# Mediterranean marine heatwaves : detection, past variability and future evolution

Sofia Darmaraki

# THÈSE

## En vue de l'obtention du

## DOCTORAT DE L'UNIVERSITÉ DE TOULOUSE

**Délivré par l'Université Toulouse 3 - Paul Sabatier**

---

**Présentée et soutenue par**

**SOFIA DARMARAKI**

Le 17 avril 2019

# Canicules océaniques en Méditerranée : détection, variabilité passée et évolution future

---

Ecole doctorale : **SDU2E - Sciences de l'Univers, de l'Environnement et de l'Espace**

Spécialité : **Océan, Atmosphère, Climat**

Unité de recherche :
**CNRM - Centre National de Recherches Météorologiques**

Thèse dirigée par
**MICHEL DEQUE et Samuel SOMOT**

Jury

**M. Michel CRéPON,** Rapporteur
**M. Gabriel JORDA,** Rapporteur
**Mme Claude ESTOURNEL,** Examinatrice
**M. Laurent LI,** Examinateur
**M. Eric OLIVER,** Examinateur
**M. Michel DEQUE,** Directeur de thèse
**M. Samuel SOMOT,** Co-directeur de thèse

# Acknowledgements

I would like to thank Samuel for his constant support and continuous help throughout this adventure. For all these stimulating discussions that sparked new ideas while advancing the limits of the already existing ones. For all the moments that answers to the questions became even more interesting questions themselves. For all those afternoon meetings that I enjoyed acquiring new knowledge and alongside confidence through his always-encouraging words. But most important of all, for all the skills and tools that he taught me in order to follow the path of my dreams. I am also thankful to Florence, Pierre and Robin for their essential and timely contributions and help at any given moment I needed, and to the people of Meteo France in the technical (or not) part that were always willing to help me solving any kind of problem, that very often tended to appear.

Last but not least, I would like to express my gratitude to the wonderful friends from all over the world that I met during these amazing three years. For their sweet and uplifting support and friendship that was always a safe refuge to come back to in moments of difficulty. And of course, to my parents and all my family that, though far away, they have been always the strongest pylon, to which I always have and I always will lean on, no matter the corner of the planet I will set to explore.

# Contents

*"If you want to discover new oceans, you must have the courage to lose the sight of the coast."*

Unknown

# Abstract

***Mediterranean Marine Heatwaves: Detection, Past Variability and Future Evolution***

The Mediterranean Sea is considered a "Hot Spot" region for future climate change and depending on the greenhouse emission scenario, the annual mean basin sea surface temperature (SST) is expected to increase from +1.5 °C to +3 °C at the end of the 21st century relative to present-day. This significant SST rise is likely to intensify episodes of extreme warm ocean temperatures in the basin, named as Marine heatwaves (MHWs), that are known to exert substantial pressure on marine ecosystems and related fisheries around the world.

In this context, the main aim of this PhD work is to study the past variability and future evolution of MHWs in the Mediterranean Sea. We propose a detection method for long-lasting and large-scale summer MHWs, using a local, climatological 99th percentile threshold, based on present-climate daily SST. MHW probability of occurrence and characteristics in terms of spatial variability and temporal evolution are then investigated, using additional integrated indicators (e.g. duration, intensity, spatial extension, severity) to describe past and future events. Within the PhD and depending on the applications, the detection method is applied to various datasets: In-situ observation at buoys, high-resolution satellite product, various high-resolution and fully-coupled Regional Climate System Models including the recently developed CNRM-RCSM6 and the multi-model (5), multi-scenario (3) Med-CORDEX ensemble. The detection method is first tested on the 2003 MHW in order to assess its sensitivity to various tuning parameters. We conclude that its characterization is partly sensitive to the algorithm setting. Hindcast and historical mode simulations show that models are able to capture well observed MHW characteristics.

We then assess past surface MHW variability (1982-2017) and their underlying driving mechanisms using the CNRM-RCSM6 model. We examine their characteristics from surface to 55m depth, where most thermal stress-related mass mortalities of Mediterranean ecosystems have been observed in the past. The analysis indicates an increase in duration and intensity of surface events with time, while MHWs of 2003, 2012 and 2015 are identified as the most severe events of the period. In particular, an anomalous increase in shortwave radiation and a lower-than-normal vertical diffusion and latent heat loss appeared to be responsible for the development of the MHW 2003, with wind playing a key role in the intensity of temperature anomalies at the sea surface. Differences on the dominant forcing, however, are sometimes evident in the different subbasin.

We finally use the Med-CORDEX RCSM ensemble to assess the future MHW evolution in the basin over 1976-2100. Our results suggest longer and more severe events with higher global-warming rates. By 2100 and under RCP8.5, simulations project at least one long-lasting MHW every year, up to 3 months longer, about 4 times more intense and 42 times more severe than present-day events. Their occurrence is expected between June-October affecting at peak the entire basin. Their evolution is found to mainly occur due to an increase in the mean SST but an increase in daily SST variability plays also a noticeable role. Up to mid-21st century MHW characteristics rise independently of the choice of the emission scenario, whose influence becomes more evident by the end of the period. Further analysis finally reveals different climate change responses in certain configurations, more likely linked to their driving global climate model rather than to the individual regional model biases.

This study provides a better understanding of Mediterranean Sea sensitivity to climate change considering for the first time the uncertainties related to global and regional climate models. We believe that this constitutes key information for the marine ecosystems and marine-related activities and societies in the basin that are under considerable risks due to the devastating effects of these events.

# Résumé

***Canicules océaniques en Méditerranée : Détection, Variabilité passée et Evolution future***

L'objectif principal de ce travail de thèse est d'étudier la variabilité passée et l'évolution future des épisodes de températures océaniques anormalement chaudes en Méditerranée. Ces évènements, appelés canicules océaniques ou Marine Heatwaves en anglais (MHW), sont connues pour exercer une pression considérable sur les écosystèmes marins et les pêcheries associées un peu partout dans le monde.

Nous proposons une nouvelle méthode de détection automatique des MHWs d'été basée sur le 99ème centile de la température quotidienne de la surface de la mer (TSM) en climat présent et tenant compte de la diversité géographique de la zone. La probabilité d'occurrence des MHWs et leurs caractéristiques spatio-temporelles sont ensuite étudiées. D'autres indicateurs intégrés tels que la durée, l'intensité, l'extension spatiale maximale ou la sévérité permettent de compléter la description des MHWs. Au cours de cette thèse et en fonction des applications, la méthode de détection est appliquée à différents types de données: observations in-situ aux bouées, produit satellitaire et différents modèles haute résolution et couplés haute fréquence du système climatique régional (RCSMs pour Regional Climate System Model en anglais) y compris le nouveau modèle CNRM-RCSM6 et l'ensemble Med-CORDEX multi-modèle (5) et multi-scénarios (3). L'algorithme de détection est d'abord testé sur la MHW de 2003 afin de montrer qu'il est peu sensible aux différents paramètres de réglage.

L'évaluation des simulations rétrospectives et historiques montrent que les RCSMs sont capables dans l'ensemble de bien reproduire l'occurrence et les caractéristiques des MHWs observées par satellite. Nous étudions ensuite la variabilité passée des MHWs de surface (1982-2017) ainsi que leurs facteurs explicatifs en utilisant le modèle CNRM-RCSM6. Nous examinons, leurs caractéristiques entre 20-55 m de profondeur, là où la plupart des mortalités de masse liées au stress thermique des écosystèmes méditerranéens ont été observées dans le passé. L'analyse indique une augmentation de la durée et de l'intensité des évènements de surface au fil du temps, tandis que les MHWs de 2003, 2012 et 2015 sont détectées comme les évènements les plus sévères de la période. Par ailleurs, pour la canicule 2003 des différences importantes dans la contribution des échanges air-mer et de la diffusion vertical de chaleur sont mis en évidence pour les différents sous-bassins méditerranéens. Nous montrons également que la tension de vent joue un rôle clé sur l'intensité des anomalies de température en surface ainsi que leur propagation verticale.

Enfin, nous utilisons l'ensemble Med-CORDEX de RCSMs pour évaluer l'évolution future des MHWs dans la région sur la période 1976-2100. Nos résultats suggèrent des évènements plus longs et plus sévères au fur et à mesure que le réchauffement climatique s'intensifie. D'ici à 2100 et dans le cadre du scénario le plus pessimiste (RCP8.5), les simulations projettent au moins une MHW de longue durée chaque année, jusqu'à 3 mois plus longue, environ 4 fois plus intense et 40 fois plus sévère que les évènements actuels. On s'attend à ce qu'elles se produisent entre juin et octobre, affectant au plus fort de leur extension l'ensemble du bassin. Cette évolution s'explique principalement par une augmentation de la TSM moyenne, mais l'augmentation de la variabilité quotidienne de la TSM joue également un rôle notable. Jusqu'au milieu du 21ème siècle, les caractéristiques des MHWs augmentent indépendamment du choix du scénario d'émission, dont l'influence devient plus évidente à la fin de la période. Enfin, l'analyse individuelle des modèles révèle différentes familles de réponses au changement climatique. Ces différences s'expliquent plus probablement par le choix du modèle global forçant, plutôt que par les biais individuels des modèles régionaux.

# Introduction (Français)

## La région Méditerranéenne

La zone méditerranéenne est un bassin de transition semi-fermé bordé par une zone tempérée au nord et une zone subtropicale au sud et à l'est. Par conséquent, les variabilités des latitudes moyennes et tropicales influencent conjointement cette zone à la topographie complexe composée de montagnes abruptes, de côtes étroites, de glaciers permanents au nord et de zones désertiques au sud, créant ainsi une région très sensible au changement climatique. De forts contrastes de températures et de précipitations sont observés au sein même du bassin qui regroupe des climats tempérés, arides et montagneux. La région se caractérise par des hivers doux et humides et des saisons estivales généralement chaudes ou sèches.

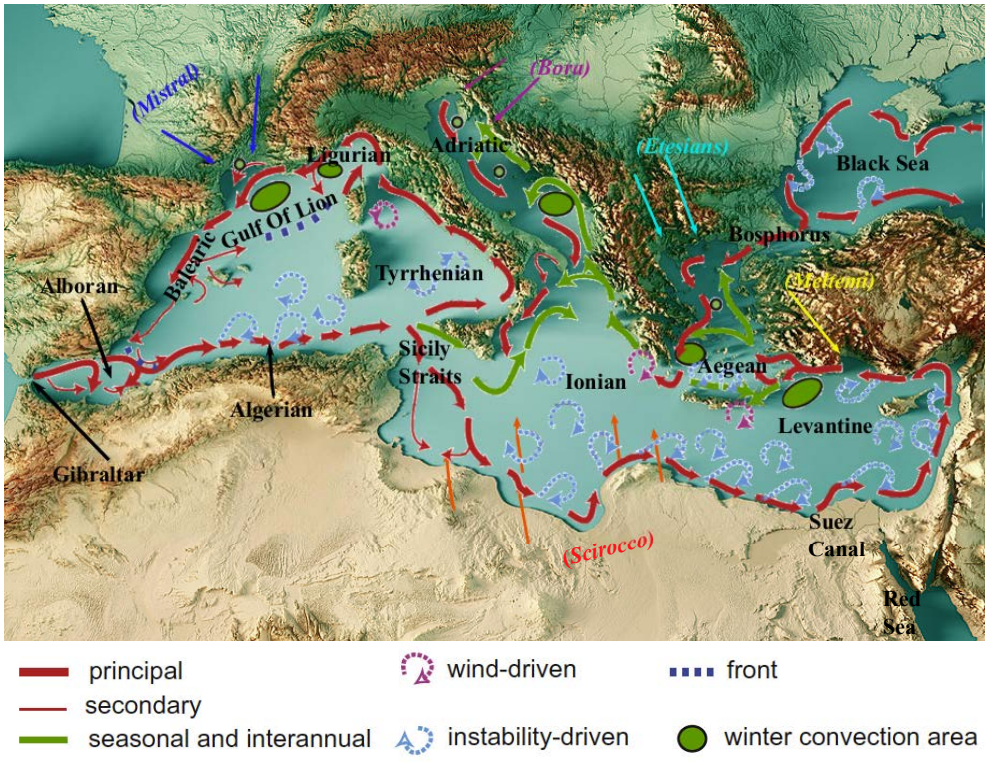


Figure 1: Région méditerranéenne et ses sous-bassins. Circulation des eaux de surface est également illustrée (redessinée d'après De Madron et al. (2011)). Les vents saisonniers et regionaux sont indiqués par des couleurs et leurs noms entre parenthèses. Modifié par S.Darmaraki. *Credits: Frank Ramspott,* https://fineartamerica.com/featured/mediterranean-sea-3d-render-topographic-map-color-frank-ramspott.html

La structure morphologique complexe du bassin méditerranéen divise la mer Méditerranée en sous-bassins, qui sont connectés avec l'océan Atlantique, la mer Noire et l'océan Indien par la mer Rouge. Le détroit peu profond de Sicile représente une barrière géographique naturelle entre la Méditerranée orientale plus chaude et plus salée, et occidentale relativement plus froid. La Méditerranée est le siège d'une circulation principalement cyclonique (Fig.1. Elle possède également une circulation thermohaline (Mediterranean ThermoHaline Circulation, MTHC) unique et active, provenant les pertes de chaleur et d'eau à la surface de la mer (Wüst, 1961).

Cette circulation anti-estuarienne est formée à partir des échanges entre le courant de surface relativement chaud et peu salé en provenance de l'Atlantique, qui se propage et s'enfonce vers la Méditerranée Est où il évolue vers une eau méditerranéenne plus salée et relativement froide. Ce courant s'écoule ensuite dans une couche intermédiaire au niveau du détroit de Gibraltar (Millot and Taupier-Letage, 2005). Cet écoulement très salin est susceptible de jouer un rôle dans la stabilisation du THC mondial (Thorpe and Bigg, 2000; Potter and Lozier, 2004; Curry et al., 2003; Reid, 1979). L'écoulement principal est en outre soutenu par les processus hivernaux de formation en eau profonde qui se produisent dans le Golfe du Lion, l'Adriatique, le sud de la mer Égée et le nord-est du bassin Levantin. Ces processus résultent de l'évaporation et du refroidissement induits par des vents régionaux froids et secs tel que le Mistral (Schroeder et al., 2012).

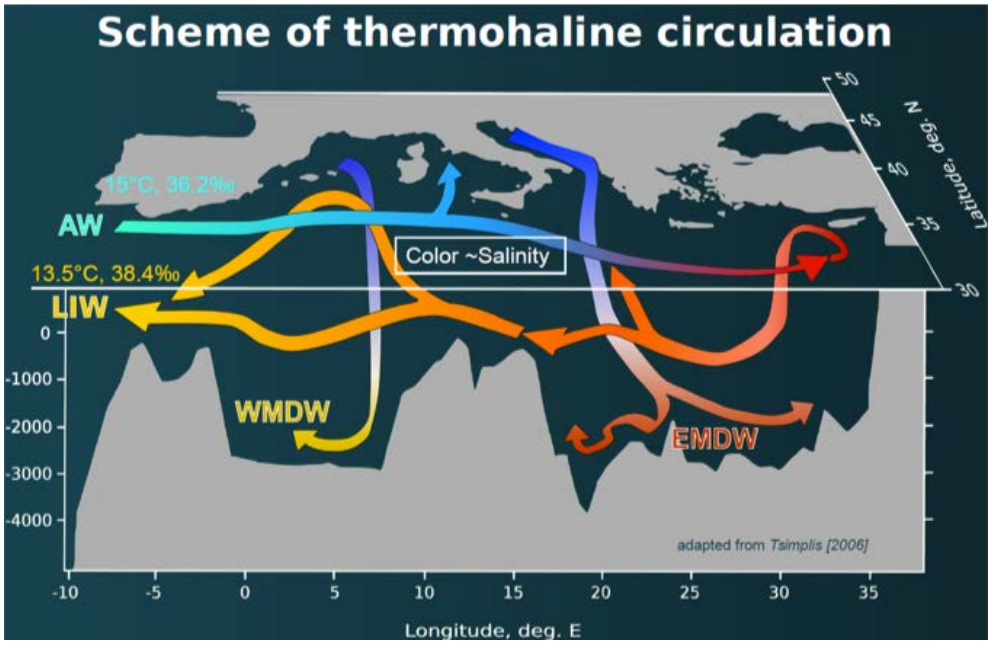


Figure 2: Schéma de la circulation thermohaline Méditerranéenne. Modifié par L.Houpert de Tsimplis et al. (2006). En anglais, AW= Atlantic Water, LIW=(Levantine Intermediate Water, WMDW=Western Mediterranean Deep Water, EMDW= Eastern Mediterranean Deep Water.

Le bassin méditerranéen abrite environ 17 000 espèces et présente un haut niveau élevé d'endémisme (Coll et al., 2010). La grande diversité des conditions climatiques a permis la coexistence d'espèces tempérées et subtropicales (Bianchi and Morri, 2000). Les zones côtières et les plateaux continentaux se caractérisent par une biodiversité plus élevée, qui diminue généralement avec la profondeur (Coll et al., 2010). Bien qu'il s'agisse d'un haut lieu de la biodiversité, le bassin méditerranéen est une zone oligotrophe en raison de l'afflux atlantique pauvre en nutriments et de l'exportation d'eau méditerranéenne riche en nutriments (Calvo et al., 2011).

La diversité et la richesse de l'environnement méditerranéen a favorisé le développement d'une communauté multiculturelle le long de ses côtes. Depuis l'Antiquité, la mer Méditerranée a représenté une voie commerciale importante et le berceau de nombreuses civilisations qui ont

échangées et prospérées. Aujourd'hui encore, elle contribue de manière significative au commerce, à l'économie mondiale, ainsi qu'à l'activité touristique. Toutefois, la mer Méditerranée est également une zone de conflit avec des tensions entre les usagers et une concurrence pour les ressources. Les villes côtières associées au 23 états modernes sont densément peuplées (500 millions d'habitants). Ces villes sont associées à de fortes différences socio-économiques et font face à de multiples défis environnementaux et sociaux. Les conditions climatiques participent notamment au déficit en eau douce, à l'augmentation du stress thermique et de la pollution qui affectent la santé, ainsi qu'à une intensification des événements extrêmes (sécheresses, inondations, vagues de chaleur) qui affectent fortement les économies (Navara and Tubiana, 2013). Source de chaleur et d'humidité pour l'atmosphère, la mer Méditerranée contribue à l'origine de aux phénomènes météorologiques extrêmes qui ont souvent lieu sur ses côtes et ont de graves conséquences sur les populations. Elle fournit néanmoins un large éventail de services écosystémiques dont dépend la qualité de vie des communautés et les activités économiques (Bleu, 2008). Par conséquent, une stratégie collective en termes d'observation, de surveillance et de gestion des ressources marines apparaît nécessaire pour accroître la résilience des socio-écosystèmes méditerranéens dans un contexte de changement climatique.

## Changement Climatique Futur en Méditerranée

Au cours du 21ème siècle, un climat nettement plus chaud - plus que la moyenne mondiale - plus sec et avec une variabilité temporelle augmentée a été envisagé pour la région méditerranéenne par plusieurs études de scénarios d'augmentation globale des émissions de gaz à effet de serre (GES). La Méditerranée est donc souvent qualifiée de «point chaud» du changement climatique (Giorgi, 2006). Si l'évolution de l'atmosphère du bassin au cours du 21ème siècle a été largement documentée, la réponse de la mer Méditerranée au changement climatique reste un sujet peu étudié jusqu'à présent. Par conséquent, les multiples sources d'incertitude quant à son évolution future sont encore moins connues. Les rares études existantes ont analysé comment l'augmentation des GES est susceptible de modifier les différentes composantes de la mer Méditerranée. D'ici la fin du siècle, ces études indiquent : une réduction des précipitations allant jusqu'à 35%, une augmentation de la perte nette d'eau à la surface de la mer (par exemple, Adloff et al. (2015); Mariotti et al. (2008)), une diminution de la perte nette de chaleur en surface sur mer (par exemple, Somot et al. (2006, 2008); Dubois et al. (2012); Adloff et al. (2015)), une augmentation de TSM de +1.5 °C à +3 °C selon le scénario d'émissions de GES, (par exemple, Somot et al. (2006, 2008); Mariotti (2010); Adloff et al. (2015)) et une augmentation possible de la salinité de surface (SSM). En raison des incertitudes associées aux propriétés de la mer Méditerranée citées précédemment, l'évolution future des phénomèneses de formation d'eau profonde et de MTHC es incertains. Par conséquent, l'évolution des caractéristiques des eaux méditerranéennes sortant à Gibraltar et leurs effets sur l'océan Atlantique restent également incertains.

## Canicules Océaniques en mer Méditerranée

Au delà de l'évolution moyenne du climat en mer Méditerranée, plusieurs études montrent que les extrêmes de température, de précipitation et de sécheresse sont susceptibles de devenir plus fréquents dans la région au cours du 21ème siècle (IPCC, 2007; Planton et al., 2012b; Giorgi and Coppola, 2009; Hertig et al., 2010) . En particulier, on s'attend à ce que le changement climatique augmente la fréquence des épisodes de chaleur extrême de 200 à 500% dans toute la région durant le 21ème siècle (Diffenbaugh et al., 2007). La concomitance de l'augmentation de la TSM attendue pour la mer Méditerranée devrait également accélérer l'occurrence d'événements thermiques extrêmes en mer, appelés Canicules océanique ou Marine Heatwaves (MHW) en anglais.

Ces épisodes représentent un réchauffement anormal des océans et ont montré lors des dernières décennies de forts impacts écologiques et des implications socio-économiques importantes (Hobday et al., 2016; Frölicher and Laufkötter, 2018). Superposées à la tendance sous-jacente du réchauffement de l'océan, les MHW se produisent régionalement de l'échelle de la côte au grand large, et peuvent modifier les écosystèmes marins en quelques semaines ou quelques mois seulement. Des réactions en chaîne ont été observées entraînant l'effondrement de la pêche commerciale, de fortes pertes financières et des tensions économiques entre les nations (Mills et al., 2013). Ces températures de la mer anormalement élevées peuvent persister dans le temps mais sont également susceptibles de s'étendre dans l'espace. Bien que de tels événements se soient probablement produits dans le passé sans avoir été détectés, le réchauffement de l'océan les rend plus pertinents dès lors que le stress thermique approche ou dépasse les seuils de thermo-tolérance de certains écosystèmes. L'amélioration récente des systèmes d'observations et de télédétection permet aujourd'hui de suivre l'évolution spatio-temporelle de la surface de la mer tandis que l'augmentation du nombre de mesures *in situ* a révélé l'extension en profondeur des MHW (Schaeffer and Roughan, 2017; Rose et al., 2012).

Nos connaissances actuelles sur les MHW passées en Méditerranée se basent principalement sur l'identification d'épisodes de mortalités massives d'espèces benthiques liées à des anomalies thermiques. Ces anomalies ont augmenté depuis le début des années 1990 (Rivetti et al., 2014; Coma et al., 2009), bien qu'elles aient été observées dès les années 1980. L'un des premiers événements de grande ampleur documenté au niveau mondial s'est produit en mer Méditerranée en 2003, avec des anomalies de surface de 2 °C à 3 °C au-dessus de la moyenne climatologique qui ont perduré pendant plus d'un mois. Cet événement a entraîné une mortalité massive d'invertébrés benthiques, la disparition de prairies marines et des changements brusques dans la composition des communautés (Garrabou et al., 2001; Diaz-Almela et al., 2007). D'autres épisodes de mortalités massives associés à des anomalies thermiques ont également été identifiés au niveau régional dans le bassin en 1994 (Marbà et al., 2015), 1999 (Perez et al., 2000; Garrabou et al., 2001), 2006 (Kersting et al., 2013; Marba and Duarte, 2010), 2008 (Huete-Stauffer et al., 2011; Cebrian et al., 2011), 2009 (Di Camillo et al., 2013; Rivetti et al., 2014) et 2010-2013 (Rodrigues et al., 2015). La plupart des épisodes documentés ont touché des espèces coralligènes (gorgones, éponges, herbiers de *posidonie*) jusqu'à 50 m de profondeur (Rivetti et al., 2014) et à quelques occasions entre 80 et 160 m (Arnoux et al., 1992; Rivoire, 1991; Vacelet, 1990). Jusqu'à

présent, les études se sont principalement concentrées sur les impacts écologiques locaux, sans évaluer systématiquement l'occurrence des MHW.

Par conséquent, un nombre d'études encore plus réduit a porté sur les mécanismes sous-jacents des MHW et leurs tendances futures dans le bassin. L'évolution de la TSM méditerranéenne extrême au 21ème siècle a jusqu'à présent été examinée uniquement par rapport aux réponses de thermo-tolérance de certaines espèces. Par exemple, en utilisant un ensemble de modèles climatiques et le scénario A1B modérément optimiste pour les émissions de GES, Jordà et al. (2012) ont suggéré une augmentation de la mortalité des herbiers marins dans l'avenir autour des îles Baléares en raison d'une augmentation prévue de la TSM maximale annuelle d'ici 2100. De la même manière, Bensoussan et al. (2013) ont évalué le risque de mortalité de masse lié au stress thermique dans les écosystèmes benthiques pour le 21ème siècle, sur la base du réchauffement moyen estimé entre 2090-2099 et 2000-2010, selon le scénario pessimiste du réchauffement futur A2. Enfin, Galli et al. (2017) ont montré une augmentation de la fréquence, de la sévérité et de l'extension verticale des MHW en supposant des dépassements des seuils de thermo-tolérance spécifiques aux espèces en utilisant le scénario à fortes émissions RCP8.5 du GIEC. Plus récemment,Oliver et al. (2018a) ont identifié une augmentation significative des MHW dans le monde au cours du siècle dernier (y compris en Méditerranée), tandis que Frölicher et al. (2018) ont prévu une augmentation des MHW dans le monde pour le 21ème siècle.

## Motivation de l'étude

Il est évident que sous l'effet continu du réchauffement climatique anthropique, les océans de la planète deviennent de plus en plus sensibles aux événements thermiques extrêmes. Compte tenu de la sensibilité du bassin méditerranéen au changement climatique, une étude plus approfondie de sa vulnérabilité et de la réponse des MHW apparaît nécessaire. Cette thèse s'inscrit dans cet objectif et tente de fournir une évaluation robuste de l'évolution des MHWS estivales méditerranéennes dans le passé, le présent et le futur en déterminant comment définir une MHW, quand et où surviennent-elles et quels sont leurs facteurs explicatifs.

Par ailleurs, la compréhension actuelle de la réponse de la mer Méditerranée au changement climatique futur repose principalement sur des ensembles de modèles climatiques de circulation générale à faible résolution spatiale (CMIP5) (Jordà et al., 2012; Mariotti et al., 2015) ou sur des expériences numériques réalisées avec un modèle océanique régional unique et utilisant très rarement plusieurs scénarios d'émission (Somot et al., 2006; Bensoussan et al., 2013; Adloff et al., 2015; Galli et al., 2017; Macias et al., 2018). Par conséquent, les études publiées dans la littérature avec des modèles adaptés à la mer Méditerranée ne tiennent pas bien compte des différentes sources d'incertitude, (i) au choix du modèle climatique et (ii) à la variabilité chaotique naturelle. Par contre, il y a quelques études que ils ont tenues compte l' incertitude associées au choix du scénario socio-économique (par exemple, Adloff et al. (2015)). Cependant, les études d'impact du changement climatique sur les écosystèmes méditerranéens et les activités maritimes sont le plus souvent basées sur une seule simulation climatique et ne peuvent donc

pas être considérées comme robuste.

Par conséquent, un autre objectif de cette thèse est d'aborder ces incertitudes. Nous considérerons pour celà différents futurs climatiques possibles par le biais d'une approche multi-modèle et multi-scénario tenant compte de la variabilité chaotique, en utilisant pour la première fois un ensemble dédié de modèles couplés et haute résolution du système climatique régional (Regional Climate System Model, RCSM, en anglais).

Dans le contexte du réchauffement climatique, l'estimation à long terme des caractéristiques spatiales des MHW pourrait aider à identifier les régions ayant une prédisposition au développement de ces événements extrêmes. La Méditerranée regroupe sur une faible superficie de nombreux risques tels que les sécheresses, la modification de la biodiversité, la croissance démographique, les migrations et les conflits. Une meilleure connaissance des risques liés aux MHW dans cette région apparaît donc essentielle afin d'assurer la durabilité des communautés qui dépendent de la mer. L'utilisation d'un algorithme automatique de detection et de description des MHW s'avère donc utile pour les systèmes de suivi et de prévision mais également pour la diffusion de l'information permet le développement de stratégies de gestion efficaces de ces événements. La méthode développée dans le cadre de ce travail de thèse s'applique aux événements estivaux uniquement et est disponible en libre accès pour les utilisateurs intéressés (industries de la pêche, centre de prévision).

Le chapitre 1 du présent manuscrit propose une introduction concernant la région méditerranéenne, son climat et les connaissances actuelles sur les MHW. Le développement original d'une méthode de détection automatique des MHW estivales en Méditerrané est décrite dans le chapitre 2, ainsi qu'un exemple de son application sur la canicule océanique bien connue de 2003 dans le bassin. Le chapitre 3 est proposé sous la forme d'un article prêt à être soumis et présente l'étude des MHW méditerranéennes passées ainsi que de leurs caractéristiques sur la période 1982-2017 avec une analyse des mécanismes explicatif. Le chapitre 4 se compose d'un article en révision qui traite de l'évolution spatio-temporelle des MHW au cours du 21ème siècle. Une analyse des incertitudes entourant les caractéristiques des événements au 21ème siècle est effectuée à l'aide d'un ensemble de modèles couplés à haute résolution et de différents scénarios d'émissions de GES. Enfin, les conclusions et perspectives de ces travaux de thèse font l'objet de la dernière partie du manuscrit, ainsi qu'une annexe sur le matériel complémentaire de ces travaux.

# List of Tables

# List of Figures

# Chapter 1

# Introduction

*"An adult scientist is a kid who never grew up."*

Neil deGrasse Tyson

## Contents

## 1.1 The Mediterranean Region

Mediterranean area is a transitional, semi-enclosed basin formed between the temperate zone to its north and the subtropical zone to its south and east. Therefore, mid-latitude and tropical variability influence a complex topography of sharp mountains and mild coasts, permanent glaciers on the north and desert areas on the south, creating a highly responsive region to climate change. The area features mild and wet winters and a mostly warm or dry summer season. Its southeastern part is exposed to the Asian Monsoon during the warm months, while it remains under the influence of the descending branch of Hadley cell for most of the year (Lionello et al., 2012). Northern regions, however, are strongly linked to mid-latitude teleconnection patterns, such as NAO (North Atlantic Oscillation), EA (East Atlantic pattern) and others, associated with moisture transport from the North Atlantic (Xoplaki, 2002; Xoplaki et al., 2003). As a result, strong contrasts in temperature and precipitation behaviour arise within the basin, distributing temperate, arid but also mountain climates throughout its surface. These spatiotemporal patterns are also affected by the location of the basin at the limit of the North Atlantic storm tracks.

To its west, the Mediterranean Sea connects to the Atlantic Ocean through the straits of Gibraltar and to its northeast, through the Bosphorus Strait to the Black Sea (main freshwater inflow for the east basin). Connection with the Red Sea and the Indian Ocean is also established, through the Suez Canal. Meanwhile, the ten largest rivers discharging in the basin (e.g. Nile, Po, Ebro, Rhone, etc.) account for about half the average river input in the Mediterranean (Ludwig et al., 2009). The complicated land-sea patterns divide the Mediterranean Sea into smaller subbasins, such as the Ionian, Tyrrhenian, Aegean, Adriatic, Alboran, Balearic and Ligurian Sea. The shallow Straits of Sicily (~ 400m) geographicaly separate the warmer and more saline eastern Mediterranean (EM) from the relatively colder and fresher, western Mediterranean (WM) subbasin, throughout which, a major cyclonic (mostly) circulation is shaped (Fig.1.1).

It is a unique and active thermohaline circulation (MTHC) driven by heat and water losses at the sea surface (Wüst, 1961). An anti-estuarine circulation is formed based on the exchange between a relatively fresh and warm surface inflow from the Atlantic (36.2 psu, 15.4°C), which spreads and sinks towards EM transforming into a relatively cool and saltier Mediterranean water (38.4 psu, 13°C) that then outflows in an intermediate layer at the narrow Strait of Gibraltar (~14.5 km) (Millot and Taupier-Letage, 2005). This very saline outflow may have a role to play in stabilizing the global THC (Thorpe and Bigg, 2000; Potter and Lozier, 2004; Curry et al., 2003; Reid, 1979). The main flow is further sustained by winter-time deep-water formation (DWF) processes that occur in the Gulf of Lion, Adriatic, the south Aegean and northeast Levantine basin, due to evaporation and cooling induced by cold and dry regional winds (e.g. Mistral) (Schroeder et al., 2012). It is one of the few places in the world where convection cells, analogous to the polar Atlantic ones, are formed and ventilate intermediate

and deeper ocean layers (Malanotte-Rizzoli et al., 2014). The vertical mixing that takes place provides oxygen to deeper Mediterranean waters but also enriches surface waters with nutrients (Auger et al., 2014) that favor marine ecosystems (Fig. 1.2).

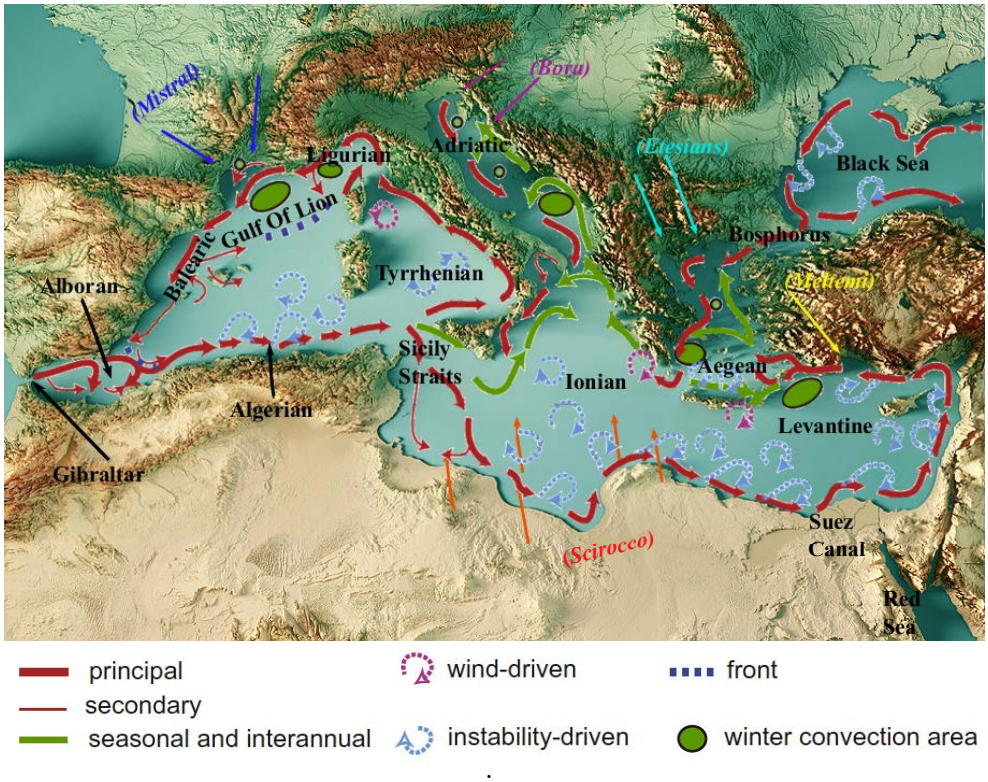


Figure 1.1: Mediterranean region and its subbasins. Circulation of surface water masses is also illustrated (redrawn from De Madron et al. (2011)). Seasonal, regional winds are indicated with colours and their names in parenthesis. Modified by S.Darmaraki. *Credits: Frank Ramspott,* https://fineartamerica.com/featured/mediterranean-sea-3d-render-topographic-map-color-frank-ramspott.html

Unlike the global ocean conveyor belt, MTHC is a much smaller in size and timescale (~100 years) open cell, which balances the excess of evaporation over the Mediterranean Sea, expressed through a net buoyancy flux towards the atmosphere (Lionello et al., 2012). Vertically, however, it forms 3 distinctive water masses that span the whole basin: The Atlantic water (AW) occupying a surface layer approximately between 100-200m, the Levantine Intermediate Water (AW) approximately between 300-800m and the Deep Water that extents to the bottom (~5.267m). Internal thermohaline cells exist in the western and eastern subbasins, which are endowed with well-known boundary currents, jets that bifurcate, mesoscale eddies and gyres (Robinson et al., 2001), some of which are wind-driven (Amitai et al., 2010; Rinaldi et al., 2010). Continental shelves, on the other hand play a significant role, since they constitute 20% of the total Mediterranean Sea surface, relative to a corresponding 7.6% of the global ocean (Pinardi et al., 2006). Its orographic surroundings and small-scale islands induces a highly diverse, regional and seasonal wind regime (e.g. Mistral, Meltemi, Sirocco, Tramontane, Bora), generating strong air-sea interactions that affect dense-water formation, MTHC and major

Mediterranean Sea features through latent heat and evaporation transfer (e.g. Romanou et al., 2010). As a source of heat and moisture for the atmosphere, the Mediterranean Sea prompts the development of extreme weather events, with often severe consequences for the surrounding communities.

Although the region accounts for 0.32% of the global ocean volume, it hosts approximately 17000 species and a high level of endemism (Coll et al., 2010). A variety of different habitats is developed in its coastal lagoons, salt marshes, estuaries, deltas, rocky and sandy coastlines, sea grass and coralligenous beds, canyons, plateaux and undersea mountains, favoring the diversity of organisms (Benoit, 2006). The wide range of climate conditions has also allowed the co-existence of both temperate and subtropical species (Bianchi and Morri, 2000). Apart from the many sensitive habitats existing across the coasts (Blondel and Aronson, 1999), there are several endangered species, such as the endemic *Posidonia Oceanica*, corraligenous assemblages, sea turtles and Mediterranean monk seals (Coll et al., 2010). The basin is also known as a spawning ground for the Atlantic Bluefin Tuna (*Thynnus thunnus*) (MacKenzie et al., 2009). Despite being a biodiversity hot spot, it is mainly an oligotrophic area due to the nutrient-poor Atlantic inflow and the nutrient-rich Mediterranean water export (Calvo et al., 2011). Nevertheless, there is a northwest-southeast gradient in productivity (decrease towards south-east), since mesoscale features in the western basin fertilize the waters regionally. Coastal areas and continental shelves, however, are characterised by a higher biodiversity which generally decreases with depth (Coll et al., 2010).

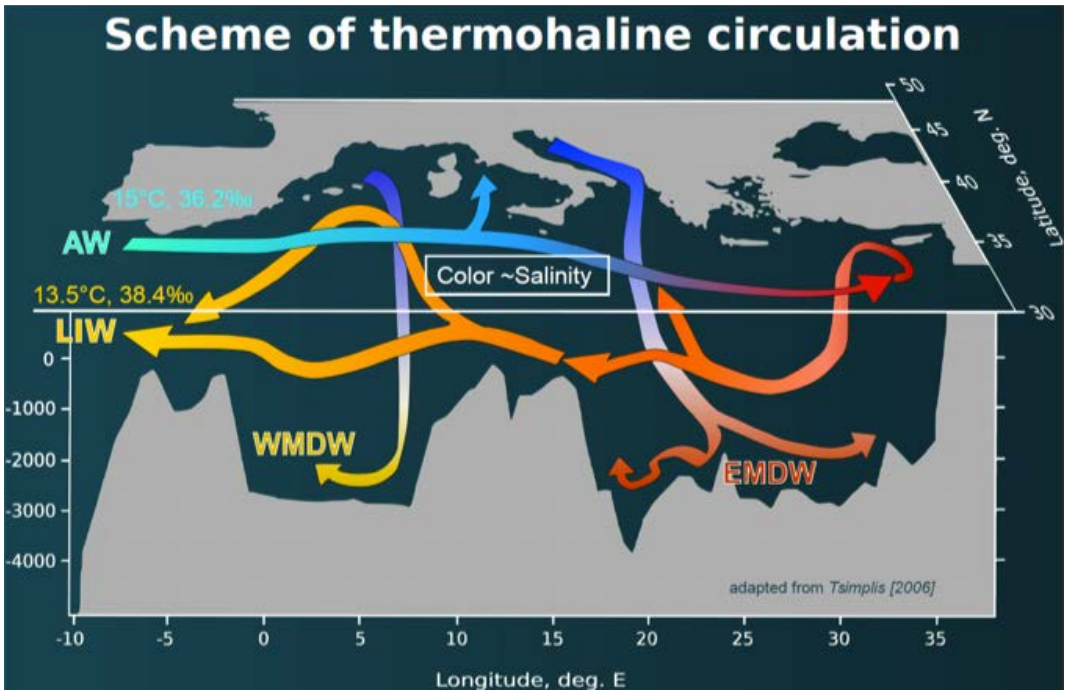


Figure 1.2: Schematic of Mediterranean Thermohaline Circulation. Modified by L.Houpert from Tsimplis et al. (2006). AW=Atlantic Water, LIW=(Levantine Intermediate Water, WMDW=Western Mediterranean Deep Water, EMDW=Eastern Mediterranean Deep Water)

The heterogeneous nature of Mediterranean environment has always also fostered a multi-cultural community around its coastlines. Since the ancient times, Mediterranean Sea has been an important trading route and a cradle of many different civilizations, which flourised and interchanged. Today, it continues its significant contribution to global trade and economy, being also a hot spot for tourist activity. It is also a disputed space, with tensions between users and competition for resources. However, its densely-populated coastal cities (500 million inhabitants) of 23 modern states, are characterised by strong socioeconomic differences and face multiple environmental and social challenges. For example, in part related to climate conditions, they are exposed already to a deficit in freshwater resources, to an increase in heat stress and pollution that affect health systems, as well as to an intensification of extreme events (e.g droughts, flooding, heatwaves) that impact economies disproportionately (Navara and Tubiana, 2013). There seems to be a north-south gradient of increasing vulnerability to climate change similar to the north-south gradient in the area's climate character. Relative to the northern countries, the southern regions demonstrate a lower adaptive capacity to changes in climate, due to reduced financial and technical resources, inadequate infrastructures and governance (Lionello et al., 2012). As a result of the great variety of socioeconomic activities, including tourism, recreation, fisheries, aquaculture, energy, cultural heritage uses, desalination, waste discharges, oil spills and maritime transport, the basin itself is under great human pressure. At the same time, it provides a wide range of ecosystem services upon which, the quality of life of neighboring communities and economic activities depend (Bleu, 2008). Therefore, a collective strategy in terms of management of marine resources, observation, monitoring and controls is required to increase resilience under climate change conditions.

The unique character of the Mediterranean Sea stands in that it is the largest and deepest enclosed sea on Earth (along with the Arctic Ocean) and a laboratory for the investigation of physical processes of global importance that operate within its small-scale subbasins. Apart from hosting a reduced version of the large-scale oceanic conveyor belt (Malanotte-Rizzoli et al., 2014), due to its semi-enclosed nature, it can be also used as a test bed for the evaluation of air-sea heat fluxes and the study of heat-budget (Bunker, 1982) and freshwater budget closures. Despite its small size, it is a biogeographical crossroad that responds quickly to atmosphere forcing and to anthropogenic influences. It represents only the 1.5% of the earth's surface, yet, a plethora of risks encountered on global scale, for example, warming, drying, water cycle and biodiversity changes, land degradation, population growth, migration and conflicts, occur simultaneously and are aggravated here. Therefore, amongst the many pressures exerted on its fragile ecosystems, resources and communities, comprehension of the interplay between the large-scale forcing and the regional influences is of outmost importance. But a high-resolution is required to adequately represent the effect of the morphological diversity on its atmospheric and oceanic circulation. For this reason, the present doctoral thesis approaches the occurrence of extreme climate events in the Mediterranean Sea, using the latest available, high-resolution ensemble of dedicated, coupled Regional Climate System Models (RCSM) from the Med-CORDEX framework.

## 1.2 Modeling of the Mediterranean Climate System

For the assessment of climate changes in the Mediterranean domain between 1950-2100, different socio-economic scenarios and types of model projections have been used:

**1**. General Circulation Models (GCMs), coupled Atmosphere-Ocean Global Climate Models (AOGCMs) and also Earth System Models (ESM), as part of coordinated Coupled Model Intercomparison Projects (CMIP). CMIP3-based results on the Mediterranean have been widely analyzed so far, whereas those by CMIP5 are still ongoing and outcomes of CMIP6 are to be expected in the coming years (Giorgi and Lionello, 2008; Lionello et al., 2012).

**2**. High-resolution, regional climate models (RCMs) dedicated to the Mediterranean region, by means of dynamically downscaled GCMs (AGCMs or AOGCMs). The RCMs then include:

- **2a)** Atmosphere-only models that are used to study the change of the atmosphere above the Mediterranean region, as part of international coordinated programs. For instance, in the following sections results from the multi-model ensembles of simulations developed within the PRUDENCE (Christensen and Christensen, 2007) and ENSEMBLES (Van der Linden and Mitchell, 2009; Goodess et al., 2009) European projects will be often mentioned. They comprise a number of GCMs and RCMs under the SRES-A2/B2 (PRUDENCE, 50km) and SRES-A1B (ENSEMBLES, 25km) emission scenario. An extension to these is the EURO-CORDEX program (Jacob et al., 2013) that has a 12km horizontal resolution, run under RCP4.5 and RCP8.5 emission scenarios and cover a domain from Ireland to Red Sea.

- **2b)** Forced regional ocean models used to assess changes for the sea (e.g. Somot et al., 2006; Macias et al., 2018) and

- **2c)** Fully-coupled, atmosphere-ocean regional climate system models (RCSM), where a high-resolution and high-frequency coupling is established between the various components of the regional climate system. For example, the European project CIRCE (e.g. Dubois et al., 2012; Gualdi et al., 2013) has made a coordinated effort to analyze the performance of such models, which have only recently emerged (e.g. Somot et al., 2008; Carillo et al., 2012), over the Mediterranean. More recently, however, the Med-CORDEX initiative (Ruti et al., 2016) has coordinated simulations using RCSMs under the RCP2.6, RCP4.5, RCP8.5 emission scenarios, with a ~30-50 km resolution in the atmosphere (or even 25-50 Km AWI model, ENEA) and 9-25km varying resolution in the sea. For the purposes of this thesis, datasets from this ensemble of simulations will be used, which currently constitutes the latest available, high-resolution Mediterranean-related multi-model ensembl.

**3**. Finally, statistical downscaling methods are also a common practice for the analysis of climate changes on atmosphere and land (e.g. Ozturk et al., 2015; Hertig and Jacobeit, 2008)

but have been rarely used over the sea (Macias et al., 2013) due to the lack of in situ data.

The various modeling approaches used so far present strengths and weaknesses and their performance on present and future climate conditions should be, therefore, considered complementary. Although Earth System Models include all the components of the global climate system (e.g. atmosphere, ocean, cryosphere, land) on a coarse resolution, RC(S)Ms work on a dynamically downscaled version of a small, limited area of interest. That way, regional processes can be examined on a finer resolution than in GCMs. For future climate projections, the climate calculated by GCMs is used as an "input" at the edges of the RC(S)Ms, which in turn can represent the effects of the regional influences better.

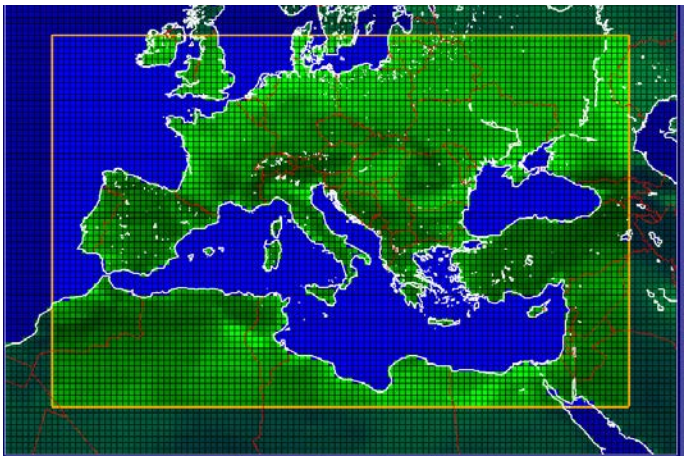

Figure 1.3: Figure representing the minimum domain prescribed for the representation of the Mediterranean area, by the Med-CORDEX ensemble of models.(https://www.medcordex.eu/simulations-phase1.php).

## 1.3 Climate Change Scenarios and Uncertainty

Investigation of climate changes is generally performed by means of model simulations that follow different greenhouse gas emission (GHG) aerosols and land-sea scenarios linked to human activities. These emissions take into account the radiative forcing from trace gases, such as $CO_2$, $CH_4$ but also aerosol particles that influence climate through absorption and reflection of solar radiation. They are proposed by the Intergovernmental Panel on Climate Change (IPCC) Working group III, which is responsible for assessing options for the mitigation of climate change effects. However, they are nothing but estimates of possible future scenarios based on socioeconomic development, population growth and technological progress, aspects of human societies which are highly unpredictable in the long-term.

The IPCC 4th Assessment Report (AR4, IPCC (2007)) yielded 4 scenario families, out of which, the impacts of the most optimistic SRES-B1, intermediate SRES-A1B and pessimistic SRES-A2 have been mostly analyzed over the Mediterranean area. The characterisation is related to the estimated $CO_2$ concentrations in 2100 (600ppm, 850ppm and 1250ppm respectively) linked to the optimistic, intermediate and pessimistic evolution of socioeconomic indices men-

tioned before. The next generation of GHG trajectories was developed within the IPCC-AR5 (Moss et al., 2010) and were named as Representative Concentration Pathways, RCP2.6 (optimistic), RCP4.5 (intermediate), RCP6.0 (intermediate) and RCP8.5 (pessimistic). They are based on assumptions of abundant fossil fuels in the future, yielding a radiative forcing of +2.6, +4.5, +6.0, and +8.5 W/m2 with respect to pre-industrial levels, respectively (Van Vuuren et al., 2011). A few studies have analyzed ecosystem and climate evolution in the Mediterranean under these scenarios, including the current work, which will focus on projections over the Mediterranean Sea under RCP2.6, RCP4.5 and RCP8.5 scenarios.

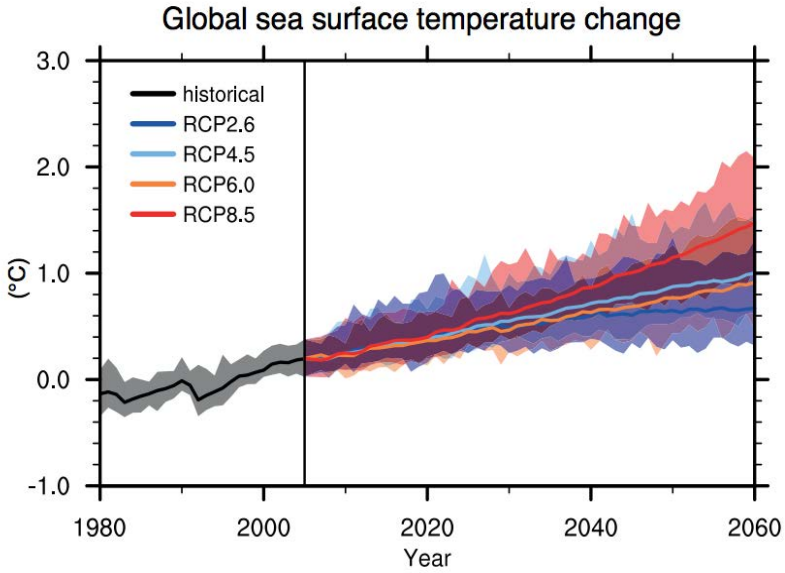


Figure 1.4: Projected changes in annual averaged, globally averaged, surface ocean temperature based on 12 Atmosphere–Ocean General Circulation Models (AOGCMs) from the CMIP5 multi-model ensemble, under 21st century scenarios RCP2.6, RCP4.5, RCP6.0 and RCP8.5. Shading indicates the 90% range of projected annual global mean surface temperature anomalies. Anomalies computed against the 1986–2005 average from the historical simulations of each model.(Kirtman et al., 2013).

In the scope of assessment of future climate changes, however, considering the different sources of uncertainties is critical. One way to deal with this is by performing several simulations under the same forcing, combining different physical descriptions of climate from different models or by varying one models' initial conditions. A robust range of climate behavior will be then aqcuired. The second source of uncertainty, where we have a higher control and chance to improve is the one related with the structural errors of the models. Description of climate equations and definition of input parameters is often poorly known or lacking. To this aim, we assume that the use of multi-model ensembles covers a sufficiently wide range of model hypothesis and can give a robust assessment over key aspects of climate (Planton et al., 2012a). Finally, as stated already, the final source of uncertainty stems from the choice of the anthropogenic emission scenario. As before, that kind of uncertainty could be investigated through simulations with different emission scenarios. Part of the current thesis is, therefore, dedicated to document both the uncertainty related to the choice of the model and the choice of the socioeconomic scenario for the Mediterranean Sea in the 21st century. We also assume

that the chaotic/natural climate variability is included in the multi-model one.

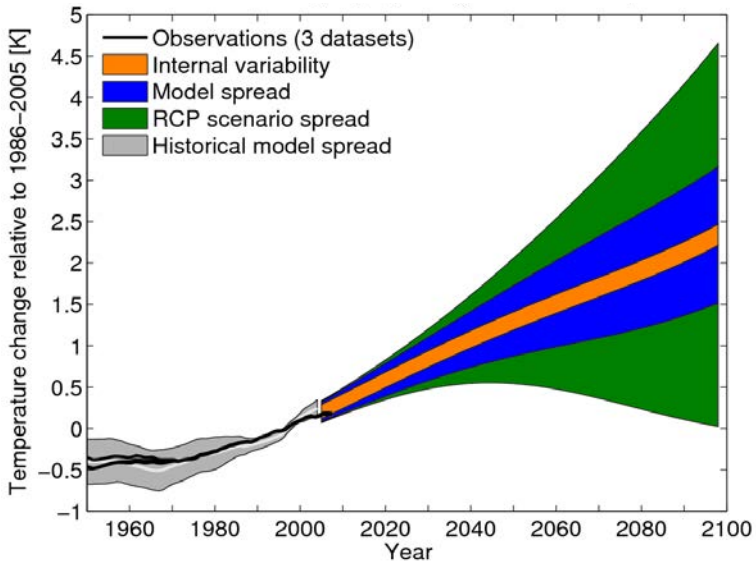


Figure 1.5: Example of the sources of uncertainty in global decadal temperature projections. Each coloured area corresponds to a different contribution, representing a 90% confidence interval (Kirtman et al., 2013).

# 1.4 Projections for the Mediterranean Region

## 1.4.1 Mean Climate

Mediterranean region is often characterised as a Hot Spot for climate change (Giorgi, 2006) and global models project significant climate changes in the 21st century as a result of the global increase on the greenhouse gas (GHG) emissions. In the following chapter, the general climate evolution anticipated for the area during the 21st century will be first summarized. Then, the analysis will focus on the model projections of the future Mediterranean Sea physical characteristics, referring also to its impacts on the marine ecosystems and socioeconomics. In the course of the 21st century, a substantially warmer -more than the global mean- and drier climate has been simulated for the Mediterranean area, by several studies. Especially during the summer season, a pronounced decrease in precipitation is projected besides a maximum warming, which would enhance the intensity and occurrence of extreme high-temperature events and droughts over the region. In fact, observed or simulated trends during the last half of the twentieth-century indicate already a decrease in river runoff (e.g. 20% reduction between 1960-2005, (Ludwig et al., 2009)) and increase in evaporation and temperatures in the region.

### Air Temperature Evolution

The ensemble mean projections of 17 GCMs under the 4th Assessment Report (AR4) of IPCC (IPCC, 2007) and the intermediate-emission scenario A1B shows a mean warming over the 2070-2100 relative to the 1961-1990 for the summer season, between 3°C-4°C over the sea

and 4°C-5°C over the land (Giorgi and Lionello, 2008). The equivalent warming under the higher/lower-emission scenario IPCC-A2/B1 is estimated to be higher/lower by 0.5°C/1°C, respectively (Giorgi and Lionello, 2008). The corresponding future changes described by RCM simulations seem to fall roughly within the range predicted by the previous GCM study (e.g. Planton et al., 2012b; Giorgi and Coppola, 2009; Christensen and Christensen, 2007).

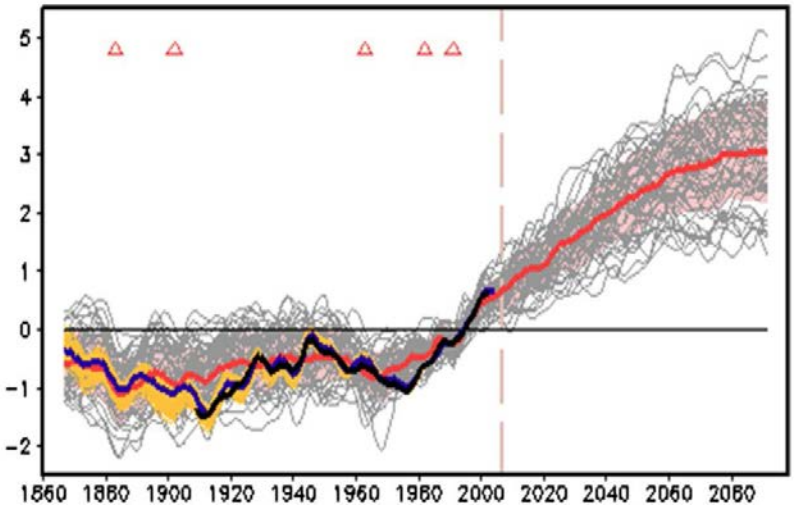


Figure 1.6: Summer, surface air temperature anomalies over the period 1860-2098 relative to 1980-2005, averaged over the Mediterranean land area only, from an ensemble of CMIP5 by (Mariotti et al., 2015). Ensemble mean temperatures (°C) are indicated in red, individual model simulations in grey and observational datasets in black, blue and yellow. Red triangle at the top of each graph indicate the years with major volcanic eruptions while vertical dash line in 2005 separates historical run from future projections .

In the more recent Fifth Assessment IPCC Report (AR5), estimates of the mean land warming by 2100 under the newer high-emission scenario RCP8.5 augment to 5°C to 7°C in the summer and 3°C to 5°C in the winter, similar to results under A2 emission scenario. By contrast, mean land warming under the newer, low-emission scenario RCP2.6 has no equivalent in the low-emission scenario of AR4 and should not exceed 1.5°C/2°C in winter/summer (Thiébault and Moatti, 2016). As it considers the implementation of climate change mitigation polices, smaller-scale climate changes should be in order. All the above results are in line with the direction of changes already seen in the 20th Century. For example, air-temperature increase over 1960-2005, based on a CMIP5 multi-model ensemble, was estimated between 0.19°C-0.25°C/decade by Mariotti et al. (2015) and 0.1 °C/decade by Xoplaki et al. (2004).

### 1.4.2 Future evolution of Mediterranean Sea Characteristics

On the contrary to the extensive literature on the basin's atmospheric evolution in the 21st century, the response of Mediterranean Sea to climate change has not been adequately examined so far. The various sources of uncertainties regarding its future evolution are even less investigated. A few studies only have dealt with how the increasing GHG forcing may alter the different components of the Mediterranean Sea.

## Water Cycle

Concerning the hydrological cycle in the basin, its particular sensitivity to temperature and precipitation changes (Sanchez-Gomez et al., 2009) is affected by their uncertain spatial distribution in the future. Many studies have pointed out that since the 1970s, the Mediterranean area has entered a pronounced dry period interrupted temporarily by some wet years (Dünkeloh and Jacobeit, 2003; Hasanean, 2004; Mitchell and Jones, 2005). Twentieth-century simulations and observation trends, designate already an increase in evaporation as well as long-term negative trends in mean precipitation, leading to an increase in freshwater deficit (Béthoux et al., 1998; Tsimplis et al., 2006; Xoplaki et al., 2006; Mariotti, 2010) e.g. a precipitation reduction of 2.5 mm/yr per decade was found for that century, based on an ensemble of coupled CMIP3 models by Mariotti et al. (2008).

According to climate change simulations this tendency should be also maintained in the future. The effective precipitation – evaporation (P-E) decrease by the end of the 21st century, is a well-known climate change feature of the area (Gibelin and Déqué, 2003; Giorgi, 2006; Mariotti et al., 2008; Sanchez-Gomez et al., 2009; Kitoh, 2007) along with an estimated river and Black Sea runoff decrease (Elguindi et al., 2011). For instance, based on the same CMIP3 ensemble from Mariotti et al. (2008), the total mean precipitation by the end of the 21st century is expected to be ~15%-20% less than the equivalent at the end of the 20th century, as a response to radiative forcing under the emission scenario IPCC-A1B. These results are in agreement with other studies performed with different GCMs or RCMs such as (Giorgi and Lionello, 2008; IPCC, 2007; Giannakopoulos et al., 2009; Chenoweth et al., 2011). Especially for the warm months, an analysis from a different GCM ensemble by Giorgi and Lionello (2008) indicated an average reduction in precipitation over the area between 25%-30%. Like in temperature, this decrease is again following the strength of the forcing and is found higher (30%-40%)/lower under the A2/B1 emission scenario, whereas it is minimised during the winter. In fact, during the cold season Giorgi and Lionello (2008) found an increase of precipitation only over the northern Mediterranean regions (e.g. the Alps). Under the newer emission scenarios of AR5 though, uncertainty in annual precipitation projections is larger, ranging from no change at all to a 40% reduction, depending on the area and season. Especially under RCP2.6 it should not be larger than 1 standard deviation from the internal variability (Thiébault and Moatti, 2016).

By default, Mediterranean Sea is characterised by an excess of evaporation towards the atmosphere and a much lower freshwater input from rivers, the Black Sea and precipitation, which is compensated by the Atlantic inflow. The above can be better described as:

$$WaterBudget \approx E - P - R - B = GibraltarNetTransport \tag{1.1}$$

where E stands for evaporation, P for precipitation, R for river discharge, B as the Black Sea freshwater net inflow into the Mediterranean Sea and Gibralta Net Transport considered

positive (Mariotti et al., 2002).

In response to greater radiative forcing by the end of the 21st century, most of the models predict a reduction in precipitation approximately between 5% to 35% over land and up to 25% over the sea (Thiébault and Moatti, 2016). Mariotti et al. (2008) found a higher, anthropogenically-forced P-E decrease over land (3.6mm/yr) but projected even more dramatic changes over the sea (~ 146mm/y) under the intermediate emission scenario IPCC-A1B. This corresponds roughly to the total amount of freshwater that Mediterranean Sea typically receives on an annual basis from neighbouring rivers and the Black Sea (Mariotti et al., 2002). Such a large freshwater loss at the sea surface (~24%) is accompanied by a mean increase in evaporation as a result of the rising SST expected under GHG warming.

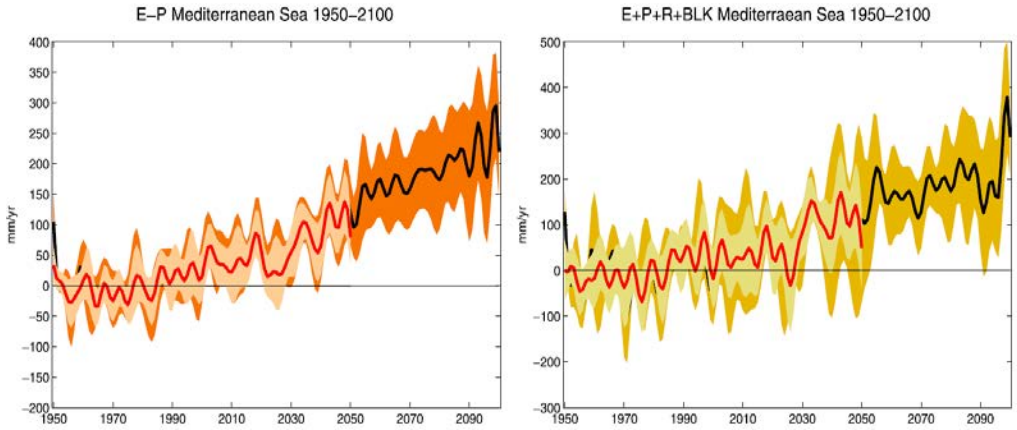


Figure 1.7: Mediterranean Sea area-averaged anomalies of the Evaporation - Precipitation (*left*) and the total freshwater deficit (*right*) for the period 1950-2100 relative to 1950-1999 from Regional Climate System Models, taken from Sanchez-Gomez et al. (2009). The black line represents the multi-model ensemble mean filtered to remove period shorter than 5 years. The coloured shading indicates uncertainty interval for the 90% level.

In combination with an estimated reduction of the river and Black Sea discharge down to -87% and -102% respectively (Thiébault and Moatti, 2016), the current freshwater deficit is expected to exacerbate in the future. According to Adloff et al. (2015), the severity of the water budget response depends on the choice of the socio-economic scenario: The higher the greenhouse gas forcing, the greater the freshwater loss.

However, the projected changes in the hydrological cycle, are non-homogeneous with a strong seasonality and geographical dependence. Due to the large variability and relatively small forced-change signal of the precipitation, changes are anticipated to emerge from internal variability around 2050 and progressively intensify by the end of the period (Sanchez-Gomez et al., 2009; Planton et al., 2012b; Giorgi and Bi, 2009; Mariotti et al., 2008). Although climate change projections typically suffer from great uncertainties (IPCC, 2007), there seems to be a remarkably high consensus among them towards the increasing freshwater deficit in the basin, as the major water budget characteristic by 2100. That is, both GCMs and RCMs future trends agree on a decrease of precipitation, river discharge and Black sea input and

increase of evaporation (Mariotti et al., 2008; Sanchez-Gomez et al., 2009). On the contrary, the contribution from the significant Nile discharge on the basin, remains still an open issue.

## Heat Budget

The direct dependence of surface heat fluxes on the GHG emission scenarios drives changes in the heat cycle that follow the intensity of the forcing. The semi-land-locked nature of the basin requires the net positive heat transport through the Gibraltar Strait to be compensated by the net sea surface heat loss over the sea. Some studies have confirmed this heat-budget closure hypothesis (Rixen et al., 2005; Ruiz et al., 2008). However, (Sanchez-Gomez et al., 2011) showed large discrepancies among atmospheric-only RCMs (between -40 W/m$^2$ to 21 W/m$^2$), most of which do not seem to satisfy it. Originally, the heat balance is described as:

$$HeatBudget = SW - LW - SENS - LAT \approx GibraltarHeatTransport(GHT) \tag{1.2}$$

where SW and LW stands for the net shortwave and longwave radiation and SENS and LAT for the sensible and latent heat flux respectively. The GHT is the net positive heat transport estimated in the Strait of Gibraltar (~5 W/m$^2$, Planton et al. (2012b)). Heat budget changes have already been observed and current research indicates a decrease in surface heat loss over the sea in the 21st century (e.g. Somot et al., 2006, 2008; Dubois et al., 2012; Adloff et al., 2015). Depending on the GHG forcing, models predict on average a surface heat gain between 25% to 118%. For instance, in the framework of the CIRCE project the ensemble mean of 5 RCSMs showed a 77% decrease of the net heat loss over the sea towards 2020-2049 relative to the 1950-1999 mean, designating a warming of the Mediterranean waters in the coming years (Gualdi et al., 2013; Dubois et al., 2012). Meanwhile, the heat content of the Mediterranean Sea is expected to augment further by the increasing temperatures of the incoming Atlantic waters, as a result of higher global ocean temperatures.

## Temperature and Salinity

Long-term observations of the ocean are fewer and often suffer from spatiotemporal homogeneity issues. Consequently, estimates based on them may not convey the overall signal of change. Still, available observations of the Mediterranean Sea during the last part of the 20th century point to a progressive increase in SST (e.g. 0.2-0.3 °C/decade, Mariotti (2010); Sevault et al. (2014)) but no significant trend is found for the sea surface salinity (SSS) (Ulbrich et al., 2013).

By the end of the 21st century, available ensemble mean scenarios indicate a basin-mean warming and salinity increase both at the surface and at deeper layers. For the mean annual SST rise in particular, GCMs and RCMs projections lie between 1.5°C–3.1°C, depending on the scenario, the time horizon and the modeling tools (e.g. Thorpe and Bigg, 2000; Shaltout

and Omstedt, 2014; Adloff et al., 2015). For example, Somot et al. (2006) used a forced, high-resolution, ocean stand-alone RCM under the IPCC-A2 scenario and concluded on a nearly spatially homogeneous SST increase for 2070-2099 relative to the 1960-1999 period. In good agreement with the forced simulation by Thorpe and Bigg (2000) those results are also close to Sevault et al. (2009) and Somot et al. (2008): A warming is projected under the IPCC-A2 emission scenario over the total water column but more pronounced at the surface, by means of the forced RCM NEMOMED8 (a regional version of NEMO ocean model) in the first case and by a coupled RCSM for the first time in the latter.

Regarding the SSS, a general and progressive increase from 0.06-1 psu is estimated over the next 100 years, yet with a large uncertainty. A greater water transport at the Strait of Gibraltar is likely to occur in order to compensate for the freshwater deficit in the basin, leading probably to an increase in its salinity. Yet, the direction and strength of salinity changes of the Atlantic waters are also very uncertain (e.g. Marcos and Tsimplis, 2008; Carillo et al., 2012; Somot et al., 2016) since some global models suggest more saline and others fresher Atlantic waters in the future. In the meantime, the simulated SSS patterns of change in the basin are geographically heterogeneous and seasonally dependent (Somot et al., 2006). A more pronounced salinification is identified, however, in the Aegean and the Adriatic, driven probably by the strong Black Sea and Po river runoff decrease (Planton et al., 2012b; Adloff et al., 2015).

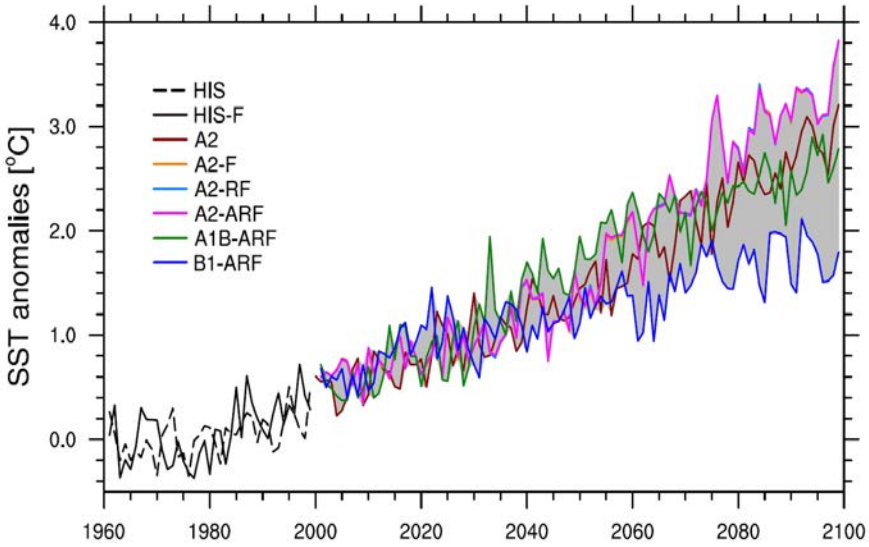


Figure 1.8: Basin-mean, yearly-averaged sea surface temperature anomalies between 1960-2100 relative to 1961-1990, by Adloff et al. (2015), using the regional ocean model NEMOMED8 and an ensemble of different socio-economic scenarios, based on the Special Report on the Emisson Scenarios. Spread of the ensemble is indicated in grey, while A2-F, A2-RF and A2-ARF curves are overlapping.

In other words, the climate change impacts coming from the different Mediterranean Sea forcings (e.g. Atlantic inflow, air-sea fluxes, river and Black Sea input) can affect the evolution of the basin's oceanic features. This could explain why the spatial patterns of SST and SSS appeared inhomogenous in the coupled simulation. Meanwhile, Adloff et al. (2015) identified the Balearic islands, the Levantine Basin, the northwest Ionian and the Aegean Sea as the

areas of maximum warming in the 21st century. From the surface, the climate change signal propagates in deeper layers and simulations show that it is transferred through convection-advection processes rather than vertical diffusion Somot et al. (2006); Adloff et al. (2015). It is the 20th-century state of MTHC that seems to be a key in how the subsurface anomalies reach at depth in the future (Adloff et al., 2015).

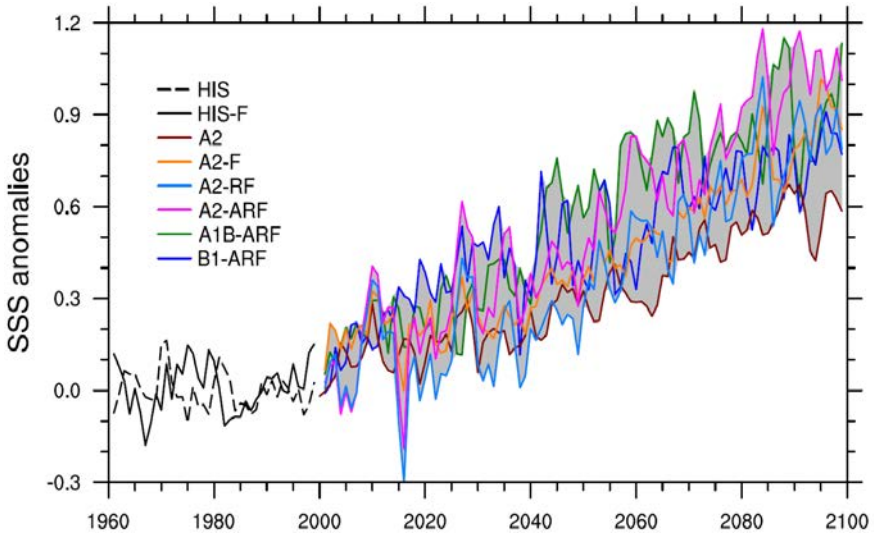


Figure 1.9: Same as Fig.1.8 but for sea surface salinity.

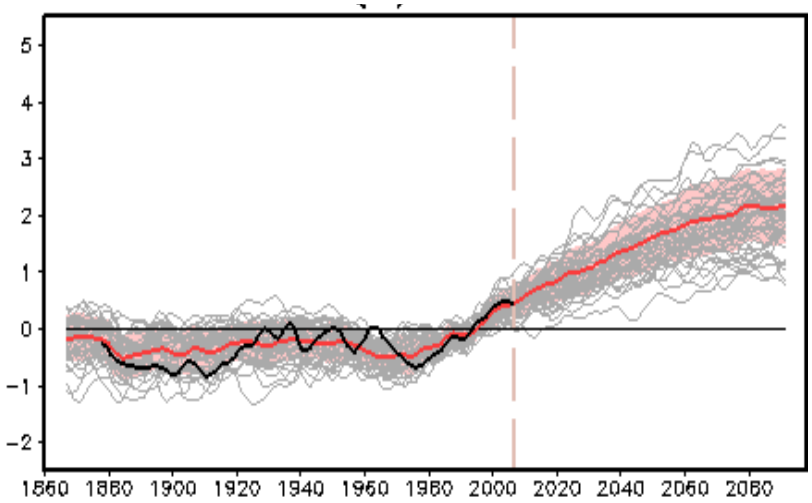


Figure 1.10: As in Fig.1.6 but for the area-average SST over the Mediterranean Sea. Observational SST is from the HadISST dataset (black line). Adapted from Mariotti et al. (2015). On the contrary to Fig.1.8, this is the SST spread given from an ensemble of GCM models.

Similar findings are shared by Tsimplis et al. (2008) that argues the predominant role of the formation of intermediate waters in the Adriatic Sea and by Marcos and Tsimplis (2008) using coupled GCMs. In this context, a marked increase in temperature and salinity of deeper layers has been observed by the 1980s and this trend seems to continue in the 21st century (Somot et al., 2006; Adloff et al., 2015; Macias et al., 2018). The strong deep-layer warming depends on the choice of the model, the modeling strategy and the socio-economic scenario.

On the contrary, no specific trend is identified for the salinity of the water column in the mid 21st century, while an uncertain increase between 0.2 -0.9 psu is given by studies towards the end of the period (Somot et al., 2006; Adloff et al., 2015; Macias et al., 2018). The main source of uncertainty for salinity, however, seems to be mostly related to the river runoff, the characteristics of the Atlantic water and MTHC and not so much to the GHG emission scenario (Somot et al., 2016).

## Mediterranean Thermohaline Circulation

From an oceanic point of view, the potential salinification indicated by the models is linked to the projected reduction in the total Mediterranean Sea hydrological budget and could lead to changes in the MTHC, through an increase in density of water masses. At the same time, an opposing SST increase due to the heat gain would counteract the salinity effect, by lightening the surface water masses. This can cause a reduced or ceased DWF affecting that way the strength of MTHC. As the MTHC is driven by both the net heat fluxes and the net surface water exchanges, its future evolution depends on the dominant factor between the two. Generally speaking, the competing effects of salinity and temperature increase on water density are not well-known. As a result, an uncertainty is induced in the projections of their implications in the future DWF processes and MTHC.

Some studies have shown that the increase in SST has a stronger influence than the increase in SSS, resulting in a weakening of the MTHC (Thorpe and Bigg, 2000; Somot et al., 2006; Adloff et al., 2015). Some project an increase in density due to a dominant contribution from the SSS at the Gibraltar Straits (Somot et al., 2016). In the coupled simulation by Somot et al. (2008) the MTHC remained stable (but slightly weakened with respect to present due to warmer deeper layers) versus the uncoupled one that used the same but forced ocean model by Somot et al. (2006). This demonstrates the importance of the coupling but also the strong link between the future MTHC evolution and the state of the vertical stratification defined during the historical simulations.

What most studies seem to agree on, however, is an increase in the stratification of the water column and a decrease of the mixed layer depth (MLD) and, therefore, of the convection processes by the end of the period (e.g. Sevault et al., 2009; Thorpe and Bigg, 2000) owing to the warming likely to occur during wintertime in the future. Particularly the western part of the MTHC is expected to undergo a strong weakening (20% - 40% for intermediate waters and 60% - 80% for deep waters) already from the early 21st century (Somot et al., 2006). On the other hand, models seem not to agree on the evolution of the eastern Mediterranean Sea thermohaline cell. Some of them display a weakening (Somot et al., 2006), whereas others suggest enhanced convection and intesified thermohaline circulation (Adloff et al., 2015). Nevertheless, estimations about how MTHC will evolve in the future are still at debate.

### Mediterranean Sea Outflow

In turn, changes in the MTHC determine (and are influenced back by) heat and salt exchanges at the Strait of the Gibraltar. Rigorous currents, temperature and salinity changes construct a complex transport of mass with the Atlantic Ocean. One that models do not currently resolve sufficiently, inducing that way a large uncertainty in future projections. For example some studies simulate a reduction of the net heat gain and the salt loss at the strait of Gibraltar (Somot et al., 2006), whereas others find an increase (e.g. Adloff et al., 2015). Adloff et al. (2015) projected an increase in the net water flux by around +0.02 Sv (current value is ~0.05 Sv), via a decrease of the outflow by ~-0.02 Sv and a slight increase of the inflow by ~0.01 Sv, in order to balance the increased surface water loss. According to the study by Somot et al. (2008) the Mediterranean Outflow becomes saltier, lighter and warmer in the future. This could result to a different outflowing position and therefore, effect on the Atlantic circulation. Nevertheless, since models do not agree on the future MTHC evolution and exchanges in the Gibraltar Strait, the characteristics of the Mediterranean Outflow are uncertain and consequently so is its effect on the Atlantic Ocean.

### Wind Changes

Finally, even fewer studies have examined changes in the wind regime over the sea (e.g. Somot et al., 2006; Dubois et al., 2012). Based on them, a decrease in speed and direction of wind is expected everywhere except for the Aegean Sea, towards the end of the 21st century. The regime shift, however, will become more evident after the middle of the period.

## 1.4.3 Impacts on Marine Ecosystems

*This section is part of the work performed during the MARmaED project (https://www.marmaed.uio.no/), in collaboration with researchers: Christina Henseler, Abo Akademi University*

The above mentioned physical changes, such as seawater warming, already have severe consequences for the Mediterranean ecosystem affecting the growth, survival and migration of several benthic and pelagic species (e.g. Marbà et al., 2015). In this section we will describe the predicted impacts of these physical changes on the ecosystem for the future. One major consequence of the expected seawater warming in the Mediterranean represents the loss of climatically suitable habitats for various organisms causing distribution shifts, but also species extinction (Jordà et al., 2012; Albouy et al., 2013; Bensoussan et al., 2013). As an example, the diversity of coastal fish assemblages is predicted to be affected very severely by the projected seawater temperature rise due to the loss of suitable climatic niches (Ben Rais Lasram et al., 2010; Albouy et al., 2013). For the end of the 21 st century it is predicted that 54 fish species will have entirely lost their habitats in the Mediterranean eventually leading to their extinction.

This will include species that are endemic to the Mediterranean Sea such as the starry sturgeon (*Acipenser stellatus*), but also fish targeted by fisheries like the flounder (*Platichthys flesus*) (Albouy et al., 2013). In total, 70% of the continental shelf area of the Mediterranean is projected to experience a decline in fish species richness by the end of this century. In the last decades several mass mortality events of invertebrates have occurred in the Mediterranean which have been linked to the documented seawater temperature rise (Rivetti et al., 2014). Responding thus to the projected temperature increase there is also an increased possibility of the occurrence of these mass mortality events in the future. One example represents the red gorgonian *Paramuricea clavata*, which is a key species in the coastal ecosystem of the north-western Mediterranean (Bensoussan et al., 2013).

In general, the summers in the Mediterranean are characterized by high temperatures and a strong stratification of the water column, which leads to a low food availability making summer periods energetically very challenging for organisms such as the red gorgonian. Due to the expected seawater warming, it is predicted that summers will be 40% longer and also warmer in the Mediterranean in the future. Experiments showed that these conditions would lead to a biomass loss of over 35% of *P. clavata*, which is equal to the mortality occurring at mass mortality events (Coma et al., 2009; Bensoussan et al., 2013). In particular, Bensoussan et al. (2013) modelled the expected mortality risk of *Paramuricea* caused by rising temperatures for the end of the 21 st century showing that there will be an extreme increase in the mortality risk over large parts of the Mediterranean coast which is likely to induce distribution shifts for this species (Fig.1.11)

The loss of climatic niches is also predicted to affect the seagrass *Posidonia oceanica*, which is endemic to the Mediterranean and represents the dominant ecosystem on sandy grounds. Seawater warming triggers an increased seagrass shoot mortality and current warming trends suggest an enhanced mortality of *Posidonia* meadows for the future (Marba and Duarte, 2010). Projections even predict that it will result in the extinction of seagrass meadows by the middle of the 21 st century with severe consequences for the Mediterranean since these meadows provide important ecosystem services (Jordà et al., 2012).

Climate change is additionally assumed to affect the productivity of Mediterranean ecosystems in the course of this century. Simulations project that rising temperatures will generally enhance metabolic rates leading to an intensification of the gross primary production of 5% by 2100, as an example (Lazzari. P, 2014). Experiments have shown that with a seawater temperature rise of 6 °C, the increase of the mean planktonic primary production of coastal communities (9% increase) will be lower than the increase of planktonic respiration rates (24% increase) rendering coastal ecosystems heterotrophic. As a consequence ecosystems would emit CO 2 to the atmosphere and deplete the O 2 -pool leading to hypoxia in coastal ecosystems with serious effects for organisms (Vaquer-Sunyer and Duarte, 2013).

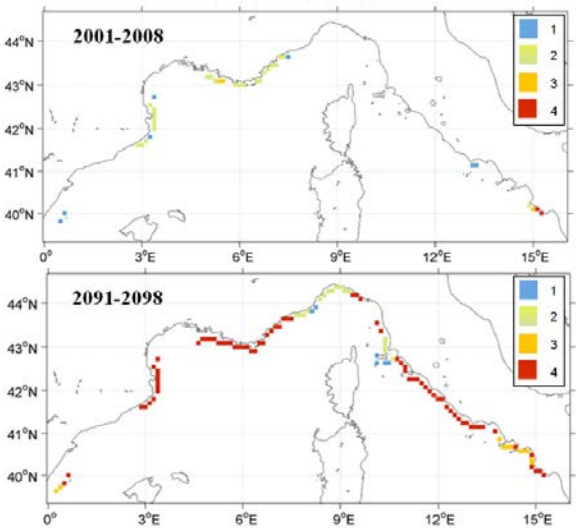


Figure 1.11: Impact mapping on the risk of mortality outbreak for *Paramuricea clavata* at the beginning (Top) and end (Bottom) of the 21st century along the continental coastal stripe north of 39 °N in the NW Mediterranean Sea. The colour scale, from 1 to 4, corresponds to sub-lethal, moderate, high and extreme lethal impacts respectively (Bensoussan et al., 2013)

Rising seawater temperatures might also trigger an increased spreading of pathogens through the Mediterranean in the future affecting both marine organisms, but also human health (Danovaro et al., 2009). When sea surface water is warming and water column stability is increased, marine snow can form huge aggregates, called mucilage, which contain large numbers of prokaryotes and viruses, but also host high abundances of pathogenic species that are absent in the surrounding seawater. Since the spreading of mucilage is enhanced by surface water warming, mucilage events are assumed to amplify in the future resulting in the potential spreading of pathogens (Danovaro et al., 2009).

### 1.4.4 Uncertainties in Mediterranean Future Projections

The collective picture from the model projections consists of an almost certain and severe warming and drying of the basin over the 21st century, especially in the warm season. These changes are related to an increase in the mean but also in the interannual variability of temperature and precipitation-minimum frequency during the summer season, which is part of a significant shift and broadening expected in general for both distributions in the future (Giorgi and Coppola, 2009). These signals are robust in that they are present and similar in most GCM and RCM projections at the broad scale (e.g. Gibelin and Déqué, 2003; Sanchez-Gomez et al., 2009), but also across any emission scenario and future time frame chosen. They corroborate a faster warming but lower drying over land than over the sea (negative feedback due to ocean thermal inertia). The magnitude of the climate-change induced signal increases with the intensity of the forcing more evidently after 2050, resulting in an enhanced land-sea contrast (between 0.4°C - 0.6°C, reaching 0.9 °C in summer, Thiébault and Moatti (2016)). A warming of the Mediterranean Sea surface and deeper layers is also predicted by both GCM and RCM models, without a model consistency over the warming rates, however. Alterations in MTHC under

the influence of warming are also anticipated but similarly to salinity changes, their direction is still under debate (Thiébault and Moatti, 2016).

To a certain extent, the way and timing of the emergence of all these changes depends on the first type of uncertainty that future projections are inherited with: The internal chaotic variability, which in this case is also connected with the large-scale modes of variability (e.g. NAO, Atlantic Multi-Decadal Oscillation) and how these may modify the climate change signal of the region (Mariotti, 2011). The actual values of the changes, however, depend on the modeling tool used and the greenhouse gas (GHG) emission scenario considered (Planton et al., 2012b). First, concerning the model structural uncertainties, their ability to reproduce properly the past and present Mediterranean Sea features determines the level of confidence on future projections. For example,Mariotti et al. (2008) argues that future projections described by the CMIP3 GCMs are uncertain, albeit to the same direction with RCM results. Due to their low resolution they fail to adequately represent the exchanges at the Gibraltar Strait, therefore they most likely do not represent realistically the mean Mediterranean Sea circulation and its potential changes. The local thermal and dynamical processes are also insufficiently described and particularly the air-sea exchanges that strongly depend on the correct representation for the temperature, humidity and wind effects (Sanchez-Gomez et al., 2009). Compared to GCMs, RCMs have been seen to improve the representation of the river and Black Sea runoff (Planton et al., 2012b), which depends on small-scale processes (Giorgi and Lionello, 2008). In turn, it has been shown that a better representation of the complex orography, the land-sea contrast and the ocean feedback, through a higher-resolution (regional) model yields water budget estimates that are more quantitatively consistent with observed values (Elguindi et al., 2011; Herrmann and Somot, 2008; Giorgi and Lionello, 2008; Sotillo et al., 2005).

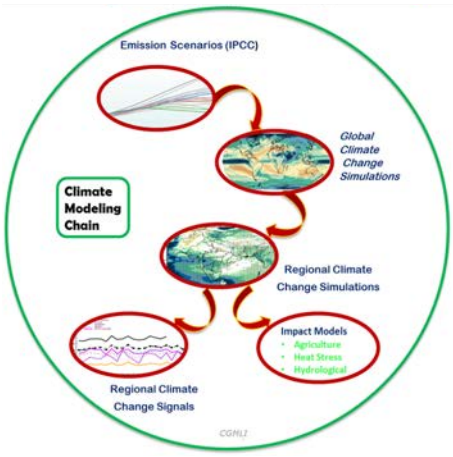


Figure 1.12: Chain of Regional Climate Modeling. Credits: Climate and Glaciers Modeling Lab, http://home.iiserb.ac.in/ kumarp/pages/research.html.

Then, regional climate modeling is characterised by an additional source of uncertainty related to its boundary conditions. In particular, the choice of the GCM used to prescribe the RCM's boundary forcing (Planton et al., 2012b). Déqué et al. (2007) performed an assessment

of the PRUDENCE ensemble, used to describe the Mediterranean area, and showed that the boundary conditions play a more dominant role in their uncertainties than climate variability. This designates the need to use a well-designed multi-model ensemble that will cover the climate change spread with different GCM forcing and RCM. Although a similar assessment, using the ENSEMBLES project this time (Goodess et al., 2009), found an equal contribution from the GCM forcing and RCM to the uncertainty factor, both ensembles indicated the dependence of the results on the climate variable, season and region. The most characteristic example for this is the water budget components of the Mediterranean Sea. Even though there is a high intermodel consistency on the direction of its changes (qualitative), the spread in the amplitude of the future freshwater deficit has been found larger in the RCMs than in GCMs, according to Sanchez-Gomez et al. (2009), implying this additional degree of uncertainty in RCMs (Déqué et al., 2005).

Concurrently, the Atlantic hydrography, air-sea fluxes and the river runoff as boundary forcing are equally influencial to the direction of the Mediterranean Sea evolution. A sensitivity study performed by Adloff et al. (2015) showed that the choice of Atlantic boundacy forcing has a large impact on Mediterranean water masses than the choice of the socio-economic scenario followed by the river run-off and the air-sea fluxes. Mariotti et al. (2008) also argues the sensitivity of the deeper-layer salinities in the river input and the current state of MTHC as well as the dependence of the ocean heat content changes on the choice of the model and the socio-economic scenario.

Finally, an additional source of uncertainty in regional climate modeling is related to coupling. A coupled simulation was seen to represent differently Mediterranean SST response to climate change versus a non-coupled one (Somot et al., 2008), leading to significant differences in the climate change responce of temperature over Europe. On the other hand, Gibelin and Déqué (2003) showed a consistency in the drying and warming projected over Mediterranean area from a coupled simulation and from a forced, low-resolution model. Although a clear signal of the impact of regional coupling is not identified yet from the literature, amongst the many added-value in their use stands their ability to reproduce air-sea fluxes that are free to evolve.

Generally speaking, high-resolution global or coupled RCMs would be the ideal modelling tool when assessing the climate changes of regional seas as the Mediterranean. Still, GCMs are limited in the representation of regional characteristics of the Mediterranean Sea circulation and the regional feedbacks compared to RCMs (Li et al., 2012). The choice of the RCM of RCSM is also essential. An issue which highlights the interest of using multi-model ensembles of simulations to illustrate the range of uncertainty (Gibelin and Déqué, 2003). After all, uncertainties should encourage more research into understanding the complex processes that link climate with anthropogenic activity.

### 1.4.5 Climate Extremes in the Mediterranean

Extreme events are termed the climate anomalies which are rare and whose magnitudes deviate significantly from the expected values. Understanding, modeling and projecting extreme events has been identified as a major area necessitating further examination by climate research. More and more studies lately argue that future climate change will be accompanied with changes in the statistics of extreme events. However, their evolution is spatially-dependent, differs according to type and is characterised by multiple causes of uncertainty (Planton et al., 2008). In the case of Mediterranean area, global changes seem to affect the frequency of hydrometeorological and wind extremes, droughts, heatwaves and cyclogeneses phenomena that concentrate in the basin. Such natural hazards affect significantly ecosystems and communities but they are still hard to predict due to their large uncertainties. More specifically, apart from the changes in the mean Mediterranean climate described before, analyses from several RCM studies highlight that temperature, rainfall and drought extremes are likely to become more frequent in the region (IPCC, 2007; Planton et al., 2012b; Giorgi and Coppola, 2009; Hertig et al., 2010) in the 21st century under A1 and B1 scenarios. Using statistical distributions, a study by Paeth and Hense (2005) reaches the same conclusion for severe warm extremes.

In general, a dramatic increase in heat risk is expected for the end of the 21st century in the Mediterranean along with an increase in frequency of extreme hot temperature events by 200% to 500% throughout the region (Diffenbaugh et al., 2007) under A2 and B2 emission scenarios. Several other studies share this view pointing out, in addition, longer and more intense events in the future (e.g. Schär et al., 2004; Beniston et al., 2007; Kitoh, 2007; Fischer and Schär, 2010). For instance, Barriopedro et al. (2011) showed, with a multi-model ensemble of RCMs from the ENSEMBLES project, that weekly heat spells, analogous to the magnitude of weekly temperatures observed during the severe European heatwave of 2003 (7-day anomaly of 3.7 standard deviation of the 1979-1999 climatology), might occur every 2 or 4 years towards 2100 under A1B emission scenario. These findings align with those by Lelieveld et al. (2014), where the hottest summers of 1961-1999 along the Eastern Mediterranean basin demonstrated high probability to constitute cooler summers by the end of the 21st century and under every emission scenario considered (A2, A1B, B2). According to Diffenbaugh et al. (2007), a preferential warming of the hot tail of the daily temperature distribution will be more severe for parts of the basin where higher drying signals are detected. In this context, the Eastern Mediterranean has been identified especially vulnerable to longer and more intense heatwaves (Kuglitsch et al., 2009; Kuglitsch, 2010; Kuglitsch et al., 2010). As a matter of fact, the 10 most severe atmospheric heatwaves in terms of intensity and spatial length have occurred in that part of the basin in 1987, 1988, 1994, 1998, 1999, 2000, 2001, 2002, 2003 and 2006 (Kuglitsch, 2010), while for the Western Mediterranean the event of 2003 was the hottest for at least the last half of the millenium with unprecedented impacts (Luterbacher et al., 2004).

The changes in temperature extremes are linked not only to a strong mean summer warming

(e.g. Goubanova and Li, 2007) but also to an enhanced temperature variability. That is, they are a combination of a shift and a broadening of the temperature frequency distribution. Specifically for the summer temperature, its variability is expected to change in interannual and subseasonal timescales (Fischer and Schär, 2009). For example, Goubanova and Li (2007) argued that the changes at the end of the 21st century further amplified relative to those in the middle of the century.

Investigation of driving mechanisms from past heatwaves in the area suggested a coupling between large-scale atmospheric circulation and regional surface influences, such as land-surface (e.g Ferranti and Viterbo, 2006; Fischer et al., 2007a,b) and SST feedbacks (as seen in the heatwave of 2003 that will be described later in Chapter 2, e.g. Black and Sutton (2007); Feudale and Shukla (2007)). For instance, Zittis et al. (2016), in line with Diffenbaugh et al. (2007) general results, showed that a decrease in soil moisture might play an amplifying role on heatwaves in the Eastern Mediterranean, through a reduced cooling caused by evaporation. Due to the great spatial variability obtained for present and future Mediterranean temperature extremes, high-resolution RCMs are considered appropriate tools to improve our understanding about them (Sánchez et al., 2004; Gao et al., 2006).

## 1.5 Marine Heatwaves

Episodes of anomalous ocean warming have been observed in recent decades, with widespread ecological impacts and important socio-economic implications (Hobday et al., 2016; Frölicher and Laufkötter, 2018). Superimposed on the underlying warming trend of the ocean, these events, referred to as Marine Heatwaves (MHWs), occur regionally from coastal to open ocean and may force changes in marine ecosystems in a matter of weeks or months. Cascading effects, have been also driven commercial fisheries driving to the point of collapse, with huge financial losses and even economic tensions between nations (Mills et al., 2013). Such anomalously warm seawater temperatures can be persistent in time but also extended in space. Although they likely occurred in the past and remained undetected, in a continuously warming ocean they become more relevant as thermal stress approaches or exceeds ecosystem thermotolerance thresholds. Their spatiotemporal evolution at the ocean surface has been captured by improved observing and remote sensing systems in recent years, while an increasing number of *in situ* data reveal their extension at depth(e.g. Schaeffer and Roughan, 2017; Rose et al., 2012).

MHWs constitute a relatively new field of research, therefore, little is known of their forcing mechanisms and the effect of the regional ocean variability on their characteristics. However, an insight is offered from the analysis of individual events around the globe, gradually drawing a picture not only of their dominant driving factors but also of their impacts on natural systems. For this reason, the current PhD work aims to present the state of affairs of MHWs in the Mediterranean Sea, in the context of the wider MHW occurrence on the planet. In the following section, a detailed overview of current MHW knowledge (modulating factors, trends, impacts)

is given based on events and studies from all over the world. It should be noted, however, that the literature described in this section will be also, partly mentioned in the introductory parts of Chapters 3 & 4, which are in the form of articles for submission (Chapter 3), accepted (Chapter 4).

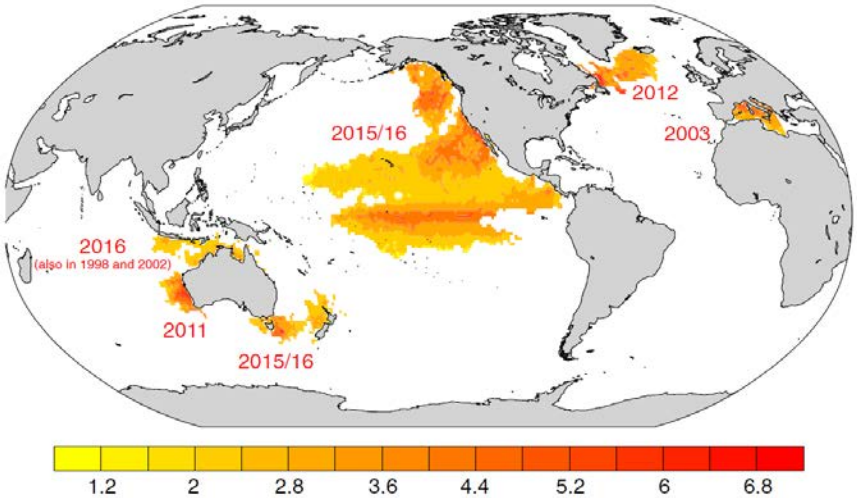


Figure 1.13: Examples of prominent MHWs that have occurred recently and have been analyzed in the literature. Maximum sea surface temperature anomaly above regional 99th percentile is indicated here, using the NOAA Optimum interpolation sea surface temperature dataset. Reference period is 1982-2016. Image taken from Frölicher and Laufkötter (2018).

### 1.5.1 Driving Mechanisms

The bulk of MHW-related research so far has explored the modulating factors behind well-known, individual MHWs. Their drivers are often a complex combination of local oceanic processes and large-scale atmospheric forcing, whose variations among the events depend on the location and season of occurrence (Pearce and Feng, 2013). Often climate-modes of variability such as ENSO, Pacific Decadal Oscillation, or Madden-Julian Oscillation are also found at play. In this section we will summarize the main physical drivers behind specific events so far.

#### Angola Benguela MHW 2001

Remotely forced warm SST anomalies were observed in the Angola Benguela Upwelling System during the austral summer of 2001, persisting around 3 months. The event has been linked to an anomalous ocean-atmosphere interaction in the Tropical Atlantic, along the equator, that facilitated the propagation of warm waters across the Angolan coast. The contribution from Kelvin waves in the propagation of the anomalies along the Equator was also implied (Rouault et al., 2007).

### Australian MHWs 2010/2011, 2012/2013

Australian waters, have experienced abnormal warming on multiple occasions, driven by different factors every time. A MHW off the west coast of Australia during the austral summer of 2011, or else named as "Ningaloo Niño", was attributed to an intensification of a poleward-flowing (Leuuwin) current that advected anomalously warm temperatures along the coast. This unusually strengthened transport was linked to a remotely-forced oceanic circulation due to a rapid transition from El Niño to La Niña conditions that year. The large-scale atmospheric teleconnection also induced high air temperatures and record reduction of opposing southerly winds associated with low sea level pressure anomalies (Feng et al., 2013; Benthuysen et al., 2014). As a result, SST anomalies peaked at 3°C-5°C (in some coastal regions) above normal for more than 10 days, boosted in turn, by mostly a reduction in latent and sensible heat loss to the atmosphere (Pearce and Feng, 2013). During the peak of the abnormally high heat fluxes the local thermal stress of an inner coral reef-lagoon system at Coral Bay was also found exacerbated (Zhang et al., 2013).

The importance of regional influences was further noted in the contrasting heat budget dynamics between that particular MHW and a less widespread event that occured again in Western Australia under the same large-scale driver (La Niña) but during the austral summer of 2012/2013. Observed differences in the extreme SST warming patterns were related to differences in the La Niña strength and to spatial differences in the wind conditions and the air-sea heat exchanges. Analysis of the ocean heat budgets revealed a more significant contribution of warm advection in the first case but a more dominant role of air-sea fluxes in the second (Xu et al., 2018). That study highlights the complex regional atmosphere-ocean interactions that ultimately regulate the development of extreme warming in coastal regions, which are preconditioned for a MHW by large-scale climate drivers.

### Atlantic MHW 2012

The record-breaking (for the past 150 years) MHW reported off the norteastern U.S coast during the first half of 2012, brought about SST anomalies of 3-4°C (exceeding 3 standard deviations) from the Gulf of Maine to Cape Hatteras. It has been mostly attributed to atmosphere-related forcing due to the anomalous northward shifts of the jet stream during that period. As a consequence, air temperature and humidity in the region rose and in combination with relatively weak wind stress resulted in reduced latent and sensible heat loss from the ocean (Chen et al., 2014). Warm temperature anomalies extended throughout the water column, increasing the continental shelf heat content. Further examination by Chen et al. (2015) confirmed the dominant role of air-sea fluxes over cold advection that acted to counteract atmosphere heating. The effect of ocean advective fluxes was more evident at local scales though and was dominated by smaller-scale processes.

### The Pacific "Blob"

One of the largest perhaps MHWs was the multi-year warm anomaly that developed in the Pacific Ocean during 2013-2016 (the largest SST anomaly in the area in at least the last 30 years), most commonly known as the "Pacific Blob" (see Fig.1.14). The start of this event (boreal winter of 2013-2014) was generally attributed to an unusually strong and persistent weather system of high sea level pressure. This system suppresed the ocean heat loss to the atmosphere and weakened the usual cold advection in the upper NE Pacific ocean (initially in the Gulf of Alaska), which was the first center of action. In particular, record low wind speeds (and wind stress) at that time were found in part responsible for a weaker than normal Ekman transport of colder water from the north, while possibly also acted to reduce the entrainment at the base of the shallower MLD (Bond et al., 2015). Observations over the Gulf of Alaska region suggested, in addition, that anomalous sensible and latent heat fluxes (due to weakened westerlies) contributed most to this warming, as opposed to surface solar and longwave radiation that offsetted each other (Myers et al., 2018). Ultimately those results indicate a lack of wintertime cooling rather than processes that actively warmed the mixed layer in 2013-2014. Warm temperature anomalies were up to 100m until 2014, after which they penetrated to depths of 300m, warmer by 2 standard deviations relative to the 1981-2010 climatology (Walsh et al., 2018). The near-surface temperature anomalies of >2°C expanded and reached coastal waters by the spring and summer of 2014 (Bond et al., 2015; Gentemann et al., 2017).

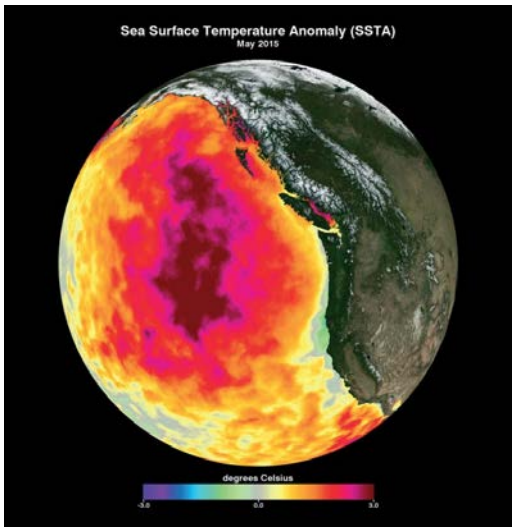


Figure 1.14: SST anomaly of May 2015 with respect to 2002-2012 climatology shows the "Pacific Blob". (Map by American Geophysical Union)

For instance, according to Chao et al. (2017) Californian coasts were affected by warm anomalies in early 2014 in addition to anomalously warm atmosphere fluxes and western boundary heat transport. Later however, the poleward propagation of ENSO signal appeared to have contributed to the warming in the area until 2016 (Jacox et al., 2018). The degree of influence from the El Niño event of 2015-2016 though, is still under debate (Jacox et al., 2016). Zaba and Rudnick (2016) confirmed but also argued a predominant atmospheric influence on

the MHW development in the southern California coast between 2014-2015. In particular, they showed that an abnormally high downward heat flux (dominated by increased shortwave radiation) led to a high stratification in the upper ocean, in combination with weak winds that depressed thermocline and reduced mixing and upwelling. Observed downward anomalies revealed then that depressed thermocline led to subsurface warming and freshening. By contrast, the evidence suggested no direct link with equatorial dynamics (northward advection of southern water masses), yet a broad connection with the general MHW state of NE Pacific was speculated. More to the south, Robinson (2016) associated the low wind intensity during extraordinary warm temperatures of 2014-2015 across the coasts of Baja California with an unusually low SLP pattern in the area associated probably to the high-pressure ridge in the NE Pacific. An analysis of the region's MLD budget further concluded on the atmosphere as the dominant driver of the local ocean heating, pointing though to the significant role of the cloud-ocean surface feedback (Myers et al., 2018). That is, a deficit in cloud cover was found to have increased downwelling (shortwave) radiation, which in turn was responsible for record-breaking warm SST in the area lasting nearly 2 years. The warm anomalies there were further amplified by the positive feedback between SST and clouds (increased solar radiation) despite a significant heat loss to the atmosphere observed during 2015/2016.

As a whole over the entire MHW-touched surface, the multi-year persistence of the event was linked to an interchange between teleconnection dynamics of extratropical and tropical origin rather than to ocean internal processes (Di Lorenzo and Mantua, 2016; Hu et al., 2017; Tseng et al., 2017). According to this theory, the "arrival" of MHW onshore (second center of action) was not due to an eastward propagation of the initial Warm Blob but rather a consequence of an entirely different atmospheric pattern formed (Arc Pattern). Then, an atmospheric transition from the Arc Pattern led to the Baja Warming Pattern, whose development is still relatively unkonwn (Amaya et al., 2016). In fact, Joh and Di Lorenzo (2017) pointed to a winter-to-winter transition between modes of Pacific decadal variability as the leading atmosphere drivers for the multi-year persistence of MHWs like this. The case of the Pacific Blob is a representative example of the complexity of the factors that drive MHWs because it included a superposition of multiple drivers. Apart from weakened wind stress and large-scale climate modes, additional mechanisms, such as the reemergence of spring/summer mixed layer temperature anomalies in winter, may also likely be at play (Jacox et al., 2018).

### Australian MHWs 2015-2016

At a certain point during 2016, 70% of the global ocean was covered by MHWs resulting in several MHWs that year. For example, during the austral summer of 2015/2016 a MHW occured over tropical Australia, with large-scale SST anomalies (>2°C) persisting for 3-4 months. The event was mainly driven by atmospheric conditions related to the strong El Niño and a weakened monsoon activity of that year. Analysis by Benthuysen et al. (2018) indicated large-scale atmospheric modes resulting in weakened winds and reduced cloud cover. This led to enhanced

ocean heating by the atmosphere (extended also at depth), primarily through positive shortwave radiation and to a lesser extent from latent heat flux anomalies. Although contribution from horizontal advection was not found predominant to the build-up of this extreme heating, the intensity of the event might have been further amplified in some areas, due to local changes in the upper ocean density structure and the shallowing of MLD. On the contrary, the anomalous warming off southeast Australia (Tasman Sea) during 2015/2016 was mainly driven by anomalous ocean heat advection, although air-sea fluxes contributed as well. This MHW lasted about 8 months, had a maximum intensity of 2.9°C above average and was both the longest and most intense event in the area up to that year. The warming signal reached down to 100-200m depth and was primarily associated to an anomalous southward flow of the East Australian current (Oliver et al., 2017). However, despite its co-occurrence with the large El Niño of that year there are no scientific evidence attributing the intensity and duration of this MHW solely to this large-scale climate mode.

**East China Sea MHW 2016**

In August 2016 East China Sea (ECS) also encountered a record-breaking warming of 2°C above normal due to the combined effects of oceanic advection and net heat flux increase. The latter, however, was shown to be the dominant contributor, largely accounted for by a positive downward solar radiation anomaly and the absence of clouds in the region affected by the event. An anomalous (atmospheric) anticyclonic circulation formed above the area not only enhanced radiative heating in the ocean but was also responsible for the advection of warm water from Kuroshio current across the ECS shelf. The event was further linked to tropical large-scale drivers such as the El Niño and the Indian Ocean Dipole (Tan and Cai, 2018).

**Tasman Sea MHW 2017**

In November 2017 another large-scale MHW hit the southeast coast of Australia (Tasman Sea), which lasted around 7 months with maximum anomalies of 2.5°C. Unlike the 2015/2016 event this MHW was more widespread and mainly linked to an increase in local air-sea heat fluxes rather than to ocean advection. Anomalously low winds and clear skies, under a persistent high sea level pressure system established over the area, caused a remarkably shallow MLD this time, due to which temperature anomalies developed and were confined in the upper 100m (Perkins-Kirkpatrick et al., 2018). This anomalous atmospheric circulation was only weakly connected to the La Niña conditions of that year. However, across New Zealand's coasts the broader oceanic heat content did not exhibit significant departures from normal rather the weaker than normal vertical mixing caused SST anomalies of about +3.7°C (Salinger et al., 2019).

### Southwest Atlantic Shelf MHW 2017

In February-March 2017 an anomalously warm event (4.3°C) occurred across the Atlantic coasts between Brazil and Argentina. It lasted for 22 days and was the longest and most intense event recorded between 1988-2017 in the area (Manta et al., 2018). A persistent atmospheric blocking circulation linked most probably to the MJO climate mode, led to anomalous heating in the ocean through turbulent heat fluxes. In addition, abnormally weak winds were responsible for a strong stratification of the water column. Although the majority of the MHW was explained by air-sea heat fluxes, a part of it was hypothesized to have occurred due to advection from a warm inner estuary discharges.

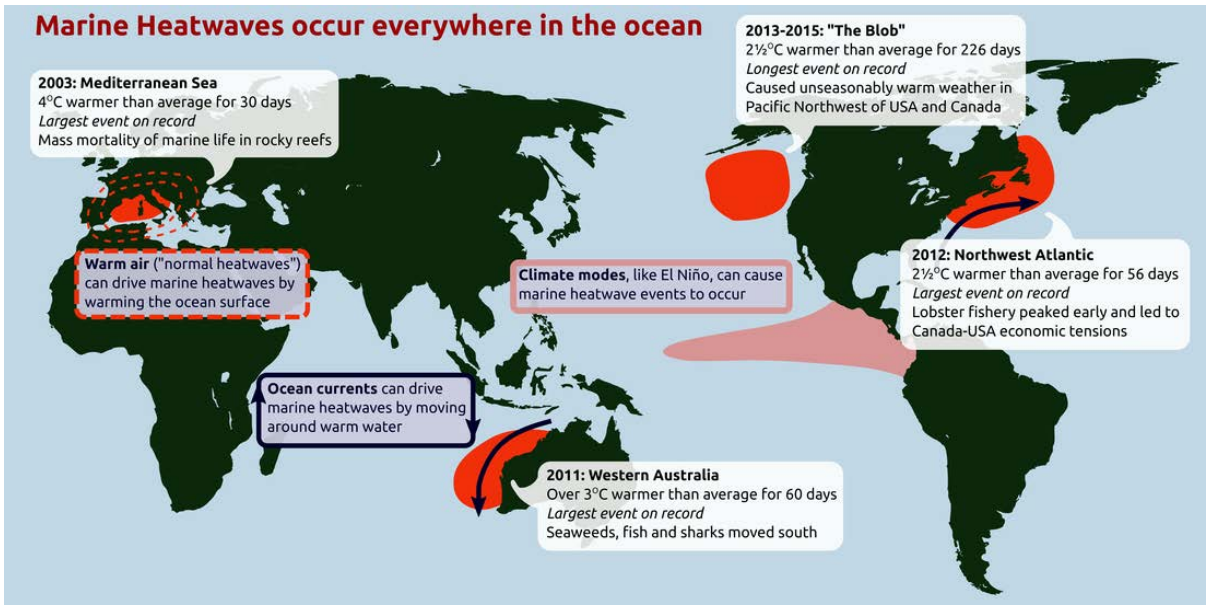


Figure 1.15: Most prominent MHWs during the last decade and their driving mechanisms. Credits, Eric Oliver, Dalhousie University.http://www.marineheatwaves.org

Aside from these well-documented events there is still little understanding of the general forcing (if there is) behind multiple MHWs around the globe. Despite the complex effects of large-scale climate modes on oceanic circulation and the radiative heating to the ocean, the scale of forcing required for a coastal MHW to occur remains an open question. In fact, Schlegel et al. (2017b) showed that the formation of onshore MHWs in South Africa was far less related to the occurrence of offshore temperature anomalies. Therefore, a closer look on broader yet regional oceanographic processes and their interactions with local features (e.g. direct atmosphere heating or coastal heating) of a (coastal) area is necessary to determine the MHW dynamics and comprehend their evolution with time. Further analysis of a series of coastal MHWs in South Africa between 1982-2017 by Schlegel et al. (2017a) confirmed the multimodality of the predominant driving patterns behind the events of that area. Clustering of atmospheric and oceanic conditions during the identified events showed that although abnormal ocean heat advection, anomalously warm air and onshore (aseasonal) winds were predominant patterns behind the development of some MHWs, most of the events were not accompanied by

a consistent oceanic or atmospheric pattern. The latter category included, in fact, the events with the highest severity and duration of the period and therefore, with the potential to cause the most harm on marine ecosystem. For some of the events a linkage with mesoscale eddies was also implied. Nevertheless, the results of these studies reinforce the importance of examining the meso-scale dynamics for the formation of local MHWs and are pertinent to the analysis that will follow in this work about the Mediterranean Sea MHWs, which develop in a highly-diverse oceanic circulation and atmospheric field.

Using a similar statistical technique (Self Organising Maps) Oliver et al. (2018b) developed a "typology" of MHWs around the Tasman Sea. That is, a number of different anomalous oceanic and atmosphere states accompanying each MHW identified between 1993-2015 in the region. In that case, the dominant drivers yielded a combination of (East Australian Current) ocean advection and warm air temperatures, while many of them included influence from anticyclonic eddies and wind anomalies. Therefore, it proved that MHW underlying mechanisms are somewhat difficult to separate and difficult to predict.

### 1.5.2 Detection Methods

Until recently, MHW identification has been based on the analysis of ecosystem-oriented events or on event-based trends of positive temperature anomalies or on anomalously warm ocean temperatures relative to a mean state. The transition to a consistent definition and characterization occurred through a standardized framework proposed by Hobday et al. (2016) whereby MHWs properties are quantified through a set of dedicated statistical metrics. According to this definition a MHW is now described as a "discrete, prolonged, anomalously warm water event at a particular location". Quantitatively this requires daily temperatures of a given point to be above a pre-defined threshold (anomalously warm) for 5 consecutive days or more (prolonged).

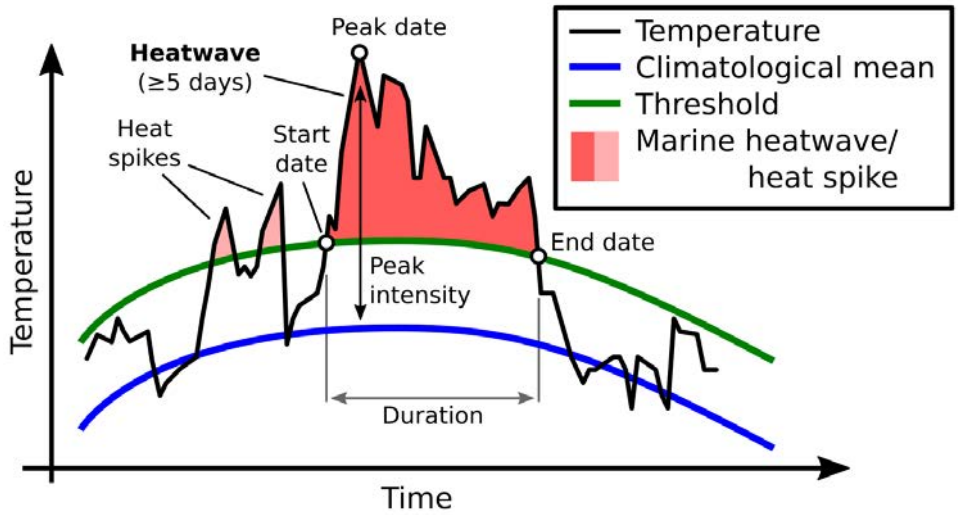


Figure 1.16: Schematic of MHW definition by Hobday et al. (2016). Credits: http://www.marineheatwaves.org/all-about-mhws.html.

This threshold was set to be the seasonally-varying 90th percentile climatology. The climatological threshold is calculated for every calendar day within an 11-day window centered on that day and across all years. The discrete nature of the event also requires a well-defined start (the first day when the local SST threshold is exceeded) and end (the day after the last day for which the temperature threshold is exceeded). This definition allowed gaps of two cool days (days that fall below the threshold) or less to be counted as part of an event, if they are followed by 5 or more consecutive MHW days.

The advantage of a percentile threshold versus an absolute value is that it can identify extreme temperatures independently from their distribution in space and time. That way, seasonal and local variations are taken into account. The 5-day minimum duration, was then chosen as a balance to identify a uniform number of MHWs around the world. This ultimately stems from the fact that with a different minimum number of MHW days some regions showed less and some others more events when compared with each other. The spatial extent of a MHW is then calculated by the sum of the area where the threshold is exceeded. Once a MHW is identified a set of primary, secondary and tertiary metrics are calculated to characterise the event. The primary metrics include the duration (total number of MHW days), mean and maximum intensity (mean and maximum temperature anomaly during the event) and cumulative intensity that represents the overall accumulation of heat stress throughout the event (see Fig.1.16).

A linear classification scheme was then proposed by Hobday et al. (2018), where MHWs are defined based on their temperature exceedance from the long-term local climatology of the 90th percentile. In other words events are categorised in 4 groups (moderate, strong, severe, extreme) based on their intensity relative to the threshold used to identify the MHWs (see Fig.1.17). A consistent naming convention like this facilitates public awareness for the events as well as preparation for effective management practices.

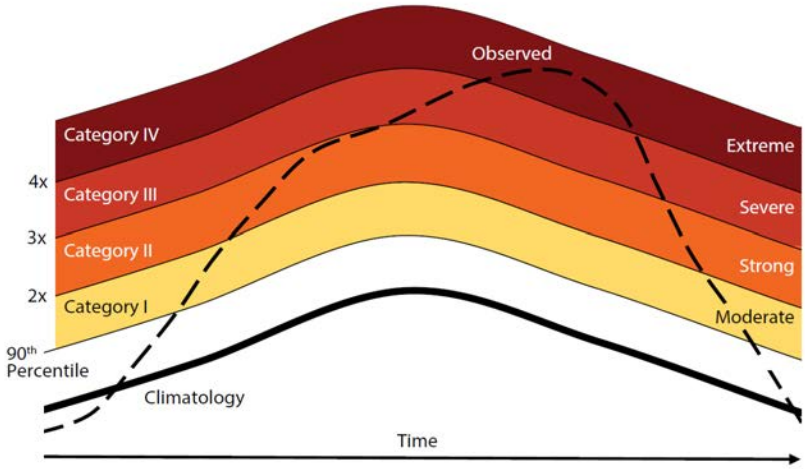


Figure 1.17: Schematic of MHW classification by Hobday et al. (2018)

Nevertheless, there are studies that did not follow the Hobday et al. (2016) standardized

framework. For instance, King et al. (2017) that investigated the Australian climate extremes at 1.5°C and 2°C of global warming and Frölicher et al. (2018) that analyzed future MHW occurence on a global scale and under different IPCC emission scenario. In the former case temperature anomalies in the ocean around Australia were defined relative to the 1961-1990 climatology. In the latter case, events were identified as MHWs when local temperatures were above the regional 99th percentile of SST (see Fig.1.13). In similar ways, the current PhD work did not follow the above-described MHW framework either. Instead, inspired by the principles presented in Hobday et al. (2016) and following some of the key requirements we developed a MHW detection method based on the 99th percentile of the local daily SST that will be further analyzed in Chapter 2.

### 1.5.3 Trends in the Past and the Future

#### MHW Trends in the 20th century

Despite the growing body of MHW-related literature, systematic examination of MHWs as distinct exceptional events with intensity, frequency and duration has only just emerged. Although marine extremes have been investigated before, only a few studies have analysed past trends in extreme ocean temperatures (e.g. MacKenzie and Schiedek, 2007). For example, an extensive proxy of MHW historical variability is provided by thermal-stressed related coral bleaching records, with relevant studies designating an increase in the frequency of SST extremes globally, already from late 1970s (Lough, 2000; Selig et al., 2010; Hughes et al., 2018). Lima and Wethey (2012) also found a heterogeneous but increased frequency of extremely warm temperatures in some coastal areas during the years 1982-2010.

Using the Hobday et al. (2016) definition, more recently, Oliver et al. (2018a) identified significant increases in MHWs globally between 1925-2016 as a result of anthropogenic climate change. In particular, using a range of observational data they showed that, on average, MHW frequency and duration have increased by 34% and 17% respectively, resulting in a 54% increase of annual marine heatwave days globally throughout the period (see Fig.1.18). This practically means an increase of about 30 additional MHW days per year by the end of the period relative to around 25 days during the 1980s. However, the spatial distribution of MHW intensity and duration across the global ocean was found inhomogeneous. Regions with western boundary currents were characterized by high MHW intensities, while the longest events were seen in the eastern Pacific region. According to that study, those trends can be explained by an increase in mean ocean temperatures but changes in SST variability contribute as well. While large-scale climate modes have a role to play in MHW variations they do not seem to affect significantly their trends. Furthermore, over the 35-year satellite SST record Hobday et al. (2018) found a 33% increase in the area of the ocean affected by MHWs at any time during the year. Especially for the strong events (Category II) there seems to be a 24% increase in the area they affect. In agreement with those studies Frölicher et al. (2018) observed a doubling in the number of MHW

days between 1982-2016 underlying also a significant increase in their duration and intensity.

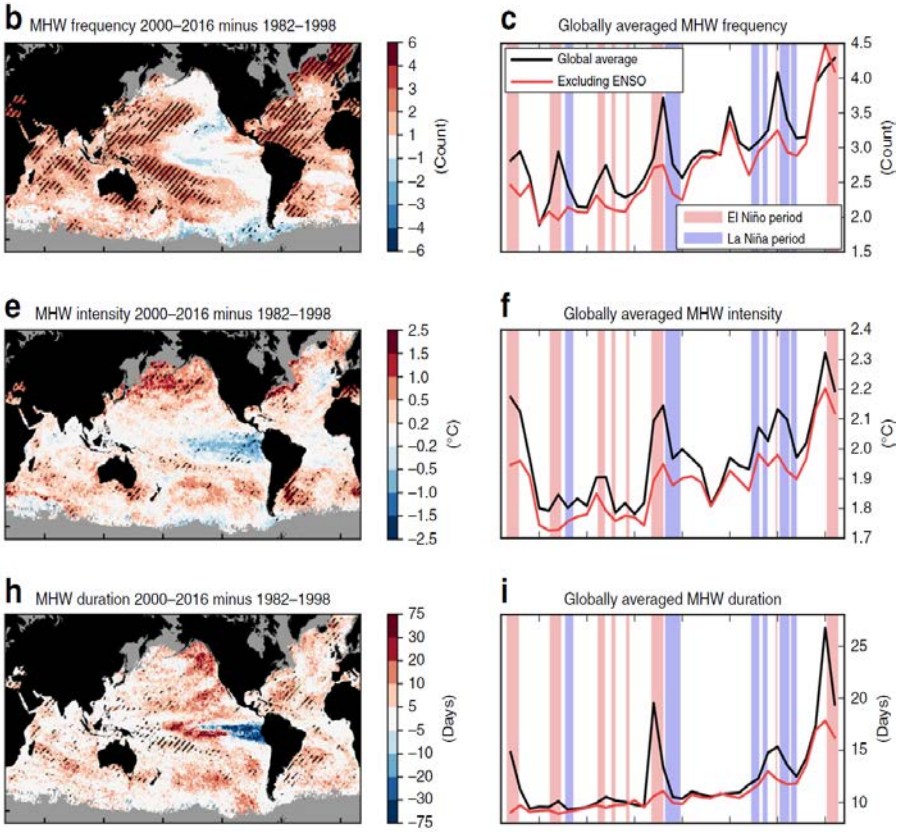


Figure 1.18: Difference of MHW properties between 1982-1998 and 2000-2006 (**b,e,h**) and their respective globally-averaged annual mean timeseries (**c,f,i**) with (black) and without (red) ENSO effect. Hatching denotes that the difference is statistically significant at the 5% level while red and blue denote El Niño and La Niña periods respectively. Figure taken from Oliver et al. (2018a).

In regional scale, using the same definition Oliver et al. (2018b) found positive trends in MHW frequency, intensity, duration and penetration depth off eastern Tasmania over 1993-2015. However, their properties exhibited regional variations. Much like Mediterranean Sea, the surface waters off eastern Tasmania are generally considered as a marine hotspot with mean temperatures increasing nearly four times the global average rate. Meanwhile, Schlegel et al. (2017b) identified positive decadal trends in annual MHW occurrence around South Africa for 1982-2015, while an increasing trend in MHW days duration and intensity was found for the Southerwestern Atlantic Shelf over 1988-2017 by Manta et al. (2018). Schaeffer and Roughan (2017) demonstrated intense subsurface MHWs that occurred all year long in coastal SE Australia between 1953-2016. Scannell et al. (2016) on the other hand, used a MHW definition based on probability of occurrence and studied large-scale warming events in the N.Atlantic and N.Pacific Ocean over 1950-2014. They argued an influence from region-specific, intrinsic climate variability for the size-frequency patterns of MHWs in those regions on interannual timescales, replaced by random weather-like processes that regulate mixed layer temperatures once the long-term anthropogenic warming is removed. Not surprisingly, they noted they higher frequency of occurrence of small-scale events than large-scale anomalies,

suggesting that MHW occurrence is a trade off between size, intensity and duration.

### Anthropogenic Influence in MHWs

Despite the different definitions used for the MHW detection almost all studies conclude to a progressive increase in their occurence and intensity throughout 20th century. MHWs are,in fact, expected to become more common in the future under continued global warming. Therefore a few studies have attempted to quantify the role of anthropogenic forcing in modifying the likelihood of MHWs with present-day properties in the future. To do so they have performed an extreme event attribution analysis or else named as Fraction of Attributable Risk (FAR) approach. They have compared the likelihood of MHW occurrence in a world with only natural forcing (pre-historical climate simulations) with that under both anthropogenic and natural forcing (historical simulations that represent the present-day climate) and/or with the MHW distribution in the 21st century under elevated greenhouse gas emissions. In most cases a compounding effect of an enhanced human-induced signal and natural variability were conducive to the MHW development. More specifically, the NE and Western Tropical Pacific MHW of 2014 (Weller et al., 2015), the Tasman Sea MHW 2015/2016 (Oliver et al., 2017), the MHW 2016 in Tropical Australia (Benthuysen et al., 2018; Oliver et al., 2018c) the MHW 2016 in the Gulf of Alaska (Oliver et al., 2018c; Walsh et al., 2018), the multi-year persistent (2014-2016) MHW in the California Current System (Jacox et al., 2018) and the Tasman MHW 2017/18 (Perkins-Kirkpatrick et al., 2018) were found to be several times more likely to occur with anthropogenic influence than in a naturally varying world. In other words, the intensity and duration of these events was virtually impossible without anthropogenic forcing. On a global scale, 87% of present-day MHWs are attributable to human-induced warming (Frölicher et al., 2018)

## Marine Heatwaves in the 21st century

While trends of the long-term warming of the ocean are relatively well-studied, fewer studies have dealt with the future evolution of extreme ocean temperatures. Therefore, little is known about the future évolution of MHWs. In general though, it is anticipated that their frequency, duration and intensity will increase in the future (Oliver et al., 2017, 2018a). On a global scale, Hobday and Pecl (2014) identified 24 discrete regions that up to 2050 seem to warm at a rate faster than 90% of the rest of the ocean. Named as marine "Hot Spots", most of them were associated with western and eastern boundary currents, while some of them were lately affected by large-scale MHWs e.g. Tasman Sea, (Oliver et al., 2017). More recently, however, Frölicher et al. (2018) investigated future MHW evolution in global scale under different IPCC scenario and suggested a significant increase in their frequency, duration, intensity and spatial extent in the 21st century. In particular, they used 12 coupled CMIP5 Earth System Models and detected an increase in MHW days that surpass the pre-industrial 99th percentile SST, by a factor of 16 and 23 at 1.5°C and 2°C global warming, respectively. According to the same study, the current

projections, point towards a 3.5°C global warming scenario, whereby the probability of MHW occurence increases by a factor of 41. This practically means that, a one-in-a-hundred-days event at pre-industrial levels is expected to become a one-in-three-days event at this level of global warming. Moreover, MHWs are expected to have an average spatial extent 21 times bigger than pre-industrial levels, last on average 112 days with a maximum intensity of 2.5°C. Human-induced warming in that case can be accounted for their occurrence nearly at 100%. However, if the warming is kept below 1.5-2°C the probability of MHW occurence and their characteristics were found substantially reduced. Finally, the tropics and the Arctic Ocean demonstrated the highest increase in future MHW frequency on the contrary to the Southern Ocean that showed a lower probability of occurrence (Frölicher et al., 2018).

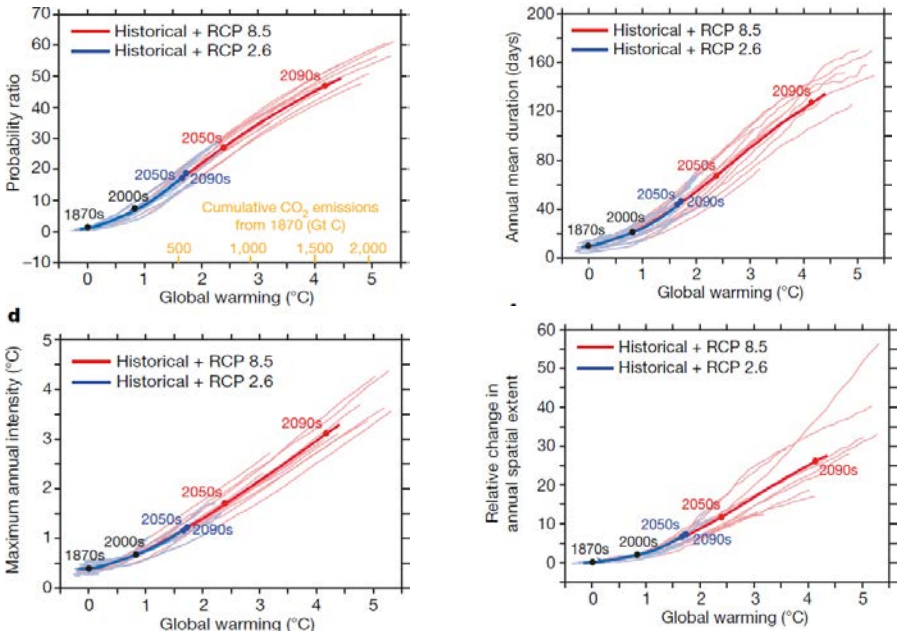


Figure 1.19: Simulated changes in MHW probability of occurence (top left), mean intensity(down left), duration (top right) and spatial extent (down right) for different levels of global warming. Figure taken from Frölicher et al. (2018).

On a similar vein, only a few studies exist that have investigated MHW occurrence at regional scales. For example, under the IPCC A1B intermediate emission scenario and by the end of the 21st century, Oliver et al. (2014) found a non-uniform increase of extreme SST in Tasman Sea, using a Bayesian hierarchical model (extreme value approach). RCP8.5 simulations indicated also that by 2020-2040 the likelihood of a MHW with similar characteristics to the Tasman Sea MHW 2015/2016 is increased in the region with a 66% higher possibility to be due to anthropogenic factors (Oliver et al., 2017). King et al. (2017) noted a doubling in the frequency of MHWs, like the one that hit the Great Barrier Reef in 2016, under a 2°C global warming. Projections for 2100 under the RCP8.5 over the Northeast Pacific suggest an increasing trend in large-scale climate modes that favor multi-year warm events (>1°C) with high spatial extent and maximum intensity. In fact, an ensemble of CMIP5 model simulations under RCP8.5 found that MHWs up to 2020 have a higher probability to be larger and more

intense than the ones that occurred in Northern Australia and Gulf of Alaska in 2016 (Oliver et al., 2018c). More recently it was shown that the MHW 2017 across New Zealand's coasts will probably occur as a typical summer condition in the area in the 21st century under RCP4.5 or RCP6.0 scenario (Salinger et al., 2019).

### 1.5.4 Impacts on Marine Ecosystems

In addition to the driving mechanisms, severe impacts on marine ecosystems due to MHWs are well-documented worldwide, bringing forward the risks related to a potential future increase in MHW frequency. For example, unprecedented mass mortality events and changes in community composition were reported during extreme warming in the Mediterranean Sea in 1999, 2003, 2006, leading to mass mortalities of a wide variety of (invertebrate) species and taxa (e.g. 80 % of Gorgonian fan colonies and seagrass *Posidonia oceanica*). In 2011, record high temperatures triggered significant biodiversity die-offs and an abrupt regime shift (tropicalisation) of temperate reef communities in Western Australia during the so-called Ningaloo Nino (Rose et al., 2012; Wernberg et al., 2013, 2016). Extensive species migrations followed the MHW 2012 in northeast Atlantic (Mills et al., 2013). The latter two events impacted as well, commercial fish species e.g. (Cavole et al., 2016). In addition, disease outbreaks were observed in commercially viable species during the intense MHW 2015 in Tasmania (Oliver et al., 2017). The MHW associated to the 2015/2016 El Nino led to the third mass coral bleaching (>90%) in the northern Great Barrier Reef (Hughes et al., 2017). The strong MHW 2013-2015 in the northern Pacific led to strandings and mortalities of marine mammals, seabirds and salmon in addition to a toxic algal bloom along the Californian coast (Cavole et al., 2016) and a very low ocean primary productivity (Frölicher and Laufkötter, 2018).


Figure 1.20: Examples of MHW impacts on marine ecosystems. Coral bleaching (top left) and sea grass die-off (top right) are indicated, along with mass mortality of abalone (down left) and changes in recruitment patterns of lobsters (down right). Severe ecological and socio-economic consequences accompanied these abrupt changes. Credits:http://www.marineheatwaves.org/

All the aforementioned examples constitute only a small fraction of the numerous observed MHW impacts on marine ecosystems around the world. A study by (Smale et al., 2019) showed

deleterious impacts of MHW across a range of (foundation also) species and their biological processes around the world's oceans, with marine ecosystems in Pacific, Atlantic and Indian oceans displaying the highest vulnerability. In addition, the socioeconomic value of coastal and marine resources can be severely affected by extreme ocean conditions with cascading effects in fisheries and marine-dependent communities. For example the MHW 2012 in the Atlantic resulted in altered fishing practices and harvest patterns that led to a collapse of important lobster fisheries, creating even tension between nations (Mills et al., 2013). A similar situation occurred during the MHW 2016 in the Gulf of Maine, except for this time adaptation strategies concerning MHWs somewhat reduced losses in fishing industries (Pershing et al., 2018). During the Pacific Blob commercial and recreational fisheries were closed leading to millions of dollars in losses (Cavole et al., 2016) similar to the oyster farm closure during the MHW 2015 in Tasmanian Sea. Given the increased MHW likelihood of occurrence in the future, identification of areas at high risk as well as adaptation planning, should be a priority both for the scientific community and the managers and stakeholders that need to collaborate with each other.

### 1.5.5 Subsurface Marine Heatwaves

Devastating MHW impacts are most of the times inflicted on marine ecosystems that live below the sea surface e.g. benthic, pelagic, demersal, (Schaeffer and Roughan, 2017). Particularly for sessile or less motile organisms that cannot move to colder water (Galli et al., 2017) (e.g. plankton (Mackas et al., 2012)), metabolic processes can be severely disturbed by prolonged and anomalous warming in the water column. One can understand that investigation of subsurface MHWs is equally (or even more) important to the identification of events at surface. But research on thermal anomalies at depth has been limited and only locally performed (or observed) so far. For example, Argo floats during the MHW 2011 in Australia, indicated open-ocean temperature anomalies constrained to the mixed layer depth, while in-situ measurements on the shelf revealed their extension down to 100m-200m (Pearce and Feng, 2013; Feng et al., 2013; Rose et al., 2012). During the MHW 2015/2016 in Tropical Australia glider data revealed a substantial warming throughout the water column. In fact, temperature anomalies in some regions were greater at (60 m) depth than near the surface (15m) (Benthuysen et al., 2018). During the MHW 2015 in Tasmania record warm temperature anomalies were measured intermittently, however, at 85m depth (Oliver et al., 2017). Meanwhile, a heat budget analysis of the upper ocean during the MHW 2014 in the San Fransisco bay indicated warm temperatures anomalies confined up to 100m close to the coast but reaching depths greater than 100m offshore. By contrast the warm anomalies at the California Current System which was affected by the same MHW that year were confined to the upper 50m (Zaba and Rudnick, 2016), similar to the temperature anomalies seen during the MHW 2012 in the North Atlantic (Chen et al., 2014). Recently, Jackson et al. (2018) demonstrated that coastal subsurface anomalous warming in the NE Pacific occurred with 1-year lag but persisted for more than 4 years after the surface 2013-2015 MHW was first observed. Duration of warm anomalies at depth can be

longer than at the surface, even re-emerging to the MLD in late winter (Deser et al., 2003).

Yet, it remains unknown how frequently and deep a MHW may penetrate in the open ocean. To our knowledge, to date, systematic analysis of subsurface events has been only performed by 2 regional studies. In the first one, coastal in-situ data off southeastern Australia were examined between 1953-2016 and showed regular warming throughout the water column, and a maximum MHW intensity just below the thermocline (Schaeffer and Roughan, 2017). In the 2nd study a high-resolution regional model was used to detect MHWs at surface and at depth and their characteristics around southeastern Tasmania between 1993-2015. An average MHW depth of 90m-185m was found for the shelf and deep regions and of 20m-50m in the nearshore regions for the period examined (Oliver et al., 2018b). In addition, the MHW depth exhibited significant positive trends that indicated a deepening of MHWs in the area. In general, when it comes to MHWs current research has mostly focused on SST temperature anomalies. when most studies so far have analyzed MHWs at the ocean surface. However, there is mounting evidence of a widespread warming in the world's deeper oceans under continued global warming (e.g. Johnson et al., 2007; Purkey and Johnson, 2010; Johnson et al., 2008). Therefore, estimation of extreme events at depth, will be front line research, especially when combined with physiological knowledge on thermotolerance thresholds of species in deeper layers (e.g. mesopelagic zone).

### 1.5.6 Marine Heatwaves in the Mediterranean Sea

While investigation of MHWs worldwide is advancing, to the best of our knowledge, it is currently lacking a dedicated and quantitative assessment of past and future MHWs in the Mediterranean Sea, despite being a "Hot Spot" for climate change. The significant increase projected for the annual mean and extreme basin SST, by the end of the 21st century, is also expected to reinforce extreme thermal events. This could have a devastating impact on Mediterranean marine ecosystems. In fact, according to Rivetti et al. (2014) and Coma et al. (2009) most of the mass mortalities of coastal benthic species documented in the basin, were related to positive thermal anomalies in the water column that occured during the summer. Although they have been reported with increased frequency since the early 1990s, their occurrence has been observed as early as the 1980s. An indicative list of them is given in Rivetti et al. (2014). As a consequence, MHW-related research in the Mediterranean Sea has been mostly focused on local ecological impacts without systematically assessing MHW occurrence.

For instance, several mass mortalities related to thermal anomalies have been identified regionally in the basin in 1994 (Marbà et al., 2015), 1999 (Perez et al., 2000; Cerrano et al., 2000; Garrabou et al., 2001; Harmelin, 2004; Linares et al., 2005; Crisci et al., 2011), 2003 (Schiaparelli et al., 2007; Diaz-Almela et al., 2007; Garrabou et al., 2009; Parravicini et al., 2010; Munari, 2011), 2006 (Kersting et al., 2013; Marba and Duarte, 2010; Bensoussan et al., 2010), 2008 (Huete-Stauffer et al., 2011; Cebrian et al., 2011), 2009 (Di Camillo et al., 2013; Rivetti et al., 2014; Pairaud et al., 2014) and 2010-2013 (Rodrigues et al., 2015). Most of

the documented episodes affected corraligenous species (e.g. gorgonians, sponges, seagrass *Posidonia oceanica* meadows) up to 50m deep (Rivetti et al., 2014), with a few occasions reaching 80m-160m (Arnoux et al., 1992; Rivoire, 1991; Vacelet, 1990). Recently, however, Oliver et al. (2018a) found increasing trends in MHW intensity, duration and frequency for the northeastern Mediterranean Sea between 1925-2016 (see Fig.1.22). In terms of driving mechanisms there have been only 2 studies examining the MHW of 2003 in selected regions and the MHW 2007.

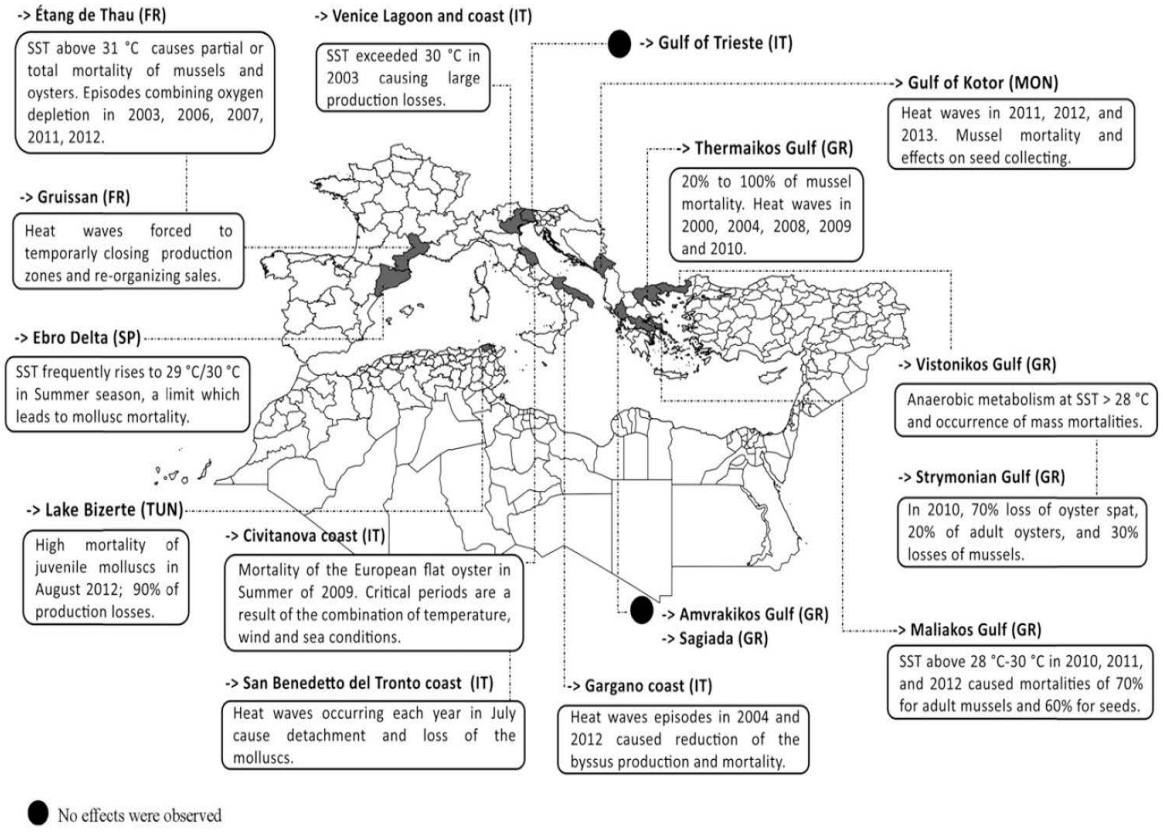


Figure 1.21: Summer Marine Heatwaves in the Mediterranean Sea during the last two decades, as they have been reported by bivalve mollusc producers from 12 coastal regions of 6 Mediterranean countries. The figure is adapted from Rodrigues et al. (2015) and is part of a questionnaire for the environmental threats encountered by the representatives of the aquaculture sector in the Mediterranean basin.

### MHW 2003

During the summer of 2003 an anomalous atmospheric high-pressure system persisted over the continental Europe, resulting amongst others to a strong overheating of the Western Mediterranean Sea (Grazzini and Viterbo, 2003). The MHW 2003 is, in fact, a well-known event and one of the first MHWs to be identified worldwide. It exhibited surface anomalies of 2-3 °C above climatological mean, which lasted for over a month. According to Olita et al. (2007) anomalously warm SST in the Straits of Sicily that summer was linked to a significant increase in air temperature, a decrease in windstress and reduction of all the upward heat flux components and mostly of the latent heat flux. Observations and model data suggested that the anoma-

lous heating was confined to the first 15m of the ocean and was associated with strong surface stratification and low mixing. In addition, model analysis indicated local currents reducing or increasing their intensity. Similar results were obtained for the Central Ligurian Sea, where the warming was found to occur within the first few meters below surface (Sparnocchia et al., 2006). This study, however, attributed the anomalous SST of that area mainly to a reduction of wind activity. Weaker than normal wind would limit vertical mixing resulting in an observed, highly stratified water column that would tend to "store" the heat in a thiner surface layer, increasing thus the SST. Finally, there are a few studies that investigated whether or not the anomalous Mediterranean SST during 2003 had an impact on the European heatwave of that summer (e.g. Feudale and Shukla, 2007, 2011; Tomassini and Elizalde, 2012). Although there is not a consensus between them on that subject a passive or small feedback of the MHW 2003 is implied on its counterpart heatwave in the atmosphere.

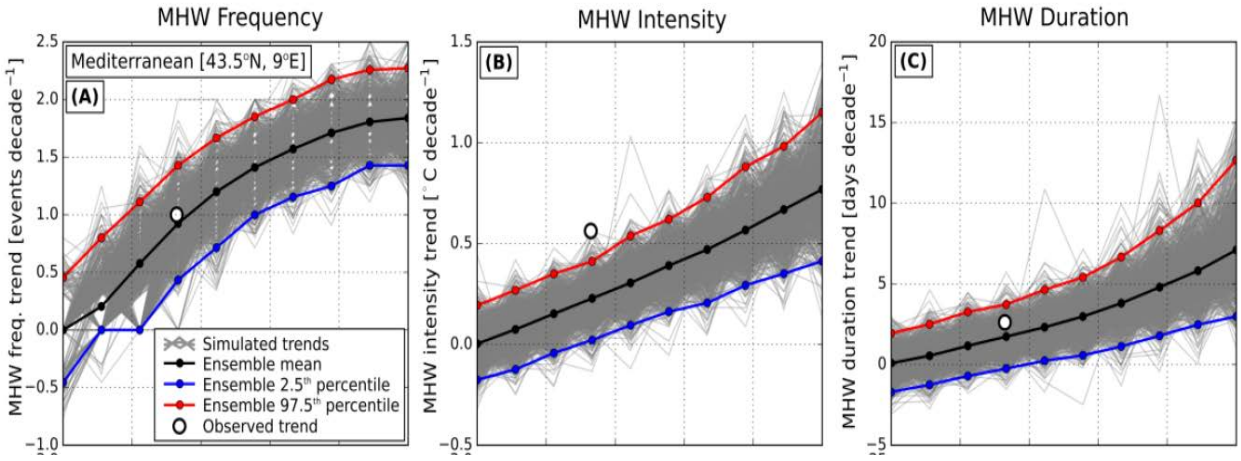


Figure 1.22: Comparison between observed and simulated MHW trends in the northeastern Mediterranean Sea. Linear trends in MHW (A) frequency, (B) duration and (C) intensity are shown as a funtion of linear trend in annual mean SST. Grey lines correspond to a 1000-member ensemble of simulated SSTs using a stochastic climate model and assuming only linear changes in the annual mean SST. The ensemble mean and 2.5th and 97.5th percentile are shown in black, blue and red lines respectively. White circle denotes the observed MHW property trends situated on the x axis, according to the observed trend in annual mean SST. Figure adapted from Oliver et al. (2018a).

### MHW 2007

An abrupt increase in SST of up to 5°C above climatology was observed in the Aegean Sea during and after the intense atmospheric heatwave of 21-30 June 2007 (Mavrakis and Tsiros, 2018). Similar to the 2003 event, a very stable anticyclonic atmospheric system prevailed at that time, which brought anomalously high air temperatures and extremely calm conditions. This combination could lead to a reduction in the upwelling processes. Further, the anomalously warm input of heat in the ocean was dominated by a higher than normal shortwave radiation and a decrease in latent and sensible heat flux.

### Future evolution of MHWs

In terms of the extreme Mediterranean SST evolution in the future, it has so far been examined in relation to the thermotolerance responses of certain species. For instance, Jordà et al. (2012) used an ensemble of models under the moderately optimistic scenario for GHG emissions A1B and suggested an increased seagrass mortality in the future around the Balearic islands due to a projected rise of the annual maximum SST by 2100 (see Fig.1.24). Similarly, Bensoussan et al. (2013) evaluated the thermal-stress related risk of mass mortality in benthic ecosystems for the 21st century, based on the average warming estimated between 2090-2099 and 2000-2010, under the pessimistic future warming scenario A2. They found an increase of temperature with time and a maximum temperature increase of 3°C higher than present-day values. Finally, Galli et al. (2017) showed an increase in MHW frequency, severity and depth extension assuming exceedances from species-specific thermotolerance thresholds under the high-emission IPCC RCP8.5 scenario (see Fig.1.23). To fill the knowledge gap on the future evolution of extreme Mediterranean Sea temperatures, the current work aims to analyze both the past and the future MHWs in the basin, based on a consistent framework that will be described in the following Chapters.

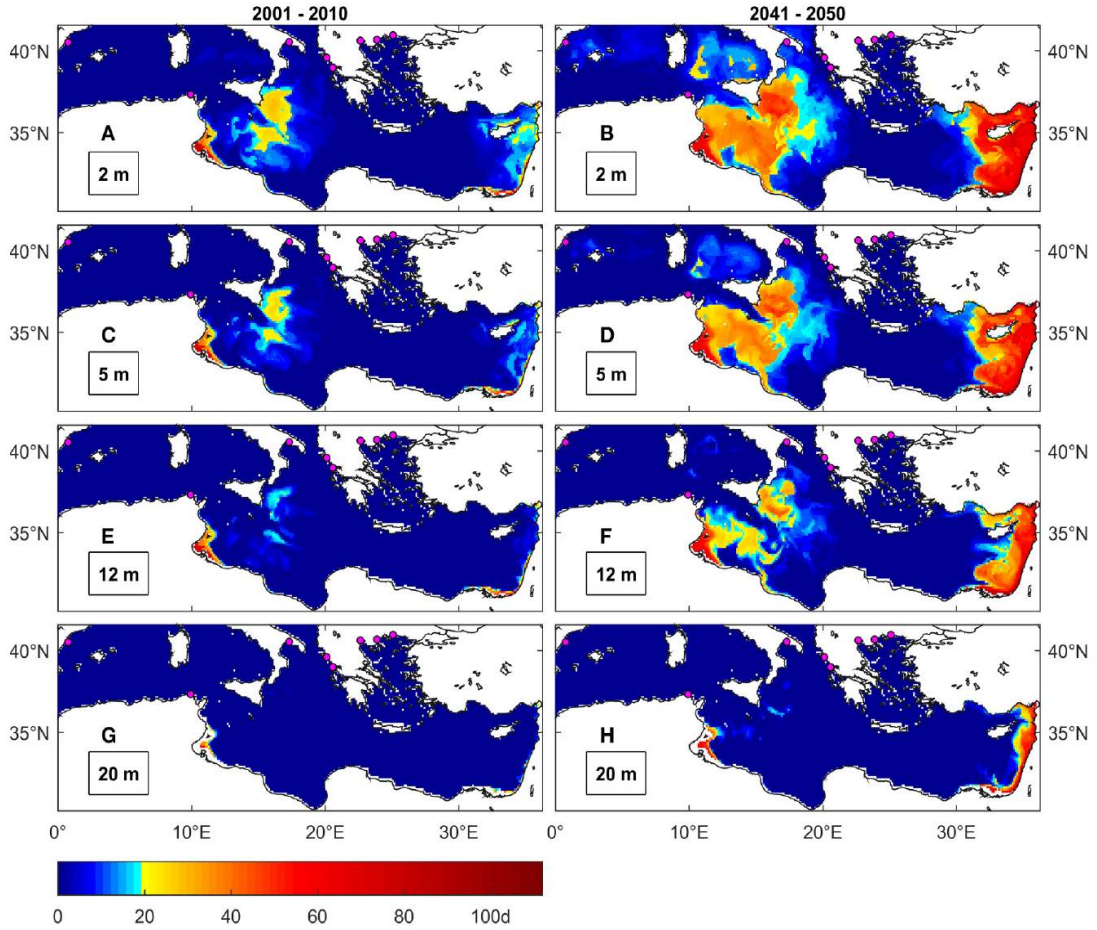


Figure 1.23: Maximum number of consecutive days above 30°C for 2001-2010 (A,C,E,G) and between 2041-2050 under RCP8.5 (B,D,F,H) at different depths. Colormap is scaled to highlight a speciedspecific 20-day lethal threshold. Magenta dots are locations of mussel farming facilities.

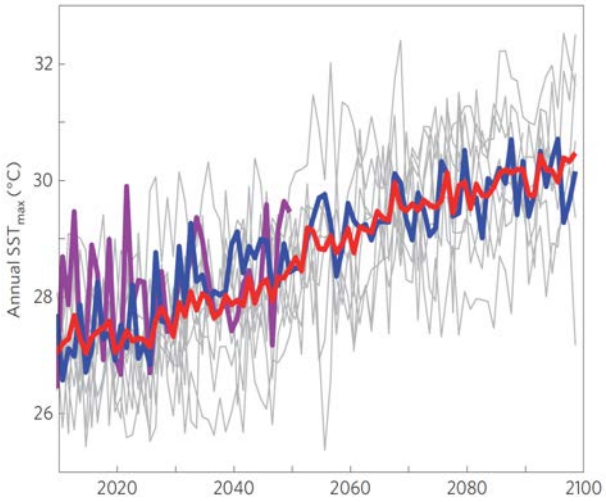


Figure 1.24: An example of 21st century projections of the annual maximum SST but averaged over the Balearic islands area. The output from 10 AOGCMs is indicated in grey, of an RCSM in purple and of an ocean-standalone RCM in blue, while the ensemble mean in red. Figure is produced by Jordà et al. (2012)

## 1.6 Conclusions

### 1.6.1 Motivation of the study

It is evident that under continuous warming, the global ocean becomes more and more susceptible to extreme thermal events. Taking into account the Mediterranean basin's sensitivity to climate changes a deeper examination is required on its vulnerability and response to MHWs. To this aim, the current thesis attempts to provide a robust assessment of summer Mediterranean MHW evolution in the past, present and future, by examining how does one define a MHW, when and where they occur and what are their driving factors.

In addition to that, the current understanding of the Mediterranean Sea's response to future climate change mostly relies on ensembles of low resolution GCMs (CMIP5) (e.g. Jordà et al., 2012; Mariotti et al., 2015) or on numerical experiments carried out with a single regional ocean model under different emission scenarios (Somot et al., 2006; Bensoussan et al., 2013; Adloff et al., 2015; Galli et al., 2017; Macias et al., 2018), without considering the various sources of uncertainty related to the choice of the socio-economic scenario (only 1 study, Adloff et al. (2015)), the choice of climate model and natural variability on the climate change impact studies on Mediterranean Sea ecosystems and maritime activities. Hence, another objective of this work is to address these uncertainties by considering different possible climate futures through a multi-model and multi-scenario set-up, using for the first time an ensemble of high-resolution, dedicated, coupled regional climate system models (RCSM).

In the context of global warming, estimation of MHW spatial patterns on the long term, might help identify regions with a physical predisposition to these extreme occurrences. That

will ensure the sustainability of marine-dependent communities such as those in the Mediterranean basin. The use of a consistent framework for the description of MHWs is, therefore, useful for monitoring and forecasting the events but also for the dissemination of information, which can lead to effective management strategies of their impacts. In the current PhD work, such a framework is developed for summer Mediterranean MHW events and is availablle for anyone interested in its applications.

In Chapter 1, an introduction to the Mediterranean region, its climate and the current knowledge on MHWs was presented. In Chapter 2, we describe the details of a consistent detection method for summer Mediterranean MHWs developed for the purposes of this thesis, along with an example of its implementation on the well-known MHW of 2003 in the basin. Chapter 3, (in the form of an article ready for submission) provides an overview of past summer Mediterranean MHW occurrences and their characteristics in the Mediterranean Sea between 1982-2017. There we also attempt to disentangle the driving mechanisms behind the MHW 2003, for the first time using atmospheric and ocean heat budgets computed online. In Chapter 4, the (accepted) article on the spatiotemporal evolution of summer Mediterranean MHWs throughout the 21st century is given. The latter deals with the uncertainty in the events's characteristics in the 21st century, using an ensemble of high-resolution coupled RCSMs and different GHG emission scenarios. Finally, conclusions and perspectives on the current work are provided, along with an Annex on the supplementary material of this work.

### 1.6.2 Scientific questions of the thesis

## 1. How do we define a summer Mediterranean MHW?

An algorithm is developed here to identify summer MHWs in the basin. However, can there be only one method to detect MHWs? How sensitive are the results to small perturbations of the definition? How much do MHW characteristics differ depending on the detection method applied on different datasets? These questions ultimately raise the issue of the objectivity in MHW identification method that we will attempt to tackle by undertaking sensitivity experiments and by making certain assumptions.

## 2. Is the current generation of Mediterranean Regional Climate System Models able to represent summer Mediterranean MHWs ?

As this study is based on coupled RCSM models, at each stage of the research we test their ability to represent Mediterranean Sea features and MHW characteristics. In that case, we are interested to see how well the models behave with respect to observations. What are their biases and how these may affect the results? Do the results between them agree? If not, why? If yes, how does the range of MHW characteristics change with the choice of the model?. We try to answer these question at each step of this work in order to present a clean and robust

representation of every issue targeted.

### 3. What are the main spatiotemporal characteristics of the past, summer Mediterranean MHWs?

Since most of the current knowledge on MHWs in the Mediterranean Sea is based on thermal-stress related mass mortalities of marine ecosystems, we would like to know what are the past events in the basin, based on a consistent MHW definition. What are their characteristics? Do they show any trends with time? What are their characteristics and trends at depth? Do subsurface events resemble surface MHWs? What is their spatial distribution?

### 4. What are the key driving mechanisms of the Mediterranean MHW 2003 ?

Identifying and characterising MHWs is only half of the story. As a relatively new research field, we are interested in understanding also why they occur. The main question here, therefore, is what dominated the spatiotemporal patterns of the MHW 2003 in the basin. Was it the ocean, the atmosphere or a combination of both? How do the driving factors change if the MHW is analyzed on a regional scale rather than at basin scale? Do the dominant atmospheric fluxes or oceanic processes change in that case? In other words, we question the importance of regional Mediterranean Sea features (e.g. currents) relative to the contribution from the atmospheric components.

### 5. How summer Mediterranean MHWs may evolve in the future ?

Although getting a first idea about the modulating factors of MHWs can help us forecasting their occurrence in the future, yet there is large uncertainty in those estimates. Do MHWs seem to increase following the projections of the Mediterranean Sea warming? If so, how much is this increase in the 21st century based on a multi-model and multi-scenario approach? How different will their characteristics be with respect to present-day and between different GHG emission scenario? A key question here is also the role of the mean and extreme Mediterranean SST future evolution in shaping the future MHW properties.

# Chapter 2

# Marine Heatwaves: Algorithm Description and Implementation

*"Be strong, whether you lose or win, I will be there with you, to fight for it, to believe it, with all my soul."*

Robogirl,Soundtrack

## Contents

In the previous Chapter we highlighted the need to study MHW occurrence in the Mediterranean Sea. Therefore, we first describe here the numerical and observational tools that we used to analyse events of the past in the basin (in Chapter 3). In particular, we evaluate the performance of two coupled RCSM models in hindcast mode in simulating mean and extreme Mediterranean Sea features between 1982-2017. We then present the details of a detection algorithm we developed for the identification of summer MHWs in the basin. An example of implementation is given for the 2003 MHW and its characteristics at local and large scale, as they are detected from the algorithm. We investigate how these properties may alter due to changes on the initial definition. The ability of the two coupled RCSM models to simulate MHWs in the past is afterwards examined in order to decide the most suitable for the study of past MHWs. The aim of this Chapter is mostly to guide the reader on a step-by-step analysis of the different aspects of the algorithm and its implementation on different datasets.

## 2.1 Model and Simulation

The numerical simulation used in this study is performed with the state-of-the-art, fully-coupled regional climate system model (RCSM) CNRM-RCSM6, one of the model contributing to the Med-CORDEX initiative (Ruti et al., 2016). CNRM center has been developing high-resolution and coupled regional climate models, often called Regional Climate System Models or Regional Earth System Models for more than 10 years to study the Mediterranean climate and sea (Somot et al., 2008; Dubois et al., 2012; Sevault et al., 2014) and to recently contribute to Med-CORDEX. The latest and 6th generation of such a model is called CNRM-RCSM6 (Voldoire et al., 2017) and is coupling at high-frequency and high resolution the various physical components of the Mediterranean regional climate system, that is to say the atmosphere, the aerosols, the land surface, the rivers and the ocean. All the components have been modified by increasing the spatial resolution and changing the physics since the last versions, CNRM-RCSM4 (Sevault et al., 2014) and CNRM-RCSM5 (Nabat et al., 2015).

The atmosphere is represented by the ALADIN-Climate model in its version 6.3 (Daniel et al., 2018) with 91 vertical levels and a spatial resolution of 12 km. The physical package used in this version is similar to the physical package of the CNRM-CM6 GCM used to perform the on-going CMIP6 experiments with some small modifications and tuning related to a higher resolution. The model domain is by far larger than the official Med-CORDEX domain in order to include most of the aerosol regional sources of Mediterranean interest (saharan dust, Atlantic sea salt, European and Middle-East pollution plumes). The natural and anthropogenic aerosols are represented by the lastest version of the TACTIC module that now includes the interactive representation of the dust, sea salt, volcanic, black carbon, organic carbon, sulfate and nitrate aerosols at the same resolution as for ALADIN-Climate (Nabat et al. (2015),Drugé et al (*in review*)). The land surface water and energy cycles are simulated by the SURFEX/ISBA model in its version 8 (Decharme et al. (subm)). It representes the natural and anthropogenized surfaces including a simple modelling of the deep hydrology and

of the lakes (SURFEX/FLAKE,Le Moigne et al. (2016). The land surface in one grid-cell is tiled into 12 patches in order to account for the variety of soil and vegetation behavior within a grid point. SURFEX has the same spatial resolution as ALADIN-Climate. The river network and discharges up to the ocean are represented at a 50-km resolution, by the CTRIP model (Decharme et al. (subm)) using the total runoff computed by SURFEX. Note that CTRIP and SURFEX are two-way coupled in order to represent the feedback of the aquifers and floodplains on the soil moisture and, therefore, the atmosphere.

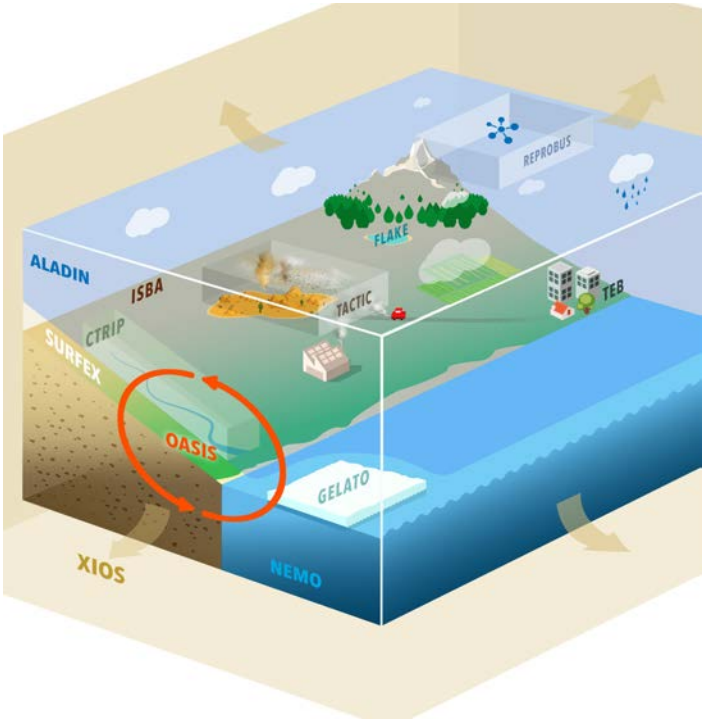


Figure 2.1: Schematic of the components of the CNRM-RCSM6 model. Credits: CNRM

Finally, the ocean component is represented by NEMOMED12 regional configuration (Beuvier et al., 2012; Hamon et al., 2016; Waldman et al., 2017) of the NEMO OGCM in its version 3.4 (Madec, 2008). NEMOMED12 has a spatial resolution varying between 6 and 7 km within the Mediterranean Sea and 75 vertical levels between 1m at the surface and 130 m at the bottom. The model domain covers the whole Mediterranean Sea excluding the Black Sea plus a so called buffer zone in the near-Atlantic Ocean. The Black Sea is therefore parameterized as a freshwater flux for the Aegean Sea by combining the total river discharges of its drainage area and the evaporation minus precipitation budget over the sea. The coupling is done through the OASIS-MCT coupler (Craig et al., 2017) and the coupling strategy follows Voldoire et al. (2017) in particular with a 1-hour coupling frequency between the various components. The ocean-atmosphere coupling is applied over the Mediterranean Sea.

At its lateral and non-coupled ocean surface boundarie outside the NEMOMED12 domain, CNRM-RCSM6 is driven by reanalysis in the so-called hindcast or evaluation mode. We use ERA-Interim (Berrisford et al., 2009) to drive the atmosphere and non-coupled ocean surfaces

and the ORAS4 (Balmaseda et al., 2013a) for the Atlantic boundary conditions (temperature, salinity, sea surface height). Note that the spectral nudging technique is applied in ALADIN-Climate (Colin et al., 2010) to better constrain the large-scale and synoptic atmospheric flow of the regional model. Therefore the large-scale day-to-day chronology of the atmosphere is close to the ERA-Interim one. The CNRM-RCSM6 hindcast simulation is continuous from 1982 to 2017 after a 10-year fully coupled spin-up, coming itself after a 7-year ocean spin-up and a 78-year CTRIP spin-up.

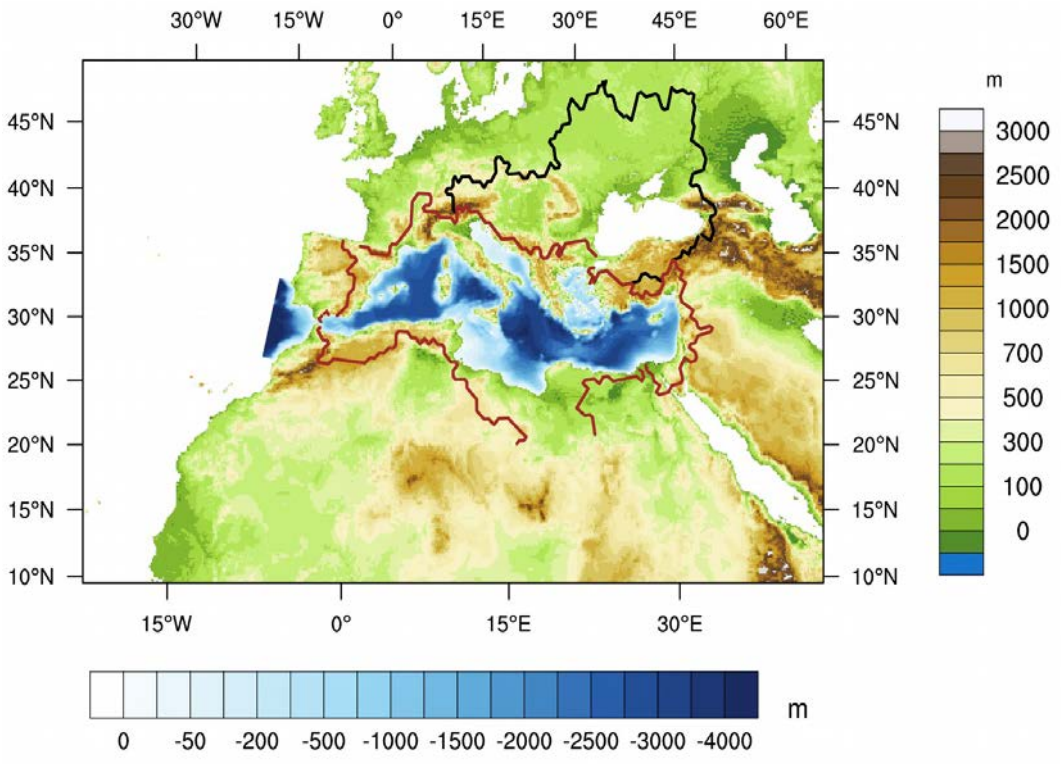


Figure 2.2: The extended Mediterranean domain covered by the CNRM-RCSM6 model. Topography, bathymetry and land-sea mask are illustrated, while the ocean and Black Sea (which are not included in the NEMOMED12) are in white. Credits:Nabat Pierre *personal communication.*

## 2.2 Choosing the RCSM model

Apart from the hindcast simulation of CNRM-RCSM6 (latest version), the same reanalysis-driven simulation of CNRM-RCSM4 was also available for this PhD work. In order to decide the most suitable model for studying summer Mediterranean MHWs during 1982-2017 we compared the performance of both. Therefore, a short description of CNRM-RCSM4 is given here from Sevault et al. (2014) for comparison purposes.

The CNRM-RCSM4 is a previous version of CNRM-RCSM6 model, in terms of model characteristics and capabilities, and it has also contributed in the Med-CORDEX initiative with hindcast but also scenario runs (see Chapter 4). It is a fully-coupled configuration with 1/8 °resolution for the ocean that does not resolve, however, mesoscale processes. It comprises the 50km-resolution and 31 vertical-levels atmospheric regional model ALADIN-Climate in

its version 5 (Herrmann et al., 2011; Colin et al., 2010), the land-surface ISBA model, a 0.5 °resolution river model (TRIP) but its oceanic component is based on NEMOMED8 (9-12km horizontal, 43 vertical levels) (Madec, 2008; J. Beuvier and Somot, 2010) this time. The OASIS coupler is responsible for the communication between the different components on a daily scale. The domain includes the Mediterranean area with a small part of the Atlantic as a buffer zone, the Black Sea budgets are parametrized and the river runoffs (except for Nile) are fully coupled (Fig.2.3). ERA-Interim Reanalysis is used as a lateral boundary condition for the atmosphere model and the non-coupled conditions. The simulation covers the 1980-2012 after a 21-year spin up of the coupled model and a 5-year ocean spin-up.

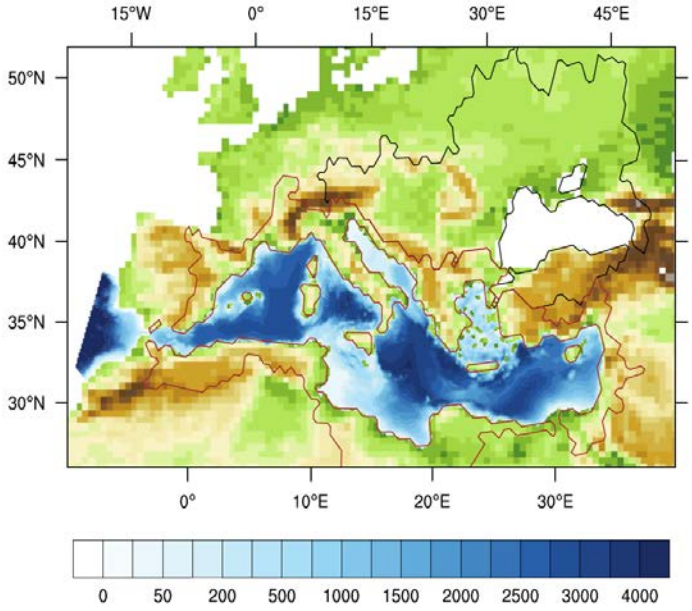


Figure 2.3: Land-sea mask orography (ALADIN-Climate) and NEMOMED8 bathymetry for the MED-CORDEX domain of CNRM-RCSM4. Drainage area of Black and Mediterranean Sea are contoured in black and red respectively. Figure from Sevault et al. (2014).

| RCSM name | CNRM-RCSM4 | CNRM-RCSM6 |
|---|---|---|
| Model Characteristics | | |
| Era Interim | 1980-2017 | 1980-2012 |
| Med.Sea Model | NEMOMED8 | NEMOMED12 |
| Ocean Res. | 9-12 km | 6-8 km |
| Num. of z-Levels (Ocean) | 43 | 75 |
| SST (1st layer depth) | 6m | 1m |
| Timestep (Ocean) | 1200 sec | 12 min |
| Atmosphere Model | ALADIN-Climate | ALADIN-Climate |
| Atmosphere Res. | 50 km | 12 km |
| Coupling Frequency | Daily | 6 hours |

Table 2.1: Differences between the characteristics of CNRM-RCSM4 and CNRM-RCSM6 models.

The differences between the 2 models are massive. CNRM-RCSM6 is a result of a 10-year development and any SST change cannot be directly attributed to a specific model property.

However, a few key elements to underline for this latest version relative to CNRM-RCSM4 is that it features a higher atmospheric and ocean resolution along with a higher coupling frequency, an interactive (versus a stable) aerosol scheme and changes in physics which resulted in better-represented heat fluxes than before.

## 2.3 Model Evaluation

At first we compared the performance of both models on the yearly mean SST ($\overline{SST}$) over the period 1982-2012 (see Fig.2.4). Each member was validated against the satellite product described in Chapter 2 (Section 2.2), which was interpolated on the respective grid each time. Figure 2.4 reveals a well-known northwest-southeast (NW-SE) gradient of Mediterranean Sea SST, with Levantine basin emerging as the warmest region (20-22°C) in all 4 datasets. By contrast, NW Mediterranean and the Aegean Sea yield a $\overline{SST}$ of around 16-18°C. Compared to CNRM-RCSM4, however, CNRM-RCSM6 appears to be somewhat warmer in the warmest regions (e.g. Levantine Basin). In general, the latter configuration presents an average warm bias (~0.35°C) relative to the observation dataset, whereas CNRM-RCSM4 shows an average cold bias of ~0.46°C (see Table.2.2). In absolute values though, the bias of CNRM-RCSM6 is slightly improved with respect to observations compared to that of CNRM-RCSM4. Nevertheless, both models seem to represent relatively well the observed patterns of $\overline{SST}$ of the period. The corresponding pattern correlation coefficients were all $\geq 0.80$ (see Table.2.3).

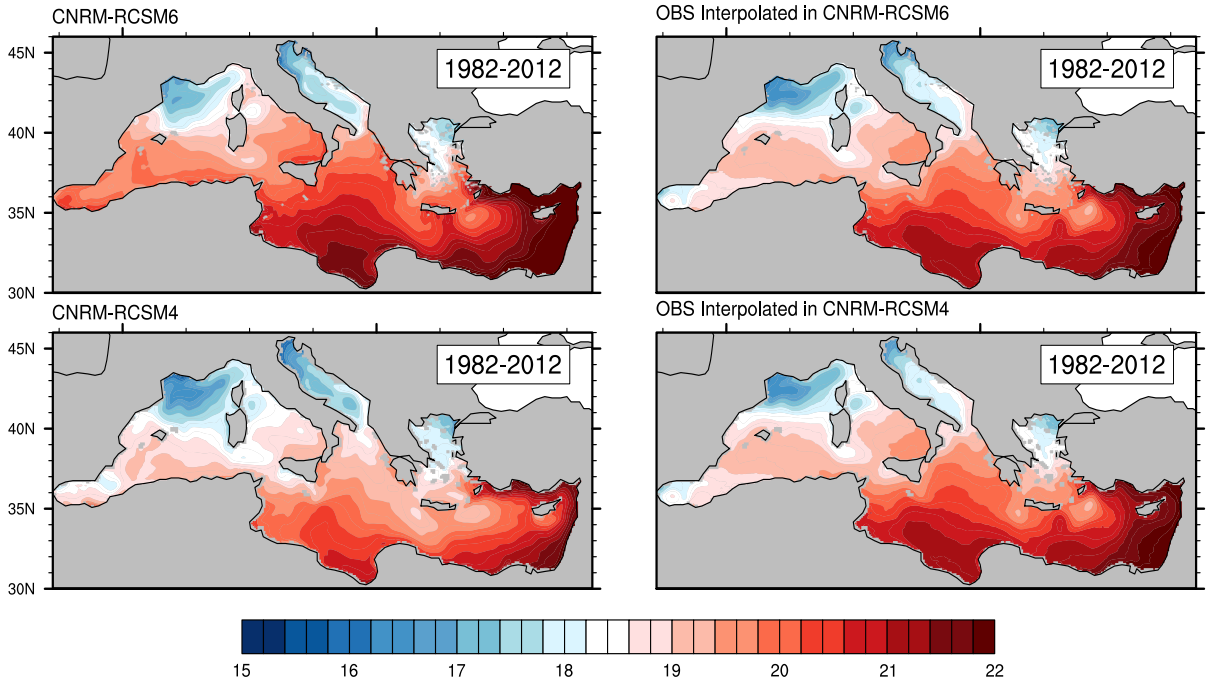


Figure 2.4: Average of yearly mean $\overline{SST}$ (°C) during 1982-2012 for CNRM-RCSM6 and CNRM-RCSM4 in hindcast mode and satellite data interpolated at each respective grid.

The equivalent maps of average $SST_{99Q}$ over the period indicated a complex spatial distribution of extreme temperatures in the basin (see Fig.2.5). In particular, in all 4 datasets, the Levantine Basin and Ionian Sea showed the most extreme SSTs (27-30°C). Gulf of Lion, the

Alboran Sea, Adriatic and Aegean Sea, on the other hand, demonstrated the lowest extreme values (22-25°C). The cold bias of CNRM-RCSM4 with respect to observations becomes more evident in the NW Mediterranean, Adriatic and Levantine Basin. Its basin-average bias is 1.1 °C (see Table.2.2). In CNRM-RCSM6, however, the bias, compared to CNRM-RCSM4, seems improved around the Adriatic, Ionian and Tyrrhenian Sea, which are now closer to the observations. Yet, extreme SSTs in CNRM-RCSM6 remain overestimated due to its basin-mean $SST_{99Q}$ warm bias (~0.71°C). It appears more pronounced though in the Alboran, Ionian Sea and in the Gulf of Lion.

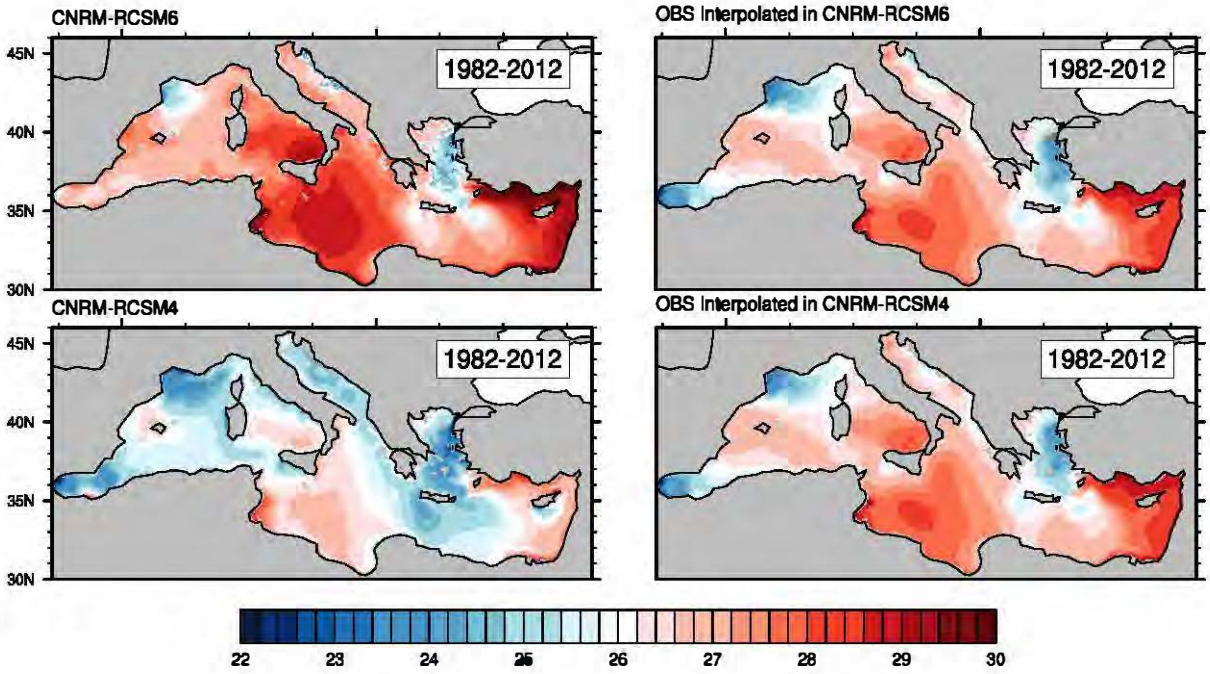


Figure 2.5: As in Fig.2.4 but for $SST_{99Q}$.

Despite that, patterns of $SST_{99Q}$ are better correlated with the observations (pattern correlation coefficient $\geq$ 0.96) compared to the $\overline{SST}$ (see Table2.3). Although CNRM-RCSM6 has a warm bias it has slightly improved the representation of mean Mediterranean Sea SST relative to CNRM-RCSM4. For the $SST_{99Q}$, however, the pattern correlations has slightly decreased compared to CNRM-RCSM4.

The improved performance of CNRM-RCSM6 becomes more evident from the corresponding area-average timeseries of the annual mean SST $\overline{SST}$ and $SST_{99Q}$ over 1982-2012. Compared to CNRM-RCSM4, simulated mean and extreme SST variability appears closer to the observed variability in CNRM-RCSM6 (Fig.2.6). Correlation coefficient between each set of CNRM-RCSM6 timeseries is indeed higher than for CNRM-RCSM4 (Table.2.3). In terms of the simulated trends, however, both configurations appear to underestimate the mean and extreme observed trends. Only the $SST_{99Q}$ trend in CNRM-RCSM6 seems improved (~0.03°C/year) yet, underestimating the trend of the observations (~0.05°C/year). The trend of $\overline{SST}$ in the meantime has remained the same in both models (~0.02°C/year) (see Table.2.2).

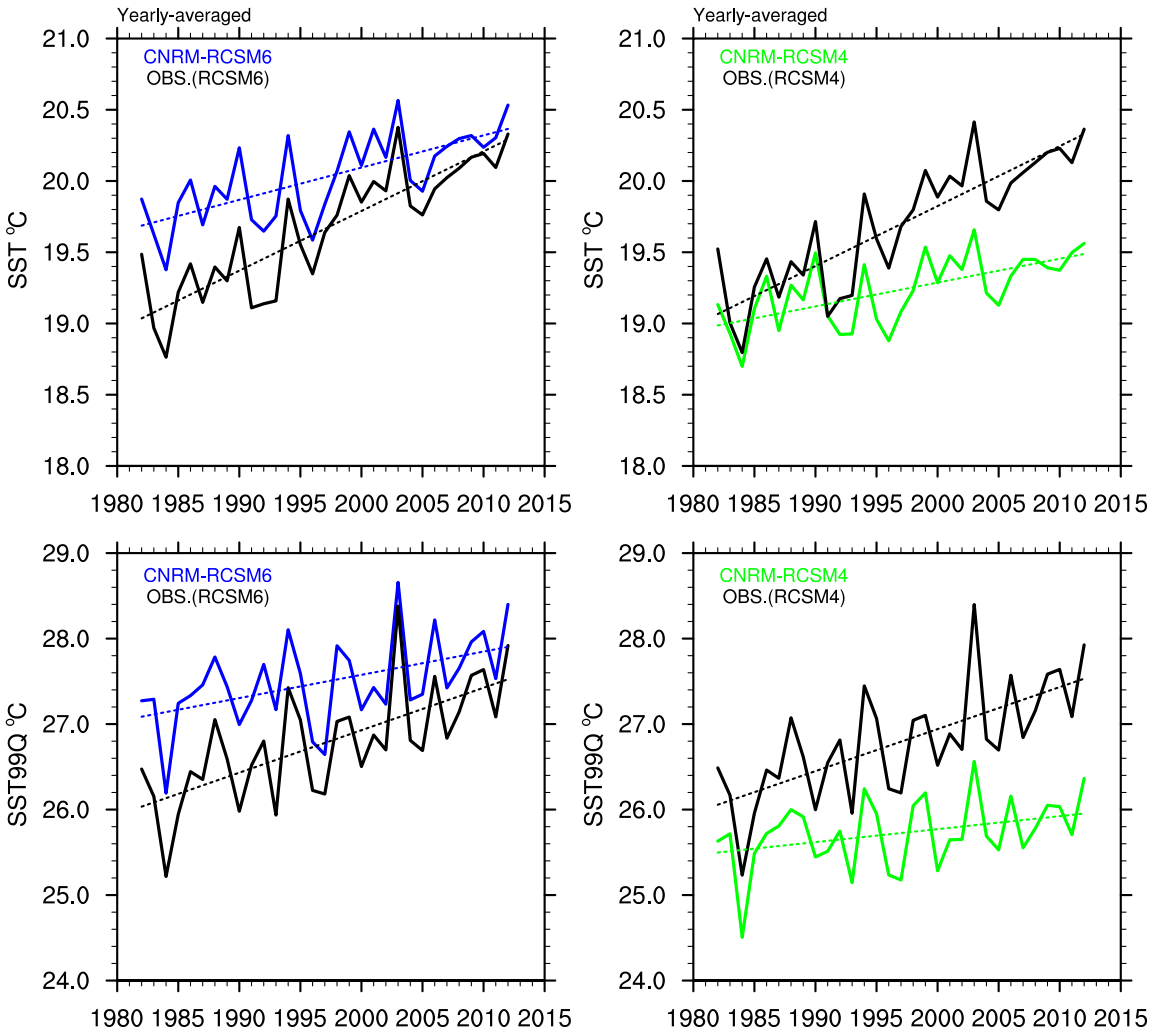


Figure 2.6: Yearly $SST_{99Q}$ (°C) during 1982-2012 for CNRM-RCSM6 and CNRM-RCSM4 in hindcast mode. Shown here is also average $SST_{99Q}$ for the same period from the satellite dataset interpolated at each respective grid.

| | $\overline{SST}$ | | $SST_{99Q}$ | |
|---|---|---|---|---|
| | Trends | Basin-Mean | Trends | Basin-Mean |
| CNRM-RCSM6 | 02.26*$10^{-2}$ | 19.92 | 02.72*$10^{-2}$ | 27.45 |
| CNRM-RCSM4 | 01.67*$10^{-2}$ | 19.14 | 01.52*$10^{-2}$ | 25.69 |
| OBS(RCSM4) | 04.20*$10^{-2}$ | 19.60 | 04.97*$10^{-2}$ | 26.75 |
| OBS(RCSM6) | 04.19*$10^{-2}$ | 19.57 | 04.91*$10^{-2}$ | 26.74 |

Table 2.2: Basin-mean, yearly-averaged ($\overline{SST}$) and extreme ($SST_{99Q}$) temperatures (°C) and their trends (°C/year) over the period 1982-2012. Values are shown respectively for CNRM-RCSM6, CNRM-RCSM4 and a satellite dataset interpolated at each different grid every time.

We note here that satellite SST refers to (night-time temperatures in) the first few mm of the ocean, whereas the models' SST is the average temperatures of the first few meters of the

mixed layer depth. Consequently, differences between them may naturally emerge. Particularly for CNRM-RCSM6, uncertainties from the aerosol scheme or missing forcing in the boundaries may be possible explanations for the underestimation of the observed trend. Nevertheless, as it was shown in Chapter 2, Section 2.4 CNRM-RCSM6 was able to capture well the characteristics of the MHW of 2003.

| Timeseries | | | Pattern Correlation | |
|---|---|---|---|---|
| $\overline{SST}$ | | | $\overline{SST}$ | |
| | CNRM-RCSM6 | CNRM-RCSM4 | CNRM-RCSM6 | CNRM-RCSM4 |
| OBS | 0.93 | 0.90 | 0.87 | 0.88 |
| SST99Q | | | SST99Q | |
| OBS | 0.93 | 0.88 | 0.96 | 0.97 |

Table 2.3: Correlation Coefficient between CNRM-RCSM6, CNRM-RCSM4 and observations. With OBS is denoted the respective interpolated observations for each model. Pattern correlations are performed, using the Pearson product-moment coefficient of linear correlation between two variables. For the timeseries, the Pearson sample linear cross-correlation at lag 0 only was used. Correlations were performed with ncl software.

## 2.4 Observational Datasets

In order to evaluate the model's ability to represent MHWs we perform comparisons with observational data. First, a satellite dataset (SATELLITE) provided by the Copernicus Marine Service (CMEMS) and CNR - ISAC ROME is employed. More specifically, it is the Mediterranean Sea high-resolution L4 dataset providing daily, reprocessed SSTs on a 0.04 °grid, an interpolation of remotely sensed SSTs from the Advanced Very High Resolution Radiometer (AVHRR) Pathfinder Version 5.2 (PFV52) onto a regular grid (Pisano et al., 2016). They are obtained over a 30-year period of January 1982 to December 2012. At this chapter, however, the dataset will be also used to validate the MHW detection algorithm that was developed in the current thesis and will be analyzed in the next section. Prior to performing any calculations and in order to compare the results between the model and observations, we first interpolated the dataset to the NEMOMED12 grid, by implementing the nearest neighbour method.

*In situ* data (BUOY) from the AZUR (7.87 °E, 43.32°N) and LION (4.68°E, 42.06°N) buoys from Meteo France are also used here (Caniaux et al., 2017; Waldman et al., 2017). They provide long-term (2000-2010) measurements of various parameters, amongst which is daily SST at the location of the buoys. This information will be used for the validation of the MHW detection algorithm of the following section. Through the course of this PhD we also intended to gather more daily, in situ data (for the open sea as well). However, we did not succeed, due to the scarce availability of long-term observations of that kind.

## 2.5 Definition of Summer Mediterranean MHWs

### 2.5.1 Objectives

In the previous Chapter we have shown that the majority of past extreme thermal events in the Mediterranean Sea have been detected based on exceedances from species-specific thermotolerance thresholds. The relatively recent definition by Hobday et al. (2016), however, has attempted to unify the identification of individual cases worldwide, with a definition based on an hierarchy of metrics. Inspired by this approach, we developed a quantitative detection method for summer Mediterranean MHWs. In this section, the reader will be introduced to the content of the algorithm developed for this purpose, while sensitivity to changes in the initial definition will be also addressed. The relatively different approach we adopted relative to, but based on, Hobday et al. (2016) targeted the following MHW characteristics, justifying the subjective choices we made on the algorithm setting:

- *Long-lasting events.* Following Hobday et al. (2016) minimum MHW duration is to 5 days or more on a given grid point. In addition, most of the summer events observed in the basin in the past had long durations with severe impacts on marine ecosystems (see Chapter 1).
- *Large-scale events.* MHWs with large spatial coverage are potentially more harmful for marine ecosystems as well due to their size. Additionaly, in order to identify events that were relatively rare, but not that rare during the last part of the 20th century, a minimum of 20% of the basin was set as the minimum MHW coverage. However, no continuity is assumed between grid points for practical reasons (see Section 2.5 for more details.)
- *Occurrence during the summer.* We choose the 99th percentile of SST as the baseline/threshold temperatures (see following sections for more details). This choice was dictated by the fact that most of the mass mortality events in the Mediterranean Sea have been observed during the summer season. However, we do not define "summer season" as a specific set of months, rather as the period of the year where temperatures exceed the 99th percentile of SST. This is a major difference with Hobday et al. (2016).
- *Daily Temperatures.* A fundamental aspect of this methodology is that it is designed for daily temperature fields. In that case, lower temporal resolution datasets are not suitable for implementing the algorithm.

### 2.5.2 Designing the Algorithm

The qualitative definition proposed by Hobday et al. (2016) prescribes a MHW to be a "discrete, prolonged, anomalously warm water event at a particular location". The reference period in that case was defined over 30 years (climatology of the yearly 90th percentile of SST), considering

the long timescales of the variability of the ocean and its large-scale climate drivers. As a baseline in our method we also used a 30-year climatology but from the yearly 99th percentile of daily SST computed at each grid point separately (e.g.Fig.2.8). Therefore, a constant in time but variable in space threshold map, named here as $SST_{99Q}$, was created separately for each dataset examined. For example, the 1982-2012 period was selected as a reference for the observed (satellite) MHWs of the same period. Depending on the availability of the data, however, reference period might be different, like in the case of buoy data (see Section 2.3.4), where 10-years were considered. In fact, the entire algorithm is based on the identification of grid points, whose daily SST deviation is equal to or positive relative to their local $SST_{99Q}$, constituting a warm day. By performing a series of tests on daily SST data the algorithm calculates the number of warm days (k) at each grid point separately, that will form the final spatiotemporal extent of the MHW.

A more qualitative illustration of the detection process is displayed in the flow chart of Fig.2.7. On a given grid point, the algorithm first identifies whether its daily SST is above, equal or below its local threshold. Then, once a warm day is found (light blue rhombus) it is registered as the start or as an additional day to an event that has already started, depending on whether a warm day has preceeded (k>0) or not (k=0), respectively. At a next step, the algorithm checks the state of the 5 following days. In particular, if a warm day is followed by 5 consecutive days with SST $<SST_{99Q}$, it is defined as the last day of the event. Then, the total number of warm days is counted and the algorithm stores as MHWs locally, those events with duration $\geq 5$. Otherwise (k<5), the event is entirely discarded (k=0) as a non-MHW. This is a subjective choice linked to the minimum duration of each event, that was set to 5 days in order to be classified as a MHW, according to Hobday et al. (2016). Likewise, it would take 5 days of below-threshold SSTs to indicate that an extreme occurrence has faded.

### 2.5.3 Gap Days

On the other hand, whenever the condition SST $<SST_{99Q}$ is not valid for each of the 5 following days and there is at least one day with SST $\geq SST_{99Q}$, it is an indication that gap (or cool) days with temperatures close to threshold values might occur. In that case, the algorithm is redirected to search for them (light red rhombus part of the flow chart) before the total number of warm days is counted. Their occurrence is a result of day-to-day SST fluctuations and their definition in our proposed method differs from that of Hobday et al. (2016). More specifically, gaps of up to 4 consecutive days or less are allowed (considered as warm days) inside a local MHW identified from the previous step (k$\geq$ 5), only when both the preceeding and following 6-day mean SST of a gap day (including the gap day in each mean) are above the local $SST_{99Q}$. For the cool day "neighbourhood" this would represent a tendency to remain above threshold, even though the SST of that particular cool day might be below limit. This also reflects the fact that minor SST deviations from the threshold cannot impact the overall warm conditions of a MHW and probably would not offer an "essential" relief to organisms or even to the less mobile

and maybe less tolerant species, once a MHW has started. By contrast, a below-threshold drop in either of the 6-day SST averages would not allow any cool day to merge with a MHW, in the same way that a sequence of five cool days or more would interrupt entirely an event. In that case, the algorithm finds when was the last time that a day was identified with SST $\geq SST_{99Q}$ and stores that as the last day of the local MHW. The total number of warm days is then counted and stored, as before.

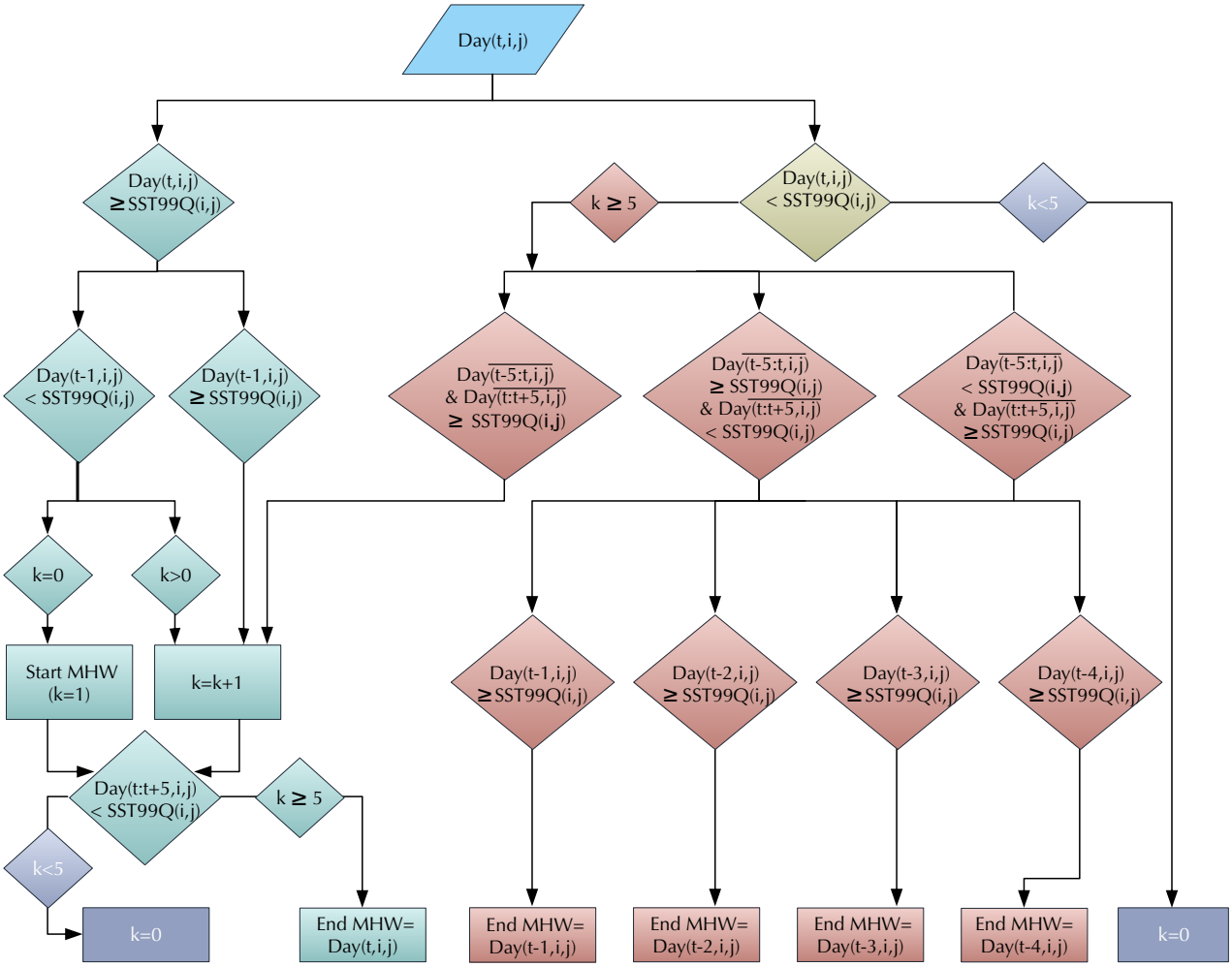


Figure 2.7: Flow chart for the grid-based detection of a summer Mediterranean MHW. Light blue rhombus refers to the detection of the starting, warm and ending day of an event, while light red signifies the part of the program where gap days are identified and treated. Dark blue rhombus represent the condition under which an event is interrupted entirely without counted as a MHW. Black line denotes the average SST over the days it comprises.

We make the assumption that a declined 6-day SST average is an indication for a considerable drop in daily SST - and not just a fluctuation of temperature, which can be caused by an event with a potential to destroy for good a MHW (e.g. wind, currents). We believe that the statistical sensitivity of the mean to outliers is appropriate to discern cold disruptions to the MHW from transitory fluctuations of SST and we chose an 11-day window around each gap day, since the minimum duration of a MHW was set to 5 days.

### 2.5.4 Example of a local MHW detection

A schematic of how a MHW looks on a random point is given in Fig.2.8. The event has a well-defined start ($t_s$) and end ($t_e$) times, whereby the daily SST is above threhold. The threshold value for each location is based on the local, 30-year climatology of the 99th percentile of daily SST and is well above the daily (30-year) climatology of that point. The MHW is characterised by a mean intensity (open circle,Imean) that is computed over the total number of days included. Imean represents the mean temperature anomaly relative to the threshold. Similarly, Icum is the sum of daily intensities and Imax the maximum intensity during the event. The gap days in that particular point were included in the MHW as they satisfied the conditions described previously.

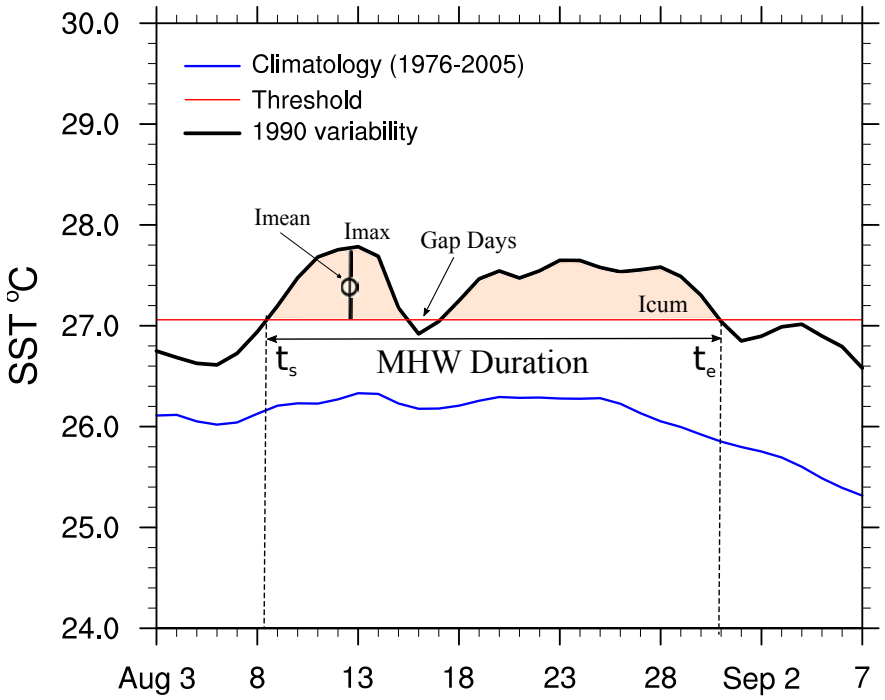


Figure 2.8: Schematic of a MHW based on Hobday et al. (2016). The black line represents daily SST variations of one grid point in a random year, red line is the local threshold ($SST_{99Q}$) and blue line is the daily 30-year climatology for this point. Also shown here also are the starting day ($t_s$) and ending day ($t_e$) above $SST_{99Q}$, gap days and the different measures of daily intensity (see text for more details). MHW metrics refer to the total event duration.

An example of implementation of the algorithm is given at the AZUR and LION buoys (Fig 2.9). In order to identify the MHW(s) in each location during 2003, the detection method was applied on the buoy data but also on daily SST data of 2003 from the CNRM-RCSM6 model and the daily satellite product. The reference period for the latter two was the 1982-2012, whereas the *in situ* data were limited to years between 2000-2012 (Azur buoy) and 2000-2010 (Lion buoy), including also days with no data. Therefore, the climatology of each local $SST_{99Q}$ was computed over the available period each time, while days without data were treated as cases with below-threshold SSTs. At this point, the advantage of a percentile-based threshold relative to an absolute-temperature limit, stands in that no assumption is made for the temperature

distribution, which might differ regionally. The same may also apply for *in situ* datasets that contain missing data, as long as they are not in large numbers. For example, a high-percentile threshold (like the 99th quantile) may not be affected by missing data, unless these occur during the summer months, as it is partly the case in Lion buoy. Absent data were not large in number and days with logged SST intervened between missing days, so the algorithm was able to "capture" the overal *in situ* temperature trend and stop the MHW within the timeframe identified from the other 2 datasets, in the month of August.

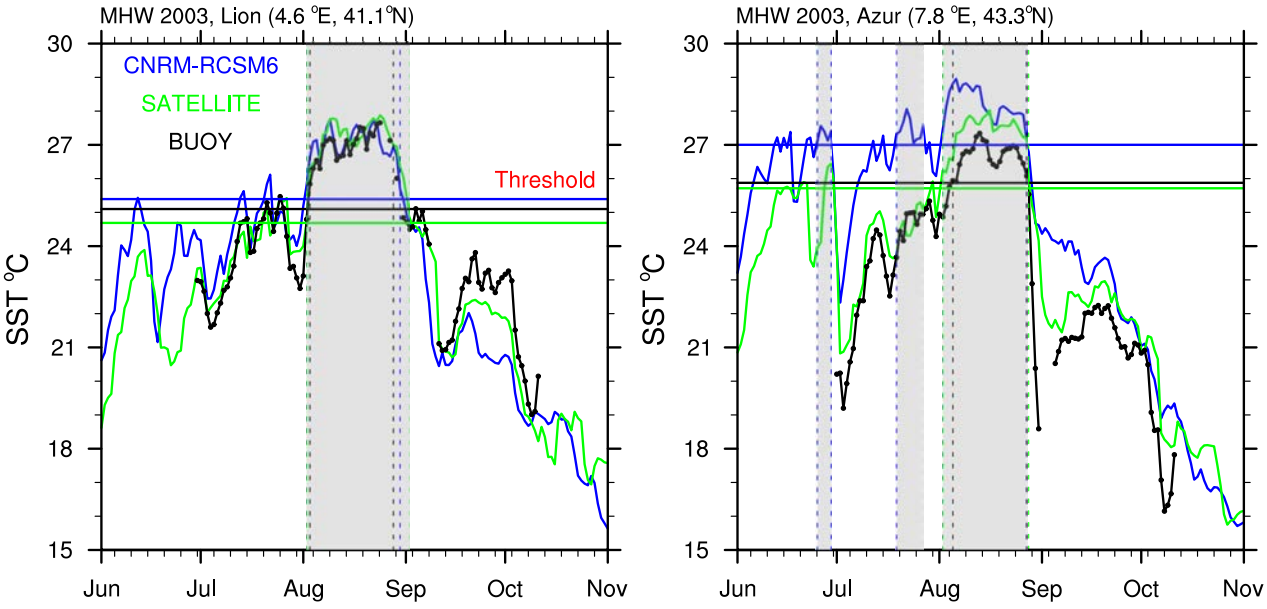


Figure 2.9: Example of the MHW(s) detected during 2003 at 2 specific, NW-Mediterranean grid points, by applying the algorithm on CNRM-RCSM6 (blue), satellite (green) and *in situ* (black dotted) data correspondingly. For each dataset, daily SST variability is displayed along with the corresponding $SST_{99Q}$ threshold line. The starting and ending day identified by each dataset is also shown within the grey area enclosed by the corresponding, in color, dashed vertical lines.

Nevertheless, the spatial and temporal resolution and the quality of the dataset examined may yield substantially different MHW characteristics, as already pointed out by Hobday et al. (2016). From Fig 2.9, it is evident that all datasets have a similar profile of temperature evolution during the summer, therefore, the MHW in Lion buoy location has been identified with similar starting and ending days, duration and even with preceeding heat spikes (not accounted as MHWs) in all 3 of them. Yet, day-to-day variability and $SST_{99Q}$ threshold clearly differs, which would result in different MHW intensities and perhaps number of events detected at each dataset. This becomes more apparent at the Azur location (Fig 2.9, right), where 3 MHWs were detected from the CNRM-RCSM6 data but only one event was registered in the other 2 datasets. This could also be a result of the warm bias of the model for June-July 2003, which is only partly compensated by the high percentile threshold. In turn, individual thresholds, depend on the choice of the reference period. It is obvious that a different number and window of years considered for the baseline period can provide a different climatology of extreme temperatures that will serve as threshold (e.g. here *in situ* data reference period is

10-12 years, while model and satellite data is 30 years). Besides being dataset-dependent, a percentile threshold at the same time removes the effect of the related biases.

### 2.5.5 Spatial aggregation

The process described above is repeated for each grid point separately, yielding every day a map of points "activated" in a MHW state. The daily MHW area, therefore, is determined by their aggregation, based on their spatial coverage and not on the contiguousness of grid cells. The option of space continuity was abandoned due to the patchy distribution of MHW points observed in many events (e.g. Fig.2.10). This practically means that the algorithm is not able to distinguish whether two areas with a simultaneous "aggregation" of MHW points, which are not contiguous and show no specific pattern (patchy), are characterised by the same or by two different events. This strongly relies on how a MHW is defined in the first place, and what are the criteria that each time determine what separates one event from another. An example of an event is given in Fig. 2.10 with the preliminary daily mean intensity (SST difference with respect to the threshold) during the MHW of 2003 illustrated between 8 July - 6 September in selected days. The final MHW, however, was registered by the algorithm between 18 July - 3 September, where its spatial coverage exceeded 20% of the Mediterranean Sea in $km^2$, consecutively.

In common with many atmospheric definitions (e.g. Schoetter et al., 2015), the minimum spatial coverage of an event to be identified as MHW was, therefore, set to 20%. The reason behind that is that we opted for large-scale events that may have a broad ecosystem impact but also represent rare occurrence for the average climate conditions of the last part of the 20th century. By that we mean that the frequency of MHWs during 1982-2017 was counted using the 20% but also a spatial limit of 10% and 30% each time. In the second case, one event was identified every year, ruling out the sense of rare, extreme occurrence, while in the third case too few MHWs were found to constitute a statistical study (Fig.2.11 a-f). Therefore, a 20% spatial limit was selected as a balance between the two. If no spatial limit is posed on the MHW coverage, one can see that only one event will be identified every time (and every year) an SST threshold exceedance is initiated.

In fact, further investigation showed that it is mostly the small-scale MHWs (coverage ~ 10%) that are more noisy in terms of spatial extent fluctuations. Compared to larger-scale MHWs, they display a higher possibility to be separated from a following event in the same year, due to MHW-affected grid points being entirely absent (0% MHW spatial coverage) during the transition between the 2 events. This practically means that small-scale events are not persistent -in time and space- structures in the ocean and can occur multiple times within a year. On the contrary, larger MHWs appear as more "stable" formations once they occur, demonstrating higher durations and less variations in their spatial extent (in agreement with Scannell et al. (2016)), hence, facilitating their examination. This can be seen as an expression

of the correlation between the time- and space-scales of MHW variability.

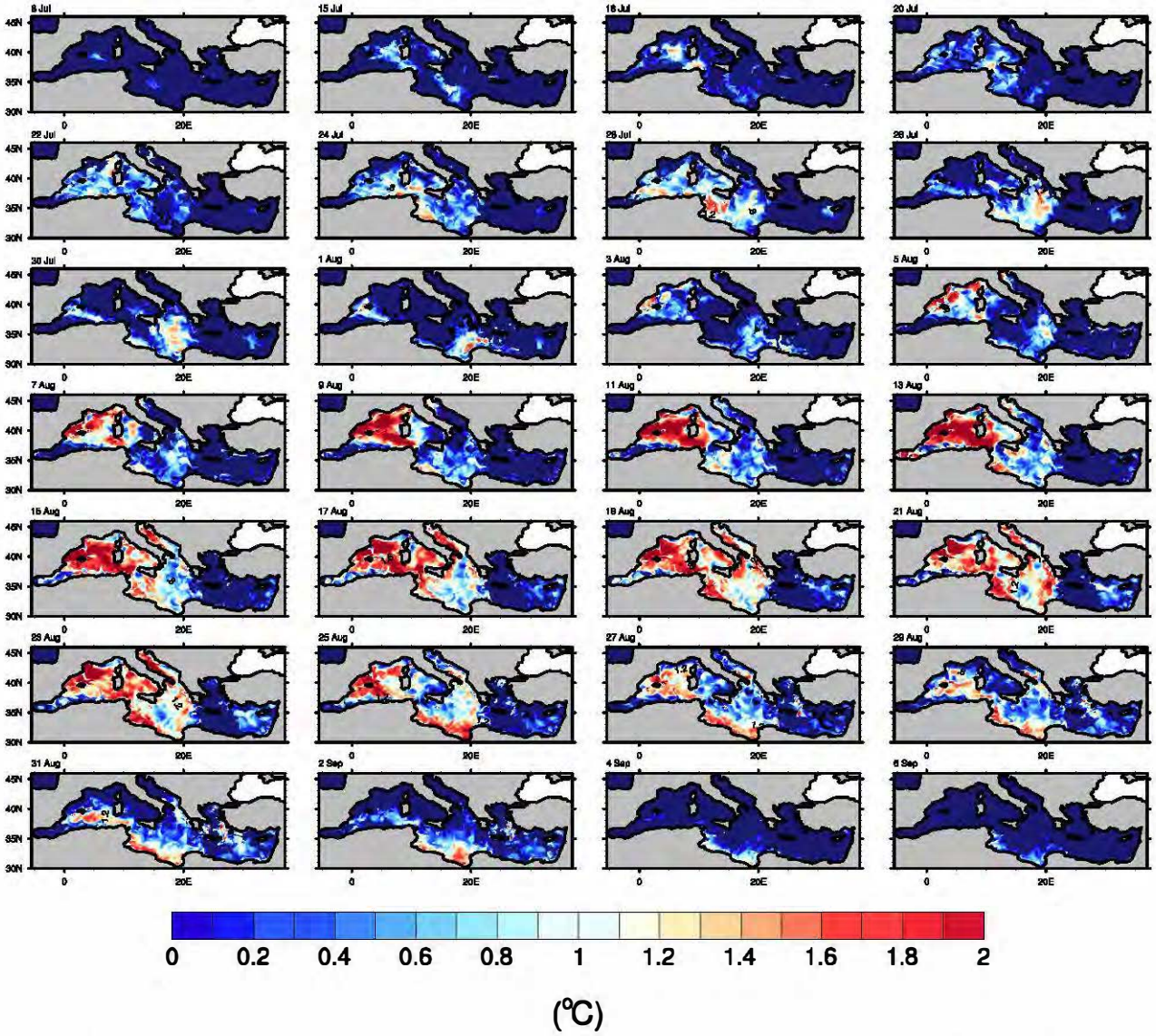


Figure 2.10: Example of the daily mean intensity of the MHW during the event of 2003, as detected by our algorithm, using the CNRM-RCSM6 in hindcast mode. Evolution of MHW area is illustrated in selected days and not throughout the entire duration of the event. Areas that were not affected by the MHW are indicated in dark blue.

Once the 20% spatial extent is reached, a subset of metrics defined in Hobday et al. (2016) is used to characterise the MHW spatiotemporal evolution (Table.2.4). In particular, we examine the frequency of MHWs (annual count of events) and their duration, which is defined as the time between the first ($t_s$) and last day ($t_e$) for which a minimum of 20% of Mediterranean Sea surface is touched by a MHW. Each event is also characterised by a mean and max intensity (mean and spatiotemporal maximum temperature anomaly relative to the threshold over the event duration in °C) and a maximum surface coverage (surfmax, in %). Finally, each MHW's severity is represented by cumulative intensity (spatiotemporal sum of daily temperature anomalies relative to the threshold over the event duration, in °C.days.km$^2$).

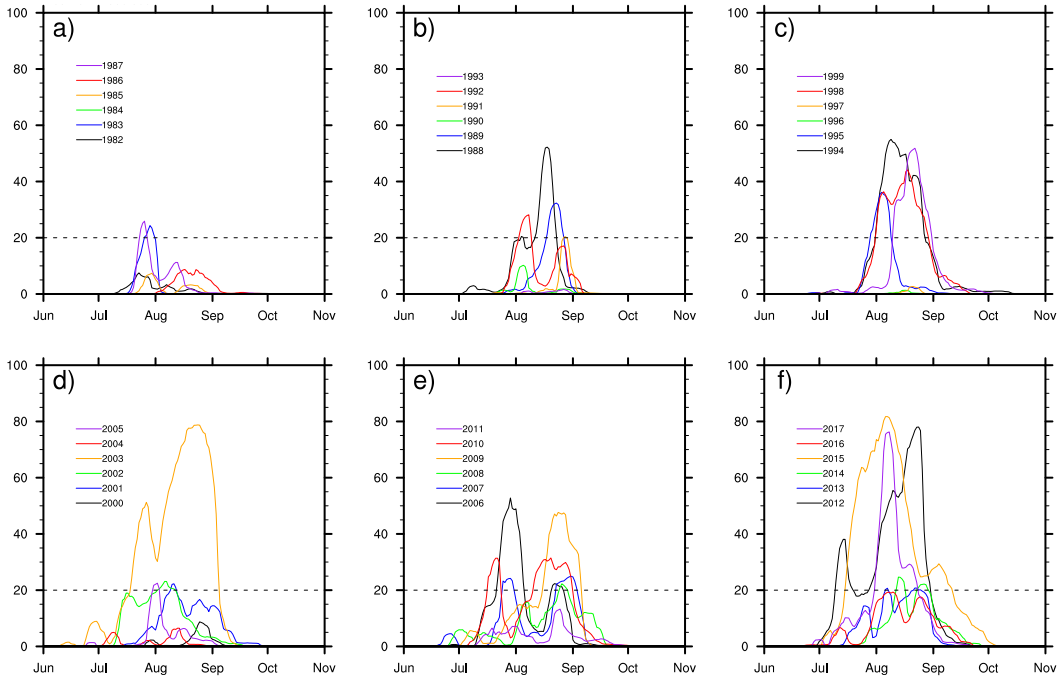


Figure 2.11: Daily MHW area summed over the basin every year between 1982-2012 and expressed in percentage of the Mediterranean Sea surface coverage in km$^2$, using the original MHW definition (Q99). Spatial threshold of 20% is indicated with dash line.

| Marine Heatwave Metrics | Description |
|---|---|
| Frequency | Number of events occuring per year |
| Duration | $(t_e - t_s) + 1$ (days) |
| Mean Intensity (Imean) | $\int [\int (SST_{(x,y,t)} - SST_{99Q}(x,y))\mathrm{dxdy}]\mathrm{dt} / \int \mathrm{dxdy} \int \mathrm{dt}$ (°C) |
| Max Intensity (Imax) | $max_{(x,y,t)}(SST_{(x,y,t)} - SST_{99Q}(x,y))$ (°C) |
| Severity (Icum) | $\int [\int (SST_{(x,y,t)} - SST_{99Q}(x,y))\mathrm{dxdy}]\mathrm{dt}$ (°C.days.km$^2$) |

Table 2.4: Marine Heatwave (MHW) set of properties and their description adapted from (Hobday et al., 2016)

## 2.6 MHW 2003 Characteristics

One of the well-known events in the Mediterranean Sea and one of the first MHWs documented worldwide was the MHW of 2003. According to Grazzini and Viterbo (2003) extreme SSTs over the Mediterranean developed during a persistent heatwave period over Europe in the summer of 2003. A warm SST anomaly built up first in the central Mediterranean Sea during the month of May. Towards the end of that month the anomaly subsided for a while, only to return in the first week of June, expanding throughout the whole basin by the end of July. According to the same study, SST anomalies of 2-3°C warmer than the climatology occured uniformly in the Mediterranean, except in the Aegean Sea, during that time. Sparnocchia et al. (2006), in the meantime, mentioned an increase of 3-4°C in the mean Mediterranean Sea

temperature during the summer of 2003. They also highlighted the remarkably high anomalies (~4°C) observed in NW Mediterranean areas (e.g. Gulf of Lion, Ligurian, Tyrrhenian, N.Ionian and Adriatic Sea) in the month of June. According to them, the event persisted in those regions during July but weaker until August, where it intensified again (anomalies ~4°C). The SST anomaly with respect to climatology simulated by CNRM-RCSM6 during the MHW is in line with the literature. It ranged between 2-3°C in the Gulf of Lion, the Tyrrhenian and the Adriatic Sea and up to 1°C higher than normal in the rest of the Mediterranean basins (not shown).

From the above description of the evolution of the event, our algorithm captured small-scale anomalies (>99th percentile of SST) in the NW Mediterranean in June, (not shown here) using the CNRM-RCSM6 model. From Fig.2.10 some progressively increasing footprints of the event are also discernible, even though in smaller-scale, during July. In August, however, the algorithm seems to have captured the bulk of the MHW, which was both intense and large-scale. The average MHW 2003 characteristics are presented in Table.2.5, as they have been identified by both the model and the observations throughout the event duration and normalized over the area that was affected.

| MHW 2003 | | |
|---|---|---|
| Characteristics | Model | Observations |
| Start Day (Calendar Day) | 18 Jul | 20 Jul |
| End Day (Calendar Day) | 3 Sep | 5 Sep |
| Mean Intensity (°C) | 0.8 | 0.9 |
| Duration (Days) | 48 | 48 |
| Severity (°C.days.km$^2$) | 60.5 | 88.9 |
| Max.Surface (%) | 78.8 | 89.9 |
| Max Intensity (°C) | 6.4 | 3.8 |

Table 2.5: Average, characteristics of MHW 2003 throughout the event duration. Starting and ending day (calendar day), duration (Number of days), mean and maximum intensity (°C), severity*$10^6$ (°C.days.km$^2$) and maximum surface coverage (%) are presented for both the model and the satellite observations.

The duration, starting (mid-July) and ending date (start of September) were, in fact, similar in both datasets. However, the model appeared to underestimate the observed mean intensity, severity and maximum surface coverage. We note here that, although SST anomalies have been detected before mid-July, they were not counted within the event as they did not satisfy the 20% spatial coverage.

To better illustrate the differences in the MHW 2003 characteristics in the 2 datasets we use the bubble plot (Fig.2.12). It is a graph that summarizes a 4D space information in 2D. More

specifically here, the maximum surface coverage of a selected MHW falls into a pre-defined range of possible spatial extents every time, represented by the size of the bubble. In similar ways, the colour of the bubble represents the range of event severity within which, the selected MHW belongs to. Finally, the y axis shows the average mean intensity of the event, normalized over the area that it touched, and in x axis is given the total number of days (duration) during which the MHW covers more than 20% of the Mediterranean Sea consecutively. However, a closer examination on the distribution of MHW characteristics in space will give us a better understanding on the reasons why the bubbles differ in shape and colour.

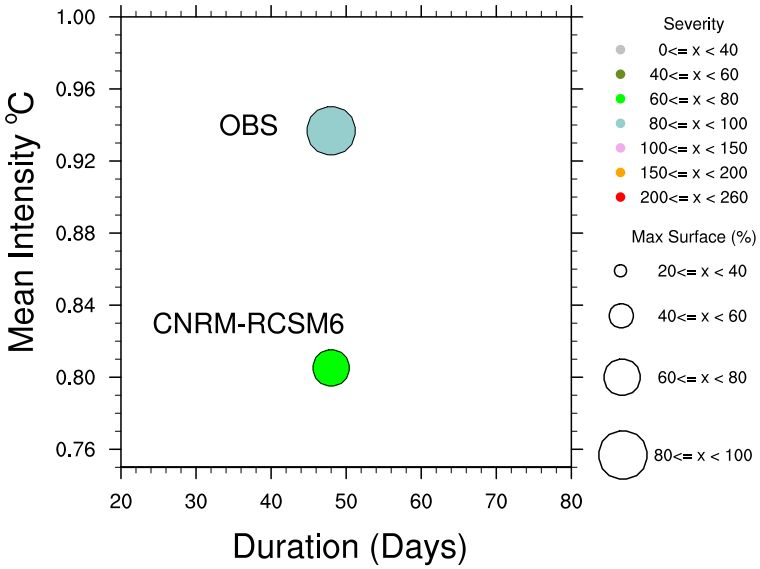


Figure 2.12: Bubble graph of MHW 2003 for both the model (NEMOMED12) and the satellite observations (OBS). Duration is in number of days, mean intensity in °C, severity*$10^6$ in °C.days.km$^2$ and maximum surface coverage in %.

For example, the impacts of MHW 2003 on marine ecosystems have been mostly documented in the NW Mediterranean region (e.g. Garrabou et al., 2009; Schiaparelli et al., 2007). This could be linked to the area's remarkably higher mean intensity compared to that of the Central and Eastern Mediterranean basin, during the event (e.g.Fig.2.10). This is a fact highlighted already in previously analysis of the event (e.g. Olita et al., 2007). In Fig.2.13 we also show the greatest intensities (departure from threshold) of 1-1.8°C located in the Gulf of Lion, the Ligurian, Tyrrhenian and N.Adriatic Sea. Even though the model underestimates the mean intensity in those areas (~0.8-1.4°C) relative to the observations, it has still simulated warmer anomalies there compared to the rest of the basin. Central Mediterranean Sea followed with anomalies between (~0-0.8°C). Eastern Mediterranean, on the other hand displayed the lowest mean intensities (~0.2-1°C), with a part of the Aegean Sea not being affected by the event, in agreement with Grazzini and Viterbo (2003). In general, the patterns of mean intensity, were relatively well correlated between model and observations (corr.coeff=0.78, not shown). For example, MHW-free regions in the model cover a higher percentage of surface compared to the observations. This could explain the lower maximum surface coverage of the simulated MHW

2003 in Fig.2.12.

Finally, we demonstrate in Fig.2.14, the spatial distribution of duration (number of MHW days) during the MHW 2003 for both datasets. Although quite patchy, certain regions were observed with durations of 40-48 days. For example, the Ionian Sea, N.Adriatic, Tyrrhenian Sea and Balearic islands and a few small areas in the Levantine basin. Most of the coastal regions around the basin remained under the MHW for almost a month, whereas some areas of the Aegean affected by the MHW displayed durations of 10-15 days. The model, however, appears to underestimate slightly the duration in some NW Mediterranean regions, the Alboran and Adriatic Sea and the Levantine Basin, while its correlation coefficient for the patterns of duration is 0.57. It captures though the low MHW persistence in some parts of the Aegean.

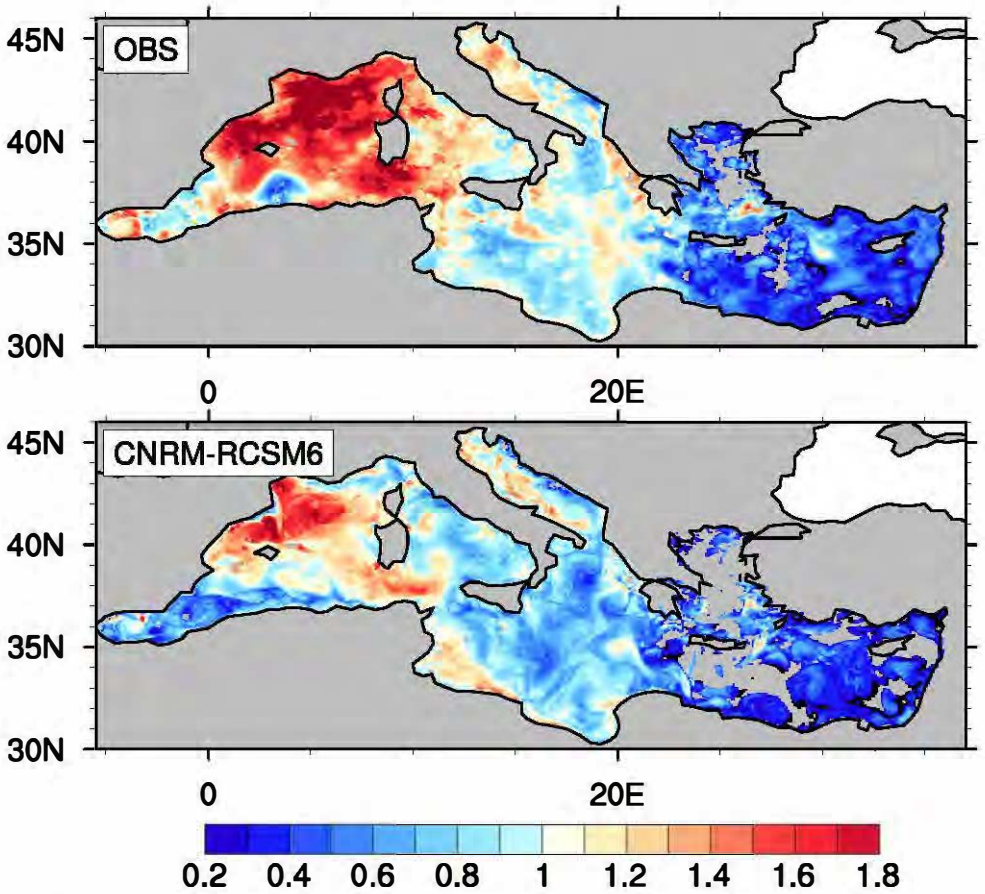


Figure 2.13: Mean intensity (°C) of the MHW 2003 throughout the event duration, as it was captured from the detection algorithm using CNRM-RCSM6 and satellite observations. Gray ocean areas represent grid points not affected by the MHW.

We can finally conclude that although the model's mean intensity and duration patterns are not well correlated with the observed ones, on average, the main warm and cold patterns during the MHW 2003 are correctly captured. Inconsistencies in the correlation coefficient most probaly emerge from the differences in missing values (areas not affected by the event). Such differences could inhibit the correct point-to-point calculation of the Pearson product-moment coefficient of linear correlation, based on which the pattern correlation is calculated

here. On the other hand, the observational dataset may also be inherited with inconsistencies. For example, the somewhat strange patterns seen in the spatial distribution of MHW duration (Fig.2.14) could be linked to the gridded analysis that fills the gaps between the days. We believe though that these pattern discrepancies are not detrimental to the overall identification of the event. For instance, despite the relatively low pattern correlation of Fig.2.14, the average duration of the overall event has been found 48 days for both the observations and the model (see. Table.2.5). Nevertheless, the model's general underestimation of mean intensity and duration values could be responsible for the lower simulated severity of the MHW relative to the observed one, since this metric is a combination of duration and mean intensity metrics in time and space.

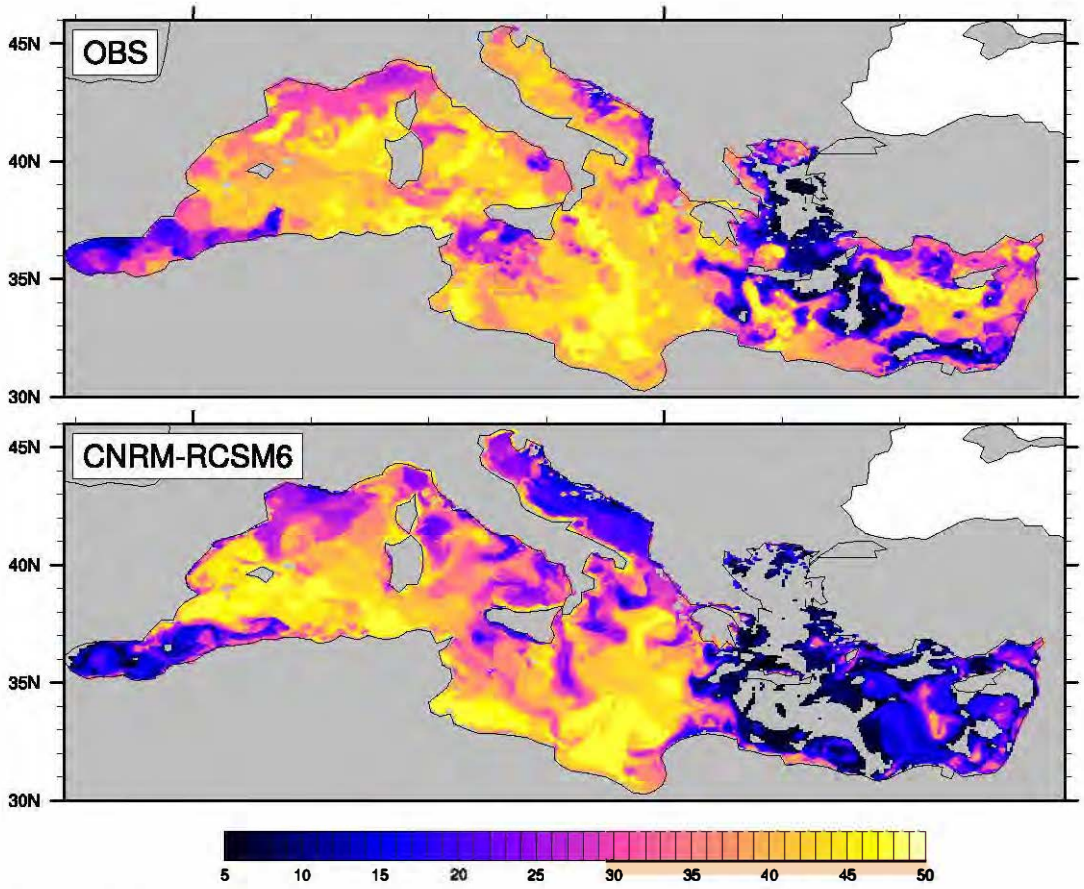


Figure 2.14: As in Fig.2.13 but for the total number of days touched by the MHW at every grid point.

## 2.7 Sensitivity Tests

From the example of MHW 2003 we can deduce that different datasets can provide a different characterisation for the same event, even though the same detection method has been used. The dataset-related reasons behind this (e.g. temporal and spatial resolution, Hobday et al. (2016)) cannot always be resolved, however. Which brings us to the next reasonable question, of how sensitive is the identification of an event from a given dataset on the detection method. In other words, is there a universal definition for MHWs? To answer this question it is important

to first take into account that every detection method is inherent with a series of subjective decisions. These decisions can be related to the choice of the reference period, the level of the temperature threshold, the number and temperature of gap days allowed, the minimum spatiotemporal extent of a MHW or to the adjacency requirements for grid points to form a MHW and others. In order to better understand how sensitive are the results to some of these perturbations on the initial definition, we performed sensitivity tests on the previously-analyzed MHW of 2003. We used only the CNRM-RCSM6 model this time in hindcast mode again and performed a series of predefined experiments that are analyzed below (Fig.2.15, Table 2.6-Table.2.7).

In the previous section we characterized the event using the algorithm that was developed in this work and was described at the beginning of this chapter. For practical reasons, in this section we will name it as the reference algorithm (REF) and compare its results (see Table.2.5) with those from the sensitivity experiments. At first, we identified the MHW 2003 using definitions with different thresholds. More specifically, we used the 30-year average (1982-2012) of the 90th (Q90), 92nd (Q92), 95th (Q95), 96th (Q96), 97th (Q97), 98th (Q98) and 99.5 (Q99.5) percentile of SST as the baseline (see Table.2.6). As before, we created a climatological map of extreme SSTs for each threshold separately and studied the properties of the MHW 2003, based on these different thresholds each time. Naturally, what can be seen by Fig.2.15 is that the lower the threshold, the longer, more intense and spatially extended appears the MHW. In some experiments in particular (Q90, Q95, Q96 and Q97), a smaller in duration, intensity and spatial coverage event seems to have occurred as well. This could either constitute an entirely different event that preceeds or follows the main MHW or could be a result of an instantaneous drop-down from the 20% spatial limit, which separates the main event from a smaller one.

| | Q90 | | Q92 | Q95 | | Q96 | | Q97 | | Q98 | **REF** | Q99.5 |
|---|---|---|---|---|---|---|---|---|---|---|---|---|
| Start Day (Cal.Day) | 12 Jun | 20 Jun | 22 Jun | 24 Jun | 7 Jul | 25 Jun | 9 Jul | 26 Jun | 10 Jul | 12 Jul | **18 Jul** | 20 Jul |
| End Day (Cal.Day) | 18 Jun | 10 Sep | 9 Sep | 4 Jul | 7 Sep | 3 Jul | 6 Sep | 29 Jun | 5 Sep | 4 Sep | **3 Sep** | 3 Sep |
| Duration (Days) | 7 | 83 | 80 | 11 | 63 | 9 | 60 | 4 | 58 | 55 | **48** | 46 |
| Imean (°C) | 1.1 | 1.4 | 1.3 | 0.8 | 1.1 | 0.8 | 1.1 | 0.9 | 1.0 | 0.9 | **0.8** | 0.7 |
| Imax (°C) | 4.4 | 8.7 | 8.2 | 4.9 | 7.3 | 4.2 | 6.9 | 3.4 | 6.4 | 5.8 | **6.4** | 3.5 |
| Surfmax (%) | 24.8 | 98.6 | 98.0 | 38.0 | 94.9 | 31.5 | 92.8 | 23.8 | 89.0 | 83.2 | **78.8** | 72.3 |
| Severity*$10^6$ (°C.days.km$^2$) | 4.6 | 251.3 | 209.5 | 7.7 | 140.0 | 5.1 | 121.3 | 2.0 | 101.9 | 81.6 | **60.5** | 45.1 |

Table 2.6: Sensitivity experiments on the MHW 2003 characteristics using MHW definitions with different baseline thresholds. Units are as in Table.2.5. Reference definition is indicated with bold. See text for more details.

Since we treated Mediterranean Sea as a "single point" that is affected (or not) by events depending on their surface coverage, such smaller-scale events most of the time stem from daily fluctuations on the number of points exceeding their local threshold. In the case of 2003, however, the smaller-scale event was identified around mid-June, before the bulk of the MHW in August, when a lower baseline SST was used. This is in agreement with observations of

that year, where a less intense SST anomaly built up around mid-June before the main event (Feudale and Shukla, 2007; Sparnocchia et al., 2006).

At a next step, we carried out experiments with perturbations on the more intrinsic part of the algorithm, such as the choice of the cool days. For example, an experiment was performed without gap days on the MHW definition but the 20% spatial threshold retained (EXP.1). Then, the MHW was also identified with a definition that allows 2 gap days and a minimum spatial threshold of 20% (EXP.2). In EXP.3, the MHW definition allowed up to 5 cool days that are lower than the initial threshold by up to 0.3 °C and a minimum spatial threshold of 20%.

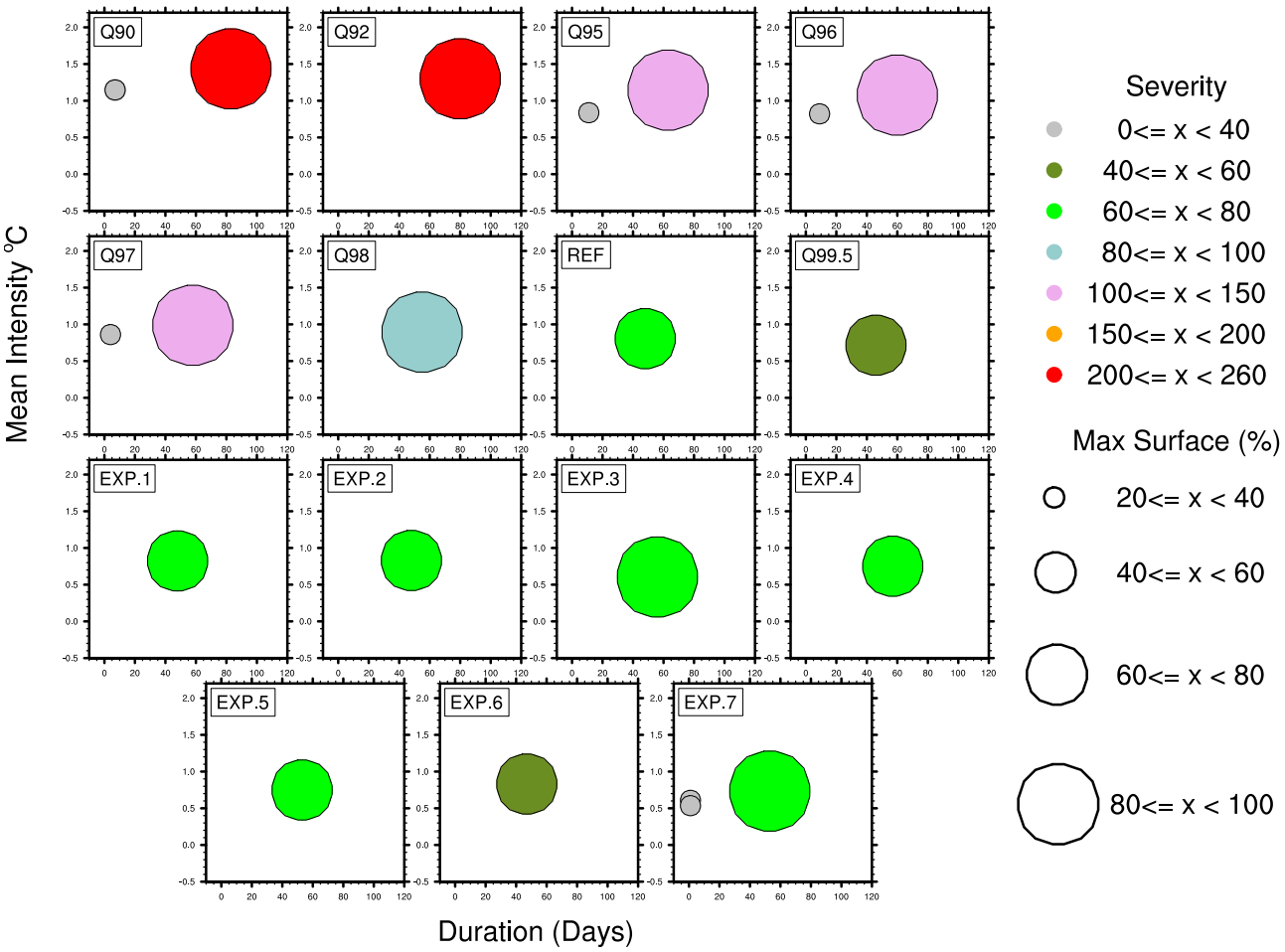


Figure 2.15: Bubble graph representing the characteristics of the MHW 2003, based on different experiments on the MHW definition. Color scale corresponds to severity ($*10^6$°C.days.km$^2$) and size of the bubbles to percentage of maximum surface coverage (surfmax) of the MHW. See the text for more details.

The starting and ending day, the overall mean intensity and severity of the events did not differ substantially between these experiments and the original definition (REF) (see Table 2.7). However, in EXP.3 the number of points that are in "MHW state" is increased and so does the MHW's duration and maximum spatial coverage (surfmax). Yet, its Imean is lower, probably due to a higher number of cool days contributing negatively to the mean intensity of the event.

To test the effect of the spatial limit on the MHWs a sensitivity test was also performed, where the original detection method was retained, apart from the minimum spatial coverage that was set to 10% (EXP.4). The latter event's characteristics were not very different from the one detected with REF except for the duration that increased from 48 to 57 days. Finally, 3 sensitivity tests, EXP.5, EXP.6 and EXP.7 were performed with a different minimum duration allowed for the MHW each time, of 3, 7 and 2 days respectively. From Fig.2.15 and Table 2.7 it is inferred that between Q99, EXP.5 and EXP.6 and EXP.7 the lower minimum durations lead to higher number, severity, Imean and maximum spatial extent of the overall event(s) that is/are identified each year, similar to the effects seen when lower percentile temperatures are chosen as a baseline. In EXP.7, for instance, 2 single-day events are identified in addition before the main MHW during August, supporting again the argument of the weak characteristics of the small in space and time MHWs.

| | **REF** | EXP.1 | EXP.2 | EXP.3 | EXP.4 | EXP.5 | EXP.6 | EXP.7 | | |
|---|---|---|---|---|---|---|---|---|---|---|
| Start Day (Cal.Day) | **18 Jul** | 18 Jul | 18 Jul | 11 Jul | 11 Jul | 13 Jul | 19 Jul | 28 Jun | 3 Jul | 13 Jul |
| End Day (Cal.Day) | **3 Sep** | 3 Sep | 3 Sep | 4 Sep | 5 Sep | 3 Sep | 3 Sep | 28 Jun | 3 Jul | 3 Sep |
| Duration (Days) | **48** | 48 | 48 | 56 | 57 | 53 | 47 | 1 | 1 | 53 |
| Imean (°C) | **0.8** | 0.8 | 0.8 | 0.6 | 0.7 | 0.7 | 0.8 | 0.6 | 0.5 | 0.7 |
| Imax (°C) | **6.4** | 6.4 | 6.4 | 6.4 | 6.4 | 6.4 | 6.4 | 2.7 | 3.5 | 6.4 |
| Surfmax (%) | **78.8** | 78.2 | 77.0 | 86.6 | 78.8 | 80.0 | 77.4 | 20.6 | 20.1 | 80.3 |
| Severity*$10^6$ (°C.days.km$^2$) | **60.5** | 60.5 | 60.1 | 61.1 | 62.1 | 62.6 | 59.2 | 0.3 | 0.2 | 63 |

Table 2.7: As in Table.2.6 but for MHW definitions with changes on gap day number, spatial threshold and minimum event duration. See text for more details.

An additional point of interest here, would be to check how the observed and simulated MHWs differ with the above-mentioned changes in the algorithm parameters. Therefore, we performed the same sensitivity tests in the observational dataset and we present them here, as before, with a bubble plot superimposed on the equivalent model results of Fig.2.15 (see Fig.2.16). In general we can say that the model-observation comparison does not differ substantially in terms of duration and mean intensity of the event. However, in terms of severity, almost all the experiments (except for Q90, Q92 and Q97) showed a somewhat reduced MHW severity in the model relative to the observations. Moreover, in almost half of the sensitivity tests the model appeared to underestimate slightly the maximum spatial coverage of the event. Nevertheless, at this point the reader is reminded that application of the algorithm on different datasets is expected to yield different results (see also Hobday et al. (2016)), which in our case here did not differ largely. Especially if we take into account the fact that the satellite SST refers to the first $\mu$m of the ocean surface, the larger maximum MHW coverage is somewhat anticipated.

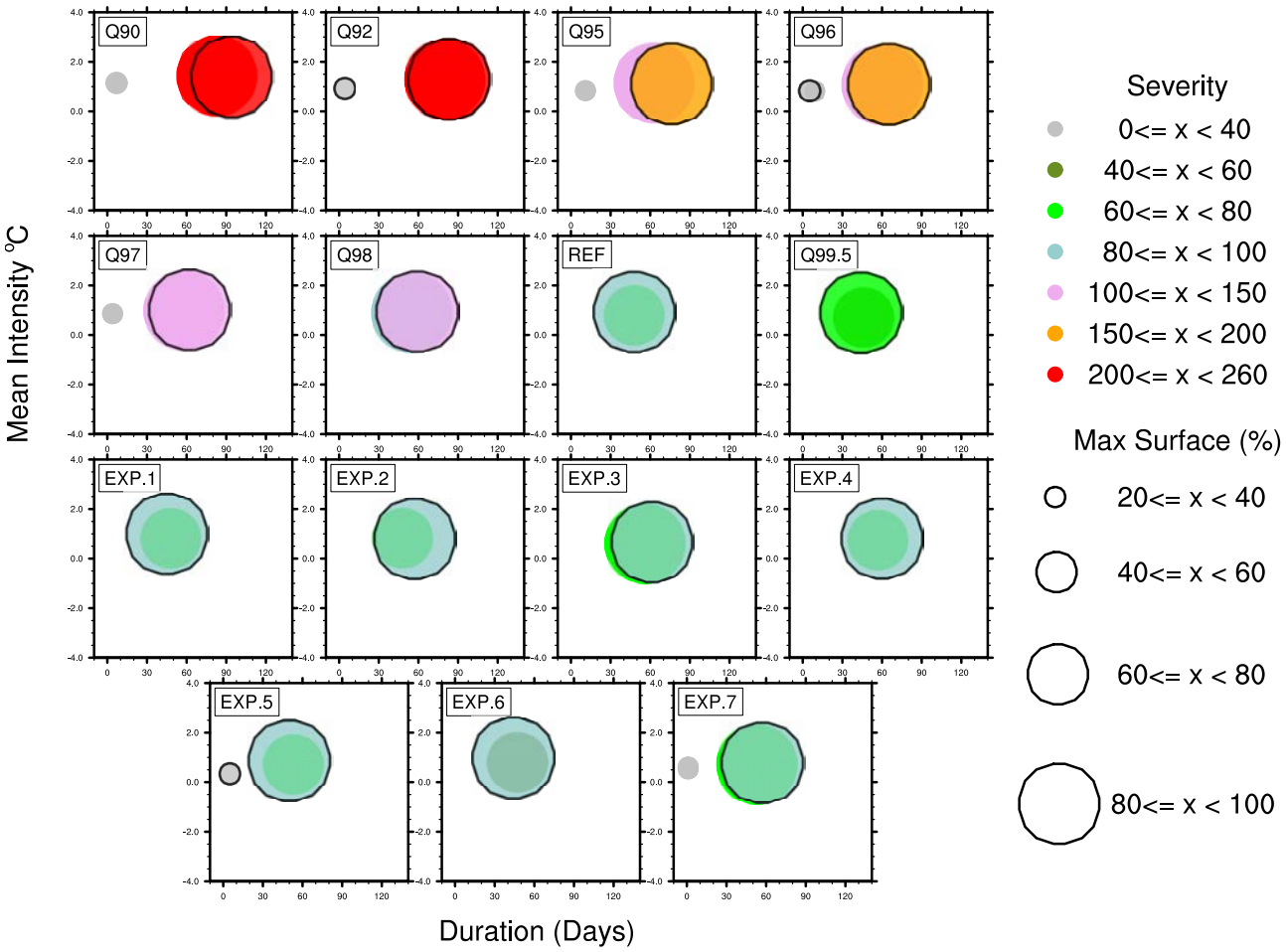


Figure 2.16: As in Fig.2.15 but with the observed MHW 2003 (bubble with bold circle, less opaque) superimposed on the simulated MHW (bubble more opaque and no bold circle).

## 2.8 MHW identification

The validation of the two RCSMs followed the evaluation of their performance in MHW detection. Preliminary tests on the number and characteristics of the summer Mediterranean MHWs detected by the models and the observations during 1982-2012 were undertaken and are analyzed below.

The bar plot of Fig. 2.17 displays the number of MHWs identified each year throughout the chosen period for all 4 datasets, as before. Both CNRM-RCSM6 and CNRM-RCSM4 appear to capture relatively well the observed events of the period. CNRM-RCSM6, in particular, identified the same number of events with the corresponding observed dataset between 1994-2004 and in 2006, 2007, 2009, 2010 and 2012. It (underestimated)overestimated though their number in (1992, 2008 and 2011)1983, 1987, 1988, 1991 and 2005. In CNRM-RCSM4 in the meantime, more MHWs were simulated than identified in the observations, especially at the beginning of the period in the 80s. An explanation for this behaviour could be the overall underestimation of the observed trend by both models, throughout the whole period examined.

As a result of this, above-threshold, daily SST can occur more often at the start of the period for both models than for the observations, which could lead to an overestimation of the simulated events (for example, see Fig.2.6, bottom row). It is noteworthy, that interpolated observations under CNRM-RCSM4 grid showed 3 events occuring in 2008, as opposed to 2 events found for the same year in the observations under CNRM-RCSM6 grid. This could be a result of the different resolution of the interpolated dataset, since no other change was applied to them. In fact, according to our definition, the extra MHW identified with CNRM-RCSM4 is an event that lasted one day and had a maximum coverage of around 20%. The equivalent day under CNRM-RCSM6 showed a MHW coverage of the Mediterranean Sea of about 19% of its surface. This pinpoints the sensitivity of the definition to the spatial threshold, which at that point could imply an activation (or not) of MHW points due to differences on the land-sea mask of each grid.

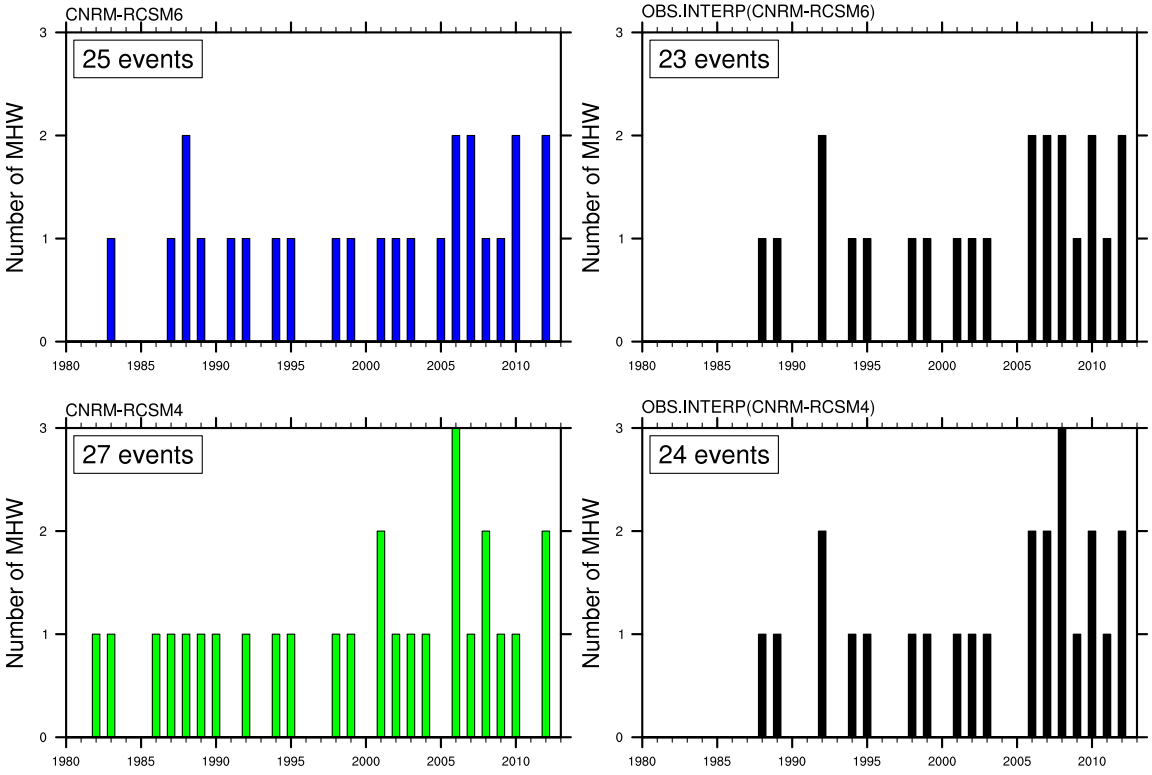


Figure 2.17: Number of summer Mediterranean MHWs per year during 1982-2012 identified by CNRM-RCSM6 (top left), CNRM-RCSM4 (bottom left) and observations interpolated in CNRM-RCSM6 grid (top right) and CNRM-RCSM4 grid (bottom right).

Finally the characteristics of all the above-identified events are demonstrated in Fig. 2.18. The Intensity-Duration-Frequency (IDF) plot categorises the total number of events (NMHW or frequency) from every dataset of Fig.2.17 into bins of mean intensity and duration. The ensemble of events shows a mean intensity of up to 1°C and maximum duration of 70 days at each dataset. For comparison purposes the observed characteristics of MHW of 2003 are indicated with red box. In the observations and in CNRM-RCSM6 it is captured as the most intense and long-lasting event of the period. In CNRM-RCSM4 though the most intense and

long-lasting event of the period underestimates/overestimates the intensity/duration of the observed MHW 2003. In general, the upper part of the events' mean intensity is underestimated in CNRM-RCSM4, although the range of their duration is well-captured.

Taking into account the better performance of CNRM-RCSM6 in terms of bias and trend of extreme temperatures, as well as its improved representation of the number and characteristics of the MHWs relative to CNRM-RCSM4, we decided to use this configuration to study further the past MHW variability in the Mediterranean. In the following section more details on summer Mediterranean MHWs during 1982-2012 will follow in the form of an article.

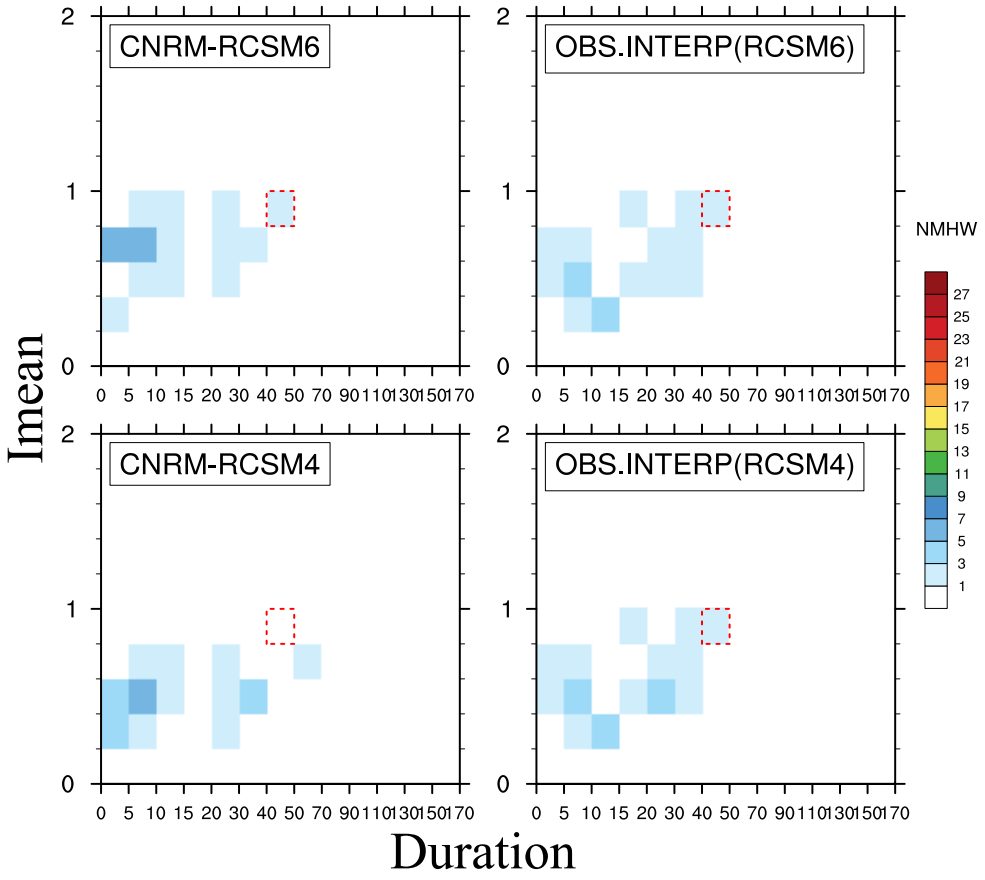


Figure 2.18: IDF plot for the MHW characteristics identified by CNRM-RCSM6, CNRM-RCSM4 and the observations interpolated in the respective grids for 1982-2012.

## 2.9 Conclusions

A consistent terminology and definition when it comes to understand anomalous temperatures in the ocean is an important requirement for the comparison between different events and relevant studies. Furthermore, a common framework can facilitate the analysis of MHW impacts on marine ecosystems and their future evolution. In this chapter, we detailed the features of a MHW detection algorithm we developed to identify summer events in the Mediterranean Sea. We applied it to a model, satellite and *in situ* dataset for the characterisation

of the well-known MHW 2003 in the basin. The analysis showed that different data can yield different MHW characteristics. On average though, the event lasted 48 days, covered more than 70% of the Mediterranean Sea, with a mean intensity of 0.8-0.9°C. In agreement with existing literature NW Mediterranean areas were more severely affected than the rest of the sub-basins.

We also assessed the stability of the methodology in terms of perturbations on its initial definition. Similar to atmospheric heatwaves, an objective MHW detection does not exist, as it is based on a series of subjective choices on the type of events that we want to track. The assumptions we do here for the MHW length, reference limits and the gap days allowed, however, are directed towards the detection of long-term, large-scale, summer thermal events, taking into account the low frequency variability of the ocean. On the contrary to atmospheric events, any type of abnormal temperature change in the ocean will require a certain amount of time to be transmitted throughout the water and "felt" by the marine ecosystems. Thus, any kind of MHW detection algorithm should resemble a type of "filter" on the abnormal temperatures in the ocean's time and space scales.

It is clear, that the characteristics of the events identified every time were more sensitive to the choice of the percentile threshold temperatures. We have shown that the lower the baseline SSTs the more intense MHWs are detected. This is followed by the effects of the minimum event duration chosen, which may alter the MHW properties in a similar way, yet on a lower pace. For the more intrinsic part of the methodology, i.e. the choice of cool days allowed and the spatial limits, they seem to be responsible for small changes in the individual events, yet, with a higher effect on the number of events detected on a given period, at local and larger scales, respectively. One should be also aware that different resolution datasets may provide substantially different MHW information, independently from the MHW detection method applied. Nonetheless, more sensitivity tests would be required to better document the uncertainty related to small changes in the MHW definition.

Ultimately, the definition of a MHW in the Mediterranean Sea was determined based on a climatology of 99th percentile of daily temperatures towards the end of the 20th century. This was dictated by the necessity to identify extremely rare occasions in the present, with an eye to place their occurrence in the future. Under continuous global warming, thermal stress in the ocean will possibly increase, transforming not only the intensity of future MHWs but also the ecosystems influenced by them. In that sense, whether MHWs should be identified based on a constant reference period from the 20th century or the reference period should be transient with time, is a subjective choice related to the questions that we want to answer every time.

# Chapter 3

# Past summer Marine Heatwave Variability in the Mediterranean Sea

*"All you have to decide, is what to do with the time that is given to you."*

Gandalf,LOTR

## Contents

In the previous Chapter we have shown the sensitivity of the properties of a single MHW (2003) on small perturbations of the initial MHW definition. We have also highlighted the fact that the application of the algorithm to different datasets may yield substantially different results for a given MHW. We have, therefore, examined the uncertainty related to the algorithm parameters and have tested for a given event the uncertainty related to various datasets. In this Chapter we examine the events occurring in the Mediterranean between 1982-2017 and their characteristics using the CNRM-RCSM6 model.The reader is reminded that current Chapter is in the form of an article under review and some of its content might have been mentioned in previous Chapters. Reference : **Darmaraki S**, Somot S, Sevault F, Nabat P, *Past trends of Mediterranean Sea Marine Heatwaves*

## Abstract

Marine heatwaves (MHWs) are episodes of anomalous warming in the ocean, responsible for widespread impacts on marine ecosystems. For the first time past summer MHW variability at surface and 3 ecosystem-relevant depths of the upper Mediterranean Sea are assessed here for 1982-2017. We apply a MHW detection algorithm on a hindcast simulation, performed with a high-resolution, fully-coupled regional climate system model. Identified surface events last, on average, 14 days with a mean intensity of 0.6°C and a maximum sea surface coverage of around 37%. Subsurface events are seasonally shifted and appear, on average, longer and more intense but less frequent and extended in space than surface MHWs. We also find significant trends of increase in all MHW properties throughout the period, with severe surface MHWs detected in 2012, 2015 and 2017. However, MHW spatial «Hot Spots» are inhomogeneously distributed at surface and deeper layers.

## 3.1 Introduction

Prolonged periods of anomalously warm temperatures in the ocean are described as Marine Heatwaves (MHWs) (Frölicher and Laufkötter, 2018; Hobday et al., 2016) and have led to detrimental impacts on marine ecosystems around the world (Smale et al., 2019). For example, they have triggered widespread mortalities and abrupt redistribution of marine species (Garrabou et al., 2001; Wernberg et al., 2013), toxic algal blooms (Cavole et al., 2016) and mass coral bleaching (Hughes et al., 2017) in a matter of weeks or months, with economic losses in fisheries and aquaculture industry (Mills et al., 2013; Oliver et al., 2017). Superimposed on the underlying warming trend of the ocean, MHWs occur regionally from coastal to open ocean, can extend up to thousand of kilometers (Scannell et al., 2016), but may also propagate deeper to the water column (Schaeffer and Roughan, 2017).

To date, our knowledge on past MHWs in the Mediterranean Sea, is based mostly on reported mass mortalities of benthic species linked to thermal anomalies, which have been seen to increase since the early 1990s (Rivetti et al., 2014; Coma et al., 2009). One of the

first documented, large-scale events occurred in 2003, where surface anomalies of 2-3°C above climatological mean lasted over a month and resulted in extensive mass mortalities of benthic invertebrates, loss of seagrass meadows and abrupt changes in community composition (Garrabou et al., 2001). Prior to this, studies focused mostly on local ecological impacts of regional events observed, for instance, in 1994 (Marbà et al., 2015), 1999 (Garrabou et al., 2001), 2006 (Kersting et al., 2013), 2008 (Cebrian et al., 2011), 2009 (Di Camillo et al., 2013) and 2010-2013 (Rodrigues et al., 2015).

Most of the documented episodes affected corraligenous species (e.g. gorgonians, sponges, seagrass *Posidonia oceanica* meadows) up to 50m deep (Rivetti et al., 2014) with a few occasions reaching 80m-160m (Arnoux et al., 1992; Rivoire, 1991). Therefore, investigation of subsurface MHWs is equally important to the identification of events at surface. However, most studies so far have analyzed MHWs at the ocean surface, suggesting already an increase in their occurrence, duration and intensity globally, over the past century (Oliver et al., 2018a). Little is known about the evolution of extreme temperatures at depth, since they are harder to observe in large spatial scales and over long-time periods. For example, Argo floats during a 2011 MHW in Australia, indicated open-ocean temperature anomalies constrained to the mixed layer depth (MLD), while in-situ measurements on the shelf revealed their extension down to 100m-200m (Feng et al., 2013). Recently, Jackson et al. (2018) demonstrated that coastal subsurface anomalous warming in the NE Pacific occurred with 1-year lag but persisted for more than 4 years after the surface 2013-2015 MHW was first observed. Duration of warm anomalies at depth can be longer than at the surface, even re-emerging to the MLD in late winter (Deser et al., 2003). Yet, it remains unknown how frequently and deep a MHW may penetrate in the open ocean or how deep events may evolve individually. The only systematic analysis to date is based on coastal in-situ data in Australia for 1953-2016 and shows regular warming throughout the water column, and a maximum MHW intensity just below the thermocline (Schaeffer and Roughan, 2017). In the case of the Mediterranean Sea, a quantitative assessment using a standarized framework is currently missing for both past surface and subsurface MHWs characteristics. There are, however, indications of an increase in surface MHW frequency and intensity in the basin for the 21st century relative to the past (Darmaraki et al., 2019).

In this study, we apply an existing MHW definition on daily-resolution temperature data between 1982-2017, and describe changes in frequency, duration, intensity, severity and spatial coverage of past MHWs identified at the surface and selected depths of the upper Mediterranean Sea. To this end, a high-resolution satellite product and a hindcast simulation, performed with a high-resolution, fully-coupled, regional climate system model (RCSM) are used.

## 3.2 Materials and Methods

### 3.2.1 Model and Simulation

The numerical simulation is performed with the state-of-the-art, fully-coupled RCSM model CNRM-RCSM6 (participating to the Med-CORDEX initiative (Ruti et al., 2016)) developed in CNRM (see Somot et al. (2008); Sevault et al. (2014); Nabat et al. (2015) for previous versions). It has a 12km-resolution atmospheric and land component (ALADIN-Climate v6, 91 vertical levels, (Daniel et al., 2018)), a 50km river model (CTRIP, (Decharme et al., subm)), an interactive aerosol scheme (TACTIC, (Nabat et al., 2015)) and a 6-8km ocean model (NEMOMED12, 75 vertical levels, Beuvier et al. (2012); Hamon et al. (2016)). The coupling strategy follows Voldoire et al. (2017) with 1-hour coupling frequency (OASIS3-HCT,(Craig et al., 2017)). The ocean model domain covers the entire Mediterranean Sea and a small part of the Atlantic as a buffer zone. The Black Sea is parametrized as a freshwater flux combining the total river runoffs of its drainage area and the evaporation minus precipitation budget over the sea. The coupled model is driven by reanalysis at its lateral boundary conditions. We use ERA-Interim (Berrisford et al., 2009) to drive the atmosphere, applying a spectral nudging technique (Colin et al., 2010) and the ORAS4 (Balmaseda et al., 2013b) at the oceanic boundary conditions (temperature, salinity, and sea surface height) in the Atlantic part of the domain. Before the simulation (1982-2017), 10 years of coupled spin-up have been performed, after a 7-year ocean spin-up and a 78-year spin-up of the river routing model.

### 3.2.2 Observations

The performance of the model on the yearly extreme sea surface temperature (SST) evolution and the identification of surface MHWs, is first evaluated against daily satellite observations between 1982-2017. We use the Mediterranean Sea high-resolution (0.04°grid) L4 dataset from Copernicus Marine Service and CNR-ISAC ROME, which provides interpolated remotely-sensed surface temperatures from the AVHRR Pathfinder Version 5.2 onto a regular grid (Pisano et al., 2016). Prior to any comparisons, observations were first interpolated to the NEMOMED12 grid using the nearest neighbor method.

### 3.2.3 MHW detection method

MHW characteristics are investigated at the sea surface using satellite observations (~µm thick) and the model's first-layer depth (~1m thick) but also at 23m (~4m thick), 41m (~6m thick) and at 55m (~8.5m thick) depth, using simulated daily seawater potential temperatures. These layers represent the average depths where most of the mass mortalities of Mediterranean marine species have been observed in the past. For this study, no connection was assumed between surface and deeper events.

Individual events are detected using a MHW identification framework, defined by Darmaraki et al. (2019). For each layer separately, daily thermal anomalies are identified relative to a climatology map of the yearly 99th percentile of daily temperatures ($SST_{99Q}$ at surface or $T_{99Q}$ at depth). A locally-defined threshold is calculated for each grid point based on the 1982-2012 period and the minimum duration of local exceedances is set to 5 consecutive days. The final MHW event, however, is only registered when a minimum of 20% of the basin is found in a "MHW state", targeting that way large-scale and long-lasting, summer MHW events.

For each surface or deeper event a set of metrics, adapted from Hobday et al. (2016), is then computed, such as the frequency (number of events per year), duration (number of days above threshold), mean (Imean) and maximum (Imax) intensity (spatiotemporal mean and maximum temperature anomaly with respect to threshold over the event duration). Further, we consider the maximum event coverage (surfmax) and the cumulative intensity Icum (spatiotemporal sum of daily temperature anomalies over the event duration), which represents the severity of each MHW.

## 3.3 Results

### 3.3.1 Extreme Temperature Evolution

In general, the model appears to simulate well the extreme SST of the upper Mediterranean Sea for the 1982-2017 period. Observed basin-mean $SST_{99Q}$ variability (Fig.3.1, *bottom*) is well-captured by the model (Corr.Coeff=0.9), despite the underestimation of its positive trend (Table.3.1). Albeit the warm model bias, the observed and simulated surface threshold patterns (Fig.3.1,*top*) are also well-correlated (Corr.Coeff=0.9). On average, the southeast Mediterranean, Ionian and Tyrrhenian Sea show the highest $SST_{99Q}$ (~28-30°C), in contrast to the northwestern Mediterranean basin, Aegean and Alboran Sea that manifest the lowest $SST_{99Q}$(~24-27°C) of the period. The model's ability to represent well surface Mediterranean Sea features, gives us confidence to assume a consistent behaviour for extreme seawater temperatures ($T_{99Q}$) at depth.

Basin-mean $T_{99Q}$ timeseries (Fig.3.1,*bottom*) reveal the same constant warming (0.02°C/year) at every layer (Table.3.1). A northwest-southeast, cold (15-24°C) - warm (25-32°C) pattern of Mediterranean Sea is more evident in the $T_{99Q}$ map at 23m. At deeper layers, however, extreme temperatures between 15-20°C span the whole basin, except for the southeast Mediterranean Sea, where $T_{99Q}$ is more pronounced.

### 3.3.2 Surface MHW characteristics

A total of 29 events were identified in the observations over 1982-2017 (Table.3.1, Fig.3.2a). On average, they lasted around 20 days, showed an Imean of about 0.6°C and covered a maximum of 44% of the Mediterranean basin. The simulated surface events exhibited severity and maximum

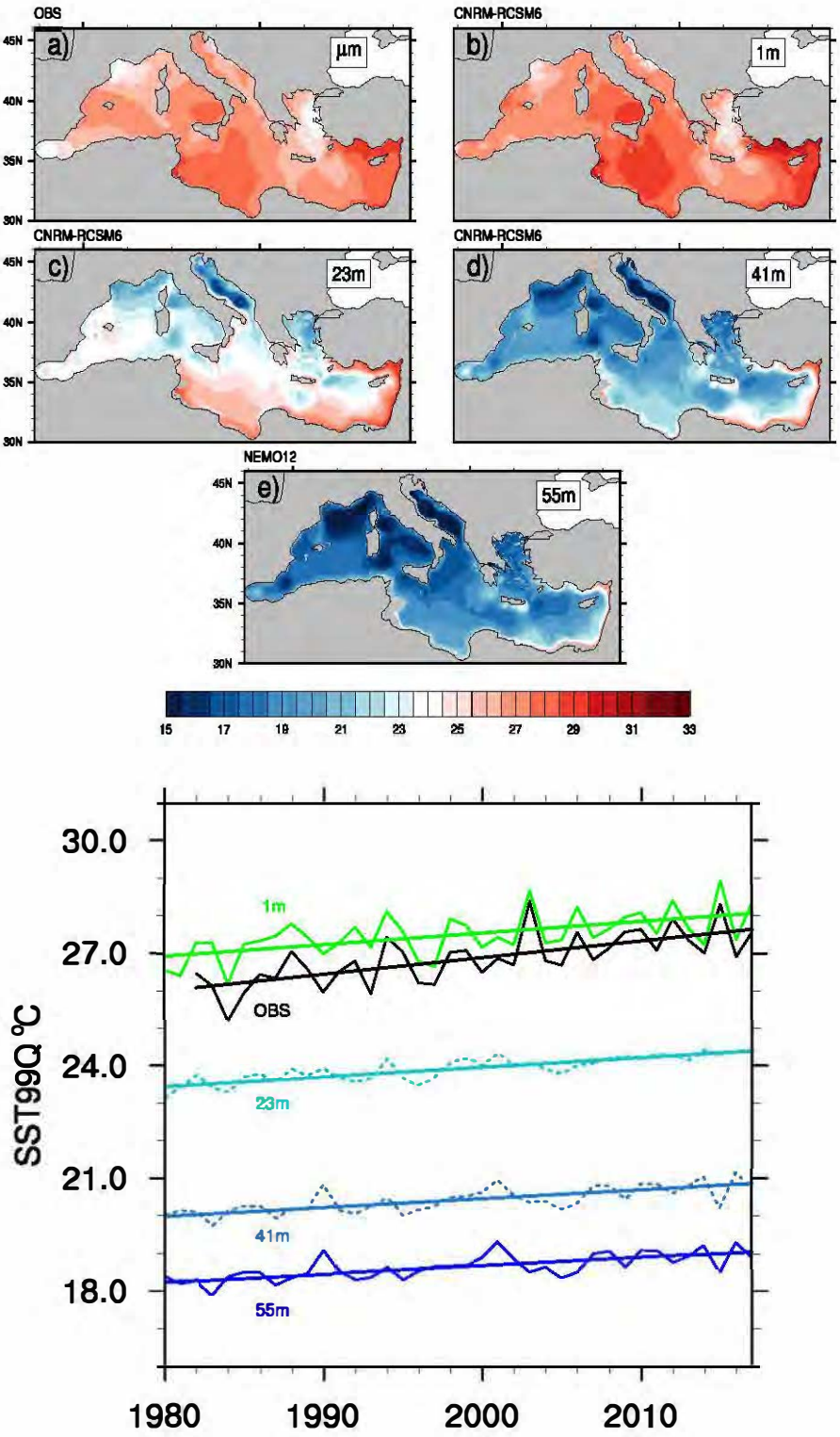


Figure 3.1: *(top)* Threshold maps ($\overline{SST_{99Q}}$,$\overline{T_{99Q}}$ over 1982-2012), for the observations (a) and the model at surface (b) and at depth (23m (c), 41m (d), 55m (e)). *(bottom)* Annual, basin-mean observed and simulated $SST_{99Q}$ and $T_{99Q}$ trends for 1980-2017 for the different layers.

spatial coverage within the observed range but with an underestimated tendency (Fig.3.2b). More events were simulated though, with slightly (higher)lower (Imean and Imax)duration values. Observed and modelled MHWs are characterized by significant (at the 95%), positive trends in all their properties (except for simulated Icum). Despite trends of the latter are

underestimated, overall the main observed MHW characteristics are well-captured.

Despite some differences in the mean behaviour, there is a good correspondence between the individual events captured by both datasets (Fig.3.2a,b). Only a few cases of less severe (0-10*$10^6$°C.days.km$^2$) MHWs did not match between them (1983,1987,1991,2005,2011,2016). The majority of severe events occurred after they year 2000 with the MHWs of 2003, 2012 and 2015 standing out as the most severe ones. Their simulated/observed duration is found at (48)48, (34)40 and (59)63 days, while their Imean at (~0.8)0.9°C, (~0.6)0.7°C and (~0.9)0.9°C, respectively (see Supplementary Material,Table.S1, Table.S2). In the model world, surface MHW of 2015 displayed the highest duration, severity (70.5*$10^6$°C.days.km$^2$) and maximum spatial coverage (~82%) of the period, while the MHW of 2010 the highest Imean (~0.9 °C). By contrast, observed highest Imean, severity (88*$10^6$°C.days.km$^2$) and spatial coverage (89%) of the period corresponded to the MHW of 2003 and the highest duration to the 2015 event.

### 3.3.3 Subsurface MHW characteristics

Relative to surface events, frequency and maximum spatial coverage of subsurface MHWs reduce, as we go deeper in the water column (see Table.3.1, Fig.2 and also Table.S3-S4). Conversely, their Imean increases. They are also characterised by higher ensemble-mean Icum, even though there are no deep events as severe as the surface MHWs of 2003, 2012 and 2015 (Table.3.1). This mean behaviour may seem counterintuitive, but it can be explained by the longer, on average, durations of events at depth (30-35 days) than at the surface (14-20 days). It is also notable, that Imax at depth are, on average, higher than at the surface. The highest/lowest mean duration of the period is found for the group of events at 55m depth/surface and the highest/lowest mean surfmax at surface/41m depth.

Individually, the most distinct MHWs at depth occur in different years from those at surface (Fig.3.2c-e). For example, the subsurface MHW 2014 was the longest (50 days), most severe (29*$10^6$ °C.days.km$^2$) and spatially largest (~43%) event of the period at 23m. Similarly, the subsurface MHW 2001 was found as the longest (53-64 days) and most severe event (32-33*$10^6$ °C.days.km$^2$) at 41m and 55m, featuring also the greatest surfmax at 55m (~45%). The greatest mean intensities though, were seen in 2015 (0.76°C), 1990 (0.95°C) and 2010 (0.78°C) events at 23m, 41m and 55m respectively. It is interesting, that the longest deep event occurred at 55m (2001) and lasted as much as the longest surface event (2015), covering, however, at peak half of its area. Likewise, the most intense MHW at depth occurred at 41m (1990), with an Imean slightly higher than the most intense surface MHW (2010), but covered a smaller area (see SM, Table S3-S4). As opposed to their mean duration, severity and frequency, the rest of the subsurface MHW properties and their positive trends do not show a monotonic variation with depth. For instance, at 41m average Imean and Imax appear higher than at 55m but average severity is similar.

As opposed to their duration and frequency, subsurface MHWs do not show a monotonic

variation with depth in the rest of their properties. For instance, at 41m average Imean and Imax appear higher than at 55m but average severity remains the same. On the other hand, the positive trends in their characteristics appear to decrease with depth.

| Characteristics | Satellite Observations | NEMOMED12 Surface | NEMOMED12 23m | NEMOMED12 41m | NEMOMED12 55m |
|---|---|---|---|---|---|
| Temperature Evaluation (1982-2017) | | | | | |
| SST99Q,T99Q (°C) | 26.9±0.2 | 27.5±0.1 | 23.9±0.1 | 20.4±0.1 | 18.7±0.1 |
| SST99Q,T99Q Timeseries Trend (°C/year) | **44.0*10$^{-3}$** | **30.7*10$^{-3}$** | **25.7*10$^{-3}$** | **23.6*10$^{-3}$** | **22.2*10$^{-3}$** |
| Average Marine Heatwave Characteristics (1982-2017) | | | | | |
| Number of MHWs | 29 | 31 | 21 | 15 | 14 |
| Imean (°C) | (57.1±06.2)*10$^{-2}$ | (64.8±05.5)*10$^{-2}$ | (68.1±02.2)*10$^{-2}$ | (81.2±04.2)*10$^{-2}$ | (69.4±02.4)*10$^{-2}$ |
| Imean Trend (°C/year) | **18.1*10$^{-3}$** | 10.0*10$^{-3}$ | **20.2*10$^{-3}$** | **20.7*10$^{-3}$** | **18.8*10$^{-3}$** |
| Duration (Days) | 20.4±5.5 | 14.1±4.8 | 29.4±4.80 | 30.2±7.4 | 35.8±10.1 |
| Duration Trend (Days/year) | **79.9*10$^{-2}$** | 40.0*10$^{-2}$ | **11.6*10$^{-1}$** | **10.1*10$^{-1}$** | **11.1*10$^{-1}$** |
| Icum (°C.days.km$^2$) | 15.1±8.0 | 10.4±5.8 | 13.6±2.9 | 15.3±4.5 | 15.4±5.1 |
| Icum Trend (°C.days.km$^2$/year) | **68.3*10$^4$** | 40.5*10$^4$ | **56.9*10$^4$** | **51.2*10$^4$** | **48.0*10$^4$** |
| Max Surface (%) | 44.1±7.9 | 37.3±6.9 | 30.1±2.3 | 27.2±2.3 | 28.4±3.4 |
| Max Surface Trend(%/year) | **15.0*10$^{-1}$** | 77.7*10$^{-2}$ | **10.1*10$^{-1}$** | **77.1*10$^{-2}$** | **78.9*10$^{-2}$** |
| Imax (°C) | 3.0±0.6 | 3.7±0.7 | 4.3±0.4 | 4.6±0.4 | 4.4±0.3 |
| Imax Trend (°C/year) | **10.8*10$^{-2}$** | **96.4*10$^{-3}$** | **14.5*10$^{-2}$** | **12.4*10$^{-2}$** | **12.1*10$^{-2}$** |

Table 3.1: Basin-mean, extreme temperature evolution at surface $\overline{SST_{99Q}}$ and at depth $\overline{T_{99Q}}$ over 1982-2017. Shown here also, are the domain-averaged mean surface and subsurface MHW frequency, Imean, Duration, Severity (Icum), Surfmax and Imax and error bar at 95% confidence level for every layer. Linear trends of domain-averaged timeseries with statistical significance higher than 95% level are indicated in bold.

### 3.3.4 MHW Seasonality

Examination of MHW timing revealed a seasonality in their occurrence, depending on the depth. Surface MHWs were detected between July-September (Fig.3.2f). Subsurface events at 23m followed between September-October, at 41m between October-November, and at 55m depth from mid-October to mid-December. Whether subsurface MHWs are always concomitant

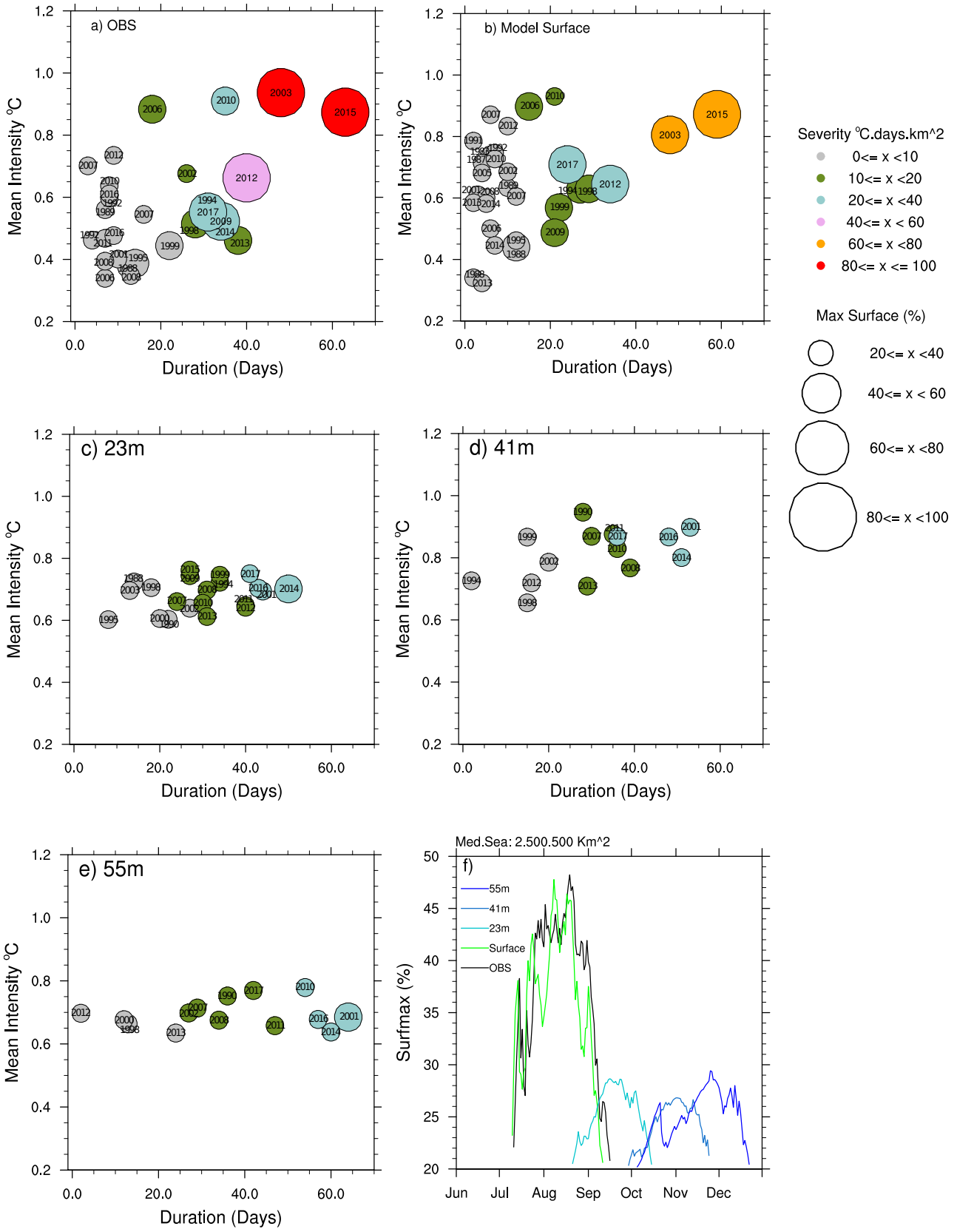


Figure 3.2: Individual MHW characteristics at surface and different depths (a-e). Color scale corresponds to severity (*$10^6$°C.days.km$^2$) and size of the bubbles to surfmax. Daily average surfmax for 1982-2017 is also depicted (f) at different layers in relation to event timing.

to the identified surface events in the same year is a hypothesis that was not investigated here. However, it is worth noting that most of the time a surface MHW was followed by a higher- or lower-intensity subsurface event and only 7(2) years exhibited MHWs only at surface (depth) (Table. S1-S4).

### 3.3.5 MHW Spatial Distribution

The spatial distribution of the average event Imean during 1982-2017 seems to vary slightly between the different depths (Fig.3.3, *top*). In general, most parts of the Mediterranean Sea show Imean between ~0.3°C and ~0.9°C at every layer. North Mediterranean regions display the most pronounced surface Imean (~1°C) both in the model and the observations. In deeper layers they only sustain a local MHW intensification (~1°C-1.7°C) that is displaced southwards with depth. In fact, the highest Imean at depth (~1°C-2°C) emerges in the Levantine, Ionian and southwestern basins. By contrast, in the corresponding patterns of mean event duration at surface, most of the areas experience MHWs for 8-13 days, except for the Levantine basin (~20-70 days) and some parts of the Aegean (~20 days) (Fig.3.3,*bottom*), whose duration is underestimated by the model. Average MHW duration appears to increase progressively from 20 days at 23m (in the Levantine basin and some regions around the northwestern Mediterranean, Ionian and Adriatic Sea) to 20-50 days almost everywhere, but far from boundary currents, in deeper layers. Surprisingly, there also seem to be specific spots in the Alboran, Ionian and Tyrrhenian Sea, which sustain MHWs between 8-13 days and others that are under MHWs for 60-167 days.

By contrast, the corresponding patterns of the average number of MHW days/event during that period reveals marked differences with depth (Fig.3.3,*right*). At surface, most of the regions seem to experience MHWs for 8-13 days, with the model underestimating their average duration around Levantine basin (~10-20 days instead of ~20-70 days) and some parts of the Aegean (~8 days instead of ~20 days). At 23m depth, Levantine basin and some regions around the northwestern Mediterranean, Ionian and Adriatic Sea are subjected to MHWs for about 20 days. As we go deeper, temperature anomalies are spreading even more to these areas and the Aegean Sea, reaching from 20-37 days at 41m to 20-50 days at 55m.

It is interesting to note that as far as the Western Mediterranean Sea is concerned, from the surface up to 23m depth, it is characterised by the most intense but infrequent events. This implies long durations of MHWs which can be especially harmful for marine ecosystems of the region.

## 3.4 Discussion

Despite the model's mean warm bias and underestimated temperature trend with respect to observations, MHW identification at the sea surface appeared consistent in both datasets. In particular, almost every event identified up to 2013 in the datasets correspond to years with

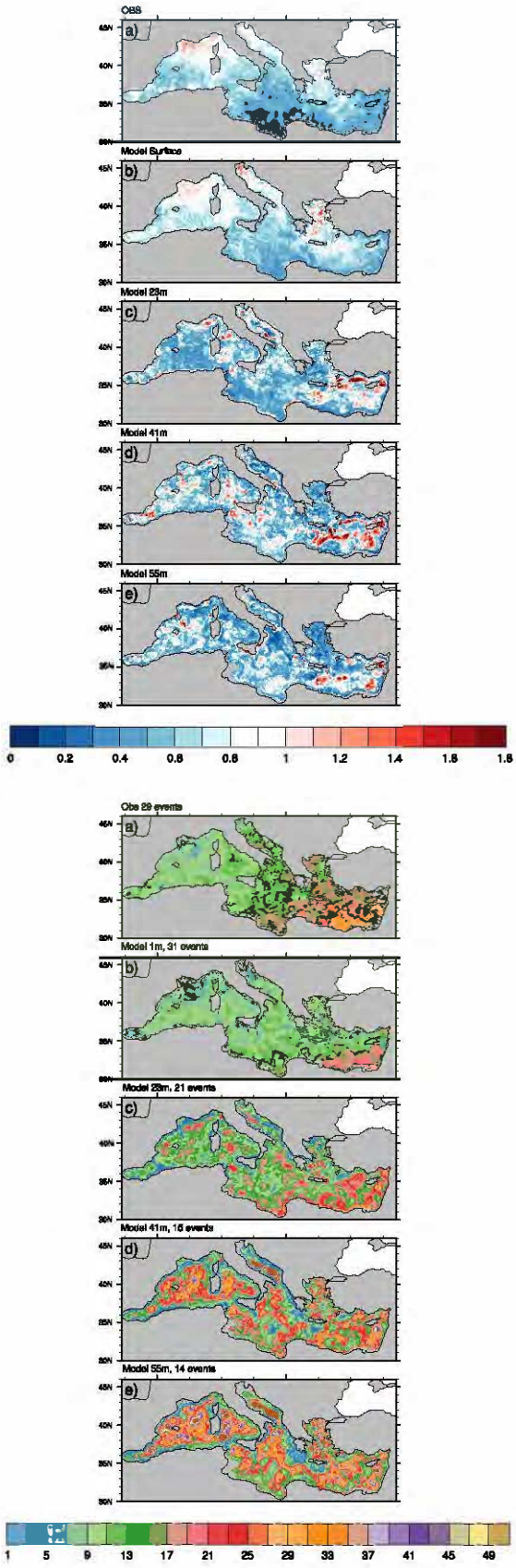


Figure 3.3: Average MHW Imean (°C) *(top)* and duration (days) *(bottom)* over 1982-2017, for the observations and the model, normalised by the number of event at each layer.

documented regional, thermal-stress related mass mortalities of marine species in the basin, whereas events identified after 2014 have not yet been discussed in the literature. Inconsistencies with respect to observed events may emerge due to the 20% minimum spatial threshold, which can inhibit the identification of smaller-scale MHWs. On the other hand, there may also be events identified here that were not observed in real-time. Surprisingly at those depths, there seem to be specific spots in the Alboran, Ionian and Tyrrenian Sea, which sustain MHWs between 8-13 days and others that are under MHWs for 60-167 days.

For the first time to our knowledge, summer Mediterranean MHWs were also investigated at different depths. Individually, they can be as long as and as intense as surface MHWs, but not as frequent and large in terms of spatial coverage. The excess heat at depth seems to accumulate in smaller regions, which could also explain the higher, on average, Imean, Imax values displayed at depth relative to the surface. The deep-layer disconnection from the air-sea exchanges allows for the long-term preservation of the heat content during the vertical MHW propagation, due to the low-frequency variability of the ocean interior, especially if no strong mixing occurs. Therefore, the longest MHW durations are found at 55m depth, far from boundary currents. As far as Imax is concerned, its increase with depth could be also linked to larger temperature variations as a result of the thermocline in agreement with Schaeffer and Roughan (2017).

In principle, for this study, surface MHWs were not associated with subsurface events. However, on a given year, the latter most of the times was concomitant to the former, especially towards the end of the period (Table.S1-S4), following the seasonal MLD deepening (Houpert et al., 2015). If a connection is to be assumed, then surface temperature anomalies developed during the summer could propagate into the water column when it is weakly stratified. Through mechanical mixing due to wind, they could reach progressively 23m and 41m during autumn and 55m in December. In particular, wind conditions may explain how (more)less intense deep events followed surface MHWs with Imean between (~0.3-0.7°C)~0.7-0.9°C respectively (see SM, Fig.1), explaining also the patterns of Fig.3.2(a-e). In the first case, for a given year, moderate wind speeds could decrease heat at the sea surface, reducing surface MHW intensities, transporting, however the energy below surface, intensifying thus, MHWs at depth. On the other hand, years with less intense or no deep MHWs at all following a surface event, could be related to two factors: 1) Strong stratification in the upper ocean, due to low wind, which intensifies surface MHWs to the expense of deeper events 2) Strong wind speeds during the autumn and winter season that does not allow summer MHWs to propagate later deeper in the water column. The cooling effect of surface latent heat flux in that case would damp warm anomalies. This is in line with Sparnocchia et al. (2006) and Schaeffer and Roughan (2017), which have already underlined the role of wind in modulating MHW properties.

Although our study highlights that intense ($>T_{99Q}$) temperature anomalies in the open ocean occur within the MLD at large scales, they may also fall below MLD at local scales (e.g. shelf) or at large scales but with more attenuated anomalies ($<T_{99Q}$). The similar mean

intensities and higher local Imax of deeper events with respect to surface ones may also indicate a higher heat content of subsurface MHWs, especially since they affect at peak a significantly lower percentage of surface. For a better understanding of this, however, further analysis of the heat content of specific events is required, which is out of the scope of this study.

## 3.5 Conclusions

We have identified Marine Heatwaves (MHW) at surface and at 3 ecosystem-relevant depths of the Mediterranean Sea between 1982-2017, by applying a MHW detection algorithm on a hindcast simulation performed with the latest version of the CNRM regional climate system model CNRM-RCSM6. Comparisons with a high-resolution satellite product show that the model is able to reproduce well extreme Mediterranean Sea surface features of that period. Despite an underestimation of their mean characteristics with respect to observed events, individual event identification was consistent between the model, the observations and the existing literature. Following a significant increase in extreme SST with time, simulated surface MHWs, on average, last around 14 days, with a mean intensity of 0.6°C and a spatial coverage of around 37% of the basin. MHWs become longer, more severe and spatially extended with time and MHWs of 2003, 2012 and 2015 are identified as the most severe surface events of the period.

We have also investigated subsurface MHWs and their evolution at 23m, 41m and 55m. Despite a reduction of extreme temperatures with depth, subsurface events are characterised, on average, by higher mean and maximum intensity and severity relative to surface MHWs, probably due to their longer durations. However, they display, on average, lower frequency and spatial coverage. Their occurrence appears to follow the seasonal mixed layer depth deepening, while the most severe deep events were identified in 2001 and 2014. North Mediterranean areas seem more vulnerable to higher mean MHW intensities at surface, whereas southern regions seem more prone to them as we go deeper in the water column. Long-lasting events on the other hand, appear to affect mostly the Levantine region at surface and spread all over the basin but far from boundary currents in deeper layers. For this study no relation was assumed between the surface and subsurface MHWs. Dedicated analysis on specific events is further required to better understand the mechanisms behind the vertical extension and heat content evolution of a MHW from the surface to depth.

## 3.6 Supplementary Material

| Years | OBSERVATIONS | | | | | | |
|---|---|---|---|---|---|---|---|
| | Start Day | End Day | Imean | Surface | Duration | Icum | Imax |
| 1982 | | | | | | | |
| 1983 | | | | | | | |
| 1984 | | | | | | | |
| 1985 | | | | | | | |
| 1986 | | | | | | | |
| 1987 | | | | | | | |
| 1988 | 224 (Aug) | 236 (Aug) | 0.38 | 48.78 | 13 | 4.6 | 2.80 |
| 1989 | 231 (Aug) | 237 (Aug) | 0.56 | 24.00 | 7 | 2.3 | 1.99 |
| 1990 | | | | | | | |
| 1991 | | | | | | | |
| 1992 | 214 (Aug) | 221 (Aug) | 0.60 | 24.89 | 8 | 2.9 | 2.49 |
| 1992 | 235 (Aug) | 238 (Aug) | 0.46 | 21.59 | 4 | 0.9 | 1.85 |
| 1993 | | | | | | | |
| 1994 | 215 (Aug) | 245 (Sep) | 0.56 | 53.54 | 31 | 19.6 | 2.76 |
| 1995 | 209 (Jul) | 222 (Aug) | 0.39 | 48.95 | 14 | 5.1 | 2.30 |
| 1996 | | | | | | | |
| 1997 | | | | | | | |
| 1998 | 214 (Aug) | 241 (Aug) | 0.51 | 40.05 | 28 | 11.9 | 2.69 |
| 1999 | 227 (Aug) | 248 (Sep) | 0.44 | 51.99 | 22 | 9.0 | 2.24 |
| 2000 | | | | | | | |
| 2001 | 237 (Aug) | 246 (Sep) | 0.40 | 24.93 | 10 | 2.3 | 1.82 |
| 2002 | 212 (Jul) | 237 (Aug) | 0.68 | 29.33 | 26 | 10.9 | 5.05 |
| 2003 | 201 (Jul) | 248 (Sep) | 0.94 | 89.88 | 48 | 88.9 | 3.79 |
| 2004 | | | | | | | |
| 2005 | | | | | | | |
| 2006 | 202 (Jul) | 219 (Aug) | 0.88 | 54.97 | 18 | 16.8 | 4.07 |
| 2006 | 234 (Aug) | 240 (Aug) | 0.34 | 25.98 | 7 | 1.4 | 1.40 |
| 2007 | 207 (Jul) | 209 (Jul) | 0.70 | 20.59 | 3 | 1.1 | 2.37 |
| 2007 | 233 (Aug) | 248 (Sep) | 0.54 | 33.99 | 16 | 6.9 | 2.38 |
| 2008 | 216 (Aug) | 222 (Aug) | 0.39 | 31.98 | 7 | 1.9 | 1.58 |
| 2008 | 240 (Aug) | 252 (Sep) | 0.35 | 23.63 | 13 | 2.5 | 1.53 |
| 2009 | 217 (Aug) | 250 (Sep) | 0.52 | 75.61 | 34 | 26.2 | 3.41 |
| 2010 | 198 (Jul) | 205(Jul) | 0.64 | 28.59 | 8 | 3.3 | 2.25 |
| 2010 | 217 (Aug) | 251 (Sep) | 0.91 | 57.34 | 35 | 29.6 | 3.76 |
| 2011 | 234 (Aug) | 240 (Aug) | 0.47 | 32.71 | 7 | 2.4 | 2.47 |
| 2012 | 191 (Jul) | 199 (Jul) | 0.73 | 39.50 | 9 | 5.3 | 3.35 |
| 2012 | 210 (Jul) | 249 (Sep) | 0.66 | 88.56 | 40 | 41.4 | 2.81 |
| 2013 | 206 (Jul) | 243 (Aug) | 0.46 | 50.59 | 38 | 14.8 | 3.41 |
| 2014 | 223 (Aug) | 257 | 0.53 | 42.95 | 35 | 15.6 | 3.06 |
| 2015 | 196 (Jul) | 258 (Sep) | 0.87 | 88.81 | 63 | 84.0 | 10.73 |
| 2016 | 216 (Aug) | 224 (Aug) | 0.48 | 23.34 | 9 | 2.4 | 2.29 |
| 2016 | 234 (Aug) | 241 (Aug) | 0.61 | 23.68 | 8 | 2.8 | 2.76 |
| 2017 | 211 (Jul) | 241 (Aug) | 0.55 | 77.07 | 31 | 20.7 | 3.18 |

Table 3.2: Marine Heatwave characteristics at the Mediterranean Sea surface as identified from the satellite dataset during 1982-2017. Here shown are, Starting day (calendar day), Ending day (calendar day), Imean (°C), surfmax (%), duration (Days), Severity*$10^6$ (°C.days.km$^2$) and Imax (°C) of every event separately.

| Years | SURFACE | | | | | | |
|---|---|---|---|---|---|---|---|
| | Start Day | End Day | Imean | Surface | Duration | Icum | Imax |
| 1982 | | | | | | | |
| 1983 | 206 (Jul) | 211 (Jul) | 0.74 | 24.32 | 6 | 2.5 | 3.00 |
| 1984 | | | | | | | |
| 1985 | | | | | | | |
| 1986 | | | | | | | |
| 1987 | 204 (Jul) | 207 (Jul) | 0.71 | 25.89 | 4 | 1.8 | 3.00 |
| 1988 | 215 (Aug) | 216 (Aug) | 0.34 | 20.46 | 2 | 0.3 | 1.58 |
| 1988 | 223 (Aug) | 234 (Aug) | 0.44 | 52.23 | 12 | 5.5 | 2.35 |
| 1989 | 229 (Aug) | 238 (Aug) | 0.63 | 32.33 | 10 | 4.5 | 2.12 |
| 1990 | | | | | | | |
| 1991 | 238 (Aug) | 239 (Aug) | 0.78 | 20.34 | 2 | 0.8 | 1.98 |
| 1992 | 214 (Aug) | 220 (Aug) | 0.75 | 28.16 | 7 | 3.4 | 2.70 |
| 1993 | | | | | | | |
| 1994 | 212 (Jul) | 238 (Aug) | 0.63 | 54.98 | 27 | 19.6 | 5.48 |
| 1995 | 209 (Jul) | 220 (Aug) | 0.46 | 36.15 | 12 | 4.3 | 1.77 |
| 1996 | | | | | | | |
| 1997 | | | | | | | |
| 1998 | 212 (Jul) | 240 (Aug) | 0.63 | 44.15 | 29 | 16.0 | 2.82 |
| 1999 | 221 (Aug) | 242 (Aug) | 0.57 | 51.81 | 22 | 12.4 | 2.79 |
| 2000 | | | | | | | |
| 2001 | 221 (Aug) | 223 (Aug) | 0.61 | 22.28 | 3 | 1.0 | 2.24 |
| 2002 | 213 (Aug) | 222 (Aug) | 0.68 | 23.12 | 10 | 3.7 | 4.47 |
| 2003 | 199 (Jul) | 246 (Sep) | 0.80 | 78.76 | 48 | 60.5 | 6.45 |
| 2004 | | | | | | | |
| 2005 | 211 (Jul) | 214 (Aug) | 0.68 | 22.48 | 4 | 1.5 | 2.35 |
| 2006 | 202 (Jul) | 216 (Aug) | 0.90 | 52.79 | 15 | 14.4 | 3.92 |
| 2006 | 232 (Aug) | 237 (Aug) | 0.50 | 22.33 | 6 | 1.7 | 2.83 |
| 2007 | 205 (Jul) | 210 (Jul) | 0.87 | 24.19 | 6 | 3.1 | 3.35 |
| 2007 | 234 (Aug) | 245 (Sep) | 0.60 | 24.96 | 12 | 4.3 | 8.00 |
| 2008 | 236 (Aug) | 240 (Aug) | 0.60 | 22.27 | 5 | 1.6 | 2.90 |
| 2009 | 227 (Aug) | 247 (Sep) | 0.49 | 47.66 | 21 | 10.4 | 2.73 |
| 2010 | 197 (Jul) | 203 (Jul) | 0.73 | 31.37 | 7 | 3.8 | 3.18 |
| 2010 | 222 (Aug) | 242 (Aug) | 0.93 | 31.45 | 21 | 14.4 | 7.54 |
| 2011 | | | | | | | |
| 2012 | 190 (Jul) | 199 (Jul) | 0.83 | 38.09 | 10 | 6.1 | 3.49 |
| 2012 | 208 (Jul) | 241 (Aug) | 0.64 | 78.01 | 34 | 29.2 | 10.12 |
| 2013 | 217 (Aug) | 218 (Aug) | 0.58 | 20.69 | 2 | 0.6 | 2.40 |
| 2013 | 233 (Aug) | 236 (Aug) | 0.32 | 20.78 | 4 | 0.7 | 2.01 |
| 2014 | 223 (Aug) | 227 (Aug) | 0.58 | 24.67 | 5 | 1.7 | 3.30 |
| 2014 | 234 (Aug) | 240 (Aug) | 0.44 | 22.17 | 7 | 1.7 | 5.92 |
| 2015 | 195 (Jul) | 253 (Sep) | 0.87 | 81.73 | 59 | 70.5 | 4.20 |
| 2016 | | | | | | | |
| 2017 | 211 (Jul) | 234 (Aug) | 0.71 | 72.26 | 24 | 21.7 | 3.48 |

Table 3.3: As in Table.3.2 but for surface MHWs identified from the model during 1982-2017.

| Years | Model 23m depth | | | | | | |
|---|---|---|---|---|---|---|---|
| | Start Day | End Day | Imean | Surface | Duration | Icum | Imax |
| 1982 | | | | | | | |
| 1983 | | | | | | | |
| 1984 | | | | | | | |
| 1985 | | | | | | | |
| 1986 | | | | | | | |
| 1987 | | | | | | | |
| 1988 | 248(Sep) | 261 (Sep) | 0.72 | 26.34 | 14 | 6.0 | 3.99 |
| 1989 | | | | | | | |
| 1990 | 253 (Sep) | 274 (Oct) | 0.60 | 23.69 | 22 | 7.3 | 3.32 |
| 1991 | | | | | | | |
| 1992 | | | | | | | |
| 1993 | | | | | | | |
| 1994 | 251 (Sep) | 284 (Oct) | 0.72 | 29.03 | 34 | 16.2 | 4.16 |
| 1995 | 256 (Sep) | 263 (Sep) | 0.60 | 21.04 | 8 | 2.5 | 3.06 |
| 1996 | | | | | | | |
| 1997 | | | | | | | |
| 1998 | 247 (Sep) | 264 (Sep) | 0.70 | 28.81 | 18 | 8.1 | 4.20 |
| 1999 | 248 (Sep) | 281 (Oct) | 0.74 | 35.45 | 34 | 18.6 | 4.33 |
| 2000 | 250 (Sep) | 269 (Sep) | 0.60 | 24.57 | 20 | 7.0 | 3.42 |
| 2001 | 243 (Aug) | 286 (Oct) | 0.69 | 34.20 | 44 | 21.9 | 3.98 |
| 2002 | 243 (Aug) | 269 (Sep) | 0.64 | 24.73 | 27 | 9.7 | 3.97 |
| 2003 | 252 (Sep) | 264 (Sep) | 0.70 | 24.11 | 13 | 5.1 | 4.13 |
| 2004 | | | | | | | |
| 2005 | | | | | | | |
| 2006 | | | | | | | |
| 2007 | 242 (Aug) | 265 (Sep) | 0.66 | 29.54 | 24 | 10.1 | 5.34 |
| 2008 | 239 (Aug) | 269 (Sep) | 0.70 | 34.32 | 31 | 15.3 | 5.76 |
| 2009 | 248 (Sep) | 274 (Oct) | 0.74 | 28.40 | 27 | 12.1 | 3.75 |
| 2010 | 243 (Aug) | 272 (Sep) | 0.65 | 29.90 | 30 | 12.7 | 4.37 |
| 2011 | 241 (Aug) | 280 (Oct) | 0.65 | 35.66 | 40 | 18.2 | 4.44 |
| 2012 | 242 (Aug) | 281 (Oct) | 0.64 | 27.10 | 40 | 15.6 | 6.42 |
| 2013 | 245 (Sep) | 275 (Oct) | 0.61 | 28.59 | 31 | 11.8 | 3.79 |
| 2014 | 238 (Aug) | 287 (Oct) | 0.70 | 42.75 | 50 | 29.2 | 4.02 |
| 2015 | 246 (Sep) | 272 (Sep) | 0.76 | 30.62 | 27 | 13.2 | 3.95 |
| 2016 | 237 (Aug) | 279 (Oct) | 0.70 | 35.43 | 43 | 21.3 | 5.40 |
| 2017 | 232 (Aug) | 272 (Sep) | 0.75 | 37.55 | 41 | 22.6 | 5.38 |

Table 3.4: As in Table.3.3 but for MHWs identified from the model at 23m during 1982-2017.

| Years | Model 41m depth | | | | | | |
|---|---|---|---|---|---|---|---|
| | Start Day | End Day | Imean | Surface | Duration | Icum | Imax |
| 1982 | | | | | | | |
| 1983 | | | | | | | |
| 1984 | | | | | | | |
| 1985 | | | | | | | |
| 1986 | | | | | | | |
| 1987 | | | | | | | |
| 1988 | | | | | | | |
| 1989 | | | | | | | |
| 1990 | 291 (Oct) | 318 (Nov) | 0.95 | 26.81 | 28 | 15.4 | 5.40 |
| 1991 | | | | | | | |
| 1992 | | | | | | | |
| 1993 | | | | | | | |
| 1994 | 312 (Nov) | 313 (Nov) | 0.72 | 20.25 | 2 | 0.7 | 3.48 |
| 1995 | | | | | | | |
| 1996 | | | | | | | |
| 1997 | | | | | | | |
| 1998 | 298 (Oct) | 312 (Nov) | 0.65 | 22.03 | 15 | 5.1 | 3.39 |
| 1999 | 300 (Oct) | 314 (Nov) | 0.87 | 22.53 | 15 | 6.7 | 4.60 |
| 2000 | | | | | | | |
| 2001 | 271 (Sep) | 323 (Nov) | 0.90 | 34.44 | 53 | 32.4 | 5.35 |
| 2002 | 291 (Oct) | 310 (Nov) | 0.78 | 23.04 | 20 | 8.4 | 4.06 |
| 2003 | | | | | | | |
| 2004 | | | | | | | |
| 2005 | | | | | | | |
| 2006 | | | | | | | |
| 2007 | 284 (Oct) | 313 (Nov) | 0.87 | 29.07 | 30 | 16.2 | 5.26 |
| 2008 | 283 (Oct) | 321 (Nov) | 0.77 | 24.76 | 39 | 16.9 | 4.37 |
| 2009 | | | | | | | |
| 2010 | 284 (Oct) | 319 (Nov) | 0.83 | 29.11 | 36 | 18.3 | 5.53 |
| 2011 | 281 (Oct) | 315 (Nov) | 0.88 | 26.35 | 35 | 18.0 | 4.42 |
| 2012 | 308 (Nov) | 323 (Nov) | 0.72 | 22.57 | 16 | 6.0 | 3.67 |
| 2013 | 295 (Oct) | 323 (Nov) | 0.72 | 29.39 | 29 | 12.4 | 4.34 |
| 2014 | 275 (Oct) | 325 (Nov) | 0.80 | 30.51 | 51 | 25.5 | 4.49 |
| 2015 | | | | | | | |
| 2016 | 280 (Oct) | 327 (Nov) | 0.87 | 34.76 | 48 | 27.5 | 5.69 |
| 2017 | 280 (Oct) | 315 (Nov) | 0.87 | 32.28 | 36 | 20.1 | 5.30 |

Table 3.5: As in Table.3.3 but for MHWs identified from the model at 41m during 1982-2017.

| Years | Model 55m depth | | | | | | |
|---|---|---|---|---|---|---|---|
| | Start Day | End Day | Imean | Surface | Duration | Icum | Imax |
| 1982 | | | | | | | |
| 1983 | | | | | | | |
| 1984 | | | | | | | |
| 1985 | | | | | | | |
| 1986 | | | | | | | |
| 1987 | | | | | | | |
| 1988 | | | | | | | |
| 1989 | | | | | | | |
| 1990 | 304 (Oct) | 339 (Dec) | 0.75 | 27.34 | 36 | 15 | 4.77 |
| 1991 | | | | | | | |
| 1992 | | | | | | | |
| 1993 | | | | | | | |
| 1994 | | | | | | | |
| 1995 | | | | | | | |
| 1996 | | | | | | | |
| 1997 | | | | | | | |
| 1998 | 315 (Nov) | 327 (Nov) | 0.66 | 23.20 | 13 | 4.4 | 4.08 |
| 1999 | | | | | | | |
| 2000 | 330 (Nov) | 341(Dec) | 0.68 | 22.34 | 12 | 4.1 | 3.28 |
| 2001 | 277 (Oct) | 340 (Dec) | 0.68 | 44.64 | 64 | 32.8 | 5.26 |
| 2002 | 311 (Nov) | 337 (Dec) | 0.70 | 26.12 | 27 | 10.7 | 4.21 |
| 2003 | | | | | | | |
| 2004 | | | | | | | |
| 2005 | | | | | | | |
| 2006 | | | | | | | |
| 2007 | 309 (Nov) | 337 (Dec) | 0.71 | 28,.21 | 29 | 12.3 | 4.35 |
| 2008 | 311 (Nov) | 344 (Dec) | 0.67 | 27.88 | 34 | 13.4 | 4.25 |
| 2009 | | | | | | | |
| 2010 | 294 (Oct) | 347 (Dec) | 0.78 | 29.66 | 54 | 26.4 | 5,.2 |
| 2011 | 298 (Oct) | 344 (Dec) | 0.66 | 24.63 | 47 | 16.4 | 4.35 |
| 2012 | 337 (Dec) | 338 (Dec) | 0.70 | 20.12 | 2 | 0.6 | 3.67 |
| 2013 | 314 (Nov) | 337 (Dec) | 0.63 | 24.56 | 24 | 8.2 | 3.24 |
| 2014 | 296 (Oct) | 355 (Dec) | 0.64 | 35.16 | 60 | 26.1 | 4.68 |
| 2015 | | | | | | | |
| 2016 | 295 (Oct) | 351 (Dec) | 0.68 | 35.85 | 57 | 27.0 | 5.14 |
| 2017 | 298 (Oct) | 339 (Dec) | 0.77 | 27.9 | 42 | 18.4 | 4.89 |

Table 3.6: As in Table.3.3 but for MHWs identified from the model at 55m during 1982-2017.

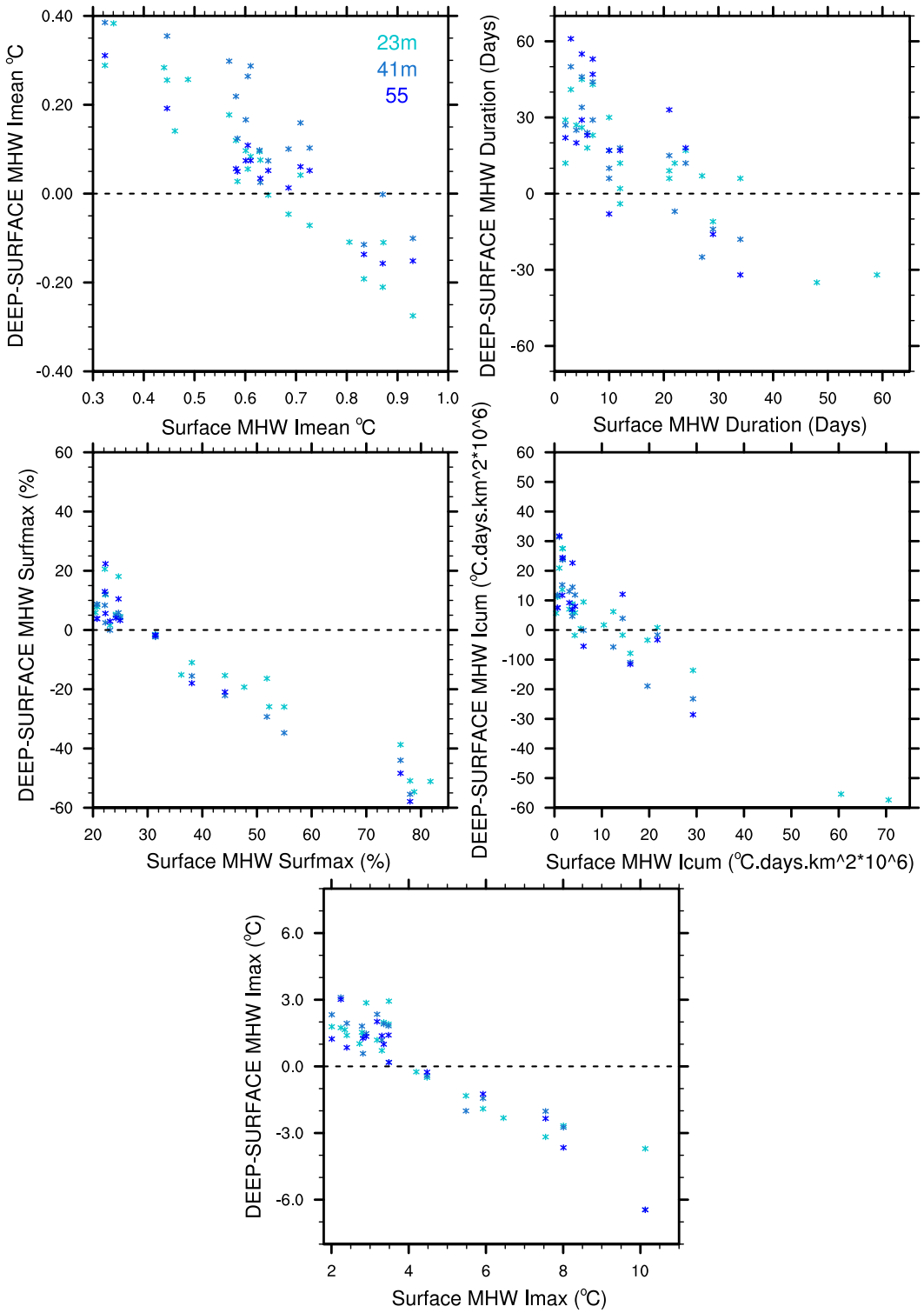


Figure 3.4: Difference between the characteristics of each subsurface MHW and its corresponding preceding surface event of a given year, versus the properties of the surface MHW. For every plot, the total number of individual subsurface MHWs identified throughout the period examined are pooled, independently from the depth where they occurred.

# Chapter 4

# Marine Heatwave 2003: Driving Mechanisms

*"Katherine Johnson knew: Once you took the first step anything was possible."*

Hidden Figures, M.L.Shetterly

## Contents

In the previous Chapter we have examined the Mediterranean MHWs occurring between 1982-2017 and their characteristics using the CNRM-RCSM6 model. In this Chapter we attempt to disentangle the driving mechanisms of the most well-known event of the period, the MHW of 2003. We will use an analysis of the mixed layer depth and atmospheric heat content during the period of its occurrence, to identify the dominant underlying forcing on a basin- but also on a regional scale. Although a well-studied event, never before in the literature the MHW 2003 has been explained using such a heat content approach. The Chapter is in the form of a paper *in preparation*.

## 4.1 Methodology

This section aims to understand the dominant driving factors behind the summer MHWs. But in order to compare the relative role of the air-sea heat flux and ocean contribution during each event we performed a temperature budget analysis using the CNRM-RCSM6 model in hindcast mode. The mixed layer (ML) heat budget was computed "online" that is to say at the model timestep frequency of 12 min while the model was running and it was stored at daily frequency. The temperature tendency equation is vertically-integrated over the ML depth whose minimum value was set to 10m throughout the Mediterranean Sea. The time rate of change in temperature T at a given location is described by the following equation:

$$\underbrace{\frac{\partial \overline{T}}{\partial t}}_{\text{Total Trend}} = \underbrace{-\overline{\boldsymbol{\nabla}(T\mathbf{u})}}_{\text{Advection}} + \underbrace{\frac{Q_{\text{net}} - Q_{\text{SW}_{(\text{-h})}}}{\rho_0 c_{\text{w}} h}}_{\text{Forcing}} + \underbrace{\overline{\boldsymbol{\nabla}_{\text{H}}(\kappa_{\text{H}} \boldsymbol{\nabla}_{\text{H}} T)}}_{\text{Lateral Diffusion}} + \underbrace{\frac{(\kappa_{\text{z}} \frac{\partial T}{\partial z})_{(\text{-h})}}{h}}_{\text{Vertical Diffusion}} - \text{Entrainment} \quad (4.1)$$

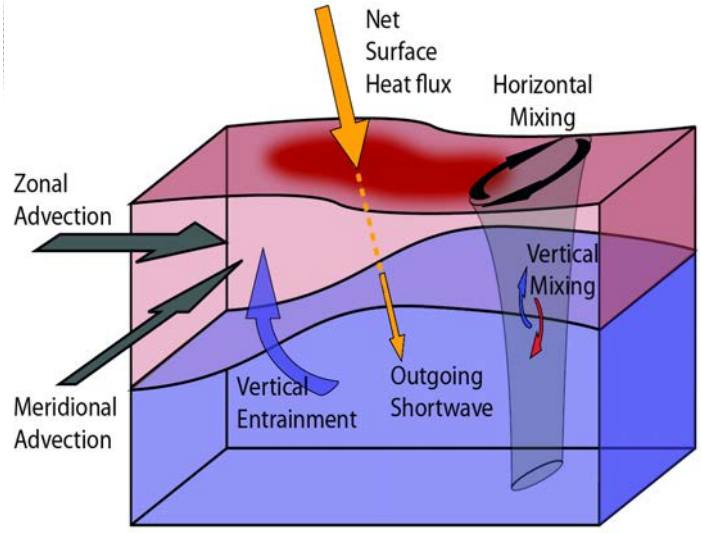


Figure 4.1: Schematic of the processes that act on the time-rate of temperature change. Based on Holbrook et al. (subm).

where $\overline{x} = \frac{1}{h}\int_{-h}^{0} x dz$, with x any variable and $h$ the mixed layer depth (MLD). The MLD is determined by the model using a vertical density profile (<0.01), with its minimum value set to 10m. $\overline{T}$ is the vertically integrated temperature over the mixed layer. Potential temperature is $T$, $\boldsymbol{u}$ is the horizontal and vertical currents, $Q_{net}$ is the net air-sea fluxes that act on the surface of the ocean while $Q_{SW}$ is the fraction of shortwave radiation at -$h$. $\kappa_h$ and $\kappa_v$ are the horizontal and vertical diffusivity coefficients respectively, $\rho_0$ is density and $c_w$ heat capacity of the water. Equation 4.1 denotes that the local change of the integrated ML temperature $\overline{T}$ (hereby names Total Trend), is affected by oceanic heat advection, the fraction of the net atmospheric forcing applied to the mixed layer (Forcing), lateral and vertical diffusion ($L_{DF}$,$Z_{DF}$) and entrainment (see also Fig.4.1). All the above terms were provided as a NEMOMED12 output from the CNRM-RCSM6 hindcast simulation of 1982-2017 (except for entrainment, see below). Due to the flux formulation of advective terms in NEMO, a physical meaning in the advection term is given when the sum of lateral and vertical advection is considered. Therefore, in Equation 4.1 a sum of all the advection components is implied in the advection term. The vertical diffusion includes both vertical diffusion and vertical component of the isoneutral mixing, while lateral diffusion is parametrized as the horizontal component of the isoneutral mixing. The remainder part in order to satisfy the MLD budget closure is the residual. We assume here, it refers to entrainment (hereby termed Entrainm) and by entrainment we consider all the processes that result in variations of the virtual MLD threshold (and therefore variations of MLD), that not include vertical transport of water. That is, we consider as entrainment the changes in the MLD that result from changes in the vertical density profile (and therefore of the position of the density threshold that defines the MLD), which partly stem from the contributions of all the terms in equation 4.1 but also from processes that are unknown so far. Indeed, its value was found zero whenever MLD was constant (except for specific coastal runoff grid points and the first day of each month that were problematic, see below). In parallel, we examined the evolution of the SST, mean temperature of the mixed layer and the MLD throughout the event duration. Finally, an error related to computational issues of the heat budget on the first day of each month, was observed but became more evident only when day-1 of a month was included in the MHW. More specifically, a "jump" on the values of each term was observed during every 1st of the month (compared to the 31st and 2nd) which was removed by reconstructing each term's 1-day (of every month) field as an average between the previous and the following day. The contribution of the corresponding error field was taken into account in the final heat budget analysis. This bug has been now corrected but not early enough to re-run a hindcast simulation in due time for the PhD.

For a complete picture of the processes at play we also decomposed the Net surface heat fluxes ($Q_{net}$) during the MHW into the sum of all the fluxes: Latent heat flux ($Q_{LH}$), sensible heat flux ($Q_{SH}$), downward shortwave radiation flux ($Q_{SWD}$), downward longwave radiation flux ($Q_{LWD}$), upward shortwave radiation flux ($Q_{SWUP}$) and upward longwave radiation flux ($Q_{LWUP}$) according to Equation 4.2. By convention, fluxes warming the ocean ($Q_{LWD}$, $Q_{SWD}$

and sometimes $Q_{SH}$) are considered positive and fluxes cooling the ocean ($Q_{LH}$, $Q_{SWUP}$, $Q_{LWUP}$ and sometimes $Q_{SH}$) negative. These fluxes are outputs of the atmospheric model (ALADIN) of CNRM-RCSM6 for the same simulation. It must be noted here that atmospheric $Q_{net}$ of equation 4.2 is slightly different from the Forcing term of equation 4.1, in that the former does not include the fraction of the solar radiation that penetrates the MLD (named $Q_{SW_{-h}}$ in eq.4.1). Before any computation atmosphere fluxes were first interpolated to NEMOMED12 grid. In addition, the 2m-air temperature and 10m windspeed (outputs from ALADIN) were also examined. Finally, every term from NEMOMED12 or ALADIN are available at daily scale in all ocean grid points.

$$Q_{\text{net}} = Q_{\text{LH}} + Q_{\text{SH}} + Q_{\text{SWD}} + Q_{\text{LWD}} + Q_{\text{SWUP}} + Q_{\text{LWUP}} \tag{4.2}$$

### 4.1.1 Temporal and Spatial Aggregation

For the identification of the ocean and atmosphere contributions during the event we examined MHW-area averaged timeseries. A MHW area is defined for every MHW by every grid point that is touched by the MHW at least one day. This MHW-area is constant in time over the event duration but it changes from one MHW to another. Each heat budget term was then averaged over this area for every day of each event. Keeping the MHW area constant over the event duration was necessary as it would be complicated to physically interpret the horizontal residual that would otherwise stem from a daily-changing MHW area. This would create inconsistencies in the ML budget closure. Thus, we examined the daily timeseries of every contributing term during an event, as well as its anomalies relative to its daily climatology of 1982-2017. The daily climatology of each term was calculated across all years and using an 11-day window centered on each day of the year. In order to get a better idea of what preconditioned the MHW and what was responsible for its fall, we expanded this daily-timeseries analysis into 7 days before and after an event. Then we split the Mediterranean into predefined different subbasins and performed the same analysis (see Section 3.9.3).

The obvious advantage of computing online diagnostics is related to the information being extracted at the model timestep with the model mathematical formulation and numerical schemes. However, the ML trends diagnostics in NEMOMED12 are, in general, known to have certain inconsistencies in coastal runoff points, whereby abnormal values are present. Therefore, in the current analysis these points were removed based on the abnormal residual values they exhibited in a twin simulation we performed with constant MLD depth. Since they only represent the 0.5% of the total area we do not expect that the analysis will be impacted by their exclusion.

## 4.2 Analysis of MHW 2003 at basin-scale

As already shown in Section 2.4 the simulated MHW 2003 lasted for 48 days (18 July-3 September) and affected almost the whole Mediterranean except for some parts of the Aegean Sea. The Western Mediterranean, the Ionian and Adriatic Sea, however, exhibited the highest intensities and durations. In this section we attempt to disentangle how and why the MHW was preconditioned, evolved and faded, first, as an average over the whole area touched by the MHW (maximum surface coverage 79% of the Mediterranean Sea) and then looking closely at selected basins (see also Fig.2.13& Fig.2.14).We perform our analysis using MHW-area averaged timeseries, where the total number of days we are interested in (x axis) are plotted against each of the parameters mentioned above on the y axis.

### 4.2.1 Ocean Heat Budget

In Figure 4.2 we show all the different oceanic and atmospheric components and their evolution with time. Starting by the ocean, before the 18th of July the SST and ML temperature are already on the rise with around 1°C difference between them. The MHW starts with a warming ocean state between 26°C (MLT) /27°C (SST), which increases up to 28°C at the surface until the end of the event. The MLD during that time remains stable at around 11 m. Towards early September (MHW end) temperatures drop by at least 2 degrees from their MHW-levels and MLD increases up to 15 m (Fig.4.2,a-b).

The reason behind this warming path can be linked to variations of the total trend, which here are mostly dominated by the atmospheric forcing. Heat supply from the atmosphere remains positive most of the time but progressively reduces from 0.2°C/day on the onset to a negative state (-0.25°C/day) after the end of the MHW. Concomitant to this progressive reduction is a gradual decline in the total Trend, which is also positive on average but falls below zero between 28th July-early August and the days after the MHW. During these 2 periods air-sea fluxes anomalies are below normal conditions with -0.10°C/day and up to -0.30°C/day respectively but the corresponding total trend decreases slightly more than them. The moderately increased $Z_{df}$ here is what probably contributes to the diminishing of the total trend. This is in contrast with the general effect of the smaller in magnitude, absolute, vertical diffusion values (~ -0.05 to -0.15 °C/day) that partly seem to counteract the air-sea fluxes along with advection (up to -0.02°C/day) (see Fig.4.2c). It turns out that anomalously positive/negative $Z_{df}$ ultimately help sustaining/destroying the MHW, as opposed to the negligible contribution of advection anomalies. Lateral diffusion (Ldf) and entrainment (Entrainm) do not contribute significantly to the total trend, while ERROR term is more important in the 1st of August than at the 1st of September.

For a MHW to develop abnormal atmospheric or oceanic heating is necessary. In our case, their anomalies are communicated through changes in the ML temperature. In that sense, the anomalously warm temperatures of that period (1°C-2°C warmer than normal) could be a

consequence of the shallower than average MLD manifested throughout the event duration (up to -1.5m) (Fig.4.2,c-d). The question is what is/are the dominant anomalous forcing(s) behind this abnormal changes? On the onset of the MHW the total trend is slightly higher

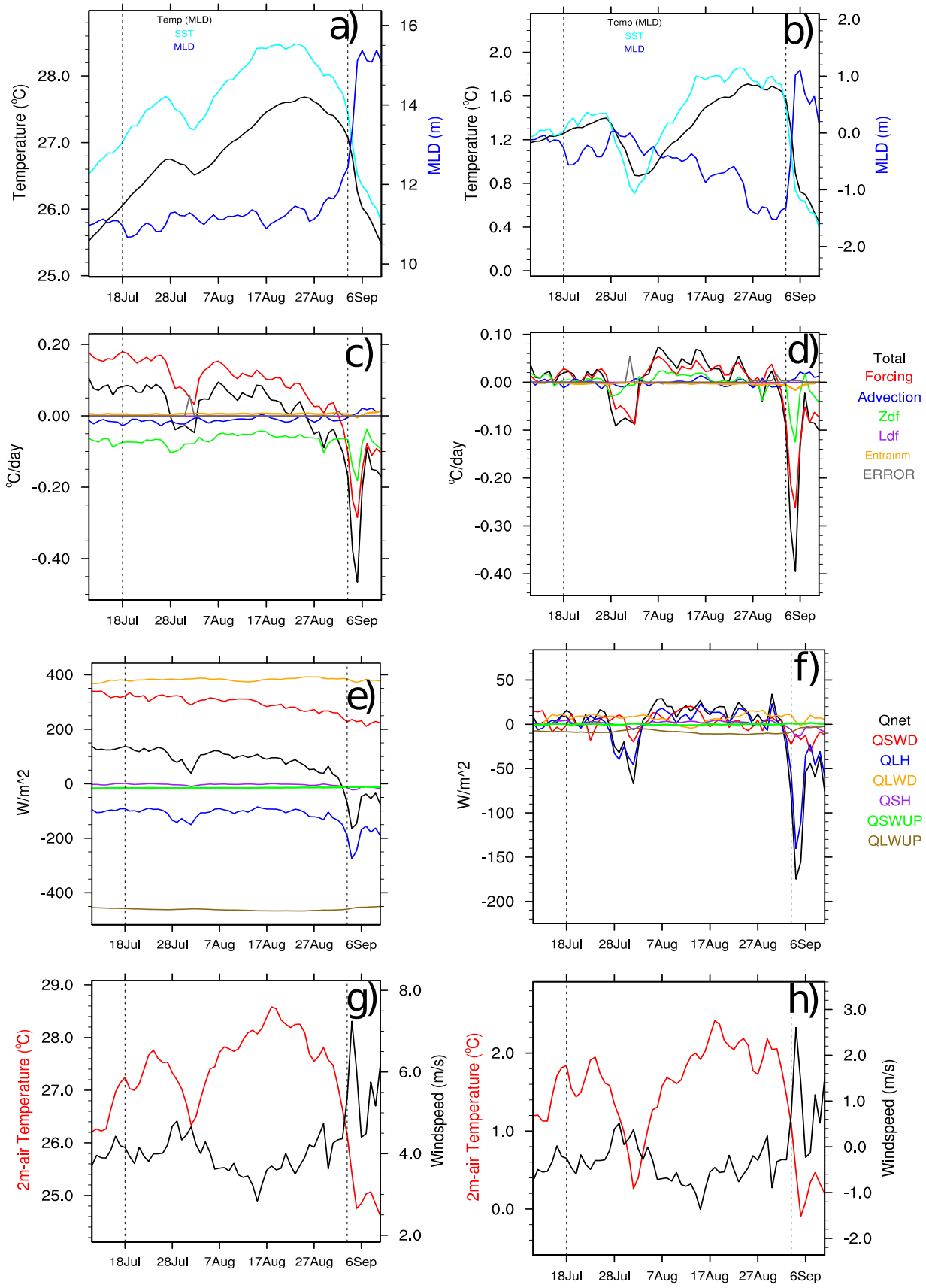


Figure 4.2: Mixed Layer (a-d) and atmosphere (e-h) heat budget decomposition 7 days before, during and 7 days after the Mediterranean MHW 2003. MHW period is displayed between dashed lines. Each term's daily timeseries is averaged over the MHW area and is shown in absolute values (a,c,e,g) and in anomalies (b,d,f,h) with respect to 1982-2017 climatology. See text for more details.

than average due to a decrease in vertical diffusion combined with an increase in atmospheric forcing (decreased latent and sensible heat flux) shortly before the beginning of the event. MLD is shallower than normal. During the MHW time the atmospheric forcing seems to exceed its seasonal value by around 0.05°C/day, combined with a higher than normal $Z_{df}$. As a consequence total trend is also higher than average by 0.08°C/day (apart from 28th July-early August) and MLD progressively shoals more than before the start of the MHW. Despite the lower MLD anomalies between 28th July-early August, the SST and the ML temperature remain warmer then average by 0.8-1.2 °C. By contrast, temperatures fall below average by the end of the event following stronger negative forcing and $Z_{df}$ anomalies (intensified vertical diffusion).

### 4.2.2 Atmosphere Heat budget

The state of the ocean described above denotes atmospheric forcing as the dominant driver during the MHW. Here, we are interested in identifying which atmospheric component is responsible for this anomalously high $Q_{net}$ (or else Forcing for the ML heat budget). Therefore, by comparing Fig.4.2c with Fig.4.2e we can first see that the variability of the Forcing is similar to that of $Q_{net}$. Both of them show a progressive declining course with time that continues after the event. The evolution of the rest of the atmosphere fluxes is shown in Fig.4.2,(e-h). The longwave radiation emitted by the ocean is almost cancelled out by the downward longwave radiation. In general, $Q_{net}$ remains positive before and until the end of the event (up to 200W/m$^2$), mostly as a result of the positive contribution from the downward shortwave radiation and the negative one from the latent heat flux. But a sudden increase in $Q_{LH}$ (up to -140 W/m$^2$) by the end of the event dominates the significant reduction in $Q_{net}$ (up to -170 W/m$^2$), although the small $Q_{SWD}$ decrease could also slightly contribute. The same air-sea exchange mechanism applies for the 28 July- early August event only that it is weaker than at the end of the MHW.

In fact, the negative $Q_{LH}$ anomalies in the first event (-40W/m$^2$) are lower than those after the MHW is over. Both events can be considered as concomitant to an increase in windspeed which induces an increase in latent heat loss and a decrease in 2m-air temperature (see Fig.4.2,g-h). In the former case, stronger windspeed anomalies of around 1m/s occur and air temperature drops around 1-2°C within a few days time. In the latter case, the windspeed anomalies are even greater (up to 3 m/s) and last longer, inducing as a result greater latent heat loss than before. The air temperature before and during the event is warmer by 1-2°C than normal except from the above-mentioned short period of decline within the MHW and after the end of it where it approaches normal conditions. The rest of the fluxes ($Q_{SH}$,$Q_{SWUP}$) show very small, mostly positive departures from the mean, which however waver throughout the whole period examined.

### 4.2.3 Overall Attribution

On average over the MHW area, we could hypothesize that before the 18th of July a combination of a slightly positive anomalous atmospheric forcing due to lower than normal windspeeds and higher than normal air temperatures along with a decline in vertical diffusion initially acted on/contributed to create the MHW. Positive anomalies of sensible and latent heat flux partly explain the MHW start since shortly (2 days) before the start of the event $Q_{net}$ becomes more positive than normal. As a result, SST started progressively to rise, preconditioning the MHW. However, the exact cause behind the onset of the event is not very clear or always evident through the MHW-area-average analysis. This could be linked to a smoothing of the signal as a result of the spatial average of the heat budget terms. For this reason, further look into the different subbasins will follow and a more clear picture of the MHW drivers will be drawn. Then, during the event an interplay between higher than normal incoming solar radiation, (and downward longwave radiation) anomalously low winds and therefore reduced latent heat loss, reinforce the MLD shallowing augmenting the SST and ML temperature more than before. A few days later wind intensifies even more and the event finally fades around 3 September due to physical processes similar to those that occurred between 28 of July-early August. Overall, it turns out that vertical diffusion and atmospheric forcing have the dominant roles on the driving of the MHW mostly through the role of wind that is critical in determining the MHW dynamics. This result is in accordance with the findings of Olita et al. (2007); Sparnocchia et al. (2006) about the MHW 2003 in the NW Mediterranean. This becomes more evident at the fading phase of the event where negative atmospheric forcing and intensified latent heat loss and vertical diffusion characterize the end of the event throughout the whole MHW area. Nevertheless, the effect of the wind on the MHW fading is somewhat unclear. By that, we mean that apart from the cooling owing to the latent heat effect, the wind speed could also act to weaken the MHW by spreading the heat out to a larger volume as a result of the deepening of the MLD. To determine,however, which of the two is the dominant factor, or if it is a combination of two, further research would be necessary. For example, sensitivity tests whereby the MLD is kept constant would help to identify the contribution from the latent heat in that case.

## 4.3 Regional MHW 2003 Analysis

Taking into account the different local oceanographic and probably also atmospheric conditions that may prevail during a single MHW in the different areas of the basin, there might be different factors that can explain the onset, duration and fall of the same event in different regions. Especially because the way the algorithm identifies MHW is by affecting points of the Mediterranean Sea that are spatially non-contiguous. Therefore, it could include points from the Eastern (EMED) and Western Mediterranean (WMED) area at the same time. Hence, to get a better idea of possible, region-specific, predominant influences on a MHW, we splitted the Mediterannean Sea into 14 subbasins. From those, we selected only the regions that

were affected by the MHW long enough (from 30 days and above) in order to get a clearer signal of the MHW driving factors (see also Fig.2.14). That is to say, for practical reasons we chose to investigate the underlying mechanisms throughout the total duration of the MHW (48 days). As a result, inconsistencies emerged on areas, such as the Alboran Sea or the Eastern Mediterranean, that were affected by the event only for a few days, since the signal was "contaminated" by non-MHW days. Besides, establishing the exact dates that each subbasin was affected by the event was complicated and due to time restrictions unfeasible. Therefore, we focused our analysis in the Gulf of Lion (GOL), the Tyrrhenian (TYR), Algerian (ALG) Ionian Sea (ION) and the area between the Sicily straits and the Gulf of Gabes (named here as GAB for simplicity). Those regions demonstrated not only the highest durations but also the highest mean intensities during the MHW. Moreover, they displayed slightly different driving features from the ones identified in the basin-scale analysis, which makes them even more interesting to examine. The subbasins are co-illustrated in Figure 4.3 with the MHW 2003 field of mean intensities on the background as calculated in Chapter 2, Fig.2.13. The names of the rest of the areas are also formed from their initials. For example,the Alboran (ALB), Adriatic (ADR), a small part of the south Ionian (SION), Aegean (AEG) ,Levantine basin (LEV) which was partitioned to North Levantine (NLEV), South Levantine (SLEV) and the far eastern part of it (EEMED).

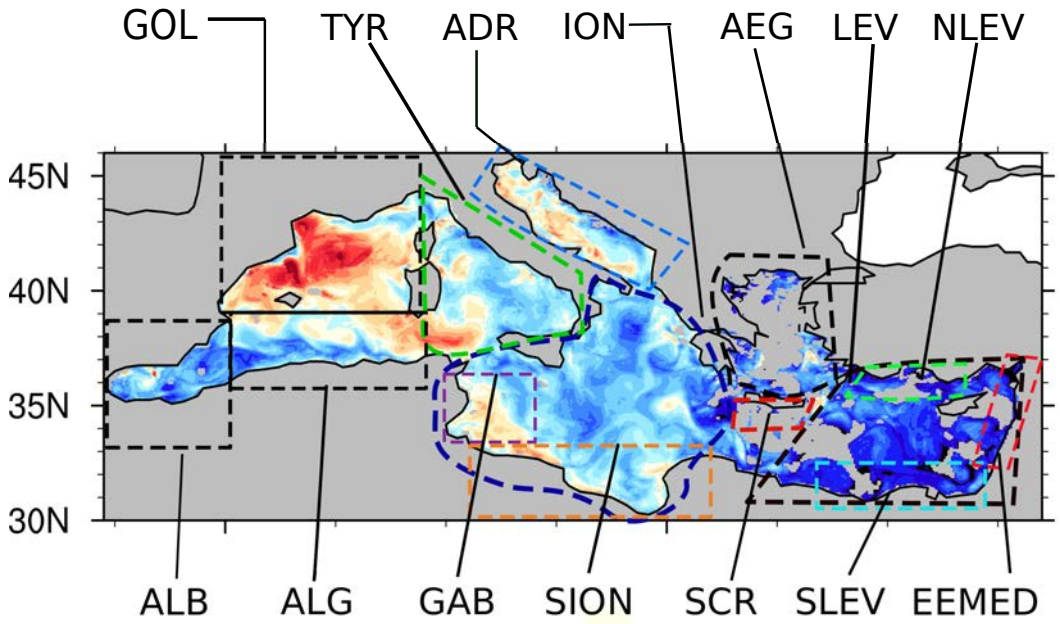


Figure 4.3: Schematic of the Mediterranean Sea separation in subbasins. The different areas are displayed with their acronyms as defined in text. On the background the spatial distribution of the mean intensity (°C) during the MHW 2003. See text for more details.

From the previous analysis we showed that anomalies of $Q_{LH}$, $Q_{SWD}$, windspeed, $Z_{df}$ and MLD stand out as critical parameters that regulate the intensity of the SST anomalies before, during and after the end of the MHW, on average over the whole MHW area. However, the exact anomalous forcing that triggered the MHW were not clear. Therefore, at this section we

perform a similar analysis as in Section 3.8.2 but according to the subbasin scheme described previously. For each subbasin absolute and anomalous values of each atmospheric and oceanic term are presented below, 7 days before, during and 7 days after the 2003 event. For a more synthetic illustration of the predominant factors, the average daily contribution of each term throughout each timeframe is displayed in the form of bars. That is, each bar represents the average contribution of every term over the respective number of days of each timeperiod. For example, the phase before and after the MHW always last 7 days, whereas the MHW-phase is 48 days. It should be noted, however, that the short cooling period between 28 July-early August may be responsible for lowering the average net atmospheric forcing of the region (over the event duration) and may not be representative of the situation in the month of August.

### 4.3.1 Western Mediterranean Basins

- *Gulf of Lion, Ionian Sea*:

  We describe these 2 subbasins together since their dominant driving factor on the onset of the MHW was anomalous atmospheric forcing, in particular an excess of $Q_{SWD}$ (~8 $W/m^2$) and a reduction in latent heat flux, combined with an anomalously low $Z_{df}$ that resulted in a positive total trend (see Figures 4.4 & 4.5). Anomalously low winds (up to -0.7m/s in ION and -1m/s in GOL) prevailed before and during the MHW in both areas. During the MHW $Q_{net}$ is higher/lower than normal in Ionian Sea/Gulf of Lion due to an interplay between the same fluxes and ocean processes that caused the warming in the first place.

  Despite the negative total trend in GOL, SST and ML temperatures are above average since the reduction of the driving terms was not very significant. MLD is shallower than normal in both regions, yet in the Ionian Sea it is shallower than in the Gulf of Lion. In fact, between the onset and during the MHW period the wind has slightly increased, yet remains anomalously low, in the Ionian Sea (on average over the event duration) but the MLD is shallower than before the beginning of the MHW. The reason for this requires further investigation. The fall of the MHW in both areas evolves much like in the total MHW-area examined. Average $Q_{net}$ is decreased from -10 to -120 $W/m^2$. A significant reduction in $Q_{SWD}$ (from -20 to -30 $W/m^2$) a slight increase of sensible heat flux, an increase of latent heat loss and intensified vertical diffusion under increased windspeeds, deepen the MLD and reduce SST and ML temperatures. The downward and upward longwave radiation most of the time cancelled each other altough this was not always clear.

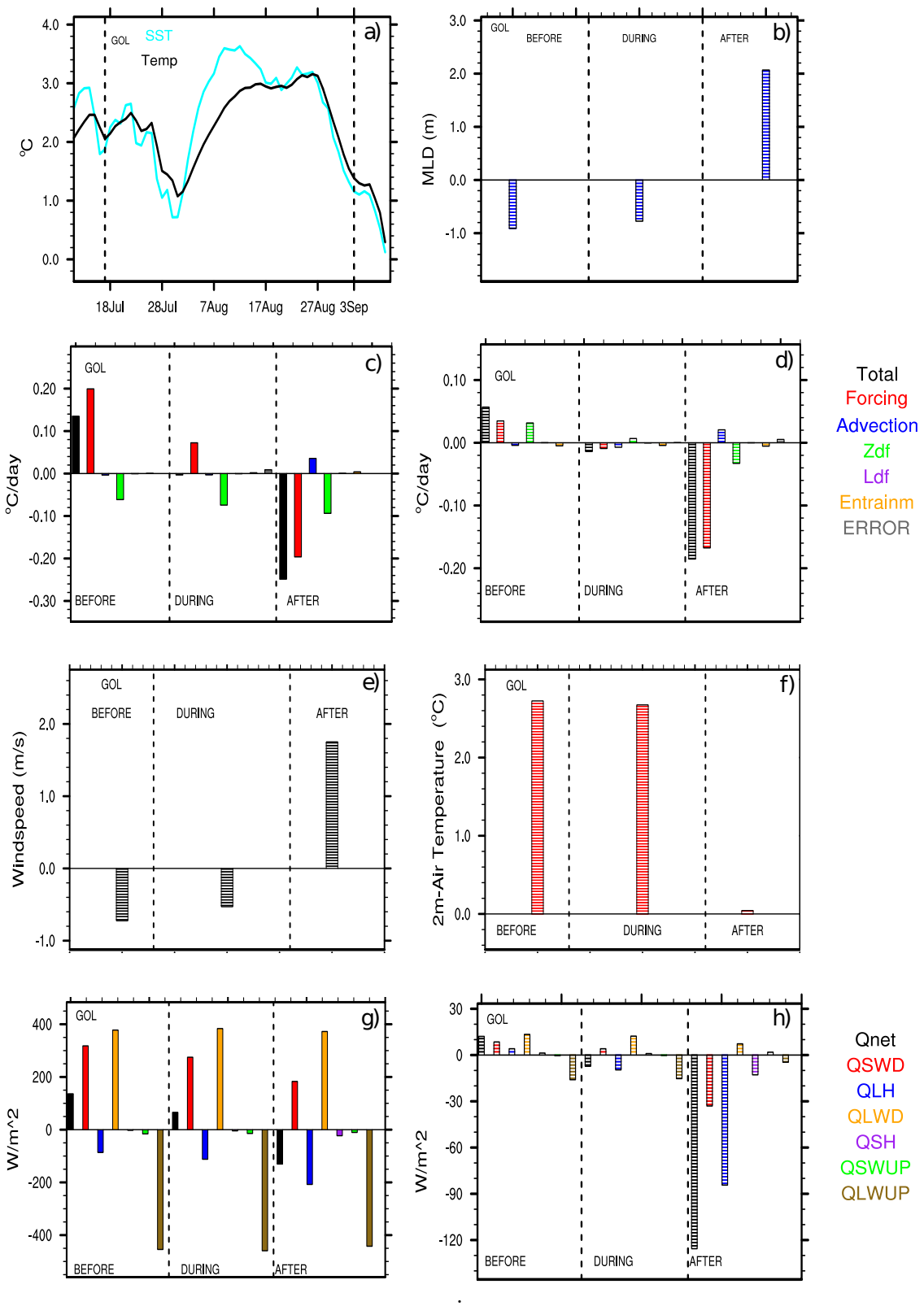


Figure 4.4: Daily timeseries of a)SST and ML temperature (Temp) anomalies, b) MLD anomalies, c) ML heat budget terms in absolute values, d) Anomalies of ML heat budget terms, e) Windspeed anomalies, f) 2m-air temperature anomalies, g) Atmosphere heat budget terms in absolute values, h) Atmosphere heat budget terms in anomalies, for the Gulf of Lion (GOL). Values are averaged for 7 days before, during and 7 days after the MHW 2003

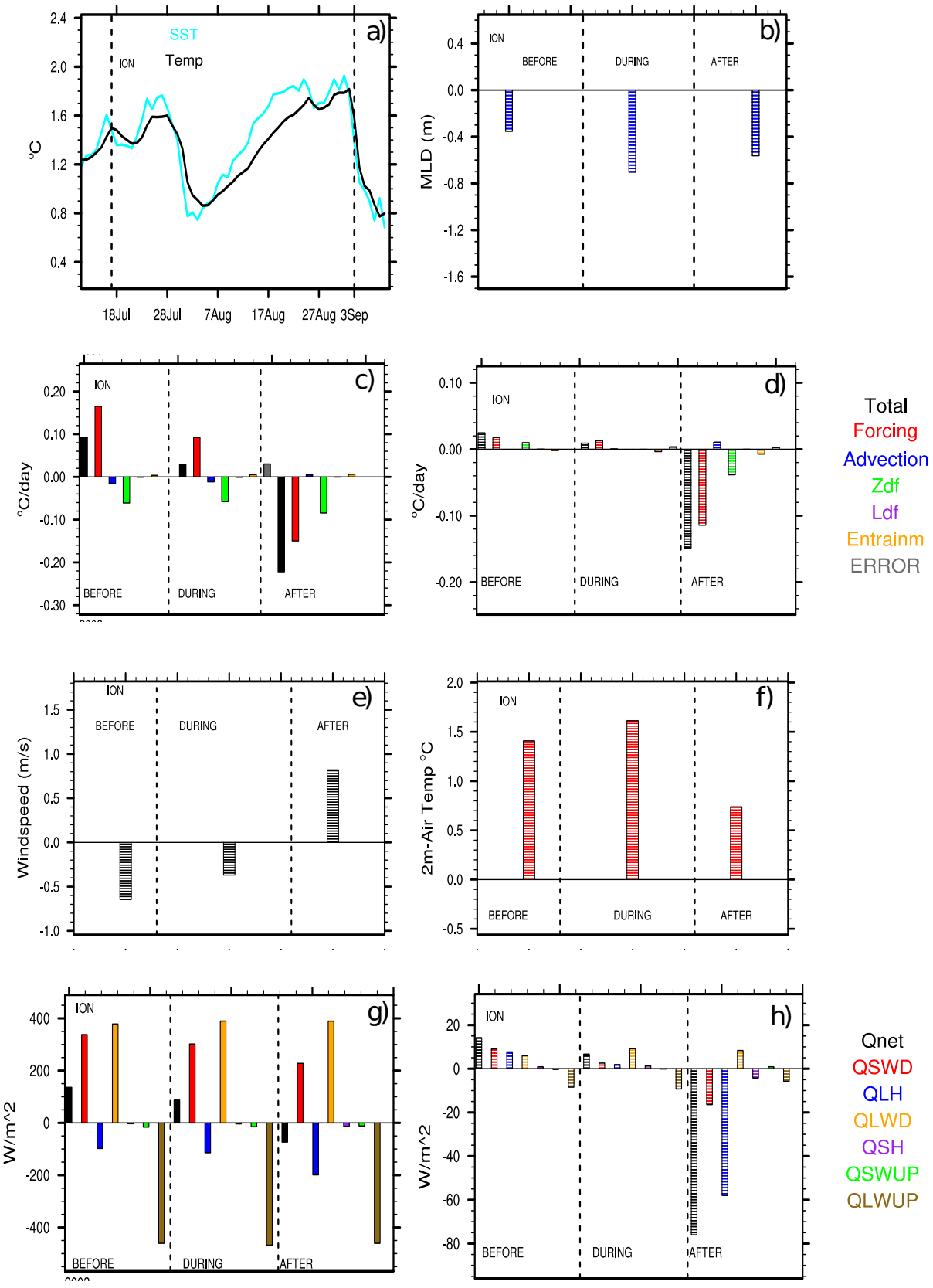


Figure 4.5: As in Fig.4.4 but for the Ionian Sea domain.

- *Tyrrhenian Sea, Algerian Sea, Gulf of Gabes domain*:

  In those 3 regions the MHW is preconditioned by anomalously high atmospheric forcing, combined with anomalously low vertical diffusion, but this time warmer than average advection contributes to the input of heat (or the absence of input of cold waters) before the 18th of July (Total trend above average) (see Fig.4.6). The anomalous atmospheric forcing is driven mostly by a decrease in latent heat loss (between 5-12 W/m$^2$) but in the case of GAB domain it is further enhanced by an anomalously high $Q_{SWD}$. Over the event duration, anomalously atmospheric forcing dominates the ocean processes and sustains the MHW in all 3 areas.

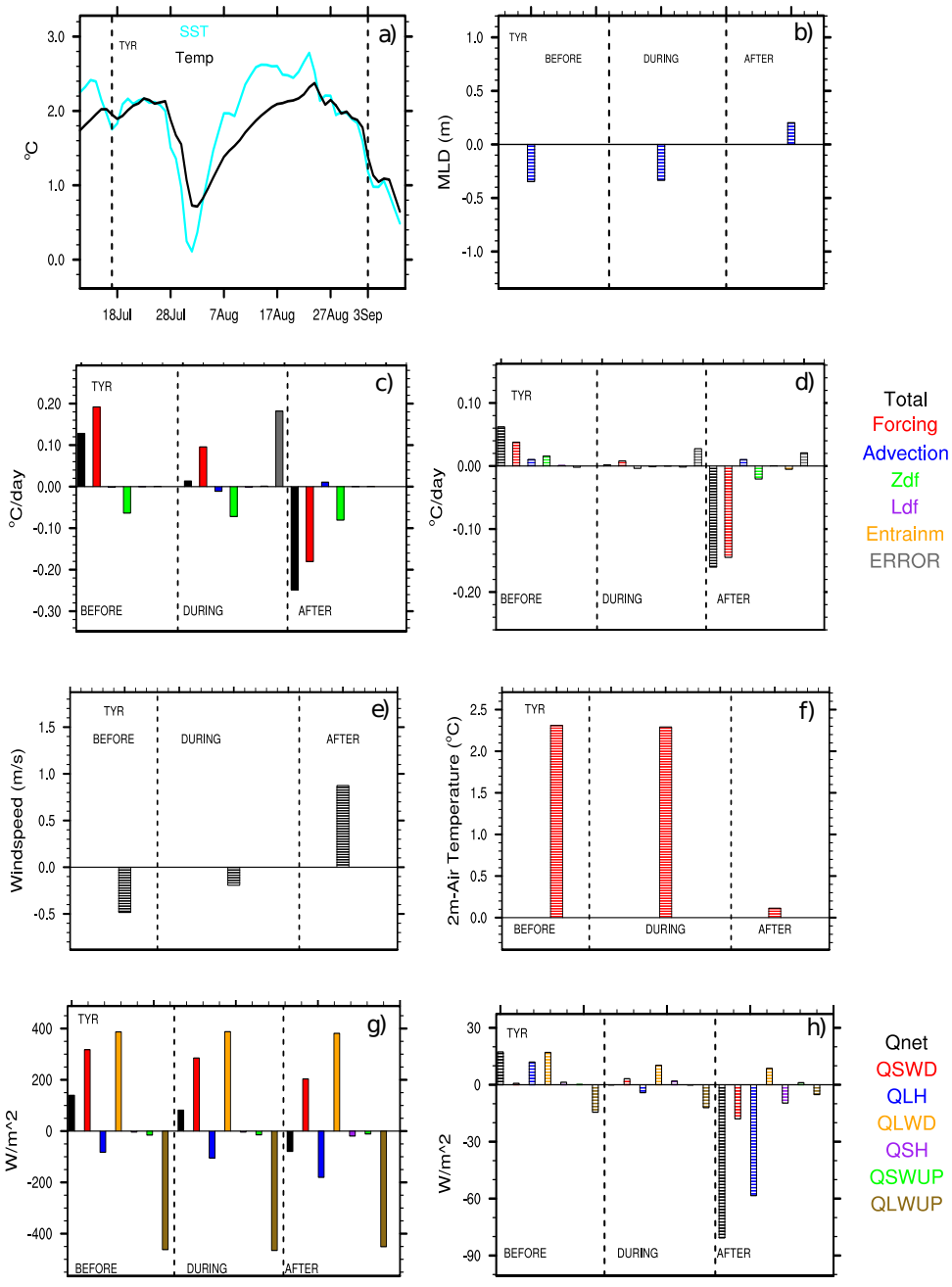


Figure 4.6: As in Fig.4.4 but for the Tyrrhenian Sea domain.

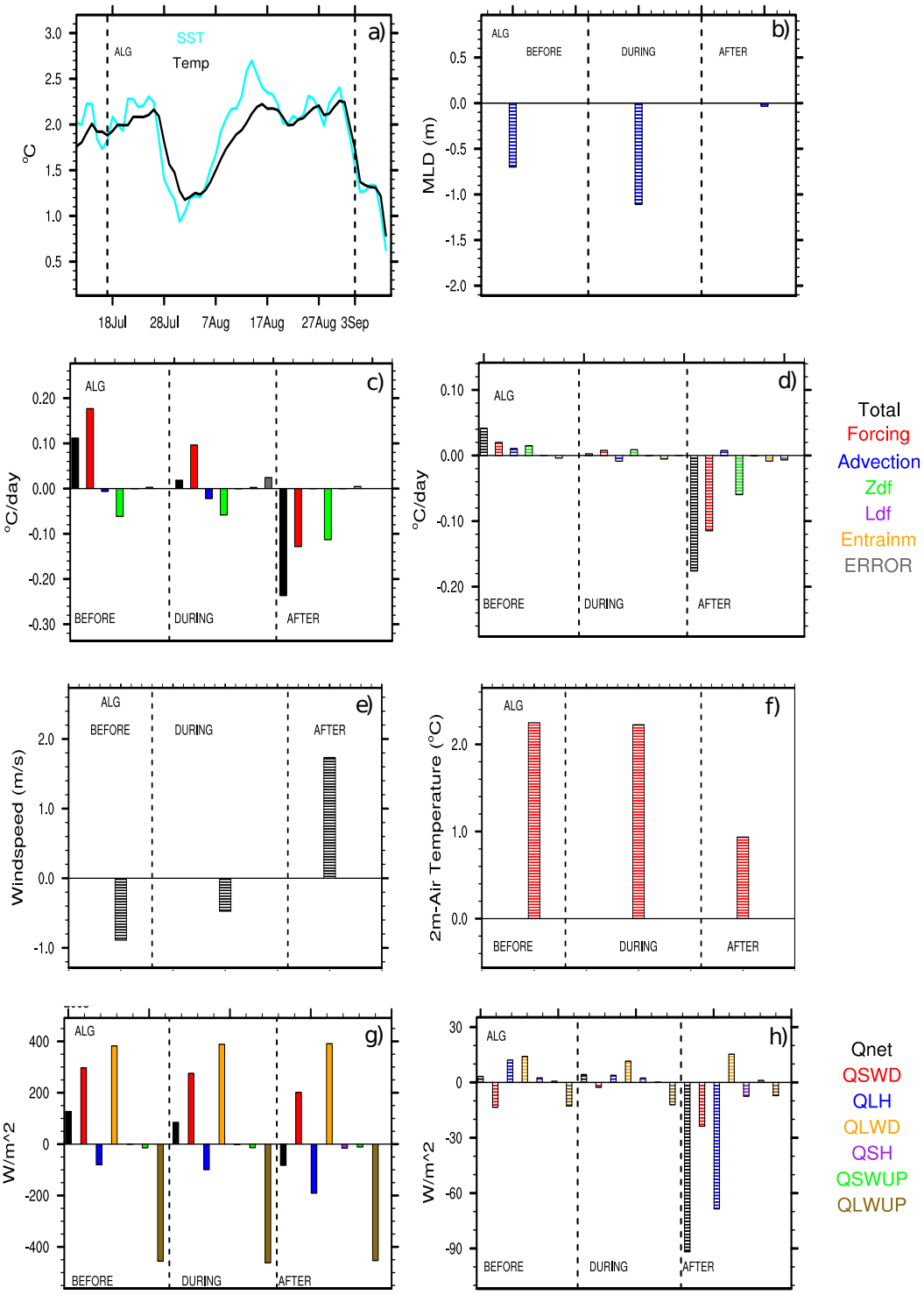


Figure 4.7: As in Fig.4.4 but for the Algerian Sea domain.

From the onset until the end of the MHW, wind and MLD remain anomalously low but both increase after the 3rd of September. In the Gulf of Gabes, however, MLD becomes lower than before. The latter could probably indicate the presence of increased stratification that opposes the wind effect. Eventually, the end of the MHW is marked by the same processes that govern the basin-scale MHW fall, although sensible heat flux appears slightly intensified along with entrainment in those domains.

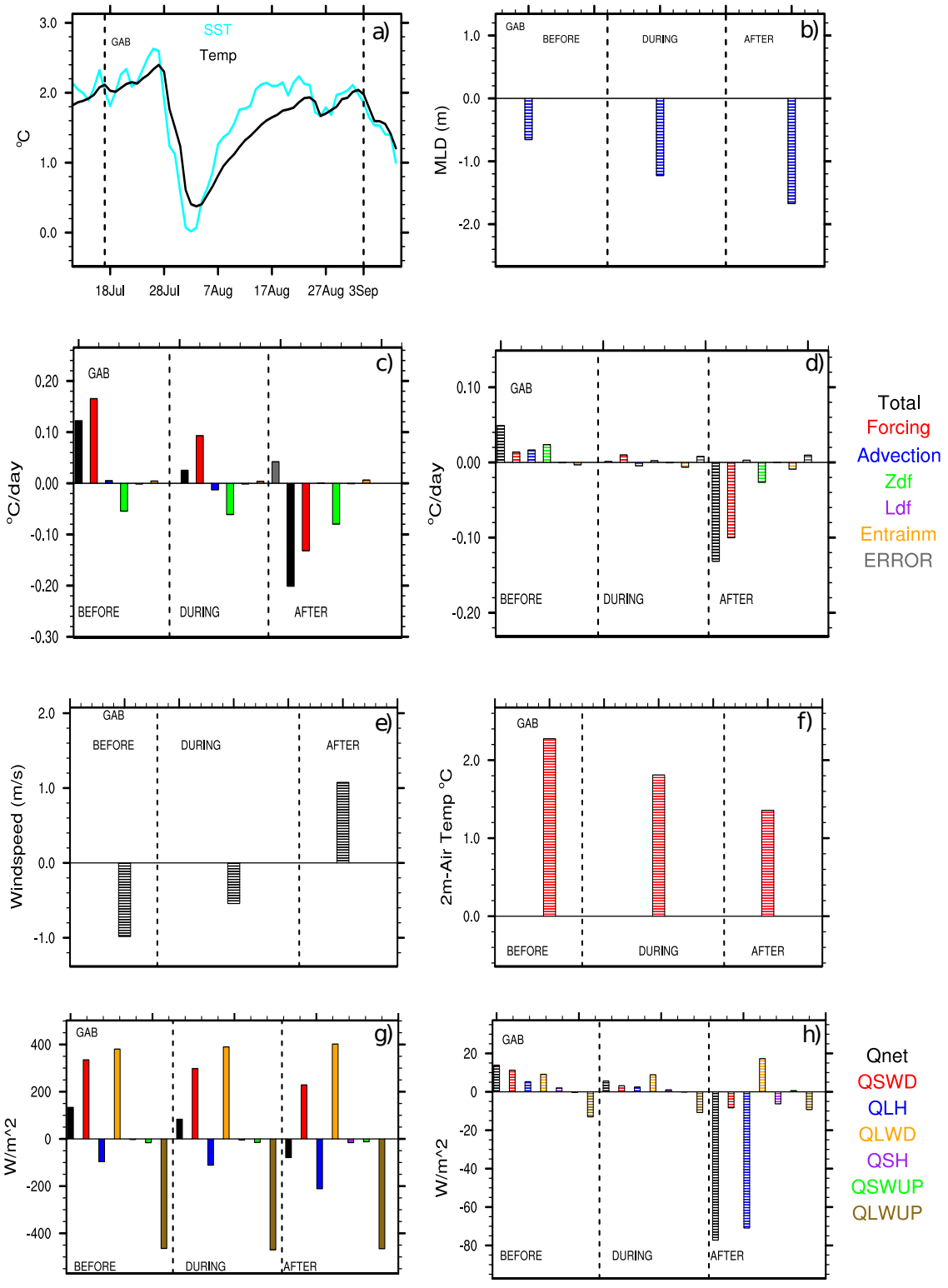


Figure 4.8: As in Fig.4.4 but for the Gulf of Gabes domain.

### 4.3.2 Eastern Mediterranean Basins

Since the MHW 2003 did not affect substantially (or a high percentage of) the EMED regions we do not include a detailed description of the dominant atmospheric and oceanic drivers of the event there. The simulated MHW lasted from 5-25 days in that part of the basin according to Fig.2.14. Thus, the low durations of the MHW do not allow us to deduce what *caused* the event there, since the subbasin analysis is focused on the average atmospheric and oceanic conditions over the event duration every time (and some days before and after the event), that is 48+14 days. Instead, what an analysis like that *can* provide us in that case is further information on what *did* weaken the MHW development, on average over the event duration in those areas. What made the MHW less warm/shorter there than in the rest of the basin?. Part of the answer to this question is given by the preconditioning phase (before the 18th of July), where most of the EMED subbasins had a negative total trend and lower than average temperatures (see Fig.4.9). This is related, in general, to lower than average atmospheric forcing, increased winds and sometimes a negative/positive contribution from the advection/entrainment (see Fig.4.10,Fig.4.11). The latter effect is probably related to the fact that most of the EMED subbasins affected by the MHW included coastal regions (e.g. EEMED, NLEV, SLEV and the remaining Aegean domain that was touched by the MHW). Since the total trend became higher than normal after the 18th of July almost everywhere in the EMED, it probably means that the MHW started later there than everywhere else. Over the event duration the same anomalous atmospheric parameters as in the basin-scale MHW emerged for the EMED regions that *were* affected by the MHW (see Fig.4.12). The only difference in that part of the basin stands in the enhanced role of warm advection found between 18 July-3 September almost everywhere. But before the event had the chance to develop further and increase its total trend and therefore the ocean temperatures everywhere, it subsided at the same dates as in the rest of the Mediterranean Sea. Therefore, the reason why the MHW did not last a long in the EMED is due to the same atmosphere and ocean forcing that ”killed” the MHW everywhere else shortly after the MHW had begun there.

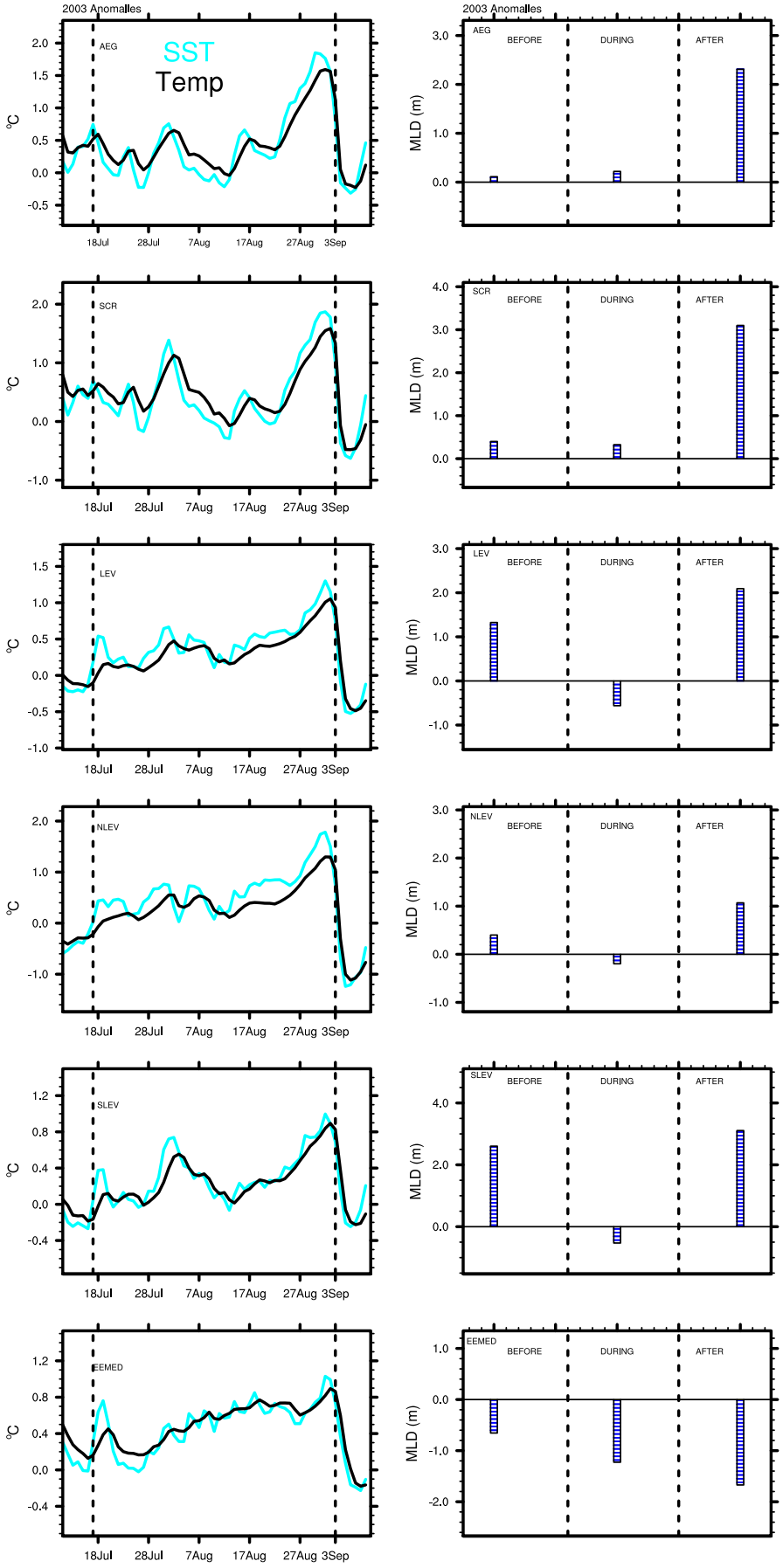


Figure 4.9: SST and ML temperature anomalies (left column) and MLD anomalies (right column) for every EMED subbasin, 7 before, during and 7 days after the MHW.


Figure 4.10: Absolute (a-f) and anomalous values (g-l)for the different MLD heat budget terms, 7 days before, over the event duration and 7 days after the MHW.

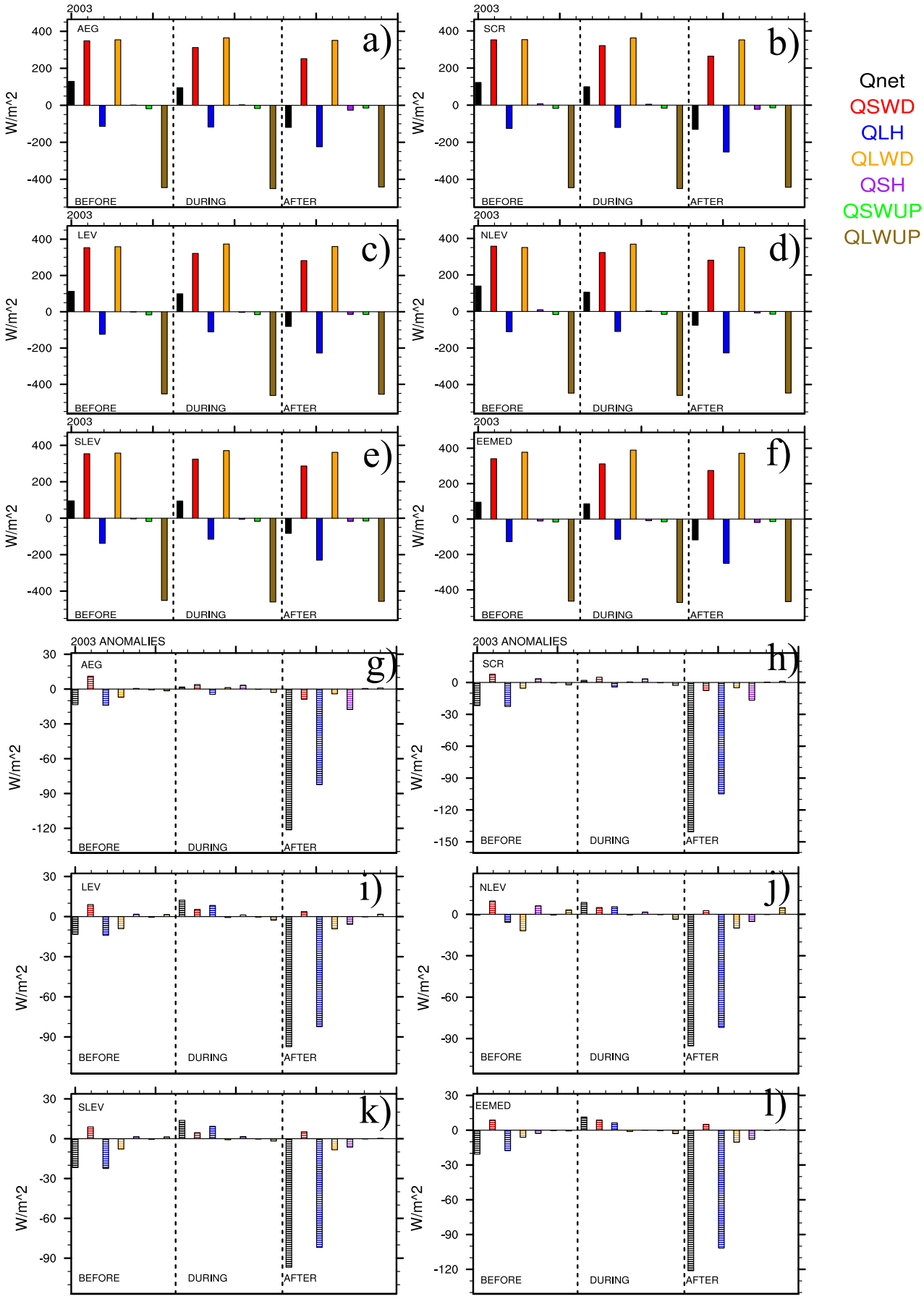


Figure 4.11: As in Fig.4.10 but for the atmosphere heat budget terms.

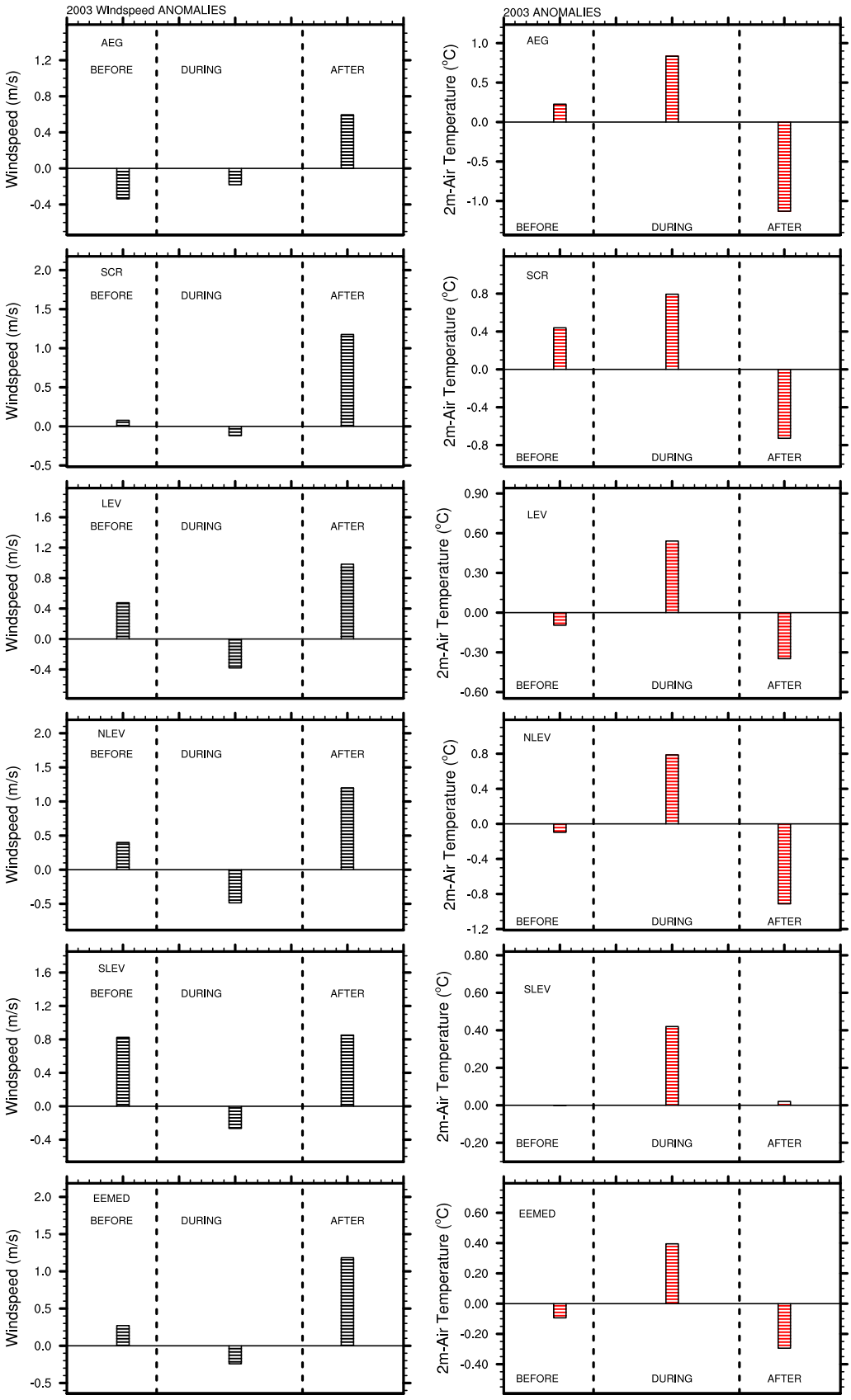


Figure 4.12: As in Fig.4.9 but for windspeed and 2m-air temperature anomalies.

## 4.4 Conclusions

Overall, both in the MHW-area average analysis and in the different subbasins analysis indicated the interplay between anomalously high incoming shortwave radiation and wind-induced anomalously low latent heat loss from the ocean as key parameters for the onset of the MHW of 2003. In addition, vertical diffusion appears to play a significant role. The wind emerges as a critical factor whose higher than average values signal the fall or the short-term weakening of the event in all the regions examined. Anomalously high SST most of the time are related to a shoaling of MLD as a result of the above-described processes. By contrast, the role of advection and entrainment was not that significant, except for a few cases where the former was enhanced and contributed critically to the input/output of heat. Finally the contributions from upward shortwave radiation and lateral diffusion most of the times were found insignificant. Sensible heat flux, however, has a small but noticeable role in some subbasins. It should be noted here that this is the first time that atmosphere and mixed layer temperature heat budget decomposition and analysis is performed for the MHW 2003. Due to time restrictions we were not able to undertake further analysis on the driving factors of the ensemble of the MHWs during 1982-2017. However, this is recognized as an important perspective that we would like to add on our future work on the PhD topic.

# Chapter 5

# Future Marine Heatwave Evolution in the Mediterranean Sea

*".. And nobody in all of Oz, no Wizard that there is or was, is ever gonna bring me down."*

Defying Gravity

## Contents



The reader is reminded that current Chapter is in the form of a published article and some of its content might have been mentioned in previous Chapters. Reference: **Darmaraki, S.** & Somot, S. & Sevault, F. & Nabat, P. & Narvaez W. D. C. & Cavicchia, L. & Djurdjevic, V. & Laurent, Li. & Sannino, G. & Sein, D. V. (2019). Future evolution of Marine Heatwaves in the Mediterranean Sea. Climate Dynamics, 1-22. Climate Dynamics. DOI: 10.1007/s00382-019-04661-z

## Abstract

Extreme ocean warming events, known as marine heatwaves (MHWs), have been observed to perturb significantly marine ecosystems and fisheries around the world. Here, we propose a detection method for long-lasting and large-scale summer MHWs, using a local, climatological 99th percentile threshold, based on present-climate (1976-2005) daily SST. To assess their future evolution in the Mediterranean Sea we use, for the first time, a dedicated ensemble of fully-coupled Regional Climate System Models from the Med-CORDEX initiative and a multi-scenario approach. The models appear to simulate well MHW properties during historical period, despite biases in mean and extreme SST. In response to increasing greenhouse gas forcing, the events become stronger and more intense under RCP4.5 and RCP8.5 than RCP2.6. By 2100 and under RCP8.5, simulations project at least one long-lasting MHW every year, up to three months longer, about 4 times more intense and 42 times more severe than present-day events. They are expected to occur from June-October and to affect at peak the entire basin. Their evolution is found to occur mainly due to an increase in the mean SST, but increased daily SST variability also plays a noticeable role. Until the mid-21st century, MHW characteristics rise independently of the choice of the emission scenario, the influence of which becomes more evident by the end of the period. Further analysis reveals different climate change responses in certain configurations, more likely linked to their driving global climate model rather than to the individual model biases.

*Keywords: Marine Heatwaves, Mediterranean Sea, Coupled regional climate models, future scenario, extreme ocean temperatures, Med-CORDEX,climate change, climate simulations*

## 5.1 Introduction

Episodes of large-scale warm temperature anomalies in the ocean may prompt substantial disruptions to marine ecosystems (Frölicher and Laufkötter, 2018; Hobday et al., 2016) and major implications for fisheries as well (Mills et al., 2013). Known as marine heatwaves (MHW), these extreme events describe abrupt but prolonged periods of high sea surface temperatures (SST) (Scannell et al., 2016) that can occur anywhere, at any time, with the potential to propagate deeper to the water column (Schaeffer and Roughan, 2017). They have received little attention until improved observational systems revealed adverse consequences emanating from them. Their occurrence is likely to intensify under continued anthropogenic warming (Frölicher et al., 2018; Oliver et al., 2018a), engendering the need for a more comprehensive examination of their spatiotemporal distribution and underlying physical causes.

In the Mediterranean area, a well-known "Hot Spot" region for climate change (Giorgi, 2006), the annual mean basin SST by the end of the 21st century is expected to increase from +1.5 °C to +3 °C relative to present-day levels, depending on the greenhouse gas (GHG) emission scenario (Somot et al., 2006; Mariotti et al., 2015; Adloff et al., 2015). This significant rise in SST is expected to accelerate future MHW occurrences, in congruence with projec-

tions for GHG-induced heat stress intensification of 200%-500% throughout the region (Diffenbaugh et al., 2007). The Mediterranean area's sensitivity to increased GHG forcing is mainly attributed to a significant mean warming and increased interannual warm-season variability, along with a reduction in precipitation (Giorgi, 2006). A recent study has already identified significant increases in MHWs globally over the last century, including the Mediterranean Sea (Oliver et al., 2018a).

In fact, one of the first-detected MHWs worldwide occured in the Mediterranean in the summer of 2003: Surface anomalies of 2-3 °C above climatological mean lasted for over a month due to significant increases in air-temperature and a reduction of wind stress and air-sea exchanges (Grazzini and Viterbo, 2003; Sparnocchia et al., 2006; Olita et al., 2007). These factors seem to have also triggered an anomalous SST warming in the eastern Mediterranean area during the heatwave of 2007, at the order of +5 °C above climatology (Mavrakis and Tsiros, 2018). Since then, numerous studies have explored the modulating factors behind individual events around the world. For instance, a combination of local oceanic and large-scale atmospheric forcing was suggested for the Australian MHW of 2011 (Feng et al., 2013; Benthuysen et al., 2014) and the persistent, multi-year (2014-2016) "Pacific Blob" (Bond et al., 2015; Di Lorenzo and Mantua, 2016). Other events have been attributed to mainly atmosphere-related drivers, such as the 2012 Atlantic MHW (Chen et al., 2014, 2015) and the extreme marine warming across Tropical Australia (Benthuysen et al., 2018), or to ocean-dominating forcing like the 2015/2016 Tasman Sea MHW (Oliver et al., 2017). The importance of regional influences was further noted in coastal MHWs in South Africa (Schlegel et al., 2017a) and during subsurface MHW intensification around Australia (Schaeffer and Roughan, 2017).

As a result of these events, severe impacts on marine ecosystems have been documented worldwide, including biodiversity die-offs and tropicalisation of marine communities (Wernberg et al., 2013, 2016), extensive species migrations (Mills et al., 2013), strandings of marine mammals and seabirds, toxic algal blooms (Cavole et al., 2016) and extensive coral bleaching (Hughes et al., 2017). In the Mediterranean Sea in particular, unprecedented mass mortality events and changes in community composition due to extreme warming were reported in the summers of 1999 (Perez et al., 2000; Cerrano et al., 2000; Garrabou et al., 2001; Linares et al., 2005), 2003 (Garrabou et al., 2009; Schiaparelli et al., 2007; Diaz-Almela et al., 2007; Munari, 2011), 2006 (Kersting et al., 2013; Marba and Duarte, 2010) and 2008 (Huete-Stauffer et al., 2011; Cebrian et al., 2011), affecting a wide variety of species and taxa (e.g. 80 % of Gorgonian fan colonies and seagrass *Posidonia oceanica*). MHWs can be especially lethal for organisms with reduced mobility that are usually limited to the upper water column; Their severity is determined by both temperature and duration (Galli et al., 2017). Finally, cascading effects have also been observed in fisheries, resulting in huge financial losses and even economic tensions between nations (Mills et al., 2013; Cavole et al., 2016; Oliver et al., 2017).

However, despite the growing body of MHW-related literature, systematic examination of MHWs as distinct exceptional events with intensity, frequency and duration has only just

emerged. Although marine extremes have been investigated before, only a few studies have analysed past trends in extreme ocean temperatures (e.g. Scannell et al., 2016; MacKenzie and Schiedek, 2007) and even fewer have dealt with their future evolution. For instance, past trends of extreme SST have been investigated in coastal regions (Lima and Wethey, 2012) and through thermal-stress-related coral bleaching records (Lough, 2000; Selig et al., 2010; Hughes et al., 2018). Using a more standardised framework, past MHW occurrences have been studied in the Tasman Sea (Oliver et al., 2018b) and the global ocean (Oliver et al., 2018a). For the 21st century, MHW projections have been performed so far on a global scale, with the use of multi-model setups from CMIP5 (Frölicher et al., 2018) and CMIP3 (Hobday and Pecl, 2014) and under different GHG emission scenarios. On a regional scale though, ocean extremes have been assessed in Australia (King et al., 2017) and the Tasman Sea (Oliver et al., 2014).

The above-mentioned studies used different definitions for extreme warm temperatures, with some adopting a recent standardised MHW approach proposed by Hobday et al. (2016). The set of dedicated statistical metrics developed in this framework allows for a consistent definition and quantification of the properties of MHWs. A MHW is now described as a "discrete, prolonged, anomalously warm water event at a particular location". Using this definition, Schlegel et al. (2017b), for example, identified an increase in MHW frequency around South Africa for the period 1982-2015, while Schaeffer and Roughan (2017) demonstrated subsurface intensification of MHWs in coastal SE Australia between 1953-2016. A linear classification scheme was also proposed by Hobday et al. (2018), where MHWs are defined based on temperature exceedance from local climatology.

In the case of the Mediterranean Sea, however, little is known about past or future MHW trends and their underlying mechanisms. The MHW-related research has mostly been focused on local ecological impacts without systematically assessing MHW occurrence. According to Rivetti et al. (2014) and Coma et al. (2009), most of the mass mortalities documented in the basin were related to positive thermal anomalies in the water column that occured regionally during the summer. Although they have been reported with increased frequency since the early 1990s, their occurrence has been observed as early as the 1980s. Meanwhile, the evolution of extreme Mediterranean SST in the 21st century has so far been examined in relation to the thermotolerance responses of certain species. For instance, Jordà et al. (2012) used an ensemble of models under the moderately optimistic scenario for GHG emissions A1B and suggested an increased seagrass mortality in the future around the Balearic islands due to a projected rise of the annual maximum SST by 2100. Similarly, Bensoussan et al. (2013) evaluated the thermal-stress related risk of mass mortality in Mediterranean benthic ecosystems for the 21st century, based on the average warming estimated between 2090-2099 and 2000-2010, under the pessimistic future warming scenario A2. Finally, Galli et al. (2017) showed an increase in MHW frequency, severity and depth extension in the basin, assuming exceedances from species-specific thermotolerance thresholds under the high-emission IPCC RCP8.5 scenario. (The A1B and A2 emission scenarios correspond to projections of a likely, mean temperature change of 1.7-4.4

°C and 2.0-5.4 °C respectively by the end of the 21st century (IPCC, 2007), whereas RCP2.6, RCP4.5 and RCP8.5 to a likely change of 0.3-1.7 °C, 1.1-2.6 °C and 2.6-4.8 °C respectively, by the end of the period (Kirtman et al., 2013)).

In addition, our understanding of the Mediterranean Sea's response to future climate change to date mostly relies on ensembles of low resolution GCMs (CMIP5) (e.g. Jordà et al., 2012; Mariotti et al., 2015) or on numerical experiments carried out with a single regional ocean model under different emission scenarios (i.e Somot et al., 2006; Bensoussan et al., 2013; Adloff et al., 2015; Galli et al., 2017). Consequently, the various sources of uncertainty related to the choice of the socio-economic scenario, choice of climate model and natural variability have not been properly taken into account by climate change impact studies on Mediterranean Sea ecosystems and maritime activities. Since there is an evident link between distinctive climate anomalies and notable ecosystem effects (e.g in the Mediterranean Sea, Crisci et al., 2011; Bensoussan et al., 2010), it is important to adress these uncertainties by considering different possible climate futures through multi-model, multi-scenario set ups when possible.

In this context, the aim of this study is to provide a robust assessment of the future evolution of summer MHWs in the Mediterranean Sea using an ensemble of high-resolution coupled regional climate system models (RCSM), driven by GCMs and a multi-scenario approach (RCP2.6, RCP4.5, RCP8.5). The RCSM's ability to reproduce Mediterranean SST features is first evaluated against satellite data. Then, a MHW spatiotemporal definition, based on SST and on Hobday et al. (2016)'s recommendations, is developed and applied to study the response of extreme thermal events to future climate change. For the first time, changes in summer Mediterranean MHW frequency, duration, intensity and severity are investigated with respect to an envelope of possible futures.

This paper is organised as follows: in section 2 we present the ensemble of RCSMs along with the methodology proposed for the detection and characterisation of summer MHWs. Model evaluation against observed mean and extreme SST is performed in section 3, using daily SST data. We also describe the future evolution of Mediterranean SST and MHW properties under different greenhouse gas emission scenarios from 1976-2100. A discussion and summary of the results are presented in Sections 4 & 5.

## 5.2 Material and methods

### 5.2.1 Model Data and Simulations

An ensemble of six coupled RCSMs (CNRM-RCSM4, LMDZ-MED, COSMOMED, ROM, EBU-POM, PROTHEUS) with different Mediterranean configurations is employed in this study. Participant members are provided by six research institutes from the Med-CORDEX initiative (Ruti et al. (2016), `https://www.medcordex.eu/`) and each simulation will be herein referred to by the name of the corresponding institute, as mentioned in Table.5.1 (e.g. simulations with

the CNRM-RCSM4 model will be referred as CNRM, etc.). Med-CORDEX can be considered as a multi-model follow-up to the CIRCE project (Gualdi et al., 2013), which studied the Mediterranean Sea under a single scenario (A1B) with most of the simulations stopped in 2050.

One novel aspect of the Med-CORDEX ensemble is that all models have a high-resolution oceanic (eddy-resolving) and atmospheric component as well as high coupling frequency (see Table.5.1). The free air-sea exchanges offered by their high-resolution interface is also an advantage for the MHW representation, which depends on ocean-atmosphere interactions. The domains cover the entire Mediterranean and a small part of the Atlantic, while the Black Sea and Nile river are respectively parametrized or represented with climatologies (except for AWI/GERICS, in which the oceanic component is global and explictly simulates the Black Sea). Boundary conditions come from 4 different general circulation models of CMIP5. Information about each coupled system is summarised in Table.5.1. To avoid biasing results towards one or more members of the ensemble, only the realization with the highest resolution is selected for each model.

| INSTITUTE | CNRM | LMD | CMCC | AWI/GERICS | U.BELGRADE | ENEA |
|---|---|---|---|---|---|---|
| Model Characteristics | | | | | | |
| RCSM name | CNRM-RCSM4 | LMDZ-MED | COSMOMED | ROM | EBU-POM | PROTHEUS |
| Driving GCM | CNRM-CM5 | IPSL-CM5A-MR | CMCC-CM | MPI-ESM-LR | MPI-ESM-LR | CNRM-CM5 |
| Med.Sea Model | NEMOMED8 | NEMOMED8 | NEMO-MFS | MPIOM | POM | MedMIT8 |
| Ocean Res. | 9-12 km | 9-12 km | 6-7 km | 10-18 km | 30 km | 13 km |
| Num. of z-Levels (Ocean) | 43 | 43 | 72 | 40 | 21 | 42 |
| SST (1st layer depth) | 6m | 6 m | 1.5 m | 16m | 1.8m | 10 m |
| Timestep (Ocean) | 1200 sec | 1200 sec | 480 sec | 900 sec | 360 sec | 600 sec |
| Atmosphere Model | ALADIN-Climate | LMDZ | CCLM | REMO | Eta/NCEP | RegCM |
| Atmosphere Res. | 50 km | 30 km | 50 km | 25 km | 50 km | 30 km |
| Coupling Frequency | Daily | Daily | 80 min | 60 min | 6 min | 6 hours |
| Numerical Simulations | | | | | | |
| SPIN UP | 130 years | - | 25 years | - | 5 years | - |
| Initial Conditions | MEDATLAS | MEDATLAS | MEDATLAS | MEDATLAS | MEDATLAS | MEDATLAS |
| HIST | 1950-2005 | 1950-2005 | 1950-2005 | 1950-2005 | 1950-2005 | 1979-2005 |
| RCP8.5 | 2006-2100 | 2006-2100 | 2006-2099 | 2006-2099 | 2006-2100 | - |
| RCP4.5 | 2006-2100 | 2006-2100 | 2006-2099 | 2006-2099 | - | 2006-2100 |
| RCP2.6 | 2006-2100 | - | - | - | - | - |
| References | Sevault et al. (2014) | 'L'Hévéder et al. (2013) | Cavicchia et al. (2015) | Sein et al. (2015) | Djurdjevic and Rajkovic (2008) | Artale et al. (2010) |

Table 5.1: Characteristics of the coupled Regional Climate System Models (RCSM) and the simulations used in this study. More information on MEDATLAS initial conditions can be found in Rixen et al. (2005).

All the numerical simulations produced daily SST data (3D temperatures were stored at a monthly scale) between 1950-2005 for the historical experiment (HIST) and for 2006-2100 under the Representative Concentration Pathway RCP8.5 (high-emission scenario), RCP4.5 (moderate-emission scenario), RCP26 (low-emission scenario) IPCC scenarios. As the models use boundary conditions from CMIP5, which are not in phase with the observed variability, simulation chronology does not represent the actual conditions that correspond to each calendar year. Instead, they are expected to represent the climate statistics of each period (e.g. average, standard deviation) well. We use SST instead of deeper layer temperatures, as both the models' behaviour and the MHW identification technique can be evaluated at a larger scale using

satellite data. A total of 17 simulations were used from six models with variable resolution (Table.5.1). For the purposes of our analysis, we define 30-year periods from the HIST run between 1976-2005 (from this moment on referred as HIST), the near future (2021-2050) and the far future (2071-2100).

In the case of ENEA, the HIST run span from 1979-2005 due to different simulation initialization, while CMCC and AWI/GERICS simulations reached 2099. The spin-up strategy of the Med-CORDEX ensemble was not prescribed, therefore it was different for every configuration. The lack of a long spin-up (e.g. U.BELGRAD, ENEA) could be detrimental for temperatures at deeper layers but not so relevant for the SST evolution. For the CNRM model, a constant monthly flux (atmosphere to ocean) correction was applied to minimise identified biases, with no significant influence on the climate change signal. Also, a slightly intense SST signal in the Alboran Sea was noted in the U.BELGRADE configuration for 2021-2050 under RCP8.5 and is probably linked to the simple representation of the connection between the Mediterranean Sea and the Atlantic Ocean in the model: The open boundary condition, as defined in the POM model, was applied in single model point defined on the strait of Gibraltar, without any buffer zone and with prescribed boundary conditions in the Atlantic Ocean; this is, on the other hand, a common approach in many models. Finally, an error has been recently reported concerning the CNRM-CM5 GCM files that were used as atmospheric lateral boundary conditions for CNRM and ENEA (http://www.umr-cnrm.fr/cmip5/spip.php?article24), but this likely has no significant effect on the long-term climate change signal.

Working from the hypothesis that MHWs are usually confined close to the surface, in this study we consider that the model SST data of the 1st layer depth represent surface temperatures between 1-16 m, depending on the model. We acknowledge, however, that MHWs may penetrate deeper to the water column under certain conditions, but assume for the time being that SST is a reliable sign of possible harmful conditions for deeper layers.

### 5.2.2 Reference Dataset

In order to evaluate the model's capability to simulate trends in regional extreme thermal events, we first perform comparisons with satellite data (OBS) provided by the Copernicus Marine Service and CNR - ISAC ROME. More specifically, the Mediterranean Sea high-resolution L4 dataset is employed, providing daily, reprocessed SSTs on a 0.04 °grid, an interpolation of remotely sensed SSTs from the Advanced Very High Resolution Radiometer (AVHRR) Pathfinder Version 5.2 (PFV52) onto a regular grid (Pisano et al., 2016). They are obtained over a 30-year period of January 1982 to December 2012 and are used as a reference for the models' performance in the mean and extreme climate in the Mediterranean Sea. With the aim of validating the "present-day" climate, we choose the 30-year period (1976-2005) in the model HIST runs that has the greatest overlap with the observed 30-year period (1982-2012). Prior to performing any calculations and in order to compare the results between the models and observations,

we first interpolated every dataset to the NEMOMED8 grid, already in use by 2 RCSMs, by implementing the nearest neighbour method.

### 5.2.3 Defining Marine Heatwaves

(*The current section has been already described in Section 2.3.2-2.3.5.*)

As for their atmospheric counterparts, there is no universal definition for MHWs. However, certain metrics can be applied to compare different events in space and time. In this research, the qualitative MHW definition proposed by Hobday et al. (2016) is followed. We use it as a baseline for developing a quantitative method that will identify MHWs, namely in the summer months, based on the climatology and the geographical characteristics of the area. Although we recognise that heatwaves in colder months might also be essential for certain species, we choose to focus on extreme events related to the highest annual SSTs, when organisms may be beyond their optima, as seen by previous mass mortality events in the Mediterranean (e.g. MHW of 1999 and 2003).

According to Hobday et al. (2016) a MHW is an "prolonged, anomalously warm water event at a particular location" and it should be defined relative to a 30-year period. In our case, a subset of the HIST experiments (1976-2005) and the 1982-2012 period for the observations are chosen, representing the average climate in the latter half of the 20th century. In order to achieve a homogenised yet area-specific temperature diagnostic, for every year of the reference period (HIST) we first compute the 99th quantile of daily SST ($SST_{99Q}$) for every grid point. Then we average these 30 years of extreme values, constructing a 2D threshold map. Note that individual threshold maps were created for each dataset separately, accounting for the different model characteristics (e.g SST bias). An "anomalously warm day" at every grid point is then any given day when the local $SST_{99Q}$ threshold is exceeded. However, in order to be classified as a "prolonged" event, we set the minimum duration of a MHW to 5 days, following Hobday et al. (2016). Further, we aim to identify long-lasting events, since most of the previous mass mortalities in the basin occured during thermal anomalies that lasted for more than 5 days (e.g. (Garrabou et al., 2009; Di Camillo and Cerrano, 2015; Cerrano et al., 2000; Cebrian et al., 2011). In addition, the average present-day MHW duration in the basin was found around 10 days (not shown). Therefore, a 3-day or 7-day minimum definition threshold would not change significantly the MHW characteristics in the future (see section 4.)

The discrete nature of MHWs also necessitates a well-defined starting and ending day, but gaps with temperatures close to threshold values can also be found, as a result of day-to-day SST fluctuations. At this point, our definition differs slightly from that of Hobday et al. (2016). More specifically, gaps of up to 4 consecutive days or less are allowed inside a local MHW (considered as warm days). This is true,however, only when both the preceeding and following 6-day mean SST of a gap day (including the gap day in each mean) are above the local $SST_{99Q}$. For the cool day "neighbourhood" this would represent a tendency to remain above threshold,

even though the SST of that particular cool day might be below limit. This also reflects the fact that minor SST deviations from the threshold cannot impact the overall warm conditions of a MHW. It would most likely not offer either an "essential" relief to organisms, even to the less mobile and perhaps less tolerant species, once a MHW has started. Taking advantage of the default statistical sensitivity of the mean to outliers (in this case cold temperatures), we make the assumption that an event with the potential to interrupt a MHW (e.g wind, current) should cause a considerable drop in daily SST. Therefore, a below-threshold drop in either of the 6-day SST averages would not allow any cool day to merge with a MHW, in the same way that a sequence of five cool days or more would interrupt an event entirely. The 11-day window around the gap day is chosen since the minimum duration of a MHW was set to five days.

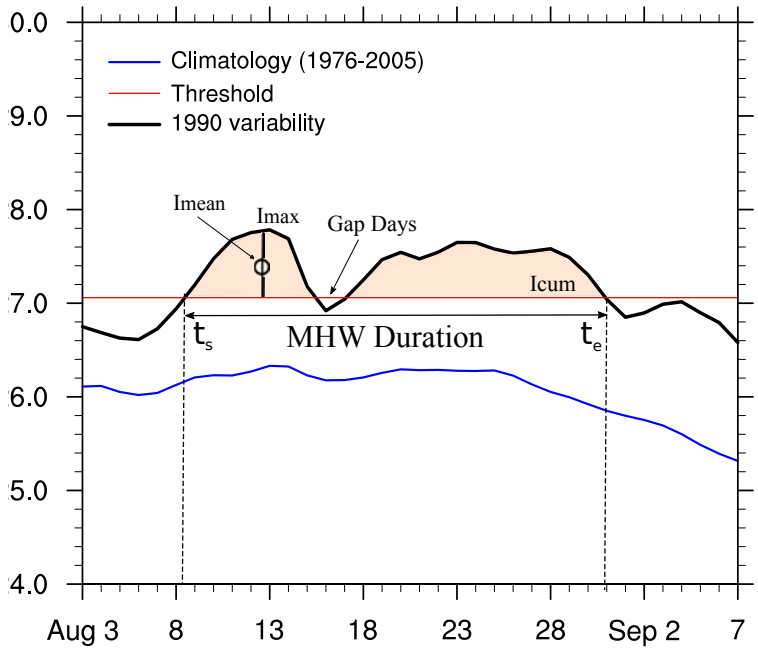


Figure 5.1: Schematic of a MHW based on Hobday et al. (2016). The black line represents daily SST variations of one grid point in a random year and red line is the local threshold ($SST_{99Q}$) based on the 30-year average of the yearly 99th quantile of daily SST for that point. The blue line is the daily 30-year climatology for this point. Also shown here also are the starting day ($t_s$) and ending day ($t_e$) above $SST_{99Q}$, gap days and the different measures of daily intensity. MHW metrics refer to the total event duration.

The spatial coverage of the MHW is then determined by aggregating grid points that are "activated" in a MHW state every day but are not necessarily contiguous. In common with many atmospheric definitions, a minimum 20% of the Mediterranean surface in $km^2$ was chosen in order to detect large-scale events that may have a broad ecosystem impact but also represent rare occurrence for the average climate conditions of HIST period. We, therefore, opt for prolonged, large-scale and extremely warm ocean temperatures that do not occur on a yearly basis in the 20th century, with a view of quantifying their evolution in the 21st century under different GHG emission scenarios. The advantage of a percentile-based SST threshold in our case is that spatial patterns are also identified independently from the different extreme

temperature levels that characterise sub-basins in the Mediterranean. We acknowledge that the detection method is developed based on subjective choices, and the sensitivity of the climate change results to these changes was also tested (See Section 4).

Once a MHW is identified, a subset of MHW metrics defined in Hobday et al. (2016) are used to characterise it. We examine the frequency of MHWs (Annual count of events), and the duration of each event is defined as the time between the first ($t_s$) and last day ($t_e$) for which a minimum of 20% of Mediterranean Sea surface is touched by a MHW. Every event is characterised by a mean and max intensity (mean and spatiotemporal maximum temperature anomaly relative to the threshold over the event duration) and a maximum surface coverage. Finally, its severity is represented by cumulative intensity (spatiotemporal sum of daily temperature anomalies relative to the threshold over the event duration) (Fig.5.1, Table.5.2).

| Marine Heatwave Metrics | Description |
|---|---|
| Frequency | Number of events occuring per year |
| Duration | $(t_e - t_s) + 1$ (days) |
| Mean Intensity (Imean) | $\int [\int (SST_{(x,y,t)} - SST_{99Q}(x,y))\mathrm{dxdy}]\mathrm{dt} / \int \mathrm{dxdy} \int \mathrm{dt}$ (°C) |
| Max Intensity (Imax) | $max_{(x,y,t)}(SST_{(x,y,t)} - SST_{99Q}(x,y))$ (°C) |
| Severity (Icum) | $\int [\int (SST_{(x,y,t)} - SST_{99Q}(x,y))\mathrm{dxdy}]\mathrm{dt}$ (°C.days.km$^2$) |

Table 5.2: Marine Heatwave (MHW) set of properties and their description after Hobday et al. (2016)

## 5.3 Results

### 5.3.1 Model Evaluation

The first goal of this paper is to evaluate each models' ability to simulate mean ($\overline{SST}$) and extreme Mediterranean Sea SST ($SST_{99Q}$) correctly. For this reason, pattern correlations were first performed, using the Pearson product-moment coefficient of linear correlation between two variables. The observed annual mean $\overline{SST}$ between 1982-2012 (Fig.5.2 OBS) shows a NW-SE pattern of cold-warm temperatures ranging from ~ 15 °C to 23 °C, respectively. Similarly, all the models demonstrate a warmer Eastern Mediterranean (EM) between 19 °C to 23 °C while colder deep water formation areas (e.g. Gulf of Lions, Adriatic) are captured well around 15 °C to 17 °C. Despite a multi-model mean (MMM) cold bias of about 0.6 °C, spatial correlations between each model mean 1976-2005 $\overline{SST}$ and observations are high (MMM~ 0.94). The lowest bias is found in ENEA and the highest in the CMCC and AWI/GERICS models (see Table.5.3). Note that satellite provides skin and night-time SST values, whereas the model SST represents averaged daily temperatures of the first few meters of mixed layer depth. Part of the model bias can be therefore explained by this difference in SST.

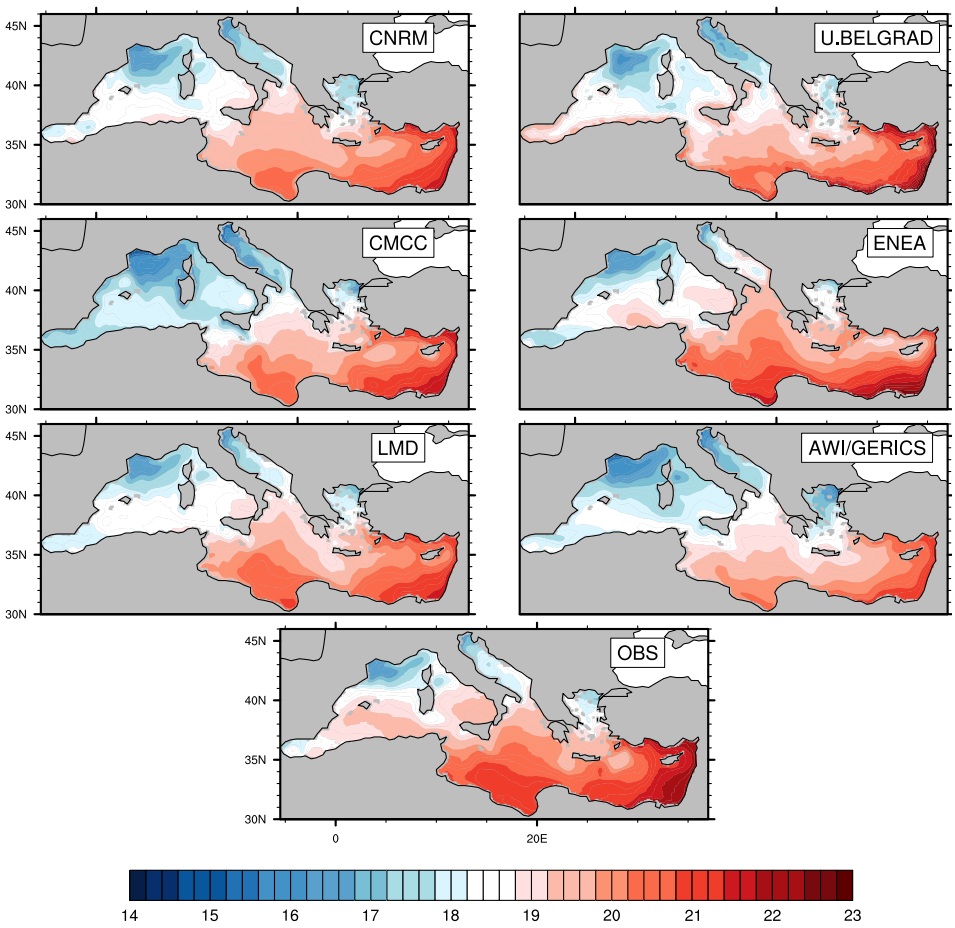


Figure 5.2: Yearly $\overline{SST}$ (°C) for the HIST run of every model (1976-2005) and satellite data during 1982-2012. Note that the HIST run for ENEA is from 1979-2005.

More complex spatial patterns are revealed when examining the 2D threshold maps used as the basis for defining Mediterranean MHWs (Fig.5.3). The highest $SST_{99Q}$ are observed in Central Ionian, Gulf of Gabes, Tyrrhenian Sea and Levantine basin varying from approximately 27 °C to 31 °C and the lowest (20-22 °C) in deep water formation areas and the Alboran Sea (Fig.5.3 OBS). In general, all the models are able to reproduce these patterns, although this time they share lower spatial correlations with the observations (MMM ~ 0.78). The ENEA model shows a warm bias whereas CMCC, U.BELGRAD and AWI/GERICS show a cold bias larger than 1 °C. The similar behaviour of the latter three could perhaps be related to the common atmospheric component (ECHAM) of their driving GCM. On the whole, the difference between the MMM mean and the extreme basinwide SST is found to be ~6.6 °C, in good agreement with the observations (7.1 °C). The corresponding MMM spread is small for the $\overline{SST}$ but higher for the $SST_{99Q}$ (~ 1 °C).

Further, the domain-averaged timeseries of SST illustrate a warming tendency of both the $\overline{SST}$ and annual $SST_{99Q}$ (Fig.5.4, Table.5.3). Even though MMM $\overline{SST}$ and $SST_{99Q}$ obtain similar trends (~0.02 °C/year) they seem to underestimate the corresponding observed trends (0.04/0.05 °C/year). Particularly for AWI/GERICS and U.BELGRAD, this is a response likely explained by their common driving GCM (MPI-ESM-LR).

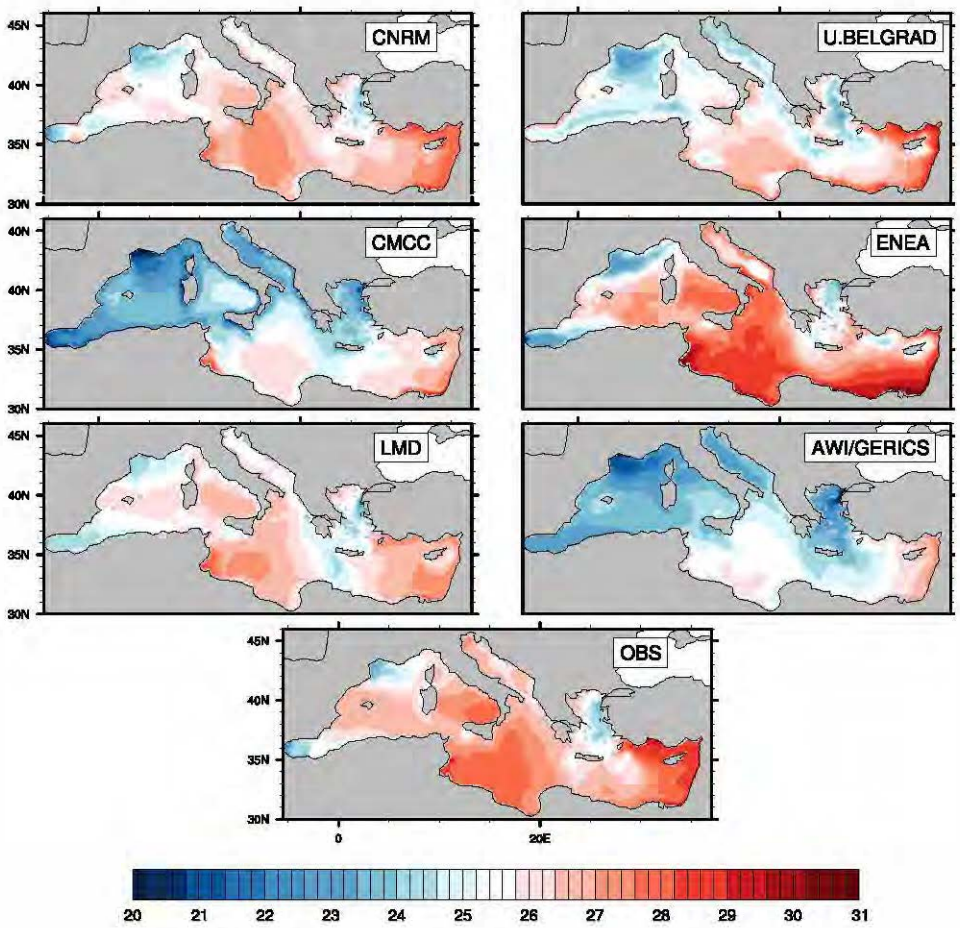


Figure 5.3: Individual MHW threshold maps of mean $SST_{99Q}$ (°C) computed from the HIST run of every model (1976-2005) and satellite data during 1982-2012. Note that the HIST run for ENEA is from 1979-2005

On the other hand, the amplitude of interannual variability is found similar to the observations for most of the models. On the whole, the observed and most of the model trends are statistically significant at a level of 95% except for certain cases indicated in Table.5.3. Interestingly, none of the simulations peaked as high as the observations during the exceptional MHW year of 2003 (20.4 °C for $\overline{SST}$ and 28.4 °C for $SST_{99Q}$). This record basinwide $SST_{99Q}$ value is on average 8.7 °C higher than the average $\overline{SST}$ °C of 1982-2012 and 2.8 °C greater than the basin-mean $SST_{99Q}$ of that period.

In terms of MHW properties during 1982-2012 (Table.5.3), observed MHW frequency is found at 0.8 events per year that last a maximum of 1.5 months and range between July and September. The mean intensity of MHWs varies from 0.3 to 0.9 °C, covering a maximum of 20% to 90% of the Mediterranean Sea surface, with a maximum intensity of 5.0 °C (2002) and a maximum severity of $8.5*10^7$ °C.days.km$^2$. The highest values over this period (except from Imax) refer to the characteristics of the well-known MHW 2003. More specifically, they correspond to a Mediterranean-scale event lasting 48 days (20 July-5 September) by our definition, in line with Grazzini and Viterbo (2003) and Sparnocchia et al. (2006). It seems that mainly the phase of the MHW that was both large-scale and intense was captured here.

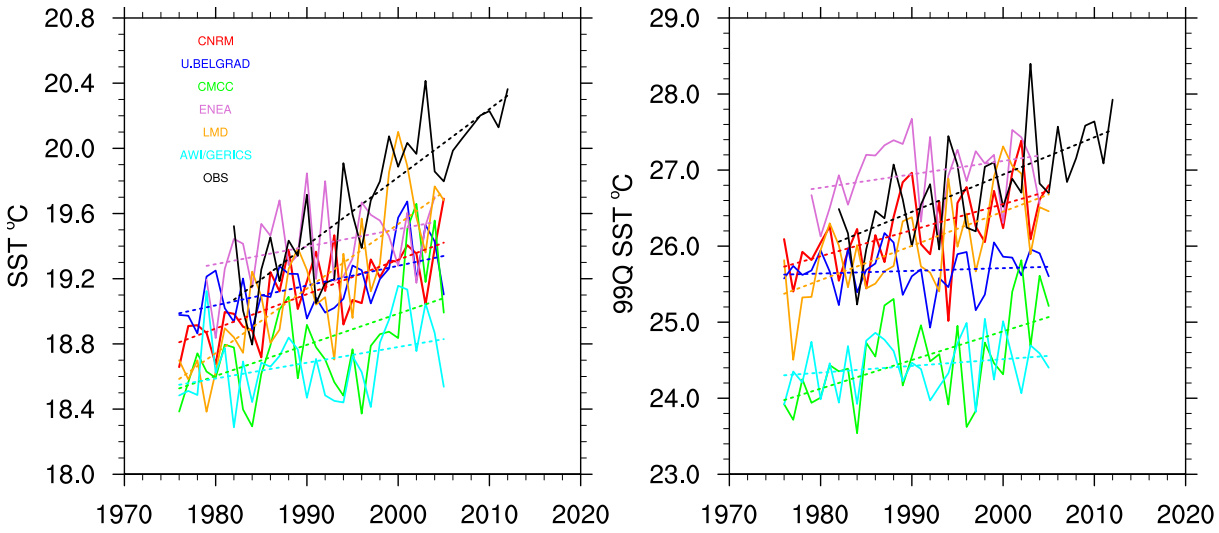


Figure 5.4: Timeseries of area-averaged, yearly $\overline{SST}$ °C (left) and $SST_{99Q}$ °C (right), during HIST for every model and satellite data, represented by a solid line. Trends are indicated in dashed lines. The different simulations are represented by different colors.

On average, the simulated events during HIST are well within the equivalent observed range of every variable. They manifest though a slightly lower annual frequency, a potential for slightly higher maximum durations and starting dates up to early September. They also appear to underestimate the upper level of the Imean, Imax and severity range. In particular, event durations of two months or more are exhibited by LMD, CMCC and AWI/GERICS models, while the ENEA model shows the highest Imax of 5.3 °C. Maximum severity, on the other hand, appears closer to the observed values only in the LMD and CMCC models. These configurations also show a MHW maximum spatial coverage above 80%, along with CNRM and AWI/GERICS. In general, the Med-CORDEX ensemble appears to perform well given that this is the first time, to our knowledge, that Mediterranean RCSMs have been evaluated for MHWs properties.

To better understand the ensemble variability of the MHW characteristics in the HIST period, we also combine Intensity-Duration-Frequency (IDF) information for every dataset separately (see Fig.5.5). The total number of events of this period are organised in bins of Imean (every 0.02 °C) and duration (5-day bins progressively increased to 10-day and 20-day bins). Although some models simulate longer events relative to MHW 2003, only CMCC exhibited equivalent MHWs in terms of duration and intensity. At the same time, 1-3 events are detected for most classes of Imean and duration, in both the observations and the models. There are only a few cases where 3-7 events appear with Imean below 0.6 °C but follow no specific duration pattern.

| Characteristics | CNRM | LMD | CMCC | AWI/GERICS | U.BELGRAD | ENEA | Multi-Model | OBS |
|---|---|---|---|---|---|---|---|---|
| SST EVALUATION | | | | | | | | |
| $\overline{SST}$ | 19.11 | 19.16 | 18.80 | 18.69 | 19.16 | 19.41 | $19.06 \pm 0.30$ | 19.70 |
| $\overline{SST}$ – OBS Corr.Coeff | 0.97 | 0.97 | 0.95 | 0.97 | 0.92 | 0.89 | $0.94 \pm 0.03$ | |
| $\overline{SST}$-OBS Bias | -0.59 | -0.54 | -0.90 | -1.01 | -0.54 | -0.29 | $-0.63 \pm 0.30$ | |
| $\overline{SST}$ Timeseries Trend | 0.02 | 0.04 | 0.02 | 0.01* | 0.01 | 0.01* | $0.02 \pm 0.01$ | 0.04 |
| $\overline{SST_{99Q}}$ | 26.23 | 26.03 | 24.52 | 24.43 | 25.68 | 26.97 | $25.64 \pm 1.00$ | 26.79 |
| $SST_{99Q}$ - OBS Corr.coeff | 0.88 | 0.84 | 0.77 | 0.84 | 0.70 | 0.74 | $0.79 \pm 0.07$ | |
| $SST_{99Q}$ -OBS Bias | -0.56 | -0.76 | -2.27 | -2.36 | -1.11 | 0.18 | $-1.15 \pm 1.00$ | |
| $SST_{99Q}$ Timeseries trend | 0.03 | 0.04 | 0.04 | 0.01* | 0.00* | 0.02* | $0.02 \pm 0.02$ | 0.05 |
| MHW CHARACTERISTICS (HIST) | | | | | | | | |
| Frequency | 0.7 | 0.6 | 0.6 | 1 | 0.7 | 0.7 | 0.7 | 0.8 |
| Duration | 2 – 32 | 4 – 67 | 1 – 74 | 1 – 61 | 4 – 38 | 4 – 44 | 2.6 – 52.6 | 1 – 48 |
| Starting Day | Jul - Sep | Jul - Aug | Jul - Aug | Jul - Sep | Jul - Aug | Jul - Sep | Jul - Sep | Jul - Aug |
| Ending Day | Jul - Sep | Aug - Sep | Aug- Sep | Aug - Sep | Jul - Sep | Aug - Sep | Aug - Sep | Aug - Sep |
| Imean | 0.4 – 0.8 | 0.3 – 0.7 | 0.3 – 0.9 | 0.2 – 0.6 | 0.3 – 0.6 | 0.4 – 0.6 | 0.3 – 0.7 | 0.3 – 0.9 |
| Imax | 1.8 – 5.5 | 1.5 – 4.1 | 1.4 – 4.9 | 1.0 – 3.0 | 1.5 – 3.2 | 1.8 – 5.3 | 1.5 – 4.3 | 1.3 – 5.0 |
| Severity (Icum) | 0.04 – 3.6 | 0.1 – 7.8 | 0.01 – 8.8 | 0.01 – 4.3 | 0.1 – 1.6 | 0.1 – 2.6 | 0.05 – 4.8 | 0.02 – 8.5 |
| Max Surface | 20.8 – 82.5 | 21.5 – 88.3 | 20.1 – 90.8 | 20.3 – 81.9 | 22.5 – 59.8 | 20.7 – 72.1 | 21.0 – 79.2 | 20.1 – 90.1 |

Table 5.3: Evaluation of SST and MHW properties during HIST run. Mean annual and threshold SST are indicated with $\overline{SST}$ (°C) and $SST_{99Q}$ (°C) respectively. The Mann-Kendal non-parametric test is used to detect the presence of linear or non-linear monotonic trends (°C/year) in domain-averaged SST timeseries. Trends with statistical significance lower than 95% level are indicated with star. Spatial correlations (Corr.Coeff) and bias with respect to observations are given for each dataset. Also shown here, are the range (min and max) of frequency, duration (days), starting day (calendar month), ending day (calendar month), Imean (°C) Imax (°C), Severity*$10^7$ (°C.days.km$^2$) and maximum surface coverage(%) of MHWs. The multi-model column indicates the ensemble average values and standard deviation for each variable.

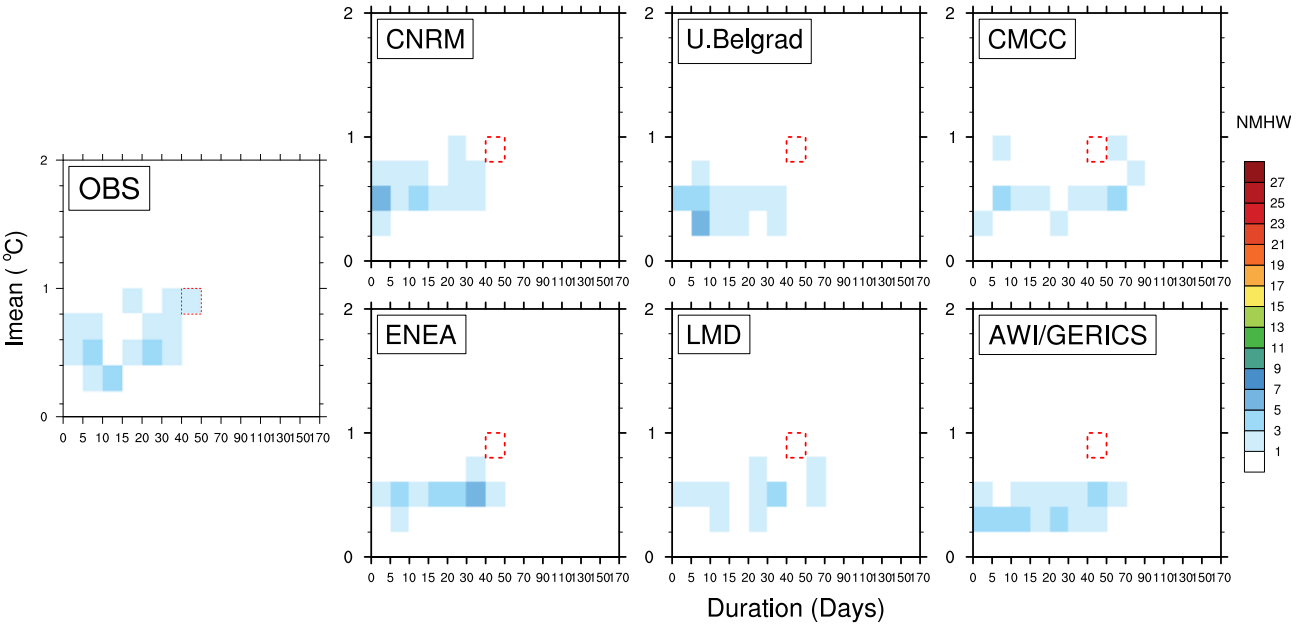


Figure 5.5: IDF plot; Intensity (Imean in °C), Duration (Days), Frequency (Number of MHW during 1976-2005). Imean is organised in bins of 0.02 °C, while duration is in bins of 5, 10 and 20 days. Red box indicates observed characteristics corresponding to the exceptional MHW of 2003.

### 5.3.2 Future Mediterranean SST evolution

In this section we analyze projections of $\overline{SST}$ and $SST_{99Q}$ in the 21st century by comparing their evolution against the reference period and under different GHG emission scenarios.

During 2021-2050 an increase is found for the domain-averaged ensemble mean $\overline{SST}$ and $SST_{99Q}$ with respect to HIST, around 0.8 °C - 1 °C and 1 °C - 1.2 °C respectively. While the mid-21st century anomalies appear almost independent from the greenhouse gas forcing, a more diverse and substantial warming occurs towards 2071-2100 (see Fig.5.6). In particular, the multi-model mean $\overline{SST}$ and $SST_{99Q}$ anomalies under RCP8.5 are 3.1 °C and 3.6 °C respectively, exhibiting nearly a doubling of their corresponding RCP4.5 rise. Similarly, the equivalent increase of CNRM $\overline{SST}$ and $SST_{99Q}$ under RCP8.5 is about 3 times as high as that under RCP2.6 for the same period. Individually, however, the highest mean and extreme SST anomalies are demonstrated by the LMD and CMCC models under every scenario and for every period (see Table.5.4). For both SST indices, the effects of the different emission scenarios become more evident by 2060, with the highest/intermediate warming occuring for every model under RCP8.5/RCP4.5 and the lowest under the (mono-model) RCP2.6 simulation. In the latter, little or no difference is found between the $\overline{SST}$ and $SST_{99Q}$ rise throughout the century. In contrast, under RCP4.5 and RCP8.5, the multi-model $SST_{99Q}$ increase appears greater than the $\overline{SST}$ rise by 20%-25% during 2021-2050 and by 16%-18% for 2071-2100 (see Table.5.4 and discussion section). This implies a higher contribution from $\overline{SST}$ to the warming towards the end of the century.

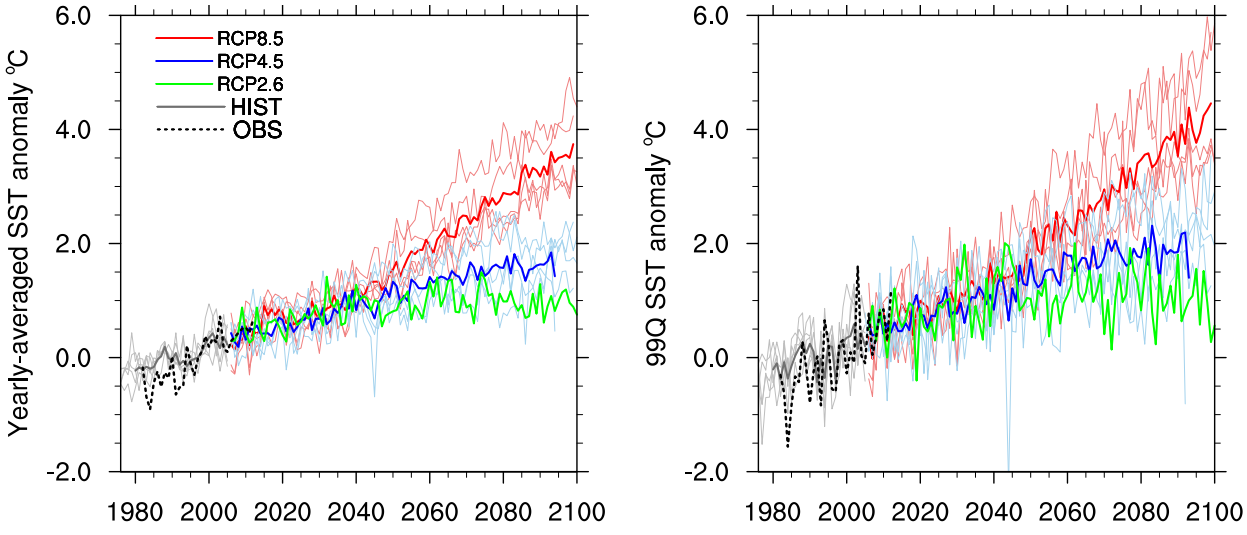


Figure 5.6: Area-average, yearly $\overline{SST}$ °C (left) and extreme $SST_{99Q}$°C (right) anomalies with respect to HIST. Bold colors represent the multi-model average and lighter colors are the individual simulations. RCP2.6 scenario has only one simulation (CNRM), HIST run is illustrated in grey and observations in dashed black.

| | CNRM | LMD | CMCC | AWI/GERICS | BELGRAD | ENEA | Multi-Model |
|---|---|---|---|---|---|---|---|
| RCP85 2021-2050 | | | | | | | |
| $\overline{SST}$ | 0.9 | 1.3 | 1.2 | 0.7 | 0.7 | - | $1.0 \pm 0.3$ |
| $SST_{99Q}$ | 1.1 | 1.7 | 1.3 | 1.0 | 1.0 | - | $1.2 \pm 0.3$ |
| RCP85 2071-2100 | | | | | | | |
| $\overline{SST}$ | 2.7 | 3.8 | 3.4 | 2.7 | 2.7 | - | $3.1 \pm 0.5$ |
| $SST_{99Q}$ | 2.9 | 4.5 | 4.3 | 3.1 | 3.1 | - | $3.6 \pm 0.7$ |
| RCP45 2021-2050 | | | | | | | |
| $\overline{SST}$ | 0.7 | 1.2 | 1.0 | 0.6 | - | 0.6 | $0.8 \pm 0.4$ |
| $SST_{99Q}$ | 0.8 | 1.4 | 1.3 | 0.8 | - | 0.7 | $1.0 \pm 0.5$ |
| RCP45 2071-2100 | | | | | | | |
| $\overline{SST}$ | 1.6 | 2.1 | 2.0 | 1.1 | - | 1.2 | $1.6 \pm 0.8$ |
| $SST_{99Q}$ | 1.8 | 2.6 | 2.5 | 1.4 | - | 1.3 | $1.9 \pm 0.9$ |
| RCP26 2021-2050 | | | | | | | |
| $\overline{SST}$ | 0.8 | - | - | - | - | - | - |
| $SST_{99Q}$ | 1.0 | - | - | - | - | - | - |
| RCP26 2071-2100 | | | | | | | |
| $\overline{SST}$ | 1.0 | - | - | - | - | - | - |
| $SST_{99Q}$ | 1.0 | - | - | - | - | - | - |

Table 5.4: Future Mediterranean-averaged, yearly mean ($\overline{SST}$) and extreme ($SST_{99Q}$) anomalies (with respect to HIST) for the near and far future under different emission scenarios. The multi-model column indicates the ensemble average values and standard deviation. Values are in °C.

The spatial distribution of the corresponding anomalies, however, appears inhomogeneous. For 2071-2100, some regions in the Levantine basin, Balearic islands, Tyrrenian Sea, Ionian Sea and North Adriatic Sea exhibit the highest MMM $\overline{SST}$ anomalies in every scenario (Fig.5.7). In contrast, the lowest anomalies of that time are located in the Alboran Sea, where cold waters are advected from the Atlantic, and depending on the scenario they may range from ~0.6 °C (RCP2.6) to ~2.4 °C (RCP8.5).

Meanwhile, the most pronounced extreme warm anomalies ($SST_{99Q}$) for 2071-2100 under RCP4.5 and RCP8.5 are projected for the NW mediterranean, Tyrrenian Sea, Ionian Sea and some parts of North Levantine basin (Fig.5.8). Under RCP2.6 though, the greatest $SST_{99Q}$ anomalies (>1.2 °C) are more confined towards the Aegean Sea, Adriatic, Tyrrhenian Sea and the area around Balearic islands. In addition to the highest $SST_{99Q}$ rise, the Adriatic Sea, Ionian Sea, Tyrrhenian Sea, some parts around the Balearic islands and the North Levantine basin display also the greatest $\overline{SST}$ rise, for every scenario during the 2nd half of the 21st century. During 2021-2050, however, they exhibit the highest mean and extreme warming under RCP26 and RCP4.5 but not under RCP8.5. The Alboran Sea and the SE Levantine basin, on the other hand, demonstrate the lowest $SST_{99Q}$ anomalies in every period and every scenario.

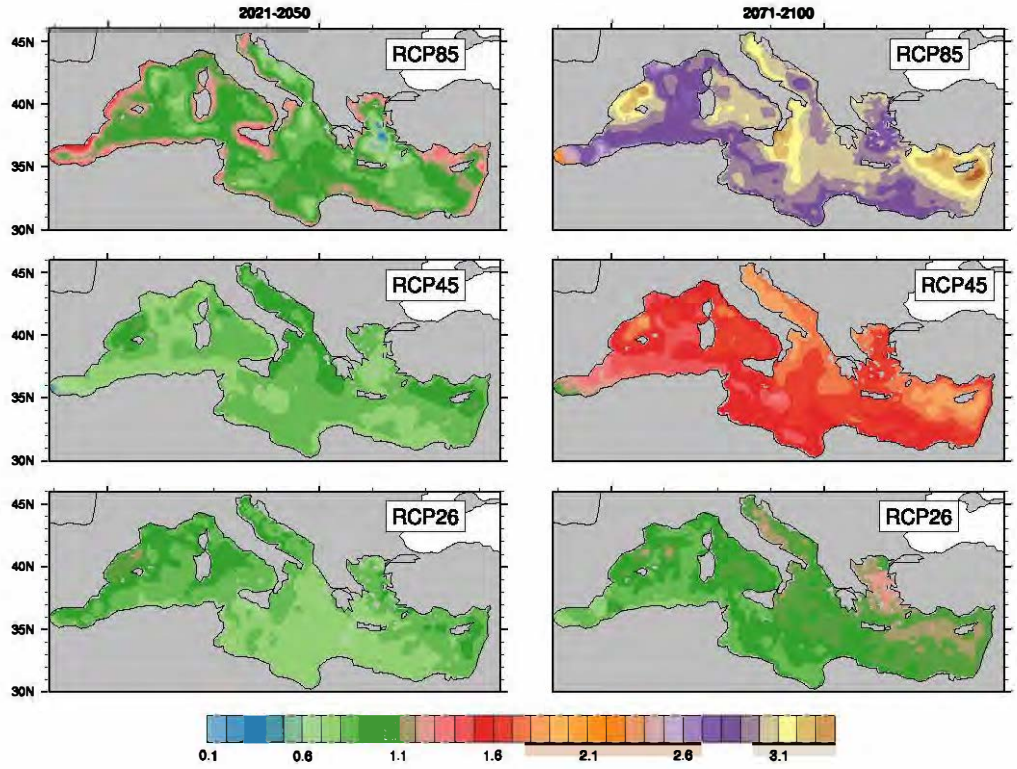


Figure 5.7: Multi-model average anomaly of yearly $\overline{SST}$ (°C) with respect to the corresponding ensemble mean HIST of each scenario, for the near and far future. The RCP2.6 scenario has only one simulation (CNRM).

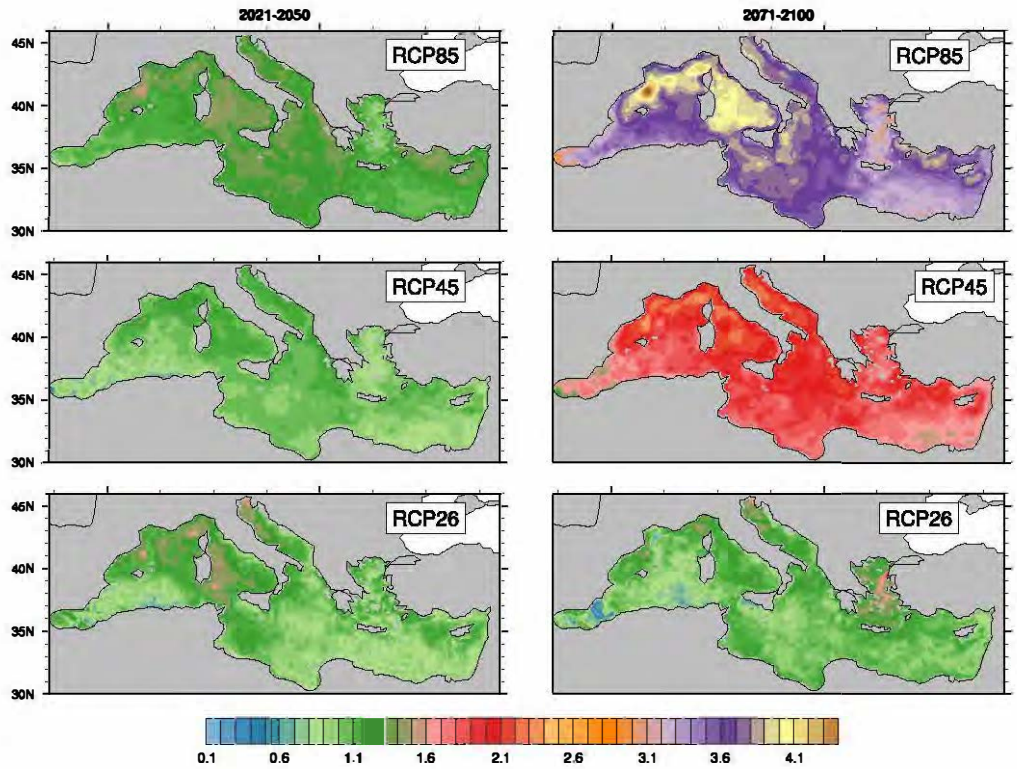


Figure 5.8: Multi-model average anomaly of extreme $SST_{99Q}$ (°C) with respect to corresponding ensemble mean HIST (1976-2005) of each scenario, for the near and far future. The RCP2.6 scenario has only one simulation (CNRM).

### 5.3.3 Future evolution of Mediterranean MHWs

The MHW climate change response is examined here using anomalies. These anomalies are computed for the average MHW characteristics in the future relative to the average MHW characteristics in HIST run, for each sub-period, model and scenario (Table.5.5).

The multi-model mean reveals an increase in frequency of 0.3-0.4 events/year for every period of RCP4.5/RCP8.5 with the mono-model RCP2.6 simulation showing a slightly greater increase of 0.5 - 0.7 events/year. In fact, individual simulations of Figure 5.9 suggest a shift from a period where years without MHWs were common (1976-2030) to a period with at least one long-lasting MHW every year. More specifically, towards 2071-2100, events can start as early as June and finish as late as October under RCP8.5, whereas for RCP4.5 and RCP2.6, the MHW temporal extent appears between July-September (Fig.5.10). It is clear that the higher the radiative forcing, the broader the window of occurrence. For example, MHWs during 2071-2100 may last on average 3 months longer in RCP8.5 than HIST MHWs (~ 21.8 days, not shown) but almost 2 months longer in RCP4.5 (see Table.5.5). This is a MMM increase in the duration, almost double the corresponding increase during 2021-2050 under RCP4.5 (~ 30.9 days) and more than double that under RCP8.5 (~ 39.2 days). Even under the optimistic RCP2.6 scenario, MHWs by 2050 may be 17.2 days longer than today and may become 1 month longer at maximum by 2100.

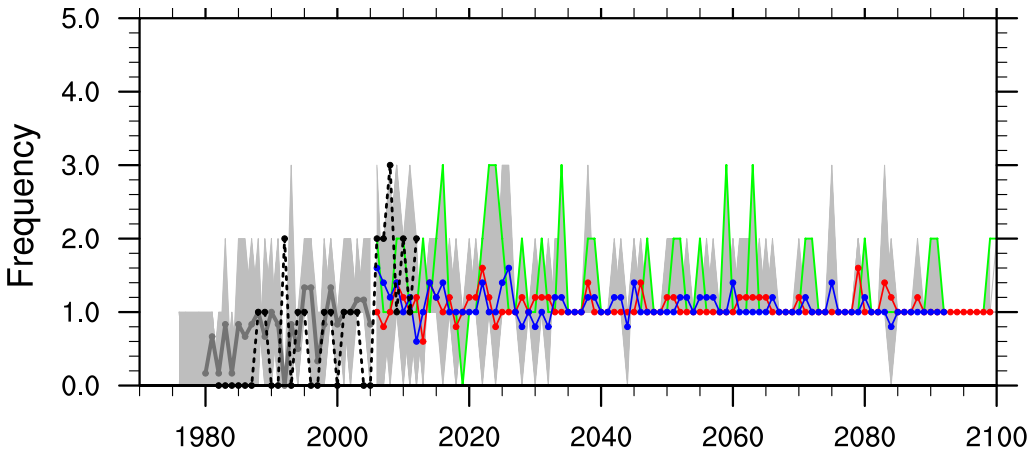


Figure 5.9: Annual number of MHWs (Annual Frequency) for RCP8.5 (red) RCP4.5 (blue) RCP2.6 (green) HIST (grey) and observations (dashed black). Bold colors indicate the multi-model mean and shaded zones represent individual MHW events identified by the models. Years without MHWs are also included, with shaded areas reaching 0. RCP2.6 has only 1 simulation (CNRM).

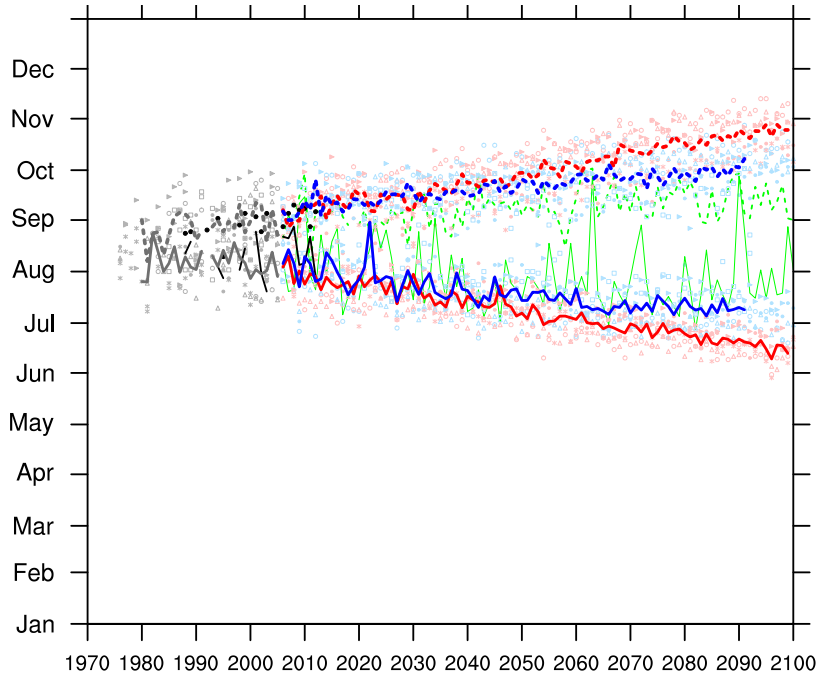


Figure 5.10: Annual earliest starting (solid lines) and latest ending (dashed lines) day of MHW events for RCP8.5 (red) RCP4.5 (blue) RCP2.6 (green) HIST (grey) and observations (black). Bold colors indicate multi-model average values, while lighter dots represent individual event dates.

Long-term projections show analogous changes in the Imean of future MHWs. They are examined through IDF plots that display the total number of MHWs identified by the ensemble during HIST (1976-2005) run, near and far future (Fig.5.11). To avoid imbalances in the present-future comparisons arising from the different sets of models for RCP4.5 and RCP8.5 (see Table.5.5), all the simulated future events are pooled for every period and juxtaposed against the corresponding sets of HIST events. Therefore, we show 3 HIST IDF plots, one for each scenario. As previously demonstrated the stronger the emission scenario, the longer the duration and the higher the Imean of the events. The MMM Imean response appears small during 2021-2050 (+0.1°C to +0.3 °C depending on the scenario) but increases towards the end of the period with higher radiative forcing. For instance, MHWs show durations of up to 170 days (Fig.5.11) in the far future of RCP8.5 and Imean of 1.8 °C on average (not shown). For the CNRM model though and under RCP2.6, the corresponding response towards 2071-2100 has doubled compared to the mid-21st century, while it becomes 4.5 times higher under RCP8.5 (see Table.5.5). Longer-lasting MHWs at the end of the period for RCP4.5 and RCP8.5 explain the lower frequency of occurrences compared to RCP2.6. A similar behaviour to Imean displays the MMM average response of Imax, with the highest anomalies indicated towards 2071-2100 (up to 3.7 °C), whereas during the mid-21st century they range between 0.5 °C (RCP2.6) and 1.2 °C(RCP8.5).

It should be also noted that for RCP4.5 and RCP8.5, events with characteristics similar to the observed exceptional MHW 2003 (Fig.5.11 red box) seem to become the new standard over 2021-2050 and even constitute weak occurrences for the distant future of RCP8.5. In the

| Marine Heatwave Characteristics | | | | | | | |
|---|---|---|---|---|---|---|---|
| Variables | CNRM | LMD | CMCC | AWI/GERICS | BELGRAD | ENEA | Multi-Model |
| RCP8.5 (2021-2050) | | | | | | | |
| Frequency | 0.5 | 0.4 | 0.5 | 0.1 | 0.4 | - | $0.4 \pm 0.2$ |
| Duration | 32.7 | 47.8 | 39.3 | 39.1 | 37.4 | - | $39.2 \pm 16.7$ |
| Starting Day | Jul | Jul | Jul | Aug | Jul | - | Jul |
| Ending Day | Sep | Sep | Sep | Sep | Sep | - | Sep |
| Imean | 0.2 | 0.4 | 0.3 | 0.2 | 0.2 | - | $0.3 \pm 0.1$ |
| Imax | 1 | 1.4 | 1.3 | 1.2 | 0.9 | - | $1.2 \pm 0.5$ |
| Max Surface | 23.5 | 39.2 | 29.4 | 36.7 | 35.6 | - | $32.9 \pm 14.6$ |
| Severity (Icum) | 3.9 | 11.6 | 7.1 | 6.7 | 4.7 | - | $6.8 \pm 3.8$ |
| RCP8.5 (2071-2100) | | | | | | | |
| Frequency | 0.3 | 0.4 | 0.5 | 0 | 0.4 | - | $0.3 \pm 0.2$ |
| Duration | 83.8 | 105.9 | 97.7 | 99.6 | 83.7 | - | $94.1 \pm 9.9$ |
| Starting Day | Jun | Jun | Jun | Jun | Jun | - | Jun |
| Ending Day | Oct | Oct | Oct | Oct | Oct | - | Oct |
| Imean | 0.9 | 1.9 | 1.6 | 1.3 | 1.1 | - | $1.4 \pm 0.4$ |
| Imax | 3.1 | 4.2 | 4.4 | 3.8 | 3.1 | - | $3.7 \pm 0.6$ |
| Max Surface | 51.7 | 50.7 | 46.1 | 58.9 | 53.5 | - | $52.2 \pm 4.6$ |
| Severity (Icum) | 29.2 | 73.1 | 63.1 | 46 | 34.1 | - | $49.1 \pm 18.7$ |
| RCP4.5 (2021-2050) | | | | | | | |
| Frequency | 0.6 | 0.4 | 0.5 | 0.1 | - | 0.2 | $0.4 \pm 0.2$ |
| Duration | 17.7 | 43.7 | 38.6 | 33.9 | - | 20.6 | $30.9 \pm 16.2$ |
| Starting Day | Aug | Jul | Jul | Jul | - | Jul | Jul |
| Ending Day | Sep | Sep | Sep | Sep | - | Sep | Sep |
| Imean | 0.1 | 0.3 | 0.2 | 0.2 | - | 0.2 | $0.2 \pm 0.1$ |
| Imax | 0.5 | 1.2 | 1.2 | 1.1 | - | 0.9 | $1.0 \pm 0.5$ |
| Max Surface | 13.5 | 34.1 | 27.9 | 33.8 | - | 27.9 | $27.4 \pm 13.5$ |
| Severity (Icum) | 1.9 | 8 | 6.7 | 4.9 | - | 3.7 | $5.0 \pm 3.0$ |
| RCP4.5 (2071-2100) | | | | | | | |
| Frequency | 0.4 | 0.4 | 0.5 | 0 | - | 0.2 | $0.3 \pm 0.2$ |
| Duration | 56.4 | 69,8 | 67,9 | 55,4 | - | 45,4 | $59 \pm 10.0$ |
| Starting Day | Jul | Jun | Jul | Jul | - | Jul | Jul |
| Ending Day | Sep | Oct | Oct | Sep | - | Sep | Sep |
| Imean | 0.4 | 0.8 | 0.7 | 0.4 | - | 0.4 | $0.5 \pm 0.2$ |
| Imax | 1.6 | 2.3 | 2.3 | 1.8 | - | 1.5 | $1.9 \pm 0.4$ |
| Max Surface | 44.4 | 48.5 | 42.6 | 51.2 | - | 39 | $45.1 \pm 4.8$ |
| Severity (Icum) | 10.6 | 25.3 | 23.9 | 11.8 | - | 8.5 | $16.0 \pm 7.7$ |
| RCP2.6 (2021-2050) | | | | | | | |
| Frequency | 0.7 | - | - | - | - | - | - |
| Duration | 17.2 | - | - | - | - | - | - |
| Starting Day | Jul | - | - | - | - | - | - |
| Ending Day | Sep | - | - | - | - | - | - |
| Imean | 0.1 | - | - | - | - | - | - |
| Imax | 0.5 | - | - | - | - | - | - |
| Max Surface | 15 | - | - | - | - | - | - |
| Severity (Icum) | 2.4 | - | - | - | - | - | - |
| RCP2.6 2071-2100 | | | | | | | |
| Frequency | 0.5 | - | - | - | - | - | - |
| Duration | 30.5 | - | - | - | - | - | - |
| Starting Day | Jul | - | - | - | - | - | - |
| Ending Day | Sep | - | - | - | - | - | - |
| Imean | 0.2 | - | - | - | - | - | - |
| Imax | 0.9 | - | - | - | - | - | - |
| Max Surface | 22.7 | - | - | - | - | - | - |
| Severity (Icum) | 3.6 | - | - | - | - | - | - |

Table 5.5: Future response (anomalies with respect to HIST) of MHW mean properties for the 6 RCSMs under RCP8.5, RCP4.5 and RCP2.6, for the near (2021-2050) and far future (2071-2100). Shown here are the average annual event count (frequency), average MHW duration (days), starting day (calendar month), ending day (calendar month), Imean (°C), Imax (°C), severity ($*10^7$°C.days.km$^2$) and maximum surface coverage (%). The multi-model column indicates the ensemble mean values for each variable and their standard deviation. Only the CNRM simulation is available for the RCP2.6 scenario, 5 simulations for RCP8.5 and 5 simulations for RCP4.5.

more optimistic RCP2.6, MHWs appear more frequent during 2021-2050 but their number is slightly decreased towards 2071-2100. Their characteristics, however, sustain a lower increase throughout the period compared to RCP4.5 and RCP8.5. For example, the response in duration and Imean is found close to that projected for CNRM during 2021-2050 and under RCP4.5 and RCP8.5 (see Table.5.5). Therefore, the possibility for an event like the MHW 2003 to occur regularly still features in a scenario close to the Paris Agreement (RCP2.6).

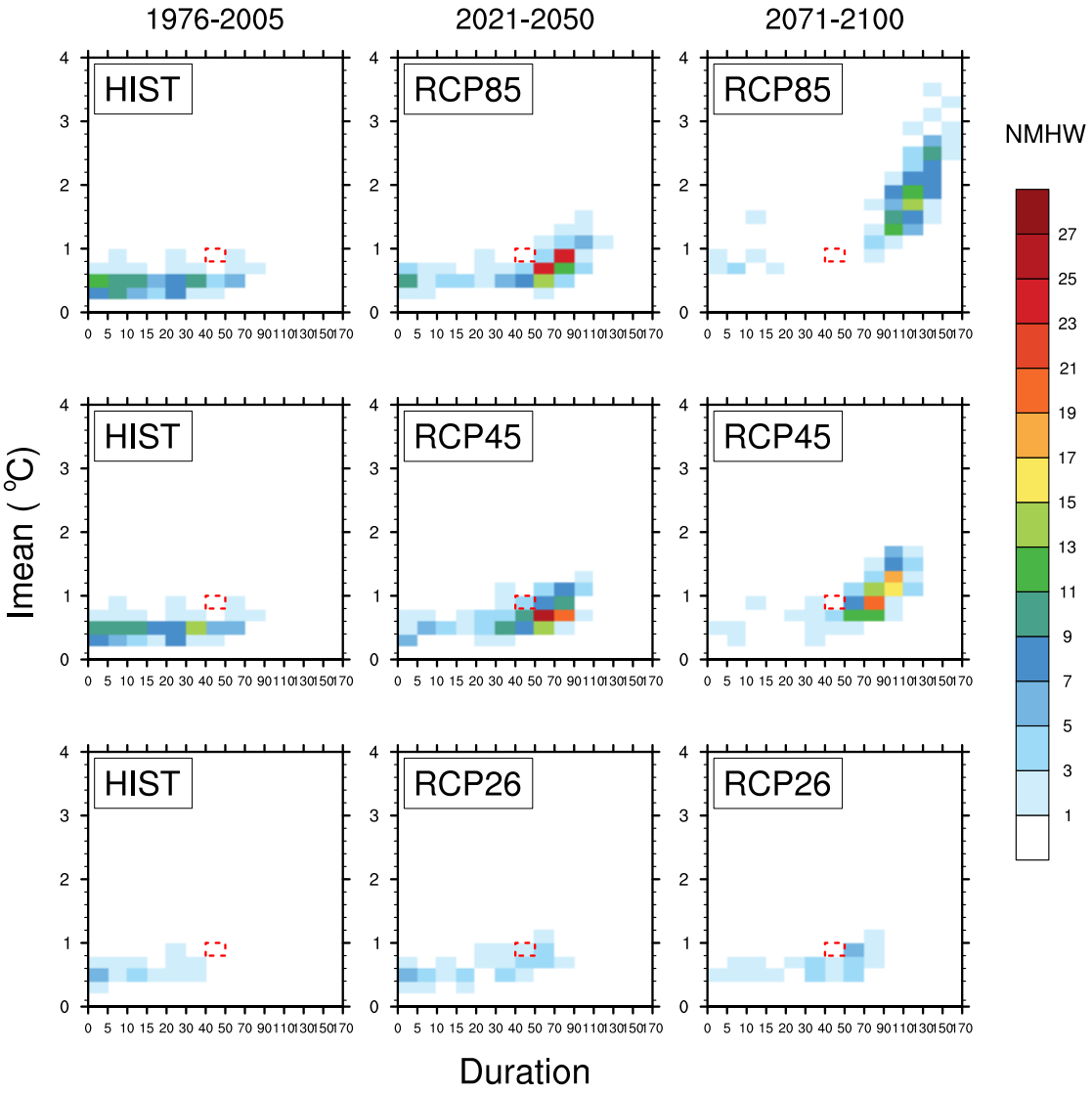


Figure 5.11: IDF (Imean, Duration, Frequency) plots display the total number of every dataset for every scenario over 2021-2050 and 2071-2100. RCP8.5 and RCP4.5 include events from 5 simulations, while RCP2.6 from only 1 (CNRM) simulation. HIST run contains MHWs from the corresponding set of models each time. The number of MHWs is calculated over each 30 year period. For contrast purposes, the red box depicts the observed characteristics of MHW 2003 in the Mediterranean.

Yet, the range of the uncertainty in future projections evolves not only in time but also throughout the different models. The severity (Icum) distribution of future MHWs was determined in that sense using Whisker diagrams. In these box plots, a specific Icum index is appointed at each simulated event of every dataset for each period and scenario (see Fig.5.12

(*left*)). By definition, Icum translates the total spatiotemporal MHW impact into numbers. It features an exponential increase from HIST towards the end of the century from ~1*$10^7$ C.days.km$^2$ to about ~50*$10^7$ C.days.km$^2$ for RCP8.5 (2071-2100-not shown). Moreover, the higher the emission forcing, the higher the rate the ensemble mean Icum response escalates from its mid- to end-of-century values; for example, Icum varies from 5 to 33*$10^7$ C.days.km$^2$ in RCP4.5 and from 6.8 to 49.1*$10^7$ C.days.km$^2$ in RCP8.5 (see Table.5.5). This becomes more evident when comparing the equivalent CNRM severity response under RCP2.6 (2.4-3.6 *$10^7$ C.days.km$^2$) with the significantly higher response under RCP4.5 and RCP8.5. Although all configurations indicate an abrupt escalation through time, there appears to be a family of models (CMCC and LMD) that share a stronger climate change response. Those models exhibit higher changes in Icum, along with higher Imean, Imax, and duration values than the remaining models (see also Table.5.5 and Discussion section).

The identified families of MHWs are also associated with a maximum spatial coverage illustrated through box plots in Figure 5.12 (*right*). It is estimated that events may affect a maximum of 40% of the Mediterranean Sea, on average, during HIST but may impact almost 100% of the basin by 2071-2100 under RCP8.5. Notwithstanding the large variability found for the mid-21st century, by 2100 the simulated maximum MHW extent seems to be an unanimous projection from every model and under RCP8.5. Conversely, MHWs under RCP2.6 increase their maximum coverage throughout the period, but towards 2071-2100 events may impact, on average, a maximum of 70% of the Mediterranean Sea.

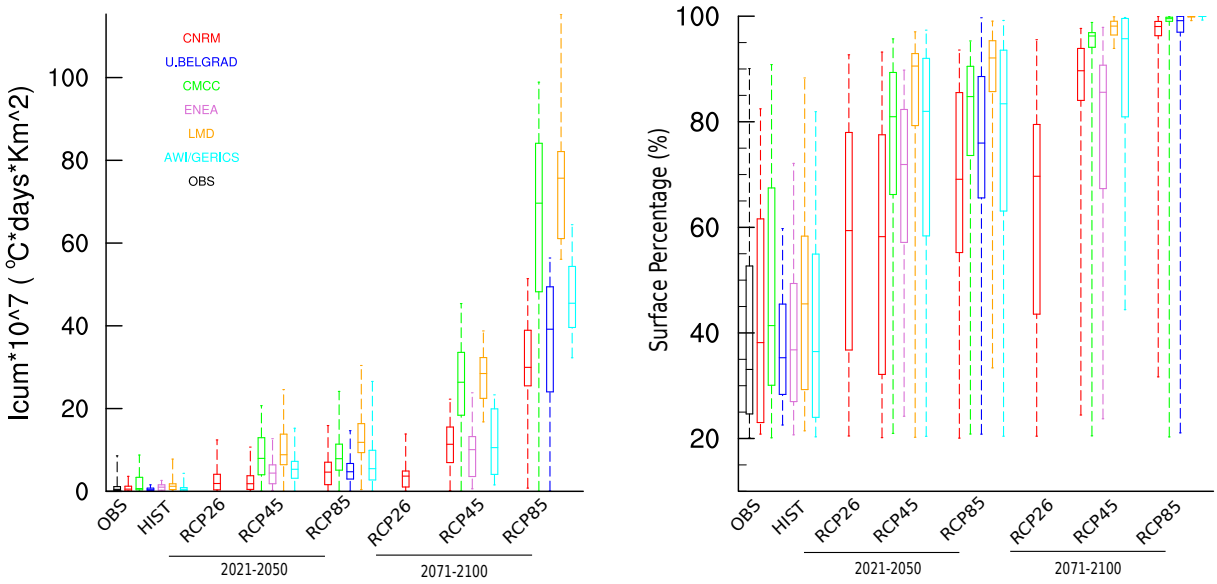


Figure 5.12: Whisker diagram of (left) Severity (Icum) and (right) maximum surface coverage of every observed and simulated MHW during HIST, 2021-2050 and 2071-2100. Box plots illustrate minimum, 25th percentile, median, 75th percentile and maximum values of each variable for a given model, scenario and period.

## 5.4 Discussion

### 5.4.1 MHW detection method

Several sensitivity tests performed on the MHW detection algorithm using only the CNRM model indicate low levels of uncertainty associated with small perturbations on the initial definition. For example, definitions with a different number of gap days, different minimum duration or minimum MHW spatial extent allowed (e.g. 10%) were tested but did not seem to change significantly the response of future MHW characteristics with respect to HIST run (see Supplementary Table.5.6). The use of different quantile thresholds also showed that climate change response of duration, Imean and Imax with respect to HIST does not differ significantly if a lower/higher threshold than the $SST_{99Q}$ is chosen. However, the severity and maximum spatial coverage appear more sensitive to such changes (see Supplementary Table.5.6).

However, certain limitations exist: assuming no spatial connectivity, the detection algorithm provides identification of large-scale (>20%) and long-lasting events but does not consider MHW effects during colder months or spatially smaller events. While it describes surface MHWs in the summer, it can be also applied to deeper layers and/or winter season when availability of data allows it.

### 5.4.2 Model-Observation Discrepancies

The discrepancies on mean and extreme Mediterranean Sea temperatures with respect to observations on the models were also evaluated using a shorter but common reference period of 1982-2005 for both datasets. Values of $\overline{SST}$, $SST_{99Q}$, their trends and pattern correlations did not change considerably. However, the multi-model mean bias was slightly reduced by 28% for $\overline{SST}$ and by 31% for $SST_{99Q}$ (see Supplementary material Table.5.7). Moreover, MHW identification appeared consistent despite the different SST layer depth of the observations (~ mm) and the models (~ m).

### 5.4.3 Model uncertainty

By default, the estimate of the uncertainty is given by the variation of the results across the ensemble members in an opportunistic way (Knutti et al., 2010). Although the models we use have a high-resolution representation of the air-sea interactions, uncertainties are introduced due to their individual biases but also due to the small number of the currently available Med-CORDEX simulations (6 RCSMs). To this purpose, more runs will be added in the future as part of the Med-CORDEX initiative. Despite this limitation, the RCSM ensemble seems to explore well the spread of SST anomalies predicted by earlier studies based on GCMs. For example, for RCP4.5 we estimate annual area-average $\overline{SST}$ anomalies from 2006-2100 with respect to HIST from approximately 0.7 °C to 2.6 °C, depending on the model (Fig.5.6). This

covers a large part of the corresponding anomalies found by Mariotti et al. (2015) for 2006-2100 with respect to 1980-2005 mean, which were between 0.5 °C to 3.5 °C for the CMIP5 ensemble of GCMs under the RCP4.5 scenario. Although our ensemble appears to underestimate the upper limit of this CMIP5 range, this could also reflect a better representation of the Mediterranean Sea dynamics by the regional models. Indeed, at higher resolutions the representation of air-sea interaction also improves (e.g. Akhtar et al., 2018; Roberts et al., 2016; Hewitt et al., 2017). At the same time, our results indicate an intensification of MHWs in the Mediterranean Sea with time, in agreement with the results obtained by Oliver et al. (2018a) and Frölicher et al. (2018), which used different MHW definitions.

Albeit some models have demonstrated lower/higher biases than others, we have chosen not to discard any of the configurations since their weak performance in some indices is not related to any specific behaviour of MHW indices in scenario. This choice also favours the holistic presentation of the uncertainty spectrum, without a considerable impact on the climate change response. More specifically, closer examination of the $\overline{SST}$ and $SST_{99Q}$ bias effect on the anomalies of the average MHW characteristics in RCP8.5 and RCP4.5 with respect to HIST suggested no particular tendency or outliers affecting the range of the outcome, for any of the periods and scenarios (Supplementary material Fig.5.14, Fig.5.15). It is however notable that LMD and CMCC have a tendency to show stronger responses in MHW or SST values. This could be due to the driving GCMs (IPSL-CMA5-MR and CMCC-CM), which demonstrate a higher mean surface temperature change over Europe by 2080 compared to CNRM-CM5 and MPI-ESM-LR, according to McSweeney et al. (2015). In that study, the performance of all the GCMs driving the Med-CORDEX RCSMs was characterised as "satisfactory" for downscaling, except that of LMD, which was found with biases.

### 5.4.4 MHW evolution and changes in SST

Present-day extreme warming at the order of $SST_{99Q}$ might constitute a rare occurrence for the Mediterranean Sea climate; however, in the future it becomes the new normal. In 2071-2100 in particular, the warming signal is found so high that almost every day from June to October can experience such extreme temperatures. This means that future warming in the Mediterranean Sea is practically able to saturate what is considered today as a severe MHW. The difference between the scenarios lies in the fact that under RCP4.5 and RCP8.5 anomalous temperatures appear more persistent and widespread and therefore fewer but longer and more intense events occur. By contrast, under RCP2.6, events appear less persistent, and therefore more "breaks" between MHWs may occur (frequency of events is increased), since a significant part of the basin is more likely to fall below the $SST_{99Q}$ threshold (Fig.5.9).

Most of the future changes in MHW characteristics were seen to increase following the GHG forcing, yet this raises the question of whether this behavior could be explained by changes in the mean (shift of distribution) or the day-to-day SST variability (distribution

flattening/narrowing). As a first indicator, we calculated (for the CNRM model only) the $\overline{SST}$ difference between RCP8.5 (2071-2100) and HIST and added it to the current $SST_{99Q}$ threshold map (see Supplementary Table.5.6). The resulting climate change response (future-present) of MHW characteristics was much lower than the one found when using the initial $SST_{99Q}$ threshold alone. This signifies that the mean SST change alone can explain a large part, but not all, of the future changes in MHWs. We estimate that 10%-20% of the MHW characteristics are due to changes in day-to-day variability.

To further test our hypothesis, we calculated the multi-model mean ratio R=$\Delta(SST_{99Q\text{Scenario}}$ - $SST_{99Q\text{Hist}})$/ $\Delta(\overline{SST}_{\text{Scenario}}$ - $\overline{SST}_{\text{Hist}})$ for every scenario and period (see Fig.5.13). In regions where R>1 SST daily variability contributes to the extreme temperature increase and only where R>2, it dominates the mean SST change contribution (distribution flattening). For R<1, a narrowing of SST daily distribution lowers the mean SST signal, which makes the dominant contribution when close to R=1. Overall, model results indicate a higher contribution from SST daily variability change in the mid-21st century compared to 2071-2100, when $\overline{SST}$ change becomes more important (Table.5.4, Fig.5.13).

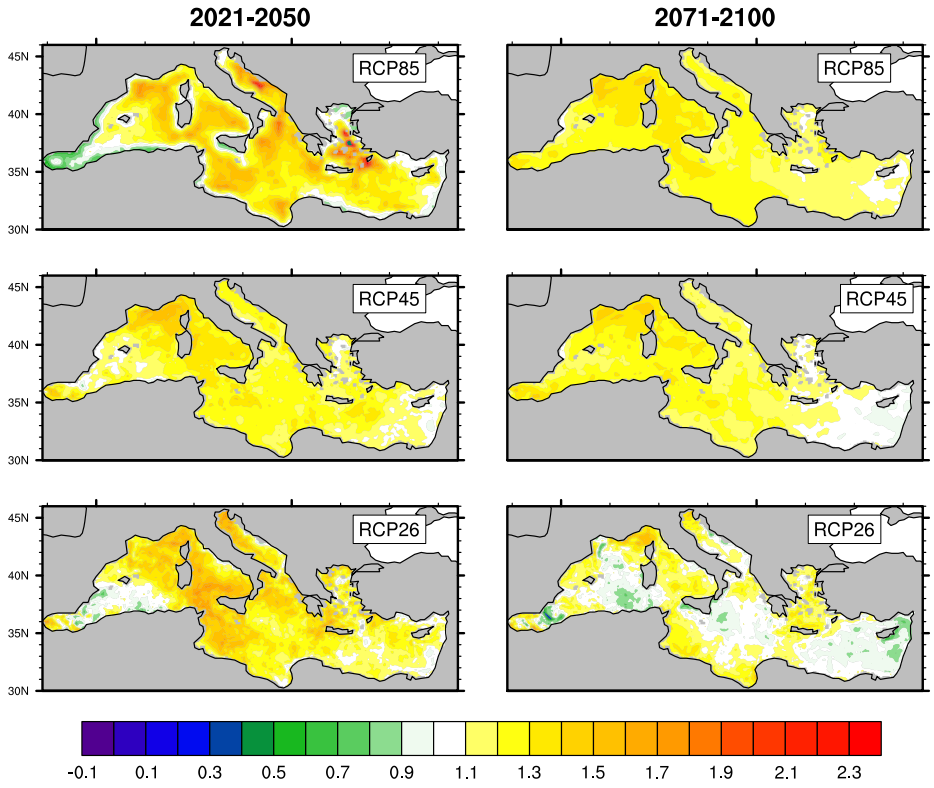


Figure 5.13: Multi-model mean ratio R of $\Delta$ $SST_{99Q}$ (°C) over $\Delta$ $\overline{SST}$ (°C) for every period and scenario. Regions where R>1/R<1 indicate regions where flattening/narrowing of SST distribution is detected in addition to the mean distribution shift. Where R~1 the $\overline{SST}$ increase can be considered as the main factor for MHW changes

During 2021-2050 and for every scenario, basin-mean R~1.2 with the Alboran Sea, some coastal parts of the Aegean Sea, Adriatic Sea and SE Levantine basin exhibiting a narrowing

(R<1) or a shift (R=1) in the SST distribution. Towards 2071-2100, however, and under RCP4.5 and RCP8.5, basin-average R is between 1<R<1.2 and more areas demonstrate a range closer to R=1.

It is worth noting that narrowing of the SST distribution is a rare situation that appears in small areas only under RCP2.6 or around the Alboran Sea under RCP85 for the mid-21st century. Flattening, on the other hand, appears more common and could possibly reflect the increase in day-to-day variability of 2m-air temperature estimated by Giorgi (2006) for the Mediterranean area in the future. Finally, a slightly stronger influence of SST daily variability is seen in the NW Mediterranean area for every scenario and period (Fig.5.13). The possible explanations for such a spatial pattern could be a future mixed layer depth shoaling, as projected by (Adloff et al., 2015). This would mean that heat fluxes would be able to change the heat content of a shallower MLD faster, creating that way an increase in daily SST variability.

## 5.5 Conclusions

The main objective of this study is to investigate the future evolution (1976-2100) of SST and marine heatwaves in the Mediterranean Sea, using the best dedicated multi-model ensemble available. Here we examine six Regional Climate System Models from the Med-CORDEX initiative, driven by 4 CMIP5 GCMs under the RCP2.6, RCP4.5 and RCP8.5 scenarios. A quantitative MHW definition and detection method based on SST and on Hobday et al. (2016) approach is developed, targeting large-scale and long-lasting events, mostly in the warmer months. The algorithm uses a climatological 99th percentile threshold based on historical simulations (1976-2005) and takes into account a spatially-varying threshold. It delivers MHW metrics such as frequency, duration, mean and maximum intensity along with severity and maximum spatial coverage.

Spatiotemporal indices under a 1976-2005 (HIST) run reveal that the Med-CORDEX ensemble simulates the present MHW characteristics well, although it appears to underestimate the warming trends of $\overline{SST}$ and $SST_{99Q}$ of that period with respect to observations from 1982-2012. The latter dataset yields an annual frequency of 0.8 events/year, with MHWs lasting a maximum of 1.5 months between July and September, while covering a maximum of 90% of the Mediterranean Sea surface. The longest and most severe event of that period corresponded to the MHW of 2003, which also demonstrates the highest mean intensity and maximum event coverage.

Analysis of future evolution shows that differences in the GHG forcing are reflected mostly towards 2071-2100, whereas uncertainty for the mid-21st century is dominated by the model uncertainty. Ensemble means by the end of the century demonstrate the highest $\overline{SST}$ (3.1 °C) and $SST_{99Q}$ (3.6 °C) increase under RCP8.5 and lowest under RCP2.6 (mono-model). The corresponding warming for 2021-2050, however, is less pronounced under RCP4.5 (~0.8°C/1°C ) and RCP8.5 (~1 °C/1.2 °C). In contrast, basinwide mean and extreme SST for RCP2.6 (~1

°C) does not differ significantly from mid- to end of 21st century.

By 2100, models project at least one long-lasting MHW occuring every year under RCP8.5 up to 3 months longer, and about 4 times more intense and 42 times more severe than today's events. Their occurrence is expected between June and October, affecting at peak, the entire Mediterranean basin. In fact, with respect to the HIST run, MMM MHW frequency increases by a factor of ~1.6 for RCP8.5 and RCP4.5 by 2021-2050 and slightly less than that towards 2071-2100 for both scenario. The equivalent CNRM comparison between the scenarios reveals a slightly greater frequency increase during 2071-2100 under RCP2.6 (by factor of 1.7) than under RCP8.5 and RCP4.5. Multi-model mean duration, on the other hand, is multiplied by a factor of 3.7 for RCP4.5 and 5.3 for RCP8.5 during 2071-2100. MHWs under RCP8.5 may also have an Imean 3.9 times as high as today's event, while the equivalent increase under RCP4.5 and RCP2.6 is significantly lower (see Table.5.5). For 2021-2050, however, there is a higher convergence in the factor of increase in frequency (~ 1.5x) duration (~ 2.4x-2.7x), Imean (~ 1.5x) and severity (~ 5x-7x) between MMM of RCP4.5 and RCP8.5.

In general, MHWs become stronger and more intense in response to increasing greenhouse gas forcing and especially towards the end of the century. RCP2.6, however, shows a slight increase in MHW signatures with time but lower than RCP4.5 and RCP8.5. Note here that certain models demonstrate stronger climate change responses than others, likely due to the choice of the driving GCM rather than to the individual RCSM biases. Much of the MHW evolution is found to occur mainly due to an increase in the mean SST, but an increase in daily SST variability also plays a noticeable role. Complementary sensitivity tests also prove that a mean shift in SST distributions alone cannot be responsible for the futures changes in MHWs.

Overall, the MHW and SST changes predicted for the 21st century will clearly impact the vulnerable Mediterranean Sea ecosystems. What was encountered as widespread consequences from the MHW 2003 could become the "new normal", since our analysis signified that future MHWs become longer and more intense than this event in the near future. Especially under RCP8.5 and 2071-2100, MHWs can become three times longer than the MHW 2003, with mean intensities three times higher. While RCP8.5 is the business-as-usual scenario, RCP2.6 is the closest to Paris agreement limits, which could offer a relative stability in both the SST increase and MHW evolution in the basin after the mid-21st century. MHWs exert a strong influence not only on marine ecosystems but also on marine-dependent economies and hence society. Therefore, more research is needed towards an improved mechanistic understanding of these events and their underlying physical drivers. In a constantly warming world, this information, along with projections of large-scale future MHW evolution, might help identify regions with a physical predisposition to these extreme occurrences. In combination with biogeochemical studies, more light could be shed on the full extent of the biological system risks related to MHWs.

## 5.6 Supplementary Material

| FUTURE RESPONSE WITH RESPECT TO HIST | | | | | | | | | | | | | | | |
|---|---|---|---|---|---|---|---|---|---|---|---|---|---|---|---|
| RCP85 2071-2100 | | | | | | | | | | | | | | | |
| | 90Q | 92Q | 95Q | 96Q | 97Q | 98Q | 99Q | 99.5Q | 99Q+SST | Exp.1 | Exp.2 | Exp.3 | Exp.4 | Exp.5 | Exp.6 |
| Number of MHW | -16 | -4 | -7 | -3 | -31 | -1 | 10 | 16 | 3 | 9 | 10 | 7 | -1 | 6 | 16 |
| Frequency | -0.53 | -0.13 | -0,.23 | -0.1 | -1.03 | -0.03 | 0.33 | 0.53 | 0.1 | 0.3 | 0.33 | 0.23 | -0.03 | -0,67 | 0,3 |
| Duration | 83.33 | 82.91 | 92.03 | 84.38 | 87 | 89.04 | 83.8 | 81 | 9.24 | 84.5 | 83.67 | 86.7 | 89.7 | 82,48 | 80,87 |
| Imean | 1.37 | 1.07 | 1.2 | 1.07 | 1.04 | 1 | 0.9 | 0.83 | 0.08 | 0.9 | 0.9 | 0.94 | 0.85 | 0,9 | 0,84 |
| Imax | 3.81 | 3.36 | 3.72 | 3.34 | 3.37 | 3.45 | 3.1 | 2.95 | 0.54 | 3.12 | 3.07 | 3.16 | 3.24 | 3,12 | 2,95 |
| Surfmax | 28.72 | 32.45 | 45.83 | 42.83 | 47.59 | 52.16 | 51.7 | 49.28 | 3.88 | 52.28 | 51.57 | 53.47 | 59.67 | 49,4 | 48,43 |
| Severity*10E7 | 57.47 | 51.21 | 45.44 | 39.78 | 37.97 | 34.75 | 29.2 | 26.74 | 0.81 | 29.3 | 29.2 | 30.3 | 29.4 | 28,52 | 28,91 |

Table 5.6: Anomalies of future MHW characteristics with respect to HIST run (climate change response) using different MHW definitions. Calculations are performed only for the CNRM model for the period 2071-2100 of the RCP85 scenario. First columns display MHW definitions with different SST thresholds (e.g 90th quantile of SST, 95th quantile of SST etc.). Climate change response of MHWs when the mean $\overline{SST}$ difference between HIST and 2071-2100 is added to the original $SST_{99Q}$ threshold is also showed in column 9. Further definitions are also tested: EXP.1 is an experiment performed without gap days on the MHW definition but the 20% spatial threshold retained. EXP.2 refers to MHWs detected with a definition that allowes 2 gap days and a minimum spatial threshold of 20%. In EXP.3 MHW definition allows up to 5 cool days that are lower than the initial threshold by up to 0.3 °C and a minimum spatial threshold of 20%. EXP.4 uses a MHW definition where gap days are defined as described in this paper but there is a 10% minimum limit on spatial threshold. Finally, Exp.5 and Exp.6 are tests of MHW definition where minimum duration of the events is set at 3 days and 7 days respectively. By MHW definition is implied the definition used in the paper with a spatial threshold of $SST_{99Q}$.

| SST Evaluation (1982-2005) | | | | | | | | |
|---|---|---|---|---|---|---|---|---|
| Characteristics | CNRM | LMD | CMCC | AWI/GERICS | U.BELGRAD | ENEA | Multi-Model | OBS |
| $\overline{SST}$ | 19.18 | 19.29 | 18.85 | 18.69 | 19.19 | 19.45 | 19.11 | 19.56 |
| $\overline{SST}$ – OBS Corr.Coeff | 0.97 | 0.97 | 0.95 | 0.97 | 0.91 | 0.89 | 0.94 | |
| $\overline{SST}$-OBS Bias | -0.38 | -0.27 | -0.71 | -0.87 | -0.37 | -0.11 | -0.45 | |
| $\overline{SST}$ Timeseries Trend | 0.02 | 0.04 | 0.03 | 0.01 | 0.01 | 0.004 | 0.02 | 0.04 |
| $SST_{99Q}$ | 26.32 | 26.15 | 24.64 | 24.47 | 25.67 | 27.04 | 25.71 | 26.61 |
| $SST_{99Q}$ - OBS Corr.coeff | 0.86 | 0.83 | 0.77 | 0.83 | 0.69 | 0.74 | 0.79 | |
| $SST_{99Q}$ -OBS Bias | -0.31 | -0.47 | -1.97 | -2.15 | -0.94 | 0.43 | -0.9 | |
| $SST_{99Q}$ Timeseries trend | 0.04 | 0.05 | 0.03 | 0.006 | 0.007 | 0.003 | 0.02 | 0.04 |

Table 5.7: SST properties during 1982-2005 years of HIST run and the observations. Mean annual and threshold SST are indicated with $\overline{SST}$ and $SST_{99Q}$. The mann-Kendal non-parametric test is used to detect the presence of linear or non-linear trends (°C/year) in domain-averaged SST timeseries. Spatial correlations (Corr.Coeff) and bias with respect to observations are given for each model dataset.

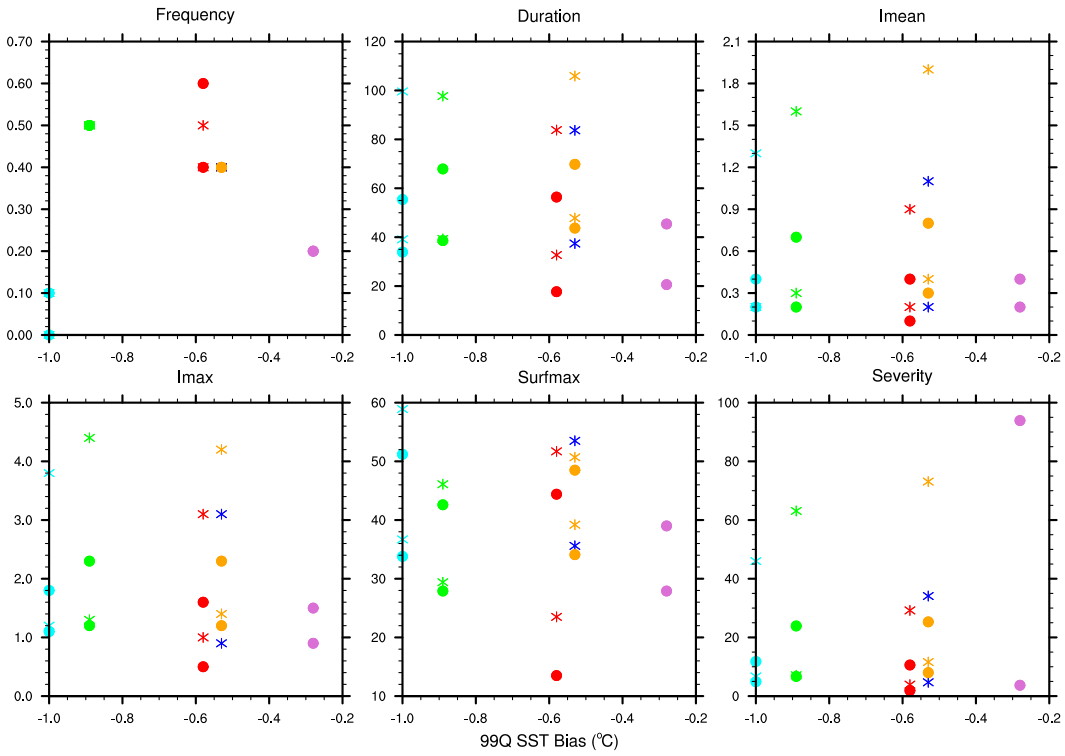


Figure 5.14: $\overline{SST}$ (°C) bias in relation to MHW characteristics anomalies of RCP45 (star) and RCP85 (circle) for both 2021-2050 and 2071-2100 periods, with respect to HIST run. For every variable model colors are represented as in main text.

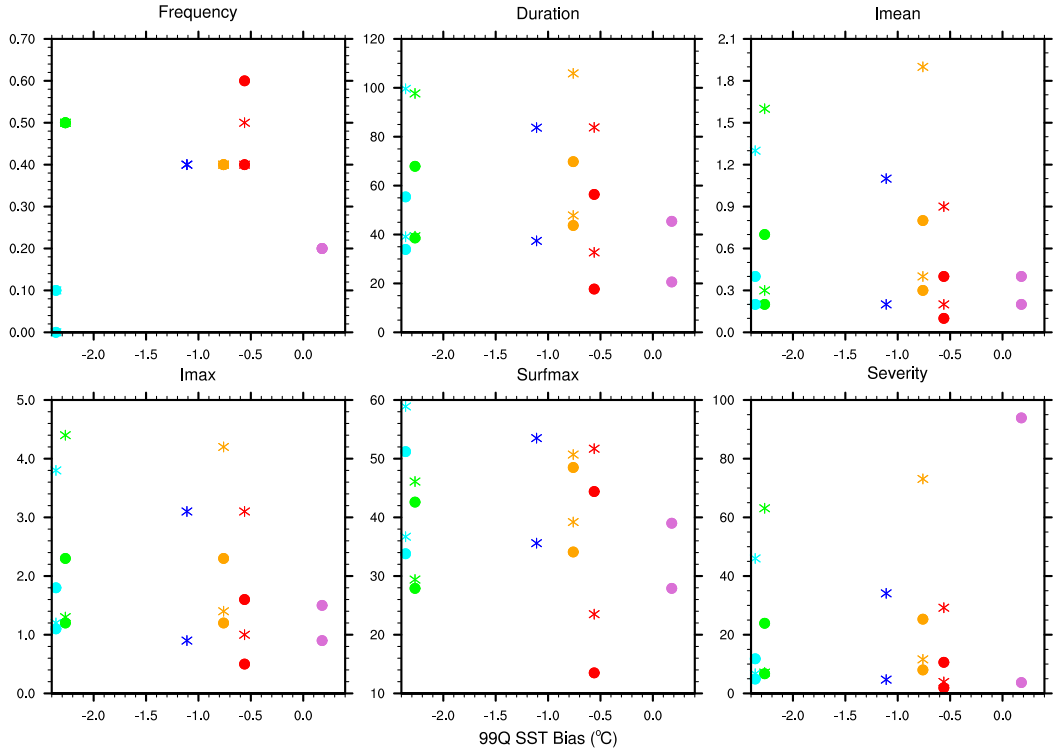


Figure 5.15: As Fig.5.14 but for $SST_{99Q}$ (°C) bias.

# Chapter 6

# Concluding Remarks

*".. Do not let the reality destroy your dreams. Use your dreams to change the reality."*

S.D

## Contents



## 6.1 Conclusions and Perspectives (English)

The high sensitivity of Mediterranean Sea to climate change is a consequence of both its location in the mid-latitudes and hotter-drier climates and of its specific topographical features. Anthropogenic factors, however, further exacerbate its vulnerability. As a result, high-impact weather and extreme events frequently affect the region, including MHWs that have been already observed to exert substantial pressure in marine ecosystems in the Mediterranean Sea. That being the case, the current PhD work has attempted to objectively define summer MHWs in the basin, with an eye to analyze how they are formed, what are their spatial patterns and to provide a robust assessment of their spatiotemporal evolution towards the 21st century. The results from the application of the developed detection method on various high-resolution observational and model datasets, provided us with interesting insights on the scientific questions we framed to this purpose in Chapter 1 and are presented below.

### 1. How do we define a summer Mediterranean MHW ?

In the present work, we have defined a general MHW detection method, targeting large-scale, long-lasting summer events in the Mediterranean. The algorithm takes into account the geographical characteristics of the area by considering local climatological thresholds of the 99th percentile of daily temperature, based on the last part of the 20th century. It can be adapted, however, to any other threshold, period or area specified from the user. For example, it can

be based on a threshold related to extreme ecosystem thermotolerance thresholds during the winter or to any other extreme cold event. Then, MHWs (or any other type of event chosen) are identified as events that exceed the selected threshold each time and their detection can be applied to 2D model (surface or deeper layers) or observational datasets as well as to local station data (including missing values inside). Further, it delivers a set of metrics that characterize each event, such as frequency, intensity, duration, severity and spatial coverage.

While this definition provides flexibility in the type of events identified, it presents certain limitations. As it requires a daily input of data, the algorithm is not applicable for *in situ* observations and deeper-layer data with lower temporal resolution (e.g. monthly). In that sense, the amount of data upon which it can be implemented is restricted, since most of the times, long-term *in situ* data (of deeper layers, for example) are hard to acquire at high frequency. At the same time though, the role of the diurnal cycle (or any other temporal variability) in MHW evolution is not assessed either and therefore, neither are the limitations due to this subjective choice.

In addition, no space continuity is assumed between the grid points that are affected by a MHW and, therefore, each event's track through space cannot be delivered. This practically means that the algorithm is not able to distinguish whether two areas with a simultaneous "aggregation" of MHW points, which are not contiguous, are characterised by the same or by two different events. This decision, however, strongly relies on how a MHW is defined in the first place, and what are the criteria that each time determine what separates one event from another. Therefore, they are subjective choices that depend on the user and the targeted application. For instance, in our case, at a local scale, one MHW was separated from another based on the minimum event duration (>5 days), while at 2D-scale it was based on the minimum spatial coverage (20 %). Another option, would be for the MHWs to be distinguished from their driving mechanisms, which may differ depending on the region, even if they occur within the same day. This is a factor which, however, is not accounted for in the present algorithm. Nevertheless, daily MHW spatial coverage is provided in this definition and under further processing by the user, both the area affected and the specific conditions that prevailed at that time can be identified, as we presented in Chapter 3. Finally, although the algorithm cannot yield a 3D representation of the MHWs, it can be applied to deeper layers of the ocean as well, just like it was demonstrated in Chapter 3.

All the above arguments prove that, similar to their atmospheric counterparts, an objective MHW definition does not exist. This is because, it is based on a series of subjective choices on the type of events we want to track. Hence, the detection of events enabled through algorithms, is inherent, by construction, with certain limitations on its initial conditions. For example, the choice of the reference period, the baseline temperatures, the minimum MHW duration and spatial extent, the gap days, need to be pre-determined, in order to facilitate the comparison between different events and datasets. In other words, there can be several different definitions that ≪ filter ≫ a certain part of the extreme ocean temperature spectrum. In our case, we

chose to detect events warmer than the 30-year climatology of temperatures above the 99th percentile, of the last part of the 20th century.

However, the different sensitivity tests we performed showed that for a given MHW the more intrinsic part of the methodology i.e. the gap days allowance and the minimum spatial limit, are responsible for small changes in its characteristics, whereas it poses a higher effect on the number of events identified on a given period at local or larger scales. By contrast, the choice of the reference period, threshold temperatures and the minimum event duration generate significant differences on the intensity (and also the number) of the MHWs identified. From that we can deduce that for the study of a particular MHW there is an important sensitivity to algorithm setting. The "ID card" of a single MHW, that is to say, depends a lot on the baseline definition.

On the contrary, in Chapter 4 we have demonstrated that change in MHW characteristics in the future do not so strongly depend on the algorithm parameters. This means that, from the perspective of MHWs as an ensemble of events in the long term, the overall direction of its properties and behaviour might be less sensitive to the algorithm setting, despite differences in individual events. This could be a result of the chaotic nature of temperature variability, in combination with the fact that the ocean "transmits" progressively a warming signal at all temperature «spectrums», captured by each algorithm tuning. It is important to highlight though, that frequency is not a very good measure for MHWs, as it appears very sensitive to the algorithm tuning. Despite that, it gives a good indication of the "character" of the extreme temperature fluctuations in the long term. For instance, a high number of large-scale MHWs indicate here a lot of fluctuations around extreme temperatures, whereas a lower number shows more stable, "agglomerating" events in terms of temperatures (see Chapter 4).

Overall, the take-away message of this work is that the sensitivity to the definition specificities depends on the scientific question asked. One should also be aware that a consistent framework of any type may deliver substantially different MHW characteristics, if applied on datasets with different spatial and temporal resolutions. Hence, to cover the uncertainty on the results many datasets should be used in combination with many different perturbations of the initial definition.

## 2. Is the current generation of Mediterranean Regional Climate System Models able to represent summer Mediterranean MHWs ?

In order to evaluate how close are the results of any kind of simulation to the real world, it is necessary first to evaluate the ability of the technical means used, to represent the basic features of the system we want to describe. Here, we evaluated the performance of RCSM models in reproducing mean and extreme SST trends in the Mediterranean Sea by identifying their biases and strong points. For this reason high-frequency and good-quality observational datasets (e.g. CMEMS satellite product used here) are necessary as a reference. Their acquisition, however,

is often not so obvious or easy.

At first, the new version of the high-resolution, coupled model CNRM-RCSM6 was used to describe the summer MHWs in the Mediterranean between 1982-2012, including therefore, the well-known event of 2003. Comparisons with a high-resolution, satellite dataset (also between 1982-2012) demonstrated that the model (in hindcast mode) represented relatively well the temporal evolution of the extreme SSTs of the period, in terms of variability and spatial patterns. It showed, however, a warm bias and underestimated the observed SST trends. The characteristics of the simulated MHWs, were also slightly underestimated with respect to the observed ones, probably related to underestimation of the observed SST trends. The previous version of this coupled model, named CNRM-RCSM4, was also available for describing MHWs in the past. It provided a relatively good capture of observed mean and extreme SST patterns. As before, the observed trend was underestimated by this configuration, which was characterized by a cold bias this time. The comparison between the 2 models showed an improved MHW representation from CNRM-RCSM6. Thus we used this model as a means of describing subsurface events for the same period.

Moreover, we evaluated the latest, available ensemble of high-resolution RCSM models for the Mediterranean area, from the Med-CORDEX initiative, this time in historical mode (1976-2005), that is to say driven by GCM runs and not reanalysis. The evaluation, again with the same observational dataset as before, showed that the Med-CORDEX ensemble simulated the mean and extreme SST evolution at the last part of the 20t century relatively well, despite a cold bias mostly in the mean SST and an underestimation of the warming trend in both the mean and extreme SST. The range of the MHW characteristics delivered matched relatively well those observed by the satellite, despite a slight underestimation of the upper part of each variable's distribution (except for duration).

This is the first time, these high-resolution models are evaluated to this respect and although they appear to represent Mediterranean summer MHWs sufficiently well, they are also characterised by biases. These biases are related to the mean and extreme temperature representation, which are somehow "eliminated" by the dataset-dependent threshold adopted by the algorithm each time. For example, none of the RCSMs in historical mode seem to have reproduced as an intense MHW 2003 as the one identified from the satellite dataset. This could be a combination of their cold bias with the fact that MHW 2003 was such an exceptional event, that longer simulations would be needed to reproduce it. The CNRM-RCSM6 in hindcast mode, on the other hand, reproduced the exceptionality of 2003 as opposed to CNRM-RCSM4 (in hindcast). But it exhibited a slightly warmer bias on extreme SST, lower though in absolute value relative to the cold bias of the ensemble of models on historical mode. Both the hindcast and historical simulations represent the "present-day" climate of the last part of the 20th century, but reproduced with different driving conditions. The former, appears to deliver an improved quality of results, despite its biases, due to probably its high-resolution characteristics and the good year-to-year climatology imposed by the reanalysis. Meanwhile, the latter dataset's biases, did

not seem to play a critical role on the future climate change response of MHWs.

At this point, it should be stressed that the satellite dataset, used as a reference here, provides skin and night-time SST values, whereas simulated SST represents averaged daily temperatures of each model's first few meters of the ocean. This practically means that simulated MLD is deeper, which can be responsible, to a certain extent, for the lower heat fluxes which have to be distributed in a larger volume of water. A thinner MLD would also mean a greater day-to-day variability of temperature. Note also that the satellite dataset is a gridded product, where optimal analysis has been performed to cover gaps in temperature measurements. This would mean that the representation of the SST evolution from the observation dataset is also characterised by potential errors, which can contribute, in turn, to the deviations of the model results.

On the whole, we can conclude that the models used here to represent the summer Mediterranean MHWs are sufficiently good to answer the questions posed in the current work. They present, however, certain limitations which means that further improvement of their skill is encouraged. In our case, the most evident discrepancies of the model relative to the observations appear to be the mean temperature bias and its lower simulated temperature trend. The different mean bias of both CNRM-RCSM6 and CNRM-RCSM4 did not seem to result in great differences on the past MHW characteristics between the two models. However, some of the event characteristics were underestimated relative to the observations. Naturally, this raises the question whether the model bias in the present is a serious handicap for future MHW projections. As we saw in Chapter 5, mean model bias in the present was independent from the MHW characteristics in the future. Generally speaking, a model bias in the "present" years does not necessarily mean that the bias will exist in the future projections as well. This could also be the case for the model trend. In an effort, to answer this question we performed a similar test for the model trend (not shown here) as we did for the model bias in the Supplementary Material of Chapter 5 and found no relationship between future MHW characteristics and model trend in the present. In the case of CNRM-RCSM6, the lower trend was probably responsible for the overestimation of MHW number at the start of the "past" period and if the model trend would remain the same in the future, it could mean an underestimation of the events in the future with respect to observations (see Chapter 2). Therefore, improvement of the model trend is identified as an important limitation in this PhD work. Other than that, the model's skill is not profound around the coasts of the Mediterranean Sea, where downscaling methods should be used to better understand the MHW evolution there. We also note here the importance of long-term and high-frequency *in situ* data (especially at depth) for model evaluation but also for monitoring MHW impact, which were difficult to be found for the purposes of that study.

## 3. What are the main spatiotemporal characteristics of the past, summer Mediterranean MHWs ?

In this PhD work, the past MHWs in the Mediterranean Sea during 1982-2017 were assessed systematically for the first time, using the above-mentioned definition framework, a high-resolution satellite dataset and the CNRM-RCSM6 model in hindcast mode. To-date knowledge on these events in the basin originated from reported mass mortalities of benthic ecosystems that have been linked to regional thermal episodes. We showed that most of the MHWs simulated firstly at surface, corresponded to the documented events in the literature (e.g. MHW of 1994, 1999, 2003, 2006, 2007, 2008). On average, simulated MHWs lasted around 15-20 days, covered around 40-44% of the Mediterranean Sea surface, with a mean intensity of about 0.6°C. They seem, however, to underestimate some of the characteristics identified using a satellite dataset. Observed MHWs were found to last a maximum of 1.5 months (between July and September), while covering a maximum of 90% of the Mediterranean Sea surface, with a mean intensity of 0.6°C (as before). Both datasets displayed a tendency for longer and more severe events with time. In particular, MHWs of 2003, 2012 and 2015 were identified as the most severe surface events of the period. To our knowledge, this is the first time the MHWs of 2012 and 2015 are identified, as they have not yet been reported by literature.

Thanks to the daily, 3D model outputs, we have also investigated subsurface MHWs and their evolution at 23m, 41m and 55m for the same period. They were characterised, on average, by higher mean and maximum intensity and severity relative to surface events, probably due to their longer durations. Yet, they displayed, on average, lower frequency and spatial coverage but increasing duration with depth, while their positive trends seem to become lower with depth. Their occurence appears to follow the seasonal mixed layer depth deepening. For example, MHWs appeared at 23m between July-September, at 41m between September-October, and at 55m between October-December. The most severe deep events of the period were identified in 2001 and 2014.

As we go deeper in the water column, the Levantine Basin, Ionian, Alboran, Tyrhennian and Balearic Seas seem more prone to higher mean intensities of subsurface MHWs, on the contrary to northwestern Mediterranean, Adriatic and Aegean Sea that seem more vulnerable to higher mean intensities of surface MHWs. Long-lasting events on the other hand, appear to affect mostly the Levantine region at surface and spread all over the basin at deeper layers. The differences in geographical patterns could be a result of regional ocean conditions that inhibit or promote the MHW development.

If we wished to see now how different are Mediterranean Sea MHWs compared to other regions of the world, we would need to apply our algorithm in different areas, which was out of the scope of this PhD work. In addition, to our knowledge, no other study has performed statistics on the MHWs of a specific region, in order to be able to make direct comparisons. Only one study by Hobday et al. (2018) has classified and compared certain well-known events,

but based on the 90th percentile of SST and a different MHW definition scheme. According to this study, the Mediterranean MHW 2003 was as intense as the event in Tasmania in 2015 and the one in the Great Barrier Reef in 2016.

## 4. What are the key driving mechanisms of the Mediterranean MHW 2003 ?

The dominant oceanic and atmospheric mechanisms that tend to drive MHWs are not always clear and certainly not the same for each event. The decomposition of the atmospheric forcing during the MHW of 2003 in the different Mediterranean basins showed that the preconditioning of the event was dominated by an anomalous incoming shortwave radiation, in addition to an abnormal reduction of latent heat flux in some regions. The interplay between these terms sustained as well the event, whereas the role of sensible heat flux and upward shortwave radiation was insignificant. Concurrently, analysis of the mixed layer heat budget, calculated online, revealed a dominant role of the atmospheric forcing in almost all the basins counteracted partly in absolute values by vertical diffusion. It turns out,however, that anomalously positive/negative $Z_{df}$ ultimately helps sustaining/destroying the MHW. By contrast, the role of advection, lateral diffusion and entrainment was not that significant, except for a few cases where the advection was enhanced and contributed critically to the input of heat. In most regions, anomalously low winds were critical for determining the intensity of the event through changes in the MLD along with changes in the latent heat loss and vertical diffusion. Most of the times a shallowing of MLD was simulated. Concomitant to this was a sea surface and mean MLD temperatures increase that driven partly by the anomalously low latent heat loss and at a smaller extent by the reduction in sensible heat flux. However, vertical stratification was also indicated as a possible factor behind the MLD shallowing, acting indirectly through the vertical advection term. The fall of the event was almost everywhere marked by a wind-induced increase of latent heat loss and vertical diffusion along with a reduction in downward solar radiation in some areas. At that phase, the mixed layer depth most of the times deepened and SST decreased although remained above climatology.

If we would wish to compare now the MHW 2003 driving factors with the ones identified in other events worldwide we could see a few similarities. For example, warm ocean currents have been seen to dominate MHW events whenever boundary currents were present (e.g. Tasmania MHW 2015). This could also be the case for the temperature anomalies that developed around the coastlines of the Mediterranean basin during the 2003 events, where we see a progressive dominance of ocean processes, although not as clear as the one found on larger-scale events. In general, the main similarity of the MHWs around the world would be the tendency of MHWs to coincide and develop during equivalent atmospheric events.

## 5. How summer Mediterranean MHWs may evolve in the future ?

Besides their driving factors, knowledge on the future MHW spatiotemporal evolution appears more critical than ever. Given their broad and accelerated impacts under a continuously warming world, it becomes even more relevant for a climate "Hot Spot" region such as the Mediterranean basin. Here, we used 6 high-resolution, coupled Regional Climate System Models (RCSM) models from the Med-CORDEX initiative, driven by 4 different CMIP5 General Circulation Models (GCMs), under the RCP2.6 (optimistics), RCP4.5 (intermediate) and RCP8.5 (pessimistic) IPCC emission scenarios, to study MHW evolution throughout the 21st century (1976-2100). A total of 17 simulations were performed. To our knowledge, this is the first use of a multi-model, multi-scenario ensemble of high-resolution models in studying the future evolution of the Mediterranea Sea.

By the end of the 21st century, the multi-model average demonstrated the highest basin-mean, SST (3.1°C) and extreme $SST_{99Q}$ (3.6 °C) increase under RCP8.5 and lowest under RCP2.6, relative to the historical period of 1976-2005. The corresponding warming for 2021-2050, however, was found less pronounced for all scenarios (0.8 °C/1.2 °C). In particular, basinwide mean and extreme SST for RCP2.6 ( ~1 °C) did not seem to differ significantly from mid- to end of 21st century.

In general, MHWs will likely become stronger and more intense in response to increasing greenhouse gas forcing and especially towards the end of the 21st century. By 2100, models project at least one long-lasting MHW occuring every year under RCP8.5 up to 3 months longer, and about 4 times more intense and 42 times more severe than today's events. Their occurrence is expected between June and October, affecting at peak, the entire Mediterranean basin. In fact, with respect to the historical run, multi-model mean MHW frequency increases by a factor of ~1.6 for RCP8.5 and RCP4.5 by 2021-2050 and slightly less than that towards 2071-2100 for both scenarios. Multi-model mean duration, on the other hand, is multiplied by a factor of 3.7 for RCP4.5 and of 5.3 for RCP8.5 during 2071-2100. For 2021-2050, there is a generally higher convergence in the factor of frequency, duration (~2.4x-2.7x), mean intensity (1~0.5x) and severity ( ~5x-7x) increase represented by the ensemble mean of RCP4.5 and RCP8.5.

The equivalent, single-model comparisons of MHWs under RCP2.6 with the previous two scenarios revealed a slightly greater frequency increase during 2071-2100 under RCP2.6 (by factor of 1.7) than under RCP8.5 and RCP4.5 and a significantly lower mean intensity. In fact, although a slight increase in MHW signatures with time is seen under RCP2.6, it is generally lower than that under RCP4.5 and RCP8.5. While RCP8.5 is the business-as-usual scenario, RCP2.6 is the closest to Paris agreement limits, which could offer a relative stability in both the SST increase and MHW evolution in the basin after the mid-21st century.

It must be noted here, that the differences due to the GHG forcing, are not reflected in

the mid-21st century, instead they become more evident by 2071-2100. What was encountered as widespread consequences from the MHW 2003 could become the "new normal" in the mid-21st century, but constitute a weak event towards the end of the century. Especially under RCP8.5 and 2071-2100, MHWs can become three times longer than the MHW 2003, with mean intensities three times higher.

This part enabled us to document the uncertainty in future MHW projections related to the choice of the model. Some models demonstrated stronger climate change responses than others, likely due to the choice of the driving GCM rather than to the individual RCSMs. A closer examination of the SST and $SST_{99Q}$ bias effect on the anomalies of the average MHW characteristics under RCP8.5 and RCP4.5 with respect to historical run, suggested no particular tendency or outliers affecting the range of the outcome, for any of the periods and scenario. Nevertheless, the uncertainty related to the choice of the model mostly dominated the mid-21st century results. Despite their imperfections, the models here provided a part of the uncertainty related to the occurrence of extreme temperatures in the basin, which seem to be in the range of those estimated by GCM models. In addition, several sensitivity tests performed on the MHW detection algorithm using only the CNRM-RCSM4 RCSM model indicated low levels of uncertainty associated with small perturbations on the intrinsic part of the definition. The use of different quantile thresholds showed that climate change response of future MHW duration, mean and maximum intensity with respect to historical run does not differ significantly if a lower/higher threshold than the $SST_{99Q}$ is chosen. However, the severity and maximum spatial coverage appearred more sensitive to such changes.

## Perspectives

Marine Heatwaves are a relatively recent field of research (10 years) with a lot of aspects that have been mostly observed but only little understood. They have lately received considerable attention due to repercussions, in marine ecosystems and maritime human activities, which even though well-known, have only just started to unfold to their full extent. The current PhD work has attempted to investigate this global phenomenon, in a small region which, however, gives a taste of what accelerated climate change looks like. Therefore, it gives an idea of how could oceans look like in the future, if warming continues at the same pace as now.

There are a lot of things that need to be examined further regarding the MHWs. One of the most crucial is the understanding of the interplay between the large-scale atmospheric forcing and the local ocean conditions that drive MHWs. For instance, in this work we have analyzed the regional atmospheric and oceanic influences in the different Mediterranean basins, but large-scale modes of variability like Atlantic Multidecadal Oscillation, North Atlantic Oscillation and others, as well as more general circulation patterns, such as atmospheric blocking and atmosphere heatwave outbreaks, have been linked to similar events around the world. Hence, such a knowledge would make MHWs potentially predictable, while identifying key regions of

concern with regard to extreme ocean warming. Concurrently, this would be a step further in disentangling the various MHW driving mechanisms. In particular, an analysis similar to the one undertaken for the MHW 2003 but for the ensemble of events in the basin between 1982-2017 is an aspect planned to be performed in the future

Another significant and relatively unknown aspect of MHWs is their subsurface spatiotemporal evolution. Since most of the marine ecosystem (observed to have been) impacted by these events inhabit at the bottom and at the continental shelf, further examination of how deep individual MHWs may reach and what are the mechanisms that facilitate or inhibit their propagation at depth, should be in the frontline of research. Especially because in a constantly warming ocean, extreme warming at depth will soon start (if not yet) to create precarious conditions even for the open-ocean species and human activities depending on them. Most of the studies so far have analysed the mean warming of the ocean interior over the years, without investigating the corresponding extreme MHWs and vice versa. Most of the MHW-related studies have dealt with their surface evolution rather than their evolution at depth. Due to the low-frequency variability of the ocean, these events have the ability to last longer at depth, therefore, causing unprecedented changes, which have yet to be revealed. To this aim, long-term *in situ* data would be essential for the detection of events at various layers, including the bottom of the ocean, as they would provide information on their penetration, development and characteristics, besides evaluating subsurface high-frequency model output. In turn, organization of field campaigns at sea could complement the investigation and documention of events at depth and enhance our understanding of them.

On top of that, a MHW identification tool can be useful for marine biologists and stakeholders, fisheries scientists and managers for predictions of possible MHW impacts on specific fish distributions. This way, management of marine-dependent human communities and Marine Protected Areas, can be more efficiently prepared. Especially when MHW predictions are combined with biogeochemical studies. For example, detection of an event, which incorporates information on its intensity and duration at depth with physiological knowledge on thermotolerance threshold of species in deeper layers, could give an idea of the probability of mass mortality or extensive migration of commercially important species (e.g. Atlantic Bluefin Tuna). Alternatively, this information could even contribute to an assessment of the additional amount of carbon dioxide released to the atmosphere once species, such as seagrass, are extirpated as a result of MHWs. A finding which has only recently been discovered. Such initiatives could also reinforce interdisciplinary scientific collaboration but also increase the involvement of the society that would be directly impacted by MHWs.

Yet, MHWs can also affect physical systems indirectly, for example, by enhancing atmospheric heatwaves and droughts at land (e.g. the case of the European heatwave of 2003), through their feedback on air-sea fluxes. On the contrary, no similar questions have been so far posed on their effect on circulation patterns at sea. For instance, one can wonder if MHWs can have an effect on surface currents and mesoscale eddies through changes in density gradi-

ents. Could these changes in density gradient, in turn, result in changes in the Mediterranean Thermohaline circulation and the Mediterranean Outflow? An ensemble of models, similar to the Med-CORDEX RCSMs, could be employed to explore these possibilities. However, these are questions that, for now, remain at a theoretical sphere, but will possibly become more important once warming of the ocean has exacerbated.

One of the main targets of this PhD, was the robust assessment of the Mediterranean Sea response to future climate change. Although in part, it was fullfilled by the current investigation, enlarging the (so far 6 model) Med-CORDEX ensemble and better cover the GCM spread is equally important to performing more simulations with different GHG emission scenarios. That way our confidence on the climate change scenarios for the Mediterranean Sea would increase. Nevertheless, the results of the future MHW evolution in the Mediterranean Sea produced here have been included in the Special Report on the Ocean and Cryosphere in a changing climate (SROCC) of IPCC that is currently under preparation.

Furthermore, the algorithm developed in the current thesis can have a direct application in services that provide MHW forecasts, similar to extreme weather warnings to the public, such as MERCATOR or CMEMS. Beyond that, forecasting of any kind of extreme (ocean) phenomena is a currently expanding territory in a continuously warming world, which can be benefited by such an automatic detection method. Whether it is related to atmospheric heatwaves, dust or extreme precipitation events, a consistent framework, which practically acts as a « filter » of extreme occurrences, can be used and transformed at will. The use of common metrics in that case advances real-time monitoring and forecasting of MHWs (or other events), by allowing warnings to be issued once an event is initiated.

Finally, despite the fact that the algorithm is freely available to any user upon request, and we encourage researchers to take advantage of it, for the moment its application is limited to one specific programming langage (ncl). Consequently, further refinements include the coding of the algorithm in another langages (e.g. Python, R), its documentation and testing the effects of the different versions of it.

## 6.2 Conclusions et Perspectives (Français)

La forte sensibilité de la mer Méditerranée au changement climatique résulte à la fois de sa localisation à la confluence des climats des latitudes moyennes et des climats plus chauds et secs, et également de sa topographie spécifique, le tout étant aggravé par des facteurs anthropiques. En conséquence, les phénomènes météorologiques à fort impact et les événements extrêmes affectent fréquemment la région. C'est notamment le cas des canicules océaniques qui exercent une pression considérable sur les écosystèmes marins dans la région. Dans ce contexte, ces travaux de thèse ont tenté de définir objectivement les canicules océaniques estivales dans le bassin afin d'analyser leur formation, leur organisation spatiale et de fournir une évaluation robuste de leur évolution spatio-temporelle au cours du 21ème siècle. L'application d'une

méthode de détection sur différents jeux d'observations et de modélisation à haute résolution a apporté des réponses aux questions soulevées dans le chapitre 1 du présent manuscrit.

## 1. Comment définir une canicule océanique estivale méditerranéenne ?

Dans le cadre de ce travail, nous avons défini une méthode de détection générale des canicules océaniques ciblant les événements estivaux de grande ampleur et de longue durée en Méditerranée. L'algorithme tient compte des caractéristiques géographiques de la région en utilisant des seuils climatologiques locaux du 99ème centile de température quotidienne de surface de la mer, ($TSM_{99Q}$) déterminés sur la fin du 20ème siècle. À noter que l'algorithme peut être adapté par l'utilisateur qui a la possibilité de spécifier un autre seuil. Des seuils relatifs aux événements thermiques extrêmes hivernaux ou aux événements froids extrêmes peuvent par exemple être utilisés. Les canicules océaniques (ou tout autre type d'événement choisi) sont ensuite identifiées comme les événements qui dépassent systématiquement le seuil sélectionné. Leurs détections peuvent être appliquées à des modèle 2D (surface ou couches profondes), à des ensembles de données d'observations ou encore à des données issues de stations locales (comprenant des valeurs manquantes). L'algorithme fournit un ensemble de paramètres caractéristiques de chaque événement tel que la fréquence, l'intensité, la durée, la sévérité et la couverture spatiale.

Bien que cette définition offre une certaine souplesse quant au type d'événement identifié, elle présente également certaines limites. Des données quotidiennes étant nécessaires en entrée de l'algorithme, celui-ci ne peut s'appliquer aux observations *in situ* et aux données des couches plus profondes ayant une résolution temporelle inférieure (par exemple mensuelle). Cela peut limiter la quantité de données sur lesquelles l'algorithme peut être implémenté, puisque la plupart du temps les données *in situ* de long terme sont difficiles à obtenir à haute fréquence (notamment pour les couches plus profondes). De plus, le rôle du cycle diurne (ou de toute autre variabilité temporelle sous-quotidienne) dans l'évolution des canicules océaniques n'est pas évalué et par conséquent, des limitations associées à ce choix subjectif demeurent.

De plus, aucune continuité spatiale n'est supposée entre les points de grille qui sont affectés par les canicules océaniques et par conséquent, la trajectoire de chaque événement dans l'espace ne peut être fournie. Cela signifie que l'algorithme n'est pas en mesure de distinguer si deux zones non contiguës associées à des canicules océaniques sont caractérisées par le même événement ou par deux événements différents. La réponse à cette question repose largement sur la manière dont un canicule océanique est définie en premier lieu et sur les critères qui déterminent de manière systématique ce qui sépare un événement d'un autre. Là encore, il s'agit de décisions subjectives qui dépendent de l'utilisateur et de l'application visée. Par exemple dans notre cas, une canicule océanique est séparée d'une autre en fonction de la durée minimale de l'événement (>5 jours) à l'échelle locale ou de la couverture spatiale minimale

(20%) pour les cas 2D. Les canicules océaniques peuvent également être distinguées à partir des mécanismes moteurs qui peuvent différer d'une région à l'autre, même pour un événement qui survient au cours d'une même journée. Ce facteur n'a toutefois pas été pris en compte dans l'algorithme. Néanmoins, la couverture spatiale journalière des canicules océaniques est prévue par cette définition et permet d'identifier après un post-traitement la zone affectée et les conditions spécifiques qui prévalent au moment souhaité, comme présenté dans le chapitre 3. Enfin, bien que l'algorithme ne puisse produire une représentation 3D des canicules océaniques, il peut être appliqué aux couches plus profondes de l'océan, comme démontré dans le chapitre 3.

L'ensemble de ces arguments montre que, comme pour leurs homologues atmosphériques, il n'existe pas de définition objective des canicules océaniques, puisqu'elles reposent sur une série de choix subjectifs faits en fonction du type d'événement que l'on souhaite suivre. Par conséquent, la détection automatique d'événements par un algorithme est inhérente par construction avec certaines limitations dans les paramétrés d'algorithme. Par exemple, le choix de la période de référence, les températures de seuils, la durée minimale de la canicule, son étendue spatiale ou encore les jours d'interruption doivent être prédéterminés afin de faciliter la comparaison entre les différents événements et les bases de données. Il existe donc différentes définitions qui permettent de "filtrer" une certaine partie du spectre des températures océaniques extrêmes. Dans notre cas, nous avons choisi de détecter les événements plus chauds que le 99ème centile de la climatologie de température quotidienne établie sur les 30 dernières années du 20ème siècle.

Les différents tests de sensibilité effectués dans le cadre de ce travail ont montré que pour une canicule océanique donnée, la partie la plus intrinsèque de la méthodologie, c'est-à-dire l'écart autorisé entre les jours et la limite spatiale minimale, sont responsables de petits changements dans ses caractéristiques, bien qu'ils aient un impact plus important sur le nombre d'événements identifiés sur une période donnée, à l'échelle locale ou plus large. En revanche, le choix de la période de référence, des températures seuils et de la durée minimale de l'événement entraînent des différences significatives sur l'intensité (et également le nombre) de canicules océaniques identifiées. On peut donc en déduire que pour l'étude d'une canicule océanique particulière, il existe une sensibilité importante aux paramétrés de l'algorithme ce qui signifie que la "carte d'identité" d'une canicule océanique donnée dépend largement des réglages choisis.

À l'inverse, nous avons montré dans le chapitre 4 l'évolution future des caractéristiques des canicules océaniques ne dépendent que peu aux paramètres de l'algorithme. Cela signifie qu'en considérant les canicules océaniques comme un ensemble d'événements sur le long terme, l'orientation générale de leurs propriétés et de leurs comportements est moins sensibles aux réglages de l'algorithme. Cela pourrait être dû à la nature chaotique de la variabilité de la température, combinée au fait que l'océan "transmet" progressivement un signal de réchauffement à toutes les "spectres" de température, capturés par chaque réglage d'algorithme. Il est important de souligner que la fréquence n'est pas une très bonne mesure pour les canicules

océaniques car elle apparaît très sensible aux réglages de l'algorithme, malgré le fait qu'elle donne une bonne indication du "caractère" des fluctuations extrêmes de température sur le long terme. Par exemple, un nombre élevé de canicules océaniques de grande échelle indique de nombreuses fluctuations autour des températures extrêmes alors qu'un nombre plus faible de canicules océaniques indique des événements "agglomérants" plus stables en termes de température (voir chapitre 4).

Finalement, le message principal qui émane de ce travail est que la sensibilité aux spécificités de la définition dépend de la question scientifique à laquelle on souhaite répondre. Il est également à noter que pour une même méthodologie, l'utilisation de données avec des résolutions spatiales et temporelles différentes peut fournir des caractéristiques de canicules océaniques très variables. Par conséquent, l'utilisation combinée de plusieurs jeux de données et de différentes perturbations sur le réglage d'algorithme doit être utilisée afin d'évolues l'incertitude sur les résultats.

## 2. La génération actuelle des modèles regionaux du système climatique est-elle capable de représenter les MHW estivales méditerranéennes?

Afin de valider dans quelle mesure les résultats de n'importe quel type de simulation sont proches de la réalité, il est nécessaire dans un premier temps d'évaluer la capacité des moyens techniques utilisés et de représenter les caractéristiques fondamentales du système à décrire. Dans notre cas les modèles RCSM, pour Regional Climate System Models en anglais. Pour cette raison, les données d'observation de haute fréquence et de haute qualité (par exemple, le produit satellite CMEMS dans cette these) sont nécessaires. Leur acquisition, cependant, n'est pas aussi évidente ou facile.

Dans un premier temps, la nouvelle version du modèle couplé haute résolution CNRM-RCSM6 a été utilisée pour décrire les canicules océaniques méditerranéennes estivales sur la période 1982-2012 (incluant donc l'événement bien connu de 2003). La comparaison avec des données satellitaires haute-résolution (également disponible sur la période d'intérêt) a montré que le modèle représente relativement bien l'évolution temporelle des TSM extrêmes sur la période en termes de variabilité, de tendance et de structures spatiales. Les caractéristiques des canicules océaniques simulées sont toutefois légèrement sous-estimées par rapport à celles observées, ce qui s'explique probablement par le biais chaud du modèle et par sa légère sous-estimation des tendances observées sur la TSM. Comme les résultats s'écartaient peu de la réalité, nous avons choisi d'utiliser le modèle afin de décrire les événements de subsurface sur la même période.

De plus, nous avons évalué le dernier ensemble disponible de modèles RCSM haute-résolution pour la zone méditerranéenne, issu de l'initiative Med-CORDEX, cette fois en mode historique (1976-2005), c'est-à-dire piloté par des modèles de circulation générale (MCG) et non pas

par des réanalyses. L'évaluation, effectuée avec le même jeu de données d'observation que précédemment, a montré que l'ensemble Med-CORDEX simulait relativement bien l'évolution moyenne et extrême de la TSM sur la dernière partie du 20ème siècle, malgré un biais de froid et une sous-estimation de la tendance au réchauffement. La gamme des caractéristiques des canicules océaniques fournie correspond relativement bien à celles observées par satellite, malgré une légère sous-estimation de la partie supérieure de la distribution de chaque variable, à l'exception de la durée.

C'est la première fois que ces modèles haute-résolution ont été évalués à cet égard et bien qu'ils semblent représenter suffisamment bien les canicules océaniques méditerranéennes estivales, ils sont également associés à des biais. Ces biais sont liés à la représentation des températures moyennes et extrêmes, qui sont en quelque sorte "éliminés" par le seuil dépendant de l'ensemble de données adopté à chaque fois par l'algorithme. Par exemple, aucun des RCSMs en mode historique ne semble avoir reproduit la canicule océanique de 2003 avec une intensité aussi importante que celle observée à partir des données satellitaires. Cela pourrait être lié à la sous-estimation des tendances observées et au fait que la canicule océanique de 2003 était un événement tellement exceptionnel, que des simulations plus longues seraient nécessaires afin de la reproduire. La RCSM en mode rétrospectif, présentait un biais chaud sur la TSM extrême, mais moins en valeur absolue par rapport au biais froid de l'ensemble des modèles en mode historique. Les simulations rétrospectives et historiques représentent toutes deux le climat "actuel" de la fin du 20ème siècle mais a partir des conditions aux bords différentes. La première, semble offrir un meilleurs résultats, malgré ses biais, peut-être a cause de ses caractéristiques de haute résolution. Les biais de ce dernier ensemble de données ne semblaient pas jouer un rôle critique sur les changements futurs des MHWs.

À ce stade, il convient de souligner que l'ensemble de données satellitaires utilisé ici comme référence fournit des valeurs de TSM pour la surface et la nuit, alors que la TSM simulée représente les températures journalières moyennes de chaque modèle sur les premiers mètres de l'océan. Les données satellitaires sont également un produit maillé, sur lequel une analyse optimale a été effectuée de manière à compléter les mesures de température manquantes. Cela signifie que la représentation de l'évolution de la TSM dans les observations est également caractérisée par des erreurs potentielles, qui peuvent à leur tour contribuer à des déviations des résultats du modèle.

Dans l'ensemble, on peut donc conclure que les modèles utilisés dans ce travail pour représenter les canicules océaniques méditerranéennes estivales sont suffisamment bons pour répondre aux question posées par cette thèse en les MHWs, mais restent imparfaits. Des améliorations supplémentaires de leur capacité sont donc encouragées. Les comparaisons avec les données *in situ* et satellitaires ont permis d'identifier leurs imperfections et donc d'orienter les pistes d'amélioration. En particulier pour les données *in situ*, l'utilisation d'un tel algorithme a souligné non seulement leur importance pour l'évaluation du modèle, mais aussi la nécessité de séries de données à plus long terme (surtout en profondeur) et à haute fréquence,

qui ont été difficiles à trouver pour les besoins de l'étude.

## 3. Quelles sont les principales caractéristiques spatio-temporelles des MHW estivales méditerranéennes passées ?

Dans le cadre de ce travail de thèse, les canicules océaniques méditerranéennes passées sur la période 1982-2017 ont été évaluées systématiquement pour la première fois, en utilisant la méthodologie mentionnée précédemment, un jeu de données satellite haute-résolution et le modèle CNRM-RCSM6 en mode rétrospectif. À ce jour, les connaissances de ces événements dans le bassin provenaient d'épisodes de mortalités massives d'écosystèmes benthiques identifiés qui ont été reliés à des épisodes thermiques régionaux. Nous avons montré que la plupart des canicules océaniques simulées en surface, correspondaient bien aux événements documentés dans la littérature (ex. canicules océaniques de 1994, 1999, 2003, 2006, 2007, 2008). En moyenne, les MHW simulées ont une durée d'environ 15-20 jours, couvrent environ 40-44% de la surface de la mer Méditerranée, et ont une intensité moyenne d'environ 0,6°C. Par contre, ces caractéristiques apparaissent sous-estimées par rapport à celles observées à partir des satellites. Les MHW observées ont montré une durée maximale de 1,5 mois entre juillet et septembre, couvrant au maximum 90% de la surface de la mer Méditerranée avec une intensité moyenne de 0,6°C (comme auparavant). Les deux jeux de données montre une tendance a des événements plus longs et plus sévères avec le temps. En particulier, les canicules océaniques de 2003, 2012 et 2015 ont été identifiées comme les événements de surface les plus sévères de la période.

Grâce aux sorties 3D du modèle, nous avons également étudié les canicules océaniques de subsurface et leurs évolutions à 23m, 41m et 55m sur la même période. Ces dernières se caractérisent en moyenne, par des intensités moyennes et maximales plus élevées ainsi que des sévérités plus importantes par rapport aux événements de surface. Cela s'explique probablement par leurs durées de vie plus importantes. Ces canicules océaniques ont également montré en moyenne des fréquences et des couvertures spatiales plus faibles, des durées de vie qui augmentent avec la profondeur tandis que leurs tendances positives semblent diminuer avec la profondeur. Leur occurrence semble suivre l'approfondissement saisonnière de la couche de mélange. Par exemple, les MHWs à 23m sont apparus entre juillet-septembre, à 41m entre septembre-octobre, et à 55m entre octobre et novembre. Les événements profonds les plus sévères de la période ont été identifiés en 2001 et 2014.

À mesure que l'on s'enfonce dans la colonne d'eau, le bassin Levantin, les mers Ionienne, d'Alboran, Tyrrhénienne et des Baléaries apparaissent plus propices à des canicules océaniques moyennes de subsurface plus importantes. À l'inverse, la région nord-ouest de la Méditerranée et les mers Adriatique et Égée apparaissent plus vulnérables à des canicules océaniques moyennes plus intenses en surface. D'autre part, les événements de longue durée semblent affecter principalement la région levantine à la surface et se répandent dans tout le bassin vers les couches plus profondes. Les différences dans la répartition géographique pourraient être le résultat

des conditions océaniques régionales qui inhibent ou favorisent le développement des canicules océaniques.

## 4. Quels sont les principaux mécanismes moteurs d'une canicules océanique estivale méditerranéenne ?

Les mécanismes océaniques et atmosphériques dominants qui sont à l'origine des canicules océaniques ne sont pas toujours clairs et certainement pas les mêmes pour chaque événement. Une contribution dominante des flux atmospherique de chaleur a été observée pour le développement de la plupart des canicules océaniques d'été en Méditerranée. Cependant, l'analyse du bilan thermique de la couche mélangée, calculé en ligne, a révélé que dans certaines régions, la diffusion verticale a un rôle important à jouer pour équilibrer en partie le forçage atmosphérique. D'autre part, le forçage local du vent détermine dans une large mesure l'apparition et l'intensité des événements. L'advection apparaît également comme un facteur important dans certaines régions.

## 5. Comment les canicules océaniques estivales méditerranéennes peuvent-elles évoluer à l'avenir ?

Les éléments moteurs mis à part, l'identification de l'évolution spatio-temporelle future des canicules océaniques apparaît plus critique que jamais. Compte tenu de leurs impacts importants dans un contexte de réchauffement climatique, ils devient encore plus pertinentes pour une région climatique "Point Chaud" comme le bassin méditerranéen. Ici, nous avons utilisé 6 modèles de système climatique régional (RCSM) couplés à haute résolution issus de l'initiative Med-CORDEX, pilotés par 4 modèles de circulation générale (MCG) CMIP5 différents, selon les scénarios RCP2.6, RCP4.5 et RCP8.5 du GIEC pour étudier les propriétés des canicules océaniques au XXIe siècle (1976-2100). A notre connaissance, il s'agit de la première utilisation d'un ensemble multi-modèles et multi-scénarios de modèles à haute résolution pour étudier l'évolution future de la mer Méditerranée.

À la fin du XXIe siècle, la moyenne multi-modèle a affiché la plus forte augmentation de la moyenne du bassin pour le scénario RCP8.5 avec 3.1°C pour la TSM et 3,6°C pour le quantile 99 quotidienne, et la plus faible pour le scenario RCP2.6. Le réchauffement correspondant pour 2021-2050 s'est toutefois révélé moins prononcé quelque soit le scénario (~0,8°/1.2 °C). En revanche, la TSM moyenne et extrême à l'échelle du bassin pour RCP2.6 ( ~1 °C) n'a pas semblé différer de façon significative entre le milieu et la fin du 21e siècle.

En général, les canicules océaniques deviendront probablement plus fortes et plus intenses en réponse à l'augmentation du forçage anthropique et particulièrement vers la fin du 21e siècle. D'ici 2100, les modèles projettent au moins une canicule océanique de longue durée chaque année en scénario RCP8.5 jusqu'à 3 mois plus longue, et environ 4 fois plus intense et 42 fois plus

sévère que les événements actuels. Leur apparition est attendue entre juin et octobre, affectant au maximum l'ensemble du bassin méditerranéen. Par rapport à la simulation historique, la fréquence moyenne des canicules océaniques multi-modèles augmente d'un facteur de 1.6 en RCP8.5 et RCP4.5 d'ici 2021-2050 et légèrement moins vers 2071-2100 pour les deux scénarios. La durée moyenne multi-modèle est multipliée par un facteur de 3.7 en RCP4.5 et de 5.3 en RCP8.5 en 2071-2100. Pour 2021-2050, il y a une convergence généralement plus élevée pour les propriétés des canicules océaniques de la moyenne d'ensemble des scénarios RCP4.5 et RCP8.5 pour le facteur d'augmentation en fréquence, en durée (~2.4x-2.7x), en intensité (~1.5x) et sévérité (~5x-7x).

Les comparaisons équivalentes de la représentation des canicules océaniques du seul modèle disponible pour le scénario RCP2.6 avec les deux autres scénarios ont révélé une augmentation de fréquence légèrement plus importante en 2071-2100 en RCP2.6 (facteur 1.7) comparé à RCP8.5 et RCP4.5 et une intensité moyenne nettement inférieure. En fait, bien qu'une légère augmentation des signatures de canicules océaniques avec le temps soit observée en RCP2.6, elle est généralement inférieure à celle en RCP4.5 et RCP8.5. Alors que le RCP8.5 est le scénario du statu quo, le RCP2.6 est le plus proche des limites de l'accord de Paris, ce qui pourrait offrir une relative stabilité tant dans l'augmentation de la TSM que dans l'évolution des canicules océaniques dans le bassin après le milieu du 21ème siècle.

Les différences dues au choix du scénario socioéconomiques ne se reflètent pas au milieu du 21e siècle, mais deviennent plus évidentes pour la période 2071-2100. Ce qui a été considéré comme des impacts forst pour de la canicule océanique de 2003 pourrait devenir la "nouvelle norm" au milieu du 21e siècle, mais constituer un événement faible vers la fin du siècle. Particulièrement en RCP8.5 et 2071-2100, les canicules océaniques peuvent devenir trois fois plus longues que la canicule océanique 2003, avec des intensités moyennes trois fois supérieures.

Dans cette partie nous avons pu documenter l'incertitude dans les projections futures des canicules océaniques liées au choix du modèle. Certains modèles ont montré des réactions plus fortes que d'autres au changement climatique, probablement plutôt en raison du choix du MCG forceur que des RCSM individuels. Un examen plus approfondi de l'effet des biais de la TSM et de la TSM extrême sur les anomalies des caractéristiques moyennes des canicules océaniques en RCP8.5 et RCP4.5 par rapport à la simulation historique n'a révélé aucune tendance particulière ou valeur aberrante affectant la plage des résultats, pour aucune période ou scénario. Il est important de noter ici que l'incertitude liée au choix du modèle a surtout dominé les résultats du milieu du 21e siècle. Malgré leurs imperfections, les modèles ont fourni ici une partie de l'incertitude liée à l'occurrence de température extrême dans le bassin, en accord avec celle estimée par les modèles de grande échelle.

De plus, plusieurs tests de sensibilité effectués sur l'algorithme de détection des canicules océaniques en utilisant uniquement le modèle CNRM-RCSM4 ont indiqué de faibles niveaux d'incertitude associés à de petites perturbations de la partie intrinsèque de l'algorithme.

L'utilisation de seuils de quantiles différents a montré que la réponse au changement climatique de la durée future des canicules océaniques, intensité moyenne et maximale par rapport à la simulation historique ne diffère pas significativement si un seuil inférieur/supérieur à la TSM seul est choisi. Cependant, la sévérité et la couverture spatiale maximale semblent plus sensibles à de tels changements.

## Perspectives

Les canicules océaniques sont un domaine de recherche relativement récent ( 10 ans) avec beaucoup d'aspects qui ont été surtout observés mais peu compris. Elles ont récemment fait l'objet d'une attention considérable en raison de leurs répercussions sur les écosystèmes marins et les activités humaines maritimes, qui, bien que désormais connues, ne font que commencer à se développer dans toute leur ampleur. Ce travail de thèse a tenté d'étudier ce phénomène mondial, dans une petite région qui, cependant, donne un aperçu de ce à quoi pourraient ressembler les océans à l'avenir, si le réchauffement se poursuit au même rythme qu'aujourd'hui.

Pourtant, il y a beaucoup de choses qui doivent être examinées plus en détail en ce qui concerne les canicules océaniques. L'une des plus cruciales serait une meilleure compréhension de l'interaction entre le forçage atmosphérique à grande échelle et les conditions océaniques locales qui déterminent les canicules océaniques. Par exemple, dans ce travail, nous avons analysé les influences atmosphériques et océaniques régionales dans les différents bassins méditerranéens. Mais des modes de variabilité à grande échelle comme l'ENSO, ou l'oscillation nord-'Atlantique entre autres, ainsi que des régimes de circulation atmosphérique plus généraux, tels que le blocage atmosphérique et les vagues de chaleur atmosphérique, ont été liés à des événements similaires dans le monde. Par conséquent, une telle connaissance rendrait les canicules océaniques potentiellement prévisibles, tout en identifiant les principales régions préoccupantes en ce qui concerne le réchauffement extrême des océans. En même temps, ce serait un pas de plus dans la compréhension des différents mécanismes d'influence des canicules océaniques. En particulier pour les canicules océaniques estivales méditerranéennes, un examen plus approfondi du rôle des différentes contributions atmosphériques avant, pendant et après l'apparition des canicules océaniques est un aspect qui doit être réalisé à l'avenir.

Un autre aspect important et relativement inconnu des canicules océaniques est leur évolution spatio-temporelle en subsurface. Étant donné que la majeure partie des écosystèms marins touchés par ces événements (ce qui a été observé) se trouve au fond et sur le plateau continental, un examen plus approfondi de la profondeur que peuvent atteindre les canicules océaniques individuelles et des mécanismes qui facilitent ou inhibent leur propagation en profondeur devrait être en première ligne des recherches amenés. D'autant plus que, dans un océan qui se réchauffe en permanence, le réchauffement extrême en profondeur va bientôt commencer (si ce n'est déjà fait) à engendrer des conditions précaires même pour les espèces de haute mer et les activités humaines qui en dépendent. Jusqu'à présent, la plupart des études ont analysé

le réchauffement moyen de l'océan interieur au fil des ans, sans étudier les canicules océaniques extrêmes correspondantes, et la plupart des études liées aux canicules océaniques ont porté sur leur évolution en surface plutôt que sur leur évolution en profondeur. En raison de la variabilité des basses fréquences de l'océan, ces événements ont la capacité de durer plus longtemps en profondeur, causant ainsi des changements sans précédent, qui n'ont sans doute pas encore été révélés. Ainsi, des données in situ à long terme et à haut-fréquence seraient essentielles pour la détection d'événements à haut-fréquence à diverse au profondeur. Car elles fourniraient des informations sur leur pénétration, leur développement et leur caractéristiques. En plus ils permettent l'évaluation des résultats des modèles à haute fréquence en subsurface. Par ailleurs, l'organisation de campagnes en mer pourrait compléter l'enquête et la documentation d'événements spécifiques et en améliorer la compréhension.

De la même façon, une algorithme de détection de canicules océaniques pourrait être utile aux biologistes et aux intervenants du milieu marin, aux scientifiques et aux gestionnaires des pêches pour prévoir les répercussions possibles des canicules océaniques sur la répartition de certains poissons. De cette manière également, la gestion des communautés humaines dépendantes de la mer et des aires marines protégés pourrait être préparée plus efficacement, en particulier si les prévisions de canicules océaniques sont combinées avec des études biogéochimiques. Par exemple, la détection d'un événement, qui intègre des informations sur son intensité et sa durée en profondeur avec des connaissances physiologiques sur le seuil de thermotolérance des espèces dans les couches profondes, pourrait donner une idée de la probabilité de mortalité massive ou de migration important d'espèces commercialement importantes. Par ailleurs, cette information pourrait même contribuer à une évaluation de la quantité additionnelle de dioxyde de carbone rejetée dans l'atmosphère lorsque des espèces, comme les herbiers marins, disparaissent à la suite de canicules océaniques. Une constatation qui n'a été découverte que récemment. De telles initiatives pourraient renforcer la collaboration scientifique interdisciplinaire, mais aussi accroître la participation de la société elle-même directement affectée par les canicules océaniques.

Les canicules océaniques peuvent aussi influencer indirectement les systèmes physiques, par exemple en renforçant les vagues de chaleur atmosphériques et les sécheresses à terre (par exemple, le cas de la vague de chaleur européenne de 2003), par rétroaction sur les flux air-mer. Au contraire, aucune question similaire n'a été posée jusqu'à présent sur leur effet sur la circulation océanique. Par exemple, on peut se demander si les canicules océaniques peuvent avoir un effet sur les courants de surface et les tourbillons mésoéchelle en modifiant les gradients de densité. Ces changements du gradient de densité pourraient-ils, à leur tour, entraîner des changements dans la circulation thermohaline méditerranéenne et l'intensité du courant d'eau méditerranéenne en Atlantique? Un ensemble de modèles, similaires à ceux de Med-CORDEX, pourrait être utilisé pour explorer ces possibilités. Cependant, ce sont des questions qui, pour l'instant, restent théoriques, mais qui deviendront peut-être plus importantes une fois que le réchauffement de l'océan se sera aggravé.

L'un des principaux objectifs de cette thèse était l'évaluation robuste de la réponse de la mer Méditerranée au changement climatique futur. Bien qu'il ait été en partie rempli, l'élargissement de l'ensemble Med-CORDEX (jusqu'à présent 6 modèles) et une meilleure couverture de la gamme d'incertitudes des MCG sont tout aussi importants pour agréger davantage de simulations avec différents scénarios socioéconomiques, augmentant ainsi notre confiance dans les scénarios de changement climatique pour la mer Méditerranée.

De plus, l'algorithme développé dans cette thèse pourrait avoir une application directe dans des services des prévision des canicules océaniques. Une application similaire aux avertissements pour situations météorologiques extrêmes au public, qui pourraient être fournis par Mercator Océan ou CMEMS. Au-delà, la prévision de tout type de phénomènes extrêmes (océaniques) est un domaine en expansion dans un monde qui se réchauffe continuellement et qui pourrait bénéficier d'une telle méthode de détection automatique. Qu'il s'agisse de vagues de chaleur atmosphériques, des événements de de poussières ou de précipitations extrêmes, un cadre cohérent, qui agit pratiquement comme un " filtre " des phénomènes extrêmes, peut être utilisé et transformé à volonté. De plus, l'utilisation de métriques communes pourrait faire progresser la surveillance et la prévision en temps réel des canicules océaniques (ou d'autres événements), en permettant d'émettre des avertissements une fois qu'un événement est déclenché. Bien que l'algorithme soit librement accessible à tout utilisateur sur demande, et nous encourageons les chercheurs à en tirer profit, pour le moment son application est limitée à un language de programmation spécifique. Par conséquent, les améliorations futures devront portes le codage de l'algorithme dans une autre language, sa documentation et les test des différentes versions de celui-ci.

# Annex

one day I'll know, how far I'll go." *Moana*

In the following sections extra material that was produced in the course of the PhD is included. First a contribution of the writer to the sub-chapter of a published Book about Mediterranean Climate Change is presented, followed by an activity report for Meteo France use (to be published) and a popular science article published in MARmaED blog.

## Book Contribution

Reference: Somot S., Jordà G., Harzallah A., **Darmaraki S.** (2016) The Mediterranean Sea in the future climate projections (sub-chapter 1.2.3). In: The Mediterranean region under climate change: A scientific Update, Editor: All-Envi in preparation of the COP22, Marrakech, 7-18 November, 2016)

Sub-chapter 1.2.3

# The Mediterranean Sea in the future climate projections

*Samuel Somot*
Météo-France, France

*Gabriel Jorda*
IMEDEA, Spain

*Ali Harzallah*
INSTM, Tunisia

*Sofia Darmaraki*
UMR CNRM, France

## Introduction

As a semi-enclosed and highly evaporative basin, the Mediterranean Sea has a specific thermohaline circulation characterized by deep convection in certain zones (Gulf of Lion, the Adriatic, Levantine and Aegean Seas). The contrast between the fresher (hence lighter) waters west of the Strait of Gibraltar compared to the saltier (hence heavier) Mediterranean waters east of it, is the principal forcing of the outflowing water vein and the compensating inflow of light Atlantic waters floating as a surface layer. The entire thermohaline circulation has a time scale of 75 to 100 years. How the circulation of the Mediterranean Sea will evolve under a changed climate is a major issue. Other key questions concern changes in the surface characteristics: sea surface temperature and salinity (SST, SSS), surface currents, sea level and waves. An overview of the projected future state of the Mediterranean Sea and associated uncertainties are presented in the following.

# Models and methods

The assessment of the effects of climate change on the Mediterranean Sea over the 1950-2100 period and under several socio-economic scenarios is based on different types of model projections from (i) general circulation models (GCM) used in the coordinated Coupled Model Intercomparison Projects (CMIP), (ii) higher resolution regional climate models (RCM) dedicated to the study of the Mediterranean region and/or Mediterranean Sea. RCMs including (1) atmosphere-only regional climate models (ARCM) from international coordinated programs (CORDEX) and European projects (e.g. PRUDENCE, ENSEMBLES) are used to assess changes in the atmosphere above the sea; (2) forced *regional ocean models* are used to assess impacts on the sea itself; and (3) fully coupled atmosphere-ocean regional climate models (AORCM), also called regional climate system models (RCSM), take into account the high resolution and high frequency coupling between the various components of the regional climate system. The use of RCSM for future projections started quite recently (Somot et al. 2008, Carillo et al. 2012) before being coordinated in the European project CIRCE (Dubois et al. 2012; Gualdi et al. 2013) and currently in the Med-CORDEX initiative (Ruti et al. 2016, see Box 1). CMIP5-based and CORDEX-based analyses are still ongoing and more results are expected in the coming years.

The various modeling approaches used up to now should be considered as complementary as they all have their advantages and drawbacks and none has been demonstrated to be better than the others in assessing the effect of climate change on the Mediterranean Sea.

Box 1
Med-CORDEX

The aim of the Coordinated Regional Downscaling Experiment (CORDEX), of the World Climate Research Program (WCRP), is to provide a coordinated framework to evaluate and improve regional climate modelling and to produce fine scale climate projections for identified regions worldwide.

The specific climate, topographical and anthropogenic factors that characterize the Mediterranean region make it a good candidate for regional climate modelling and the region was indeed chosen as a CORDEX sub-domain leading to the Med-CORDEX initiative (www.medcordex.eu) endorsed by Med-CLIVAR and HyMeX. The Med-CORDEX initiative is a voluntary-based approach and was proposed by the Mediterranean climate research community as a continuation of previous initiatives. It takes advantage of new very high resolution regional climate models (RCMs, up to 10 km) and of new fully coupled regional climate system models (RCSMs), coupling the various components of the regional climate. Med-CORDEX is a unique framework in which the research community will make use of these new modelling tools to increase the reliability of past and future regional climate information and to better understand the processes responsible for the Mediterranean climate variability and trends.

It is worth mentioning here that empirical downscaling approaches, very common over land, are only rarely used over the sea (Maciàs et al. 2013) probably due to the lack of in-situ data to train the statistical methods.

## Future evolution of the Mediterranean Sea forcings

As mentioned in the previous sub-chapter, there is a wide consensus that the future Mediterranean climate will be characterized by drier and warmer conditions. In line with these changes, the components of the Mediterranean Sea surface freshwater budget, evaporation, precipitation, rivers and Black Sea freshwater inputs, will also change (Mariotti et al. 2008, 2015, Sanchez-Gomez et al. 2009, Elguindi et al. 2011, Dubois et al. 2012, Planton et al. 2012, Adloff et al. 2015). Between the end of the 20$^{th}$ century and the end of the 21$^{st}$ century, most studies predict a decrease in precipitation of between -5% and -15% over the basin, although some studies project a reduction of up to 28%. On the other hand, evaporation tends to increase, with some models projecting an increase of up to 18%. River runoff and Black Sea water net inflow are both projected to decrease respectively by down to -87 % and -102 %. The latter value implies that, according to some future projections, the Black Sea will become an evaporative basin and as a consequence, the net water flow through the Dardanelles Strait would reverse (from the Mediterranean to the Black Sea). Changes in the components of the water budget depend to a great extent on the socio-economic scenario chosen (Adloff et al. (2015): the higher the GHG emissions, the greater the response of the water flux. However, changes in the Mediterranean Sea water budget are not expected to emerge from natural variability before the middle of the 21$^{st}$ century. It is worth noting that the future change in the Nile River discharge is a challenging issue due to the considerable influence of the management of this river, which has not been correctly tackled up to now (see Somot et al. 2006 and Dubois et al. 2012 for a discussion of this issue).

Future changes in the components of the Mediterranean Sea surface heat budget: shortwave and longwave radiation, latent and sensible heat fluxes, have been less frequently studied (Somot et al. 2006, 2008, Dubois et al. 2012, Gualdi et al. 2013, Adloff et al. 2015). These studies show that in all available climate projections, the surface heat loss from the Mediterranean will decrease. The projected change in surface heat change ranges from +25 % to +118 %, meaning some models predict that the Mediterranean Sea could even gain heat through the surface in the future. The changes in surface heat fluxes are tightly correlated with the GHG concentrations in the scenarios.

Few studies have assessed changes in the speed and direction of the wind over the Mediterranean Sea (Somot et al. 2006, Dubois et al. 2012, A. Dell'Aquila CLIM-RUN project, unpublished). From these RCM-based studies, changes are not expected before the middle of the 21st century but a decrease in wind speed is projected for the end of the 21st century. The only sub-basin where an increase in wind speed is expected is the Aegean Sea (Somot et al. 2006).

Concerning the heat and salt transport from the near-Atlantic Ocean into the Mediterranean Sea, the global temperature increase will certainly lead to an increase in the temperatures of the incoming waters through the Strait of Gibraltar. This, together with the change in the surface heat budget, would increase the heat content of the Mediterranean Sea. In addition, an increase in water lost through the sea surface would increase the net water transport at the Strait and probably increase salinization of the basin, since more salty water will enter the basin to compensate for the increase in the fresh water deficit. However, the expected change in salinity in the near Atlantic Ocean is very uncertain in GCMs (Marcos and Tsimplis 2008, Carillo et al. 2012). Some global models project an increase in salinity in the northeast, whereas other models suggest freshening. In the latter case, the waters entering the Mediterranean through the Strait of Gibraltar could be fresher and could at least partially compensate for the effects of increased water transport. The evolution of salinity forcing coming from the Atlantic Ocean is today probably one of the main uncertainties of future projections concerning the Mediterranean Sea.

# Future evolution of sea circulation, temperature and salinity

## Sea surface temperature and salinity

In the climate change scenarios, GCMs and RCMs clearly predict warming of the Mediterranean Sea surface, with a significant, nearly homogenous increase of up to 1.5 °C – 3.1 °C in the annual mean SST for the end of 21st century compared to the present (e.g. Somot et al. 2006, Adloff et al. 2015). The warming rate depends at the first order on both the time horizon and the greenhouse gas emission scenario (Shaltout et al. 2014, Adloff et al. 2015, Mariotti et al. 2015). However, warming will always remain below than that of the air due to ocean thermal inertia. Some studies indicate greater warming in summer compared to winter. Even if there is still no clear consensus on the spatial variability of the increase in SST, Adloff et al. (2015) identified the Balearic Islands, the northwest Ionian, the Aegean and Levantine Seas as the regions with maximum warming.

The future evolution of sea surface salinity (SSS) is less certain as it depends on two competing and opposite forcings (see above). This leads to non-homogeneous, geographically and seasonally dependent projected changes for SSS. A progressively higher SSS is however generally projected with values ranging from 0.06 psu to 1 psu over the next 100 years. Changes in SSS often remain undetectable until the middle of the 21st century and more pronounced salinization is identified in the Aegean and the Adriatic, possibly driven by a marked decrease in Black Sea and Po river runoff (Planton et al 2012, Adloff et al. 2015, see Figure 1).

Changes in SST and SSS have opposite effects on the density of the surface waters. Pessimistic scenarios project a decrease in surface density (due to the marked increase in temperature) whereas some optimistic scenarios project an increase in density (related to a moderate increase in temperature and sometimes major changes in SSS in the near Atlantic Ocean).

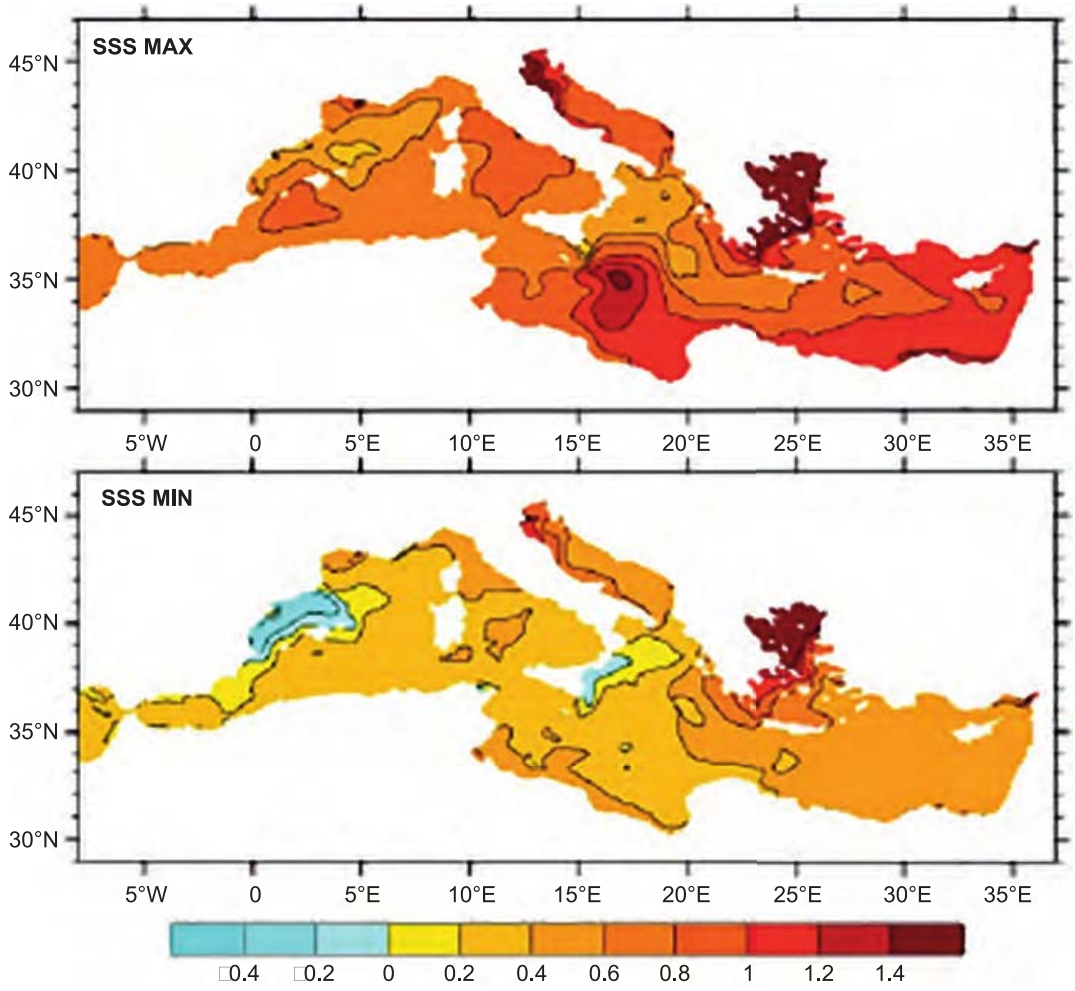


*Figure 1*
*Spatial composite of the expected minimum and maximum changes in SSS at the end of the 21st century compared with the end of the 20th century based on a 6-member ensemble covering various sources of uncertainty (adapted from Adloff et al. 2015)*

## Deep layer characteristics

The surface climate change signal is propagated efficiently towards the deeper layers through the Mediterranean thermohaline circulation and more particularly through deep convection and dense water formation processes. This leads to relatively strong signals in the deep layers of the Mediterranean Sea with a mean warming of about +0.4 °C in total heat content in the middle of the 21st century (Carillo et al. 2012) and between +0.9 °C and +2.5 °C at the end of the 21st century mostly depending on the socio-economic scenario concerned but also on the choice of the model and on the modeling strategy applied (Somot et al. 2006, Marcos and Tsimplis 2008, Adloff et al. 2015, Macià s et al. 2016). For the total salt content of the seawater, no significant signal is projected for the middle of the 21st century (Carillo et al. 2012) while values ranging from +0.2 psu to +0.9 psu, (Somot et al. 2006, Adloff et al. 2015, Macià s et al. 2016) are projected for the end of the 21st century mostly due to the uncertainty related to the changes in the near Atlantic characteristics, in river discharges, and in the strength of the thermohaline circulation under the current climate. This means the socio-economic scenario is not the main source of uncertainty in future changes in salinity.

## Sea circulation

Although sea surface circulation is difficult to assess from the published literature (only one study), it is projected to undergo some modifications with a northward shift of the eastward moving surface water veins in both the western and eastern basins. For example in Figure 1, the areas with a decrease in salinity in the Balearic area and in the northern Ionian Sea are signatures of these changes in surface circulation (Adloff et al. 2015).

All published studies agree on a weakening of the open-sea deep convection, the winter deep water formation and the related branch of the thermohaline circulation for the western Mediterranean Sea (Thorpe and Bigg 2000, Somot et al. 2006, Adloff et al. 2015), which, in some studies, is projected to be very strong and to occur very early in the 21st century (Somot et al. 2006). The picture in the eastern Mediterranean Sea is more contrasted with weakening in some simulations (Somot et al. 2006) but enhanced convection and thermohaline circulation in others and even some situations where the Aegean Sea becomes the first source of Eastern Mediterranean Deep Water (EMDW) such as during the Eastern Mediterranean Transient (EMT) in the 1990s (Adloff et al. 2015). This EMT-like situation is attributed to stronger winds over this area and to a drastic reduction in the flow of freshwater from the Black Sea into the Aegean Sea. The results concerning future changes in the Mediterranean thermohaline circulation should to be interpreted with caution as the models still have difficulty representing the current climate thermohaline circulation.

# Water transport through the Strait of Gibraltar and Mediterranean outflow water

Changes in the Mediterranean thermohaline circulation are intimately connected to the exchange of water and heat with the Atlantic Ocean through the Strait of Gibraltar. Adloff et al. (2015), project an increase of 0.02 Sv (relative to the actual value, 0.05 Sv) in the net water flux at the Strait of Gibraltar to compensate for the increase in net water loss from the sea surface. The net heat and salt transport are projected to increase by +2 $Wm^{-2}$ and +11 $10^5$ $kg.s^{-1}$, respectively. The Atlantic Ocean is therefore projected to increase its supply of mass, salt, and heat to the Mediterranean Sea. Concerning the two-way exchange, a decrease in outflow (~-0.02 Sv) and a slight change in inflow (an increase of less than +0.01) are projected. These changes reflect changes in the hydrographic characteristics of the Mediterranean Sea but also probably in those of the eastern Atlantic Ocean. However the projected changes vary among models, with some models showing a reduction in the net heat gain and in the salt loss at the Strait of Gibraltar (Somot et al. 2006). The model simulations underline the complexity of the expected changes in water transport through the Strait of Gibraltar as they are the result of competing changes in temperature and salinity.

# Mean sea level, storm surge and wind waves

## Mean sea level

Modeling mean sea level variability in the Mediterranean Sea is not straightforward. On one hand, GCMs do not have enough spatial resolution to reproduce the main mechanisms that control regional dynamics. For instance, the redistribution of heat inside the basin is strongly biased if the resolution is too coarse. This has a major impact on the reliability of temperature projections in the Mediterranean, and consequently on thermal expansion. On the other hand, at low frequencies, the variability of Mediterranean sea level is strongly influenced by changes in the nearby Atlantic, which are usually not included in regional climate models (RCMs) thus making it impossible for them to estimate long term trends of total sea level.

Up to now, studies on the projections of sea level in the Mediterranean have focused on one of the components of sea level variability, the steric component (i.e. linked to changes in the density of the water column). This is only a part of the story as long as the projected sea level changes in the nearby Atlantic (i.e. either due to land ice melting or to changes in the circulation) are not taken into account. Moreover, Jordà and Gomis (2013) showed that ignoring changes

in the amount of salt and using only the steric component to characterize the total sea level can lead to false conclusions in the Mediterranean. In particular, the steric component is equal to total sea level only in those cases where the mass in the water column is preserved. However, major changes in salt content are expected in the Mediterranean Sea that would not only increase the density of the water column but also change the mass. In other words, an increase in salinity in the basin would not imply a contraction of the water column, even if the steric component were negative. Therefore, projections based only on the steric component should be interpreted with caution.

Using the simulated evolution of the steric component in the Mediterranean, Carillo et al. (2012) found a thermal expansion of about 5 cm in 2050 under the A1b scenario. It can also be concluded from their study that differences in the temperature of the waters flowing into the Mediterranean from the Atlantic will have little effect on the thermal evolution of the basin. Gualdi et al., (2013) found an increase in the steric component of about 15 cm in 2050 under the A1b scenario, although it should be noted that this is not completely representative of total sea level as the salinity effects were not filtered out. Adloff et al. (2015) projected a basin average thermal expansion ranging from +34 to +49 cm at the end of the 21$^{st}$ century under scenario A2. These authors found that the discrepancies are mainly due to the conditions prescribed for the Atlantic forcing, thus somewhat in disagreement with Carillo et al. (2012), who found no significant sensitivity to Atlantic forcing.

In addition to the local thermal expansion, other components will play a role in future changes in sea level in the Mediterranean. In particular, melting of terrestrial ice due to global warming will be converted into a quasi-homogeneous global signal. This could mean an additional rise of between 10 and 60 cm in the level of the Mediterranean Sea (Spada et al. 2013). Changes in the northeast Atlantic circulation will also represent an additional 10-30 cm (Bouttes et al. 2012). In summary, the projected rise in the average sea level of the Mediterranean basin is estimated to be between 40 cm and 110 cm at the end of the 21$^{st}$ century with respect to the present climate. The range reflects the uncertainties linked to the GHG emissions scenario and to uncertainties in the modelling system. Finally, it is worth mentioning that changes in circulation within the Mediterranean can also sustain local changes that differ from the basin average Figure 1. These changes can be up to $\pm$ 10 cm (Figure 2) although different models differ in the patterns of change and there are no dedicated studies addressing the robustness of these regional patterns.

## Storm surge

Concerning the extreme sea level events, studies show that projections of extreme sea level events in the Mediterranean are very sensitive to the choice of atmospheric forcing. Marcos et al. (2011) point to a reduction in the average number of positive surges, whereas negative surges will increase throughout the 21$^{st}$ century. Conte and Lionello (2013) found an overall

decrease of ~-5% in the magnitude in positive surges with changes up to ~-10% in some locations along the Mediterranean coasts. However, these authors reported marked differences among simulations, and that the results were not spatially coherent.

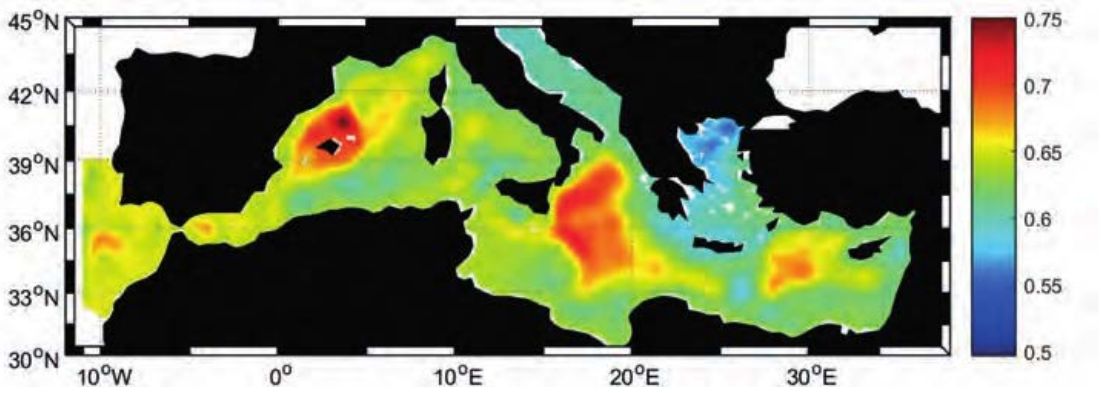


*Figure 2*
*Projection of sea level change for the period 2080-2100 with respect to the period 1980-2000. The result is the combination of outputs of an ensemble of regional climate models combined with the CMIP5 projections for the Atlantic changes all run under moderate GHG emission scenarios (A1b and RCP6.0).*

## Wind waves

Future changes in waves will be determined by future changes in the wind field over the Mediterranean Sea. Lionello et al. (2008) ran a regional wave model of the whole Mediterranean Sea under scenarios A2 and B2. These authors found that the mean significant wave height field over a large fraction of the Mediterranean Sea would be lower all year round at the end of the 21st century with a greater reduction (about -20 cm) in winter under scenario A2. The changes are similar, though smaller and less significant, under the B2 scenario, except during winter in the north-western Mediterranean Sea, where the mean significant wave height is projected to be higher than at present. Concerning extreme events, these authors also found smaller values in future scenarios than in the present climate. They also showed that, in general, changes in significant wave height, wind speed and atmospheric circulation were consistent.

Based on statistical downscaling, Pérez et al. (2016) also found a decrease in significant wave height of -5 cm under scenario RCP8.5, of -3 cm under scenario RCP4.5, and no change under scenario RCP 2.6. These results are in agreement with the above mentioned work and point to a larger decrease in wave height under higher emission scenarios.

# Conclusions

Several robust and significant conclusions can be drawn such as general warming and an increase in the salinity of Mediterranean waters, as well as the sea level rise due to the propagation of the global signal. However the changes in temperature and salinity have opposite and competing effects on the change in water density and hence on changes in vertical stratification, in the Mediterranean thermohaline circulation, and in the total steric sea level. Whereas some scenarios project a weakening of the thermohaline circulation especially in the western Mediterranean basin, others predict that the Mediterranean Sea could enter an EMT-like state. As a consequence, future changes in water and heat exchanges at the Strait of Gibraltar, being part of the thermohaline circulation, are less certain but will very likely be an increasing source of heat and salt for the deep layers of the North Atlantic Ocean during the course of the 21st century. Similarly, the uncertainty on the expected sea level rise is as high as that for oceans worldwide.

Changes related to the water cycle are not expected to emerge from the natural variability before the middle of the 21st century, whereas changes related to the heat cycle are already being observed. Concerning the end of the 21st century, as expected, the choice of the socio-economic scenario is often the most important source of uncertainty, but future changes in conditions in the Near Atlantic Ocean may outweigh salinity related changes including the Mediterranean thermohaline circulation. Future changes in river discharges could be the main source of uncertainty in some key sub-basins.

# References

**Adloff F., Somot S., Sevault F., Jordà G., Aznar R., Déqué M., Herrmann M., Marta Marcos M., Dubois C., Padorno E., Alvarez-Fanjul E., Gomis., 2015**
Mediterranean Sea response to climate change in an ensemble of twenty first century scenarios. Clim Dyn (2015) 45:2775–2802. DOI 10.1007/s00382-015-2507-3.

**Bouttes N., Gregory J. M., Kuhlbrodt T., Smith R. S., 2014**
The drivers of projected North Atlantic sea level change. *Climate Dynamics, 43:1531–1544. doi: 10.1007/s00382-013-1973-8*

**Carillo A., Sannino G., Artale V., Ruti P. M., Calmanti S., Dell'Aquila A., 2012**
Steric sea level rise over the Mediterranean Sea: present climate and scenario simulations. *Climate Dynamics*, 39(9-10):2167-2184.

**Conte D., Lionello P., 2013**
Characteristics of large positive and negative surges in the Mediterranean Sea and their attenuation in future climate scenarios. *Global and Planetary Change 111* 159–173. DOI: 10.1016/j.gloplacha.2013.09.006

**Dubois C., Somot S., Calmanti S., Carillo A., Déqué M., Dell'Aquilla A., Elizalde A., Gualdi S., Jacob D., L'Hévéder B., Li L., Oddo P., Sannino G., Scoccimarro E., Sevault F., 2012**
Future projections of the surface heat and water budgets of the Mediterranean Sea in an ensemble of coupled atmosphere–ocean regional climate

models. *Climate Dynamics*, 39(7–8):1859–1884. doi:10.1007/ s00382-011-1261-4.

**Elguindi N., Somot S., Déqué M., Ludwig W., 2011**
Climate change evolution of the hydrological balance of the Mediterranean, Black and Caspian Seas: impact of climate model resolution. *Clim. Dyn.,* 36 (1-2):205-228, doi: 10.1007/ s00382-009-0715-4

**Gualdi S., Somot S., Li L., *et al.*, 2013**
The CIRCE simulations regional climate change projections with realistic representation of the Mediterranean Sea. *Bull Am Meteorol Soc,* 94(1):65–81. doi:10.1175/BAMS-D-11-00136.1

**Jordà G., Gomis D., 2013**
On the interpretation of the steric and mass components of sea level variability: The case of the Mediterranean basin, J. Geophys. Res.: Oceans, 118, doi:10.1002/jgrc.20060

**Lionello P., Cogo S., Galati M.B., Sanna A., 2008**
The Mediterranean surface wave climate inferred from future scenario simulations. *Global and Planetary Change*, 63:152–162.

**Macias D., Garcia-Gorriz E., Stips A., 2013**
Understanding the causes of recent warming of Mediterranean waters. How much could be attributed to climate change?. *PloS one*, *8*(11), e81591.

**Macias D., Garcia-Gorriz E., Dosio A., Stips A., Keuler, K., 2016**
Obtaining the correct sea surface temperature: bias correction of regional climate model data for the Mediterranean Sea. *Climate Dynamics*, in press.

**Marcos M., Tsimplis M.N., 2008**
Comparison of results of AOGCMs in the Mediterranean Sea during the 21st century. *J Geophys Res. Oceans,* 113(C12):C12,028

**Marcos M., Jordà G., Gomis D., Pérez B., 2011**
Changes in storm surges in southern Europe during the 21st century. *Global and Planetary Change*, 77 , 116-128.

**Mariotti A., Zeng N., Yoon J., Artale V., Navarra A., Alpert P., Li L., 2008**
Mediterranean water cycle changes: Transition to drier 21st century conditions in observations and CMIP3 simulations, *Environ. Res. Lett.*, 3: 044001, doi:10.1088/1748-9326/3/044001.

**Mariotti A., Pan Y., Zeng N., Alessandri A., 2015**
Long-term climate change in the Mediterranean region in the midst of decadal variability. *Climate Dynamics*, *44*(5-6):1437-1456.

**Pérez J., Menéndez M., Camus P., Méndez F.J., Losada I.J. 2015**
Statistical multi-model climate projections of surface ocean waves in Europe, *Ocean Modelling* 96(1) 161-170 DOI: 10.1016/j. ocemod.2015.06.001

**Planton S., Lionello .P, Artale V., *et al.*, 2012**
The Climate of the Mediterranean Region in Future Climate Projections (chapter 8). In: The Climate of the Mediterranean Region, Publisher: Elsevier, Editors: Lionello, P, pp.449 – 502. DOI: 10.1016/B978-0-12-416042-2.00008-2.

**Ruti P.M., Somot S., Giorgi F. *et al.*, 2016**
MED-CORDEX initiative for Mediterranean Climate studies. *Bulletin of the American Meteorological Society.* 94, Early view. doi:10.1175/BAMS-D-14-00176.1

**Sanchez-Gomez E., Somot S., Mariotti A., 2009**
Future changes in the Mediterranean water budget projected by an ensemble of regional climate models. *Geophys Res Lett,*36:L21,401. doi:10.1029/200 9GL040120.

**Shaltout M., Omstedt A., 2014**
Recent sea surface temperature trends and future scenarios for the Mediterranean Sea. *Oceanologia*, 56, Issue 3, 411–443. doi:10.5697/ oc.56-3.411

**Spada G., J. L. Bamber J. L., Hurkmans R. T. W. L., 2012**
The gravitationally consistent sea-level fingerprint of future terrestrial ice loss, *Geophys. Res. Lett.,* 40, 482–486, doi:10.1029/2012GL053000.

**Somot S., Sevault F., Déqué M., 2006**
Transient climate change scenario simulation of the Mediterranean Sea for the twenty-first century using a high-resolution ocean circulation model. Clim Dyn 27(7–8):851–879.

**Somot S., Sevault F., Déqué M., Crépon M., 2008**
21st century climate change scenario for the Mediterranean using a coupled Atmosphere-Ocean Regional Climate Model. *Global and Planetary Change,* 63(2-3):112-126, doi:10.1016/j.gloplacha.2007.10.003

**THORPE R. B., BIGG G. R., 2000**
Modelling the sensitivity of Mediterranean Outflow to anthropogenically forced climate change. *Climate dynamics*, *16*(5):355-368.

# Meteo France Activity Report

## Mediterranean Sea Marine Heatwave On the Rise

Episodes of anomalous ocean warming have been observed in recent decades, with widespread ecological impacts and important socio-economic implications. Superimposed on the underlying warming trend of the ocean, these events referred to as Marine Heatwaves (MHWs), occur regionally from coastal to open ocean and may force changes in marine ecosystems and fisheries in a matter of weeks or months. They can be persistent in time and extended in space.

A general increase in their occurence throughout the global ocean surface was indicated over the last century, while regional and global-scale projections suggest more intense and longer-lasting events in the 21st century with higher global warming rates.

In the case of the Mediterranean Sea -a well-known "Hot Spot" region for climate change-, little is known about past or future MHW trends. A significant annual mean SST rise (+1.5°C to +3°C, depending on GHG emission scenario) projected for the basin by the end of the21st century, is expected to accelerate future MHW occurrence. To assess for the first time this evolution, we used the dedicated, fully-coupled, RCSM NEMOMED8 and a multi-scenario approach.

In response to increasing GHG forcing, events seem to become stronger and more intense under RCP8.5 than RCP2.6. Particularly for RCP85 2071-2100, simulations project at least one MHW every year, up to 4 months longer and about 4 times more intense than present-day events (HIST) (Fig.1). Meanwhile, their surface coverage at peak increases from an average of 40 % (HIST) to almost 100 % and events like the MHW 2003 become the new normal. While RCP8.5 is the business-as-usual scenario RCP2.6 is the closest to Paris agreement limits, which could restrain future MHW mean intensity and duration.

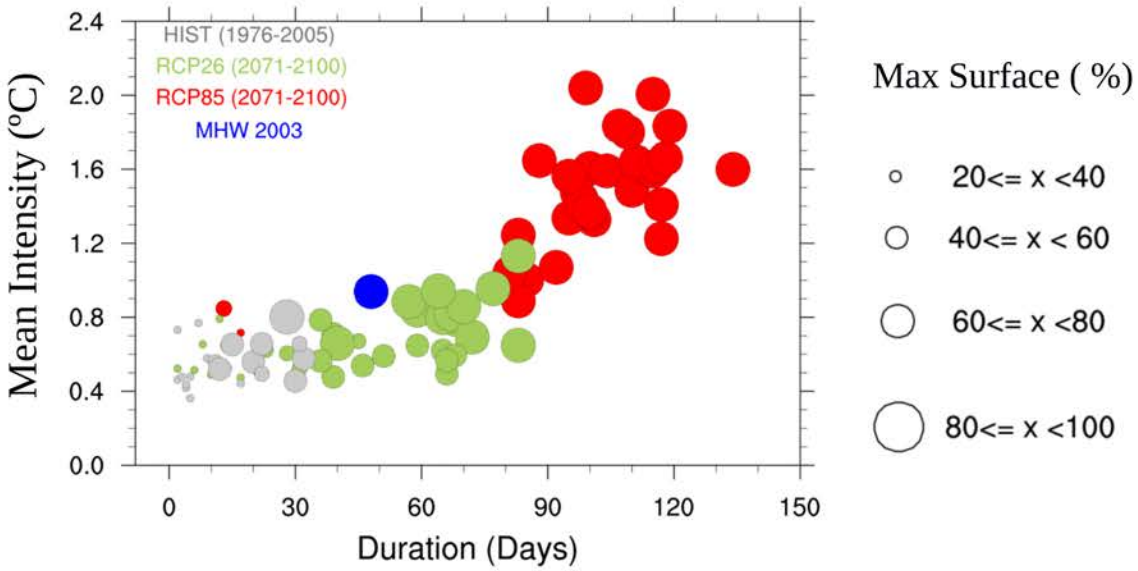


Fig.1 : MHW evolution in the Mediterranean Sea at present-day and at the end of the 21st century. Historical run (HIST) is indicated in grey, high-emission scenario RCP85 in red and low-emission scenario RCP26 in green. MHW of 2003 is also shown in blue. Size of the bubble refers to the maximum surface coverage ( %) of each event.

# Popular Science Article: Marmaed Blog

**MARINE HEAT WAVES : A silent threat**

For the second time this summer, an intense heat spell is on the rise in many European countries as temperatures go beyond 40 C. Official heatwave warnings and instructions are issued repeatedly for european citizens who often flee to the sea breeze to cool off. But exactly how cold is the water that we are turning to for a bit of comfort in days like that? We are all familiar with the idea of global warming, but have you ever wondered what happens once such extreme heat penetrates the sea surface into the marine world ? Does the ocean ever develop heatwave "fever "?

After all, it is only natural for the ocean to receive heat and sustain it for long periods of time, as part of its interaction with the atmosphere. There is ,therefore, no physical barrier that inihibits or protects near-surface marine environment from intense atmospheric signals which can trigger anomalously warm sea temperatures ,superimposed in fact, on the already underlying ocean-warming trend. Can you imagine, living in a world where heatwaves break out without any notice and with not many means of escaping from them?Surely marine inhabitants cannot read weather reports but testimonies of heatwaves occuring in the ocean have recently emerged.

We all remember the record-breaking heat wave in summer 2003 that claimed the lives of 30,000 people across Europe. One of the longest and hottest regional events, appears to have also caused mass mortality events in benthic ecosystems, across thousands of kilometres of coastline in the NW Mediterranean, with sea surface temperatures reaching 1-3 C above normal [1]. Similarly in 2011, west coast of Australia is hit by anomalously warm waters, lasting for more than 10 weeks. This hot surge was responsible for the eradication of kelp forests that never recovered, mass deaths of seaweed meadows, with knock-off effects on wildlife depending on these ecosystems. This is also when the term "marine heat wave" was first coined to describe similar extreme events like the one in 2013 : Washed up seabirds, dehydrated lions, dead whales followed by a large toxic algal bloom along the California coast and species migrations, summarize the infamous extremely warm "blob" - with its very own dedicated Wikipedia page - that swept the Pacific for 1.5 years. Then, the Great Barrier Reef is blasted in 2016 from what was experienced as possibly the worst coral bleaching ever recorded in the region, in one fell swoop.

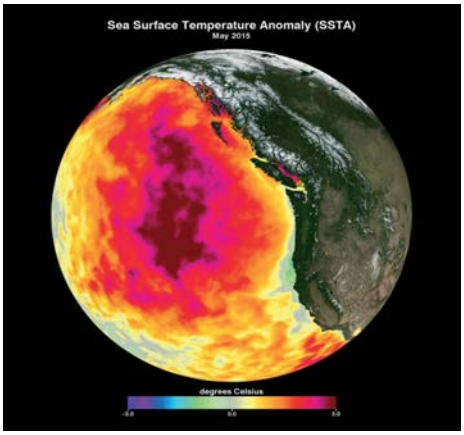


SST anomaly of May 2015 with respect to 2002-2012 climatology, reveals the "Pacific blob" signature. (Map by American Geophysical Union)

Extreme events in ocean properties happened before but received little attention until their adverse impacts started to increase in scale and frequency, (in parallel with the improving observational systems). In principle, a marine heat wave is a prolonged period of anomalously warm water extended regionally [2] and can have severe impacts on marine ecosystems. By default, an objective universal index is nearly impossible to define for comparisons between every such event which can occur almost everywhere throughout the global ocean. However, researchers have recently proposed

.

a standardised framework for their assessment. The idea is to measure characteristics like frequency, duration, (cumulative) intensity across the available observational record in an effort to understand how marine heat waves have evolved. Meanwhile, work is also conducted using climate models to study their future evolution in the 21st century and to disentangle their remote and/or local driving mechanisms.

Take for example the Mediterranean Sea. A ‘’hot spot’’ region for climate change, biodiversity , tourism and a heavily inhabited area. Inspired by the rapid changes already in place, we are using regional climate models (models with incorporated air-sea interactions) to examine how surface marine heat waves in the Mediterranean Sea will evolve in the next 100 years, under different greenhouse gas regimes. We are interested in understanding their present and future spatiotemporal patterns and how quickly these are transformed. But the big question, we are facing is whether (and how much) will their severity and frequency change under climate change and what will be the consequences in the relevant ecosystems and coastal communities. Preliminary results suggest longer and more severe extreme events in the future that follow up greenhouse gas emissions. For this reason, we are also investigating what it seems to be a complicated combination of local oceanic and large-scale atmospheric forcing components of these events, in an attempt to identify the modulating factors behind them. Deep understanding will hopefully lead to more accurate predictions.

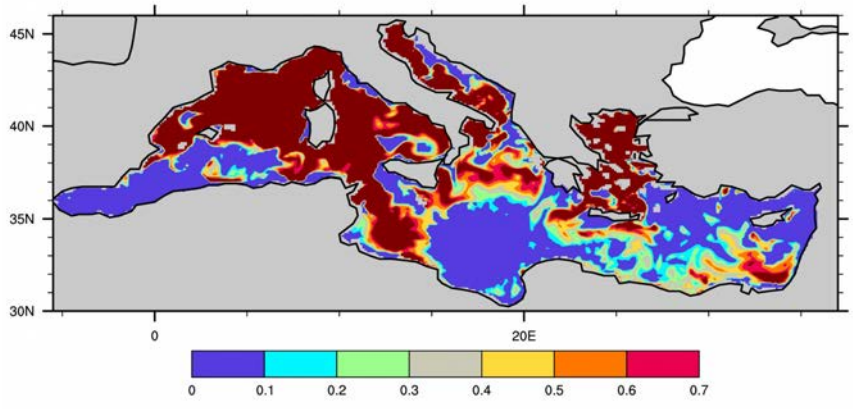


And while initially this might not look very disturbing (who doesn’t prefer tropical ocean temperatures ?), implications for society are worrying. Aside from considerable losses in biodiversity, ‘’tropicalisation » of Mediterranean waters can lead to abrupt shifts in financial balance between fisheries in the area (e.g. see here). Marine-based tourism and coastal communities will inevitably be impacted by the sudden regime shift which will sooner or later affect our food consumption habits as well.

One thing we know for sure is that as anthropogenic climate change escalates, so will marine heatwaves, like their atmospheric counterparts, spreading silently chaos in the oceans ,initially hidden from view but eventually reaching our communities. It is widely known that a small increase in average temperatures forces big changes in extreme events,notably the intensity and frequency. It is important hence, not to forget that the ocean makes up 70 % of our planet before more « noisy evidence start to emerge of what marine heat waves can cause below the seemingly calm and cool waters.

.

# Bibliography


Adloff, F., Somot, S., Sevault, F., Jorda, G., Aznar, R., Deque, M., Herrmann, M., Marcos, M., Dubois, C., Padorno, E., et al. (2015). Mediterranean sea response to climate change in an ensemble of twenty first century scenarios. *Climate Dynamics*, 45(9-10):2775–2802.

Akhtar, N., Brauch, J., and Ahrens, B. (2018). Climate modeling over the Mediterranean Sea: impact of resolution and ocean coupling. *Climate Dynamics*, 51(3):933–948.

Albouy, C., Guilhaumon, F., Leprieur, F., Lasram, F. B. R., Somot, S., Aznar, R., Velez, L., Le Loc'h, F., and Mouillot, D. (2013). Projected climate change and the changing biogeography of coastal mediterranean fishes. *Journal of Biogeography*, 40(3):534–547.

Amaya, D., Bond, N., Miller, A., and DeFlorio, M. (2016). The evolution and known atmospheric forcing mechanisms behind the 2013-2015 north pacific warm anomalies. *US Clivar Variations*, 14(2):1–6.

Amitai, Y., Lehahn, Y., Lazar, A., and Heifetz, E. (2010). Surface circulation of the eastern mediterranean levantine basin: Insights from analyzing 14 years of satellite altimetry data. *Journal of Geophysical Research: Oceans*, 115(C10).

Arnoux, A., Harmeilnn, J.-G., Monod, J., Romaña, L., and Zibrowius, H. (1992). Altérations des peuplements benthiques de roches profondes en méditerranée nord-occidentale: quelque aspects biologiques et molysmologiques. *Comptes rendus de l'Académie des sciences. Série 3, Sciences de la vie*, 314(5):219–225.

Artale, V., Calmanti, S., Carillo, A., Dell'Aquila, A., Herrmann, M., Pisacane, G., Ruti, P. M., Sannino, G., Struglia, M. V., Giorgi, F., et al. (2010). An atmosphere–ocean regional climate model for the mediterranean area: assessment of a present climate simulation. *Climate Dynamics*, 35(5):721–740.

Auger, P., Ulses, C., Estournel, C., Stemmann, L., Somot, S., and Diaz, F. (2014). Interannual control of plankton communities by deep winter mixing and prey/predator interactions in the nw mediterranean: Results from a 30-year 3d modeling study. *Progress in Oceanography*, 124:12–27.

Balmaseda, M. A., Mogensen, K., and Weaver, A. T. (2013a). Evaluation of the ecmwf ocean reanalysis system oras4. *Quarterly Journal of the Royal Meteorological Society*, 139(674):1132–1161.

Balmaseda, M. A., Trenberth, K. E., and Källén, E. (2013b). Distinctive climate signals in reanalysis of global ocean heat content. *Geophysical Research Letters*, 40(9):1754–1759.

Barriopedro, D., Fischer, E. M., Luterbacher, J., Trigo, R. M., and García-Herrera, R. (2011). The hot summer of 2010: redrawing the temperature record map of europe. *Science*, 332(6026):220–224.

Ben Rais Lasram, F., Guilhaumon, F., Albouy, C., Somot, S., Thuiller, W., and Mouillot, D. (2010). The mediterranean sea as a 'cul-de-sac'for endemic fishes facing climate change. *Global Change Biology*, 16(12):3233–3245.

Beniston, M., Stephenson, D. B., Christensen, O. B., Ferro, C. A., Frei, C., Goyette, S., Halsnaes, K., Holt, T., Jylhä, K., Koffi, B., et al. (2007). Future extreme events in european climate. *Climatic Change*, 81:71–95.

Benoit, G. (2006). Environnement et developpement en mediterranee les perspectives du plan bleu. *Futuribles*, (321):11–45.

Bensoussan, N., Garreau, P., Pairaud, I., Somot, S., and Garrabou, J. (2013). Multidisciplinary approach to assess potential risk of mortality of benthic ecosystems facing climate change in the nw mediterranean sea. In *Oceans-San Diego, 2013*, pages 1–7. IEEE.

Bensoussan, N., Romano, J.-C., Harmelin, J.-G., and Garrabou, J. (2010). High resolution characterization of northwest mediterranean coastal waters thermal regimes: to better understand responses of benthic communities to climate change. *Estuarine, Coastal and Shelf Science*, 87(3):431–441.

Benthuysen, J., Feng, M., and Zhong, L. (2014). Spatial patterns of warming off western australia during the 2011 ningaloo niño: quantifying impacts of remote and local forcing. *Continental Shelf Research*, 91:232–246.

Benthuysen, J. A., Oliver, E. C., Feng, M., and Marshall, A. G. (2018). Extreme marine

warming across tropical australia during austral summer 2015–2016. *Journal of Geophysical Research: Oceans*, 123(2):1301–1326.

Berrisford, P., Dee, D., Fuentes, M., Kallberg, P., Kobayashi, S., and Uppala, S. (2009). The era-interim archive. era-40 report series no. 1, ecmwf, shinfield park. *Reading*, 10.

Béthoux, J.-P., Gentili, B., and Tailliez, D. (1998). Warming and freshwater budget change in the mediterranean since the 1940s, their possible relation to the greenhouse effect. *Geophysical Research Letters*, 25(7):1023–1026.

Beuvier, J., Béranger, K., Lebeaupin Brossier, C., Somot, S., Sevault, F., Drillet, Y., Bourdallé-Badie, R., Ferry, N., and Lyard, F. (2012). Spreading of the western mediterranean deep water after winter 2005: Time scales and deep cyclone transport. *Journal of Geophysical Research: Oceans*, 117(C7).

Bianchi, C. N. and Morri, C. (2000). Marine biodiversity of the mediterranean sea: situation, problems and prospects for future research. *Marine pollution bulletin*, 40(5):367–376.

Black, E. and Sutton, R. (2007). The influence of oceanic conditions on the hot european summer of 2003. *Climate dynamics*, 28(1):53–66.

Bleu, P. (2008). Climate change and energy in the mediterranean. *Sophia Antipolis: Plan Bleu Regional Activity Centre*.

Blondel, J. and Aronson, J. (1999). *Biology and wildlife of the Mediterranean region*. Oxford University Press, USA.

Bond, N. A., Cronin, M. F., Freeland, H., and Mantua, N. (2015). Causes and impacts of the 2014 warm anomaly in the ne pacific. *Geophysical Research Letters*, 42(9):3414–3420.

Bunker, A. (1982). A note on the heart balance of mediterranean and red seas. *J. Mar. Res.*, 40:73–84.

Calvo, E., Simó, R., Coma, R., Ribes, M., Pascual, J., Sabatés, A., Gili, J. M., and Pelejero, C. (2011). Effects of climate change on mediterranean marine ecosystems: the case of the catalan sea. *Climate Research*, 50(1):1–29.

Caniaux, G., Prieur, L., Giordani, H., and Redelsperger, J.-L. (2017). An inverse method to derive surface fluxes from the closure of oceanic heat and water budgets: Application to the north-western mediterranean sea. *Journal of Geophysical Research: Oceans*, 122(4):2884–2908.

Carillo, A., Sannino, G., Artale, V., Ruti, P. M., Calmanti, S., and Dell'Aquila, A. (2012). Steric sea level rise over the mediterranean sea: present climate and scenario simulations. *Journal of Climate Dynamics*, pages 2167–2184.

Cavicchia, L., Gualdi, S., Sanna, A., Oddo, P., et al. (2015). The regional ocean-atmosphere coupled model cosmo-nemo_mfs. *CMCC Research Paper*, (RP0254).

Cavole, L. M., Demko, A. M., Diner, R. E., Giddings, A., Koester, I., Pagniello, C. M., Paulsen, M.-L., Ramirez-Valdez, A., Schwenck, S. M., Yen, N. K., et al. (2016). Biological impacts of the 2013–2015 warm-water anomaly in the northeast pacific: Winners, losers, and the future. *Oceanography*, 29(2):273–285.

Cebrian, E., Uriz, M. J., Garrabou, J., and Ballesteros, E. (2011). Sponge mass mortalities in a warming mediterranean sea: are cyanobacteria-harboring species worse off? *PLoS One*, 6(6):e20211.

Cerrano, C., Bavestrello, G., Bianchi, C. N., Cattaneo-Vietti, R., Bava, S., Morganti, C., Morri, C., Picco, P., Sara, G., Schiaparelli, S., et al. (2000). A catastrophic mass-mortality episode of gorgonians and other organisms in the ligurian sea (north-western mediterranean), summer 1999. *Ecology letters*, 3(4):284–293.

Chao, Y., Farrara, J. D., Bjorkstedt, E., Chai, F., Chavez, F., Rudnick, D. L., Enright, W., Fisher, J. L., Peterson, W. T., Welch, G. F., et al. (2017). The origins of the anomalous warming in the california coastal ocean and san francisco bay during 2014–2016. *Journal of Geophysical Research: Oceans*, 122(9):7537–7557.

Chen, K., Gawarkiewicz, G., Kwon, Y.-O., and Zhang, W. G. (2015). The role of atmospheric forcing versus ocean advection during the extreme warming of the northeast us continental shelf in 2012. *Journal of Geophysical Research: Oceans*, 120(6):4324–4339.

Chen, K., Gawarkiewicz, G. G., Lentz, S. J., and Bane, J. M. (2014). Diagnosing the warming of the northeastern us coastal ocean in 2012: A linkage between the atmospheric jet stream variability and ocean response. *Journal of Geophysical Research: Oceans*, 119(1):218–227.

Chenoweth, J., Hadjinicolaou, P., Bruggeman, A., Lelieveld, J., Levin, Z., Lange, M. A., Xoplaki, E., and Hadjikakou, M. (2011). Impact of climate change on the water resources of the eastern mediterranean and middle east region: Modeled 21st century changes and implications. *Water Resources Research*, 47(6).

Christensen, J. H. and Christensen, O. B. (2007). A summary of the prudence model projections of changes in european climate by the end of this century. *Climatic change*, 81(1):7–30.

Colin, J., Déqué, M., Radu, R., and Somot, S. (2010). Sensitivity study of heavy precipitation in limited area model climate simulations: influence of the size of the domain and the use of the spectral nudging technique. *Tellus A: Dynamic Meteorology and Oceanography*, 62(5):591–604.

Coll, M., Piroddi, C., Steenbeek, J., Kaschner, K., Lasram, F. B. R., Aguzzi, J., Ballesteros, E., Bianchi, C. N., Corbera, J., Dailianis, T., et al. (2010). The biodiversity of the mediterranean sea: estimates, patterns, and threats. *PloS one*, 5(8):e11842.

Coma, R., Ribes, M., Serrano, E., Jiménez, E., Salat, J., and Pascual, J. (2009). Global warming-enhanced stratification and mass mortality events in the mediterranean. *Proceedings of the National Academy of Sciences*, 106(15):6176–6181.

Craig, A., Valcke, S., and Coquart, L. (2017). Development and performance of a new version of the oasis coupler, oasis3-mct_3. 0. *Geoscientific Model Development*, 10(9):3297–3308.

Crisci, C., Bensoussan, N., Romano, J.-C., and Garrabou, J. (2011). Temperature anomalies and mortality events in marine communities: insights on factors behind differential mortality impacts in the nw mediterranean. *PLoS One*, 6(9):e23814.

Curry, R., Dickson, B., and Yashayaev, I. (2003). A change in the freshwater balance of the atlantic ocean over the past four decades. *Nature*, 426(6968):826.

Daniel, M., Lemonsu, A., Déqué, M., Somot, S., Alias, A., and Masson, V. (2018). Benefits of explicit urban parameterization in regional climate modeling to study climate and city interactions. *Climate Dynamics*, pages 1–20.

Danovaro, R., Umani, S. F., and Pusceddu, A. (2009). Climate change and the potential spreading of marine mucilage and microbial pathogens in the mediterranean sea. *PLoS One*, 4(9):e7006.

Darmaraki, S., Somot, S., Sevault, F., Nabat, P., Narvaez, W. D. C., Cavicchia, L., Djurdjevic, V., Li, L., Sannino, G., and Sein, D. V. (2019). Future evolution of marine heatwaves in the mediterranean sea. *Climate Dynamics*, pages 1–22.

De Madron, X. D., Guieu, C., Sempere, R., Conan, P., Cossa, D., D'Ortenzio, F., Estournel, C., Gazeau, F., Rabouille, C., Stemmann, L., et al. (2011). Marine ecosystems' responses to climatic and anthropogenic forcings in the mediterranean. *Progress in Oceanography*, 91(2):97–166.

Decharme, B., Delire, C., Minvielle, M., Colin, J., Vergnes, J.-P., Alias, A., Saint-Martin, D., Séférian, R., Sénési, S., and A., V. (subm). Recent changes in the isba-ctrip land surface system for use in the cnrm-cm6 climate model and in global off-line hydrological applications. *JAMES*.

Déqué, M., Jones, R., Wild, M., Giorgi, F., Christensen, J., Hassell, D., Vidale, P. L., Rockel, B., Jacob, D., Kjellström, E., et al. (2005). Global high resolution versus limited area model climate change projections over europe: quantifying confidence level from prudence results. *Climate Dynamics*, 25(6):653–670.

Déqué, M., Rowell, D., Lüthi, D., Giorgi, F., Christensen, J., Rockel, B., Jacob, D., Kjellström, E., De Castro, M., and van den Hurk, B. (2007). An intercomparison of regional climate simulations for europe: assessing uncertainties in model projections. *Climatic Change*, 81(1):53–70.

Deser, C., Alexander, M. A., and Timlin, M. S. (2003). Understanding the persistence of sea surface temperature anomalies in midlatitudes. *Journal of Climate*, 16(1):57–72.

Di Camillo, C. G., Bartolucci, I., Cerrano, C., and Bavestrello, G. (2013). Sponge disease in the adriatic sea. *Marine Ecology*, 34(1):62–71.

Di Camillo, C. G. and Cerrano, C. (2015). Mass mortality events in the nw adriatic sea: phase shift from slow-to fast-growing organisms. *PloS one*, 10(5):e0126689.

Di Lorenzo, E. and Mantua, N. (2016). Multi-year persistence of the 2014/15 north pacific marine heatwave. *Nature Climate Change*, 6(11):1042–1047.

Diaz-Almela, E., Marba, N., and Duarte, C. M. (2007). Consequences of mediterranean warming events in seagrass (posidonia oceanica) flowering records. *Global change biology*, 13(1):224–235.

Diffenbaugh, N. S., Pal, J. S., Giorgi, F., and Gao, X. (2007). Heat stress intensification in the mediterranean climate change hotspot. *Geophysical Research Letters*, 34(11).

Djurdjevic, V. and Rajkovic, B. (2008). Verification of a coupled atmosphere-ocean model using satellite observations over the adriatic sea. In *Annales Geophysicae*, volume 26, pages 1935–1954. Copernicus GmbH.

Dubois, C., Somot, S., Calmanti, S., Carillo, A., Déqué, M., Dell'Aquilla, A., Elizalde, A., Gualdi, S., Jacob, D., L'hévéder, B., et al. (2012). Future projections of the surface heat and water budgets of the mediterranean sea in an ensemble of coupled atmosphere–ocean regional climate models. *Climate dynamics*, 39(7-8):1859–1884.

Dünkeloh, A. and Jacobeit, J. (2003). Circulation dynamics of mediterranean precipitation variability 1948–98. *International Journal of Climatology*, 23(15):1843–1866.

Elguindi, N., Somot, S., Déqué, M., and Ludwig, W. (2011). Climate change evolution of the hydrological balance of the mediterranean, black and caspian seas: impact of climate model resolution. *Climate dynamics*, 36(1-2):205–228.

Feng, M., McPhaden, M. J., Xie, S.-P., and Hafner, J. (2013). La niña forces unprecedented leeuwin current warming in 2011. *Scientific reports*, 3.

Ferranti, L. and Viterbo, P. (2006). The european summer of 2003: Sensitivity to soil water initial conditions. *Journal of Climate*, 19(15):3659–3680.

Feudale, L. and Shukla, J. (2007). Role of mediterranean sst in enhancing the european heat wave of summer 2003. *Geophysical Research Letters*, 34(3).

Feudale, L. and Shukla, J. (2011). Influence of sea surface temperature on the european heat wave of 2003 summer. part i: an observational study. *Climate dynamics*, 36(9-10):1691–1703.

Fischer, E. M. and Schär, C. (2009). Future changes in daily summer temperature variability: driving processes and role for temperature extremes. *Climate Dynamics*, 33(7-8):917.

Fischer, E. M. and Schär, C. (2010). Consistent geographical patterns of changes in high-impact european heatwaves.

Fischer, E. M., Seneviratne, S. I., Lüthi, D., and Schär, C. (2007a). Contribution of land-atmosphere coupling to recent european summer heat waves. *Geophysical Research Letters*, 34(6).

Fischer, E. M., Seneviratne, S. I., Vidale, P. L., Lüthi, D., and Schär, C. (2007b). Soil moisture–atmosphere interactions during the 2003 european summer heat wave. *Journal of Climate*, 20(20):5081–5099.

Frölicher, T. L., Fischer, E. M., and Gruber, N. (2018). Marine heatwaves under global warming. *Nature*, 560(7718):360.

Frölicher, T. L. and Laufkötter, C. (2018). Emerging risks from marine heat waves. *Nature communications*, 9(1):650.

Galli, G., Solidoro, C., and Lovato, T. (2017). Marine heat waves hazard 3d maps, and the risk for low motility organisms in a warming mediterranean sea. *Frontiers in Marine Science*, 4:136.

Gao, X., Pal, J. S., and Giorgi, F. (2006). Projected changes in mean and extreme precipitation over the mediterranean region from a high resolution double nested rcm simulation. *Geophysical Research Letters*, 33(3).

Garrabou, J., Coma, R., Bensoussan, N., Bally, M., Chevaldonné, P., Cigliano, M., Diaz, D., Harmelin, J.-G., Gambi, M., Kersting, D., et al. (2009). Mass mortality in northwestern mediterranean rocky benthic communities: effects of the 2003 heat wave. *Global change biology*, 15(5):1090–1103.

Garrabou, J., Perez, T., Sartoretto, S., and Harmelin, J. (2001). Mass mortality event in red coral corallium rubrum populations in the provence region (france, nw mediterranean). *Marine Ecology Progress Series*, 217:263–272.

Gentemann, C. L., Fewings, M. R., and García-Reyes, M. (2017). Satellite sea surface temperatures along the west coast of the united states during the 2014–2016 northeast pacific marine heat wave. *Geophysical Research Letters*, 44(1):312–319.

Giannakopoulos, C., Le Sager, P., Bindi, M., Moriondo, M., Kostopoulou, E., and Goodess, C. (2009). Climatic changes and associated impacts in the mediterranean resulting from a 2 c global warming. *Global and Planetary Change*, 68(3):209–224.

Gibelin, A.-L. and Déqué, M. (2003). Anthropogenic climate change over the mediterranean region simulated by a global variable resolution model. *Climate Dynamics*, 20(4):327–339.

Giorgi, F. (2006). Climate change hot-spots. *Geophysical research letters*, 33(8).

Giorgi, F. and Bi, X. (2009). Time of emergence (toe) of ghg-forced precipitation change hot-spots. *Geophysical Research Letters*, 36(6).

Giorgi, F. and Coppola, E. (2009). Projections of twenty-first century climate over europe. In *EPJ Web of Conferences*, volume 1, pages 29–46. EDP Sciences.

Giorgi, F. and Lionello, P. (2008). Climate change projections for the mediterranean region. *Global and planetary change*, 63(2-3):90–104.

Goodess, C., Jacob, D., Déqué, M., Guttierez, J., Huth, R., Kendon, E., Leckebusch, G., Lorenz, P., and Pavan, V. (2009). Downscaling methods, data and tools for input to impacts assessments.

Goubanova, K. and Li, L. (2007). Extremes in temperature and precipitation around the mediterranean basin in an ensemble of future climate scenario simulations. *Global and Planetary Change*, 57(1-2):27–42.

Grazzini, F. and Viterbo, P. (2003). Record-breaking warm sea surface temperature of the mediterranean sea. *ECMWF Newsletter*, 98:30–31.

Gualdi, S., Somot, S., Li, L., Artale, V., Adani, M., Bellucci, A., Braun, A., Calmanti, S., Carillo, A., Dell'Aquila, A., et al. (2013). The circe simulations: regional climate change projections with realistic representation of the mediterranean sea. *Bulletin of the American Meteorological Society*, 94(1):65–81.

Hamon, M., Beuvier, J., Somot, S., Lellouche, J.-M., Greiner, E., Jordà, G., Bouin, M.-N., Arsouze, T., Béranger, K., Sevault, F., et al. (2016). Design and validation of medrys, a mediterranean sea reanalysis over the period 1992–2013. *Ocean Science*, 12(2):577–599.

Harmelin, J. (2004). Environnement thermique du benthos côtier de l'île de port-cros (parc national, france, méditerranée nord-occidentale) et implications biogéographiques. *Scientific reports of Port-Cros national park*, 20:97–146.

Hasanean, H. (2004). Precipitation variability over the mediterranean and its linkage with el nino southern oscillation (enso). *J. Meteorol*, 29:151–160.

Herrmann, M., Somot, S., Calmanti, S., Dubois, C., and Sevault, F. (2011). Representation of spatial and temporal variability of daily wind speed and of intense wind events over the mediterranean sea using dynamical downscaling: impact of the regional climate model configuration. *Natural Hazards and Earth System Sciences*, 11:1983–2001.

Herrmann, M. J. and Somot, S. (2008). Relevance of era40 dynamical downscaling for modeling deep convection in the mediterranean sea. *Geophysical Research Letters*, 35(4).

Hertig, E. and Jacobeit, J. (2008). Assessments of mediterranean precipitation changes for the 21st century using statistical downscaling techniques. *International Journal of Climatology: A Journal of the Royal Meteorological Society*, 28(8):1025–1045.

Hertig, E., Seubert, S., and Jacobeit, J. (2010). Temperature extremes in the mediterranean area: trends in the past and assessments for the future. *Natural Hazards and Earth System Sciences*, 10(10):2039–2050.

Hewitt, H. T., Bell, M. J., Chassignet, E. P., Czaja, A., Ferreira, D., Griffies, S. M., Hyder, P., McClean, J. L., New, A. L., and Roberts, M. J. (2017). Will high-resolution global ocean models benefit coupled predictions on short-range to climate timescales? *Ocean Modelling*.

Hobday, A., Oliver, E., Gupta, A. S., Benthuysen, J., Burrows, M., Donat, M., Holbrook, N., P.J. Moore, M. T., Wernberg, T., and Smale, D. (2018). Categorizing and naming marine heatwaves. *Oceanography*, page 31(2).

Hobday, A. J., Alexander, L. V., Perkins, S. E., Smale, D. A., Straub, S. C., Oliver, E. C., Benthuysen, J. A., Burrows, M. T., Donat, M. G., Feng, M., et al. (2016). A hierarchical approach to defining marine heatwaves. *Progress in Oceanography*, 141:227–238.

Hobday, A. J. and Pecl, G. T. (2014). Identification of global marine hotspots: sentinels for change and vanguards for adaptation action. *Reviews in Fish Biology and Fisheries*, 24(2):415–425.

Holbrook, N., HA, S., A Sen, G., JA, B., M, F., ECJ, O., LV, A., MT, B., MG, D., AJ, H., PJ, M., SE, P.-K., DA, S., SC, S., and T, W. (subm). A global assessment of marine heatwaves and their drivers.

Houpert, L., Testor, P., de Madron, X. D., Somot, S., D'ortenzio, F., Estournel, C., and Lavigne, H. (2015). Seasonal cycle of the mixed layer, the seasonal thermocline and the upper-ocean heat storage rate in the mediterranean sea derived from observations. *Progress in Oceanography*, 132:333–352.

Hu, Z.-Z., Kumar, A., Jha, B., Zhu, J., and Huang, B. (2017). Persistence and predictions of the remarkable warm anomaly in the northeastern pacific ocean during 2014–16. *Journal of Climate*, 30(2):689–702.

Huete-Stauffer, C., Vielmini, I., Palma, M., Navone, A., Panzalis, P., Vezzulli, L., Misic, C., and Cerrano, C. (2011). Paramuricea clavata (anthozoa, octocorallia) loss in the marine protected area of tavolara (sardinia, italy) due to a mass mortality event. *Marine Ecology*, 32:107–116.

Hughes, T. P., Anderson, K. D., Connolly, S. R., Heron, S. F., Kerry, J. T., Lough, J. M., Baird, A. H., Baum, J. K., Berumen, M. L., Bridge, T. C., et al. (2018). Spatial and temporal patterns of mass bleaching of corals in the anthropocene. *Science*, 359(6371):80–83.

Hughes, T. P., Kerry, J. T., Álvarez-Noriega, M., Álvarez-Romero, J. G., Anderson, K. D., Baird, A. H., Babcock, R. C., Beger, M., Bellwood, D. R., Berkelmans, R., et al. (2017). Global warming and recurrent mass bleaching of corals. *Nature*, 543(7645):373.

IPCC (2007). In: Solomon, S., Qin, D., Manning, M., Chen, Z., Marquis, M., Averyt, K.B., et al (eds), Climate Change 2007: The Physical Science Basis. Contribution of Working Group i to the Fourth Assessment Report of the IPCC.

J. Beuvier, F. Sevault, M. H. H. K. W. L. M. R. E. S. K. B. and Somot, S. (2010). Modeling the mediterranean sea interannual variability during 1961–2000: Focus on the eastern mediterranean transien. *J. Geophys. Res.*, 115:C08017 1–27.

Jackson, J. M., Johnson, G. C., Dosser, H. V., and Ross, T. (2018). Warming from recent marine heatwave lingers in deep british columbia fjord. *Geophysical Research Letters*, 45(18):9757–9764.

Jacob, D., Petersen, J., Eggert, B., Alias, A., Christensen, O. B., Bouwer, L. M., Braun, A., Colette, A., Déqué, M., Georgievski, G., Georgopoulou, E., Gobiet, A., Menut, L., Nikulin, G., Haensler, A., Hempelmann, N., Jones, C., Keuler, K., Kovats, S., Kröner, N., Kotlarski, S., Kriegsmann, A., Martin, E., Meijgaard, E. v., Moseley, C., Pfeifer, S., Preuschmann, S., Radermacher, C., Radtke, K., Rechid, D., Rounsevell, M., Samuelsson, P., Somot, S., Soussana, J.-F., Teichmann, C., Valentini, R., Vautard, R., Weber, B., and Yiou, P. (2013). Euro-cordex: new high-resolution climate change projections for european impact research. *Reg Environ Change*, 14:563–578.

Jacox, M. G., Alexander, M. A., Mantua, N. J., Scott, J. D., Hervieux, G., Webb, R. S., and Werner, F. E. (2018). Forcing of multiyear extreme ocean temperatures that impacted california current living marine resources in 2016. *Bulletin of the American Meteorological Society*, 99(1):S27–S33.

Jacox, M. G., Hazen, E. L., Zaba, K. D., Rudnick, D. L., Edwards, C. A., Moore, A. M., and Bograd, S. J. (2016). Impacts of the 2015–2016 el niño on the california current system: Early assessment and comparison to past events. *Geophysical Research Letters*, 43(13):7072–7080.

Joh, Y. and Di Lorenzo, E. (2017). Increasing coupling between npgo and pdo leads to prolonged marine heatwaves in the northeast pacific. *Geophysical Research Letters*, 44(22).

Johnson, G. C., Mecking, S., Sloyan, B. M., and Wijffels, S. E. (2007). Recent bottom water warming in the pacific ocean. *Journal of Climate*, 20(21):5365–5375.

Johnson, G. C., Purkey, S. G., and Toole, J. M. (2008). Reduced antarctic meridional overturning circulation reaches the north atlantic ocean. *Geophysical Research Letters*, 35(22).

Jordà, G., Marbà, N., and Duarte, C. M. (2012). Mediterranean seagrass vulnerable to regional climate warming. *Nature Climate Change*, 2(11):821–824.

Kersting, D. K., Bensoussan, N., and Linares, C. (2013). Long-term responses of the endemic reef-builder cladocora caespitosa to mediterranean warming. *PLoS One*, 8(8):e70820.

King, A. D., Karoly, D. J., and Henley, B. J. (2017). Australian climate extremes at 1.5 °C and 2 °C of global warming. *Nature Climate Change*, 7(6):412.

Kirtman, B., S.B, P., J.A., A., G.J., B., R., B., I., C., F.J., D.-R., A.M., F., M., K., G.A., M., M., P., A., S., C., S., R., S., G.J., v. O., G., V., and H.J., W. (2013). 13: Near-term climate change: Projections and predictability. in:Climate Change 2013: The physical science basis. contribution of working group i to the fifth assessment report of the intergovernmental panel on climate change.

Kitoh, A. (2007). Future climate projections around turkey by global climate models. *Final report of ICCAP*.

Knutti, R., Abramowitz, G., Collins, M., Eyring, V., Gleckler, P., Hewitson, B., and Mearns, L. (2010). Ipcc expert meeting on assessing and combining multi-model climate projections. *Good practice guidance paper on assessing and combining multi model climate projections*.

Kuglitsch, F. G. (2010). *Extreme temperature events in the Mediterranean region*. PhD thesis, Verlag nicht ermittelbar.

Kuglitsch, F. G., Toreti, A., Xoplaki, E., Della-Marta, P. M., Luterbacher, J., and Wanner, H. (2009). Homogenization of daily maximum temperature series in the mediterranean. *Journal of Geophysical Research: Atmospheres*, 114(D15).

Kuglitsch, F. G., Toreti, A., Xoplaki, E., Della-Marta, P. M., Zerefos, C. S., Türkeş, M., and Luterbacher, J. (2010). Heat wave changes in the eastern mediterranean since 1960. *Geophysical Research Letters*, 37(4).

Lazzari. P, G. Mattia, C. S. S. S. A. C. M. Z. P. O. M. V. (2014). The impacts of climate change and environmental management policies on the trophic regimes in the mediterranean sea: Scenario analyses. *Journal of Marine Systems*, page 37–149.

Le Moigne, P., Colin, J., and Decharme, B. (2016). Impact of lake surface temperatures simulated by the flake scheme in the cnrm-cm5 climate model. *Tellus A: Dynamic Meteorology and Oceanography*, 68(1):31274.

Lelieveld, J., Hadjinicolaou, P., Kostopoulou, E., Giannakopoulos, C., Pozzer, A., Tanarhte, M., and Tyrlis, E. (2014). Model projected heat extremes and air pollution in the eastern mediterranean and middle east in the twenty-first century. *Regional environmental change*, 14(5):1937–1949.

Li, L., Casado, A., Congedi, L., Dell'Aquila, A., Dubois, C., Elizalde, A., L'Hévéder, B., Lionello, P., Sevault, F., Somot, S., et al. (2012). Modeling of the mediterranean climate system. In *The Climate of the Mediterranean Region*, pages 419–448. Elsevier.

Lima, F. P. and Wethey, D. S. (2012). Three decades of high-resolution coastal sea surface temperatures reveal more than warming. *Nature communications*, 3:704.

Linares, C., Coma, R., Diaz, D., Zabala, M., Hereu, B., and Dantart, L. (2005). Immediate and delayed effects of a mass mortality event on gorgonian population dynamics and benthic community structure in the nw mediterranean sea. *Marine Ecology Progress Series*, 305:127–137.

Lionello, P., Abrantes, F., Congedi, L., Dulac, F., Gacic, M., Gomis, D., Goodess, C., Hoff, H., Kutiel, H., Luterbacher, J., et al. (2012). Introduction: mediterranean climate: background information.

Lough, J. (2000). 1997–98: unprecedented thermal stress to coral reefs? *Geophysical Research Letters*, 27(23):3901–3904.

Ludwig, W., Dumont, E., Meybeck, M., and Heussner, S. (2009). River discharges of water and nutrients to the mediterranean and black sea: major drivers for ecosystem changes during past and future decades? *Progress in oceanography*, 80(3-4):199–217.

Luterbacher, J., Dietrich, D., Xoplaki, E., Grosjean, M., and Wanner, H. (2004). European seasonal and annual temperature variability, trends, and extremes since 1500. *Science*, 303(5663):1499–1503.

L'Hévéder, B., Li, L., Sevault, F., and Somot, S. (2013). Interannual variability of deep convection in the northwestern mediterranean simulated with a coupled aorcm. *Climate dynamics*, 41(3-4):937–960.

Macias, D., Garcia-Gorriz, E., Dosio, A., Stips, A., and Keuler, K. (2018). Obtaining the correct sea surface temperature: bias correction of regional climate model data for the mediterranean sea. *Climate dynamics*, 51(3):1095–1117.

Macias, D., Garcia-Gorriz, E., and Stips, A. (2013). Understanding the causes of recent warming of mediterranean waters. how much could be attributed to climate change? *PloS one*, 8(11):e81591.

Mackas, D., Greve, W., Edwards, M., Chiba, S., Tadokoro, K., Eloire, D., Mazzocchi, M., Batten, S., Richardson, A., Johnson, C., et al. (2012). Changing zooplankton seasonality in a changing ocean: comparing time series of zooplankton phenology. *Progress in Oceanography*, 97:31–62.

MacKenzie, B. R., Mosegaard, H., and Rosenberg, A. A. (2009). Impending collapse of bluefin tuna in the northeast atlantic and mediterranean. *Conservation Letters*, 2(1):26–35.

MacKenzie, B. R. and Schiedek, D. (2007). Daily ocean monitoring since the 1860s shows record warming of northern european seas. *Global change biology*, 13(7):1335–1347.

Madec, G. (2008). Nemo, the ocean engine, note du pole de modelisation, institut pierre-simon laplace (ipsl), france, no 27 issn no 1288–1619.

Malanotte-Rizzoli, P., Artale, V., Borzelli-Eusebi, G., Brenner, S., Crise, A., Gacic, M., Kress, N., Marullo, S., d'Alcalà, M. R., Sofianos, S., et al. (2014). Physical forcing and physical/biochemical variability of the mediterranean sea: a review of unresolved issues and directions for future research. *Ocean Science (OS)*, 10(3):281–322.

Manta, G., de Mello, S., Trinchin, R., Badagian, J., and Barreiro, M. (2018). The 2017 record marine heatwave in the southwestern atlantic shelf. *Geophysical Research Letters*, 45(22):12–449.

Marba, N. and Duarte, C. M. (2010). Mediterranean warming triggers seagrass (posidonia oceanica) shoot mortality. *Global Change Biology*, 16(8):2366–2375.

Marbà, N., Jordà, G., Agustí, S., Girard, C., and Duarte, C. M. (2015). Footprints of climate change on mediterranean sea biota. *Frontiers in Marine Science*, 2:56.

Marcos, M. and Tsimplis, M. N. (2008). Comparison of results of aogcms in the mediterranean sea during the 21st century. *Journal of Geophysical Research: Oceans*, 113(C12).

Mariotti, A. (2010). Recent changes in the mediterranean water cycle: a pathway toward long-term regional hydroclimatic change? *Journal of Climate*, 23(6):1513–1525.

Mariotti, A. (2011). Decadal climate variability and change in the mediterranean region. In *US National Oceanic and Atmospheric Administration, Climate Test Bed Joint Seminar Series, NCEP, Maryland, USA*.

Mariotti, A., Pan, Y., Zeng, N., and Alessandri, A. (2015). Long-term climate change in the mediterranean region in the midst of decadal variability. *Climate Dynamics*, 44(5-6):1437–1456.

Mariotti, A., Struglia, M. V., Zeng, N., and Lau, K. (2002). The hydrological cycle in the mediterranean region and implications for the water budget of the mediterranean sea. *Journal of climate*, 15(13):1674–1690.

Mariotti, A., Zeng, N., Yoon, J.-H., Artale, V., Navarra, A., Alpert, P., and Li, L. Z. (2008). Mediterranean water cycle changes: transition to drier 21st century conditions in observations and cmip3 simulations. *Environmental Research Letters*, 3(4):044001.

Mavrakis, A. F. and Tsiros, I. X. (2018). The abrupt increase in the aegean sea surface temperature during the june 2007 southeast mediterranean heatwave–a marine heatwave event? *Weather*.

McSweeney, C., Jones, R., Lee, R. W., and Rowell, D. (2015). Selecting cmip5 gcms for downscaling over multiple regions. *Climate Dynamics*, 44(11-12):3237–3260.

Millot, C. and Taupier-Letage, I. (2005). Circulation in the mediterranean sea. In *The Mediterranean Sea*, pages 29–66. Springer.

Mills, K. E., Pershing, A. J., Brown, C. J., Chen, Y., Chiang, F.-S., Holland, D. S., Lehuta, S., Nye, J. A., Sun, J. C., Thomas, A. C., et al. (2013). Fisheries management in a changing climate: lessons from the 2012 ocean heat wave in the northwest atlantic. *Oceanography*, 26(2):191–195.

Mitchell, T. D. and Jones, P. D. (2005). An improved method of constructing a database of monthly climate observations and associated high-resolution grids. *International journal of climatology*, 25(6):693–712.

Moss, R. H., Edmonds, J. A., Hibbard, K. A., Manning, M. R., Rose, S. K., Van Vuuren, D. P., Carter, T. R., Emori, S., Kainuma, M., Kram, T., et al. (2010). The next generation of scenarios for climate change research and assessment. *Nature*, 463(7282):747.

Munari, C. (2011). Effects of the 2003 european heatwave on the benthic community of a severe transitional ecosystem (comacchio saltworks, italy). *Marine pollution bulletin*, 62(12):2761–2770.

Myers, T. A., Mechoso, C. R., Cesana, G. V., DeFlorio, M. J., and Waliser, D. E. (2018). Cloud feedback key to marine heatwave off baja california. *Geophysical Research Letters*, 45(9):4345–4352.

Nabat, P., Somot, S., Mallet, M., Sevault, F., Chiacchio, M., and Wild, M. (2015). Direct and semi-direct aerosol radiative effect on the mediterranean climate variability using a coupled regional climate system model. *Climate dynamics*, 44(3-4):1127–1155.

Navara, A. and Tubiana, L. (2013). *Regional Assessment of Climate Change in the Mediterranean: Volume3:Case Studies*. Springer Science+Business Media Dordrecht.

Olita, A., Sorgente, R., Natale, S., Ribotti, A., Bonanno, A., Patti, B., et al. (2007). Effects of the 2003 european heatwave on the central mediterranean sea: surface fluxes and the dynamical response. *Ocean Science*, 3(2):273–289.

Oliver, E. C., Benthuysen, J. A., Bindoff, N. L., Hobday, A. J., Holbrook, N. J., Mundy, C. N., and Perkins-Kirkpatrick, S. E. (2017). The unprecedented 2015/16 tasman sea marine heatwave. *Nature communications*, 8:ncomms16101.

Oliver, E. C., Donat, M. G., Burrows, M. T., Moore, P. J., Smale, D. A., Alexander, L. V., Benthuysen, J. A., Feng, M., Gupta, A. S., Hobday, A. J., et al. (2018a). Longer and more frequent marine heatwaves over the past century. *Nature Communications*, 9(1):1324.

Oliver, E. C., Lago, V., Hobday, A. J., Holbrook, N. J., Ling, S. D., and Mundy, C. N. (2018b). Marine heatwaves off eastern tasmania: Trends, interannual variability, and predictability. *Progress in Oceanography*, 161:116–130.

Oliver, E. C., Perkins-Kirkpatrick, S. E., Holbrook, N. J., and Bindoff, N. L. (2018c). Anthropogenic and natural influences on record 2016 marine heat waves. *Bulletin of the American Meteorological Society*, 99(1):S44–S48.

Oliver, E. C., Wotherspoon, S. J., Chamberlain, M. A., and Holbrook, N. J. (2014). Projected tasman sea extremes in sea surface temperature through the twenty-first century. *Journal of Climate*, 27(5):1980–1998.

Ozturk, T., Ceber, Z. P., Türkeş, M., and Kurnaz, M. L. (2015). Projections of climate change in the mediterranean basin by using downscaled global climate model outputs. *International Journal of Climatology*, 35(14):4276–4292.

Paeth, H. and Hense, A. (2005). Mean versus extreme climate in the mediterranean region and its sensitivity to future global warming conditions. *Meteorologische Zeitschrift*, 14(3):329–347.

Pairaud, I. L., Bensoussan, N., Garreau, P., Faure, V., and Garrabou, J. (2014). Impacts of climate change on coastal benthic ecosystems: assessing the current risk of mortality outbreaks associated with thermal stress in nw mediterranean coastal areas. *Ocean Dynamics*, 64(1):103–115.

Parravicini, V., Guidetti, P., Morri, C., Montefalcone, M., Donato, M., and Bianchi, C. N. (2010). Consequences of sea water temperature anomalies on a mediterranean submarine cave ecosystem. *Estuarine, Coastal and Shelf Science*, 86(2):276–282.

Pearce, A. F. and Feng, M. (2013). The rise and fall of the "marine heat wave" off western australia during the summer of 2010/2011. *Journal of Marine Systems*, 111:139–156.

Perez, T., Garrabou, J., Sartoretto, S., Harmelin, J.-G., Francour, P., and Vacelet, J. (2000). Mortalité massive d'invertébrés marins: un événement sans précédent en méditerranée nord-occidentale. *Comptes Rendus de l'Académie des Sciences-Series III-Sciences de la Vie*, 323(10):853–865.

Perkins-Kirkpatrick, S., King, A., Cougnon, E., Grose, M., Oliver, E., Holbrook, N., Lewis, S., and Pourasghar, F. (2018). The role of natural variability and anthropogenic climate change in the 2017/2018 tasman sea marine heatwave. *Bulletin of the American Meteorological Society*, pages 1–4.

Pershing, A. J., Mills, K. E., Dayton, A. M., Franklin, B. S., and Kennedy, B. T. (2018). Evidence for adaptation from the 2016 marine heatwave in the northwest atlantic ocean. *Oceanography*, 31(2):152–161.

Pinardi, N., Arneri, E., Crise, A., Ravaioli, M., and Zavatarelli, M. (2006). The physical, sedimentary and ecological structure and variability of shelf areas in the mediterranean sea (27). *The sea*, 14:1243–330.

Pisano, A., Nardelli, B. B., Tronconi, C., and Santoleri, R. (2016). The new Mediterranean optimally interpolated pathfinder AVHRR SST Dataset (1982–2012). *Remote Sensing of Environment*, 176:107–116.

Planton, S., Déqué, M., Chauvin, F., and Terray, L. (2008). Expected impacts of climate change on extreme climate events. *Comptes Rendus Geoscience*, 340(9-10):564–574.

Planton, S., Lionello, P., Artale, V., Aznar, R., Carrillo, A., Colin, J., Congedi, L., Dubois, C., Elizalde, A., Gualdi, S., et al. (2012a). Climate extremes (sub-chapter 8.5). in: The climate of the mediterranean region in future climate projections. In *The Climate of the Mediterranean Region*, pages 449–502. Elsevier.

Planton, S., Lionello, P., Artale, V., Aznar, R., Carrillo, A., Colin, J., Congedi, L., Dubois, C., Elizalde, A., Gualdi, S., et al. (2012b). The climate of the mediterranean region in future climate projections. In *The Climate of the Mediterranean Region*, pages 449–502. Elsevier.

Potter, R. A. and Lozier, M. S. (2004). On the warming and salinification of the mediterranean outflow waters in the north atlantic. *Geophysical Research Letters*, 31(1).

Purkey, S. G. and Johnson, G. C. (2010). Warming of global abyssal and deep southern ocean waters between the 1990s and 2000s: Contributions to global heat and sea level rise budgets. *Journal of Climate*, 23(23):6336–6351.

Reid, J. L. (1979). On the contribution of the mediterranean sea outflow to the norwegian-greenland sea. *Deep Sea Research Part A. Oceanographic Research Papers*, 26(11):1199–1223.

Rinaldi, E., Buongiorno Nardelli, B., Zambianchi, E., Santoleri, R., and Poulain, P.-M. (2010). Lagrangian and eulerian observations of the surface circulation in the tyrrhenian sea. *Journal of Geophysical Research: Oceans*, 115(C4).

Rivetti, I., Fraschetti, S., Lionello, P., Zambianchi, E., and Boero, F. (2014). Global warming and mass mortalities of benthic invertebrates in the mediterranean sea. *PloS one*, 9(12):e115655.

Rivoire, G. (1991). Mortalité du corail et des gorgones en profondeur au large des côtes provençales. *Les especies marines a proteger en Mediterranee. GIS Posidonies, France*, pages 53–59.

Rixen, M., Beckers, J.-M., Levitus, S., Antonov, J., Boyer, T., Maillard, C., Fichaut, M., Balopoulos, E., Iona, S., Dooley, H., et al. (2005). The western mediterranean deep water: a proxy for climate change. *Geophysical Research Letters*, 32(12).

Roberts, M. J., Hewitt, H. T., Hyder, P., Ferreira, D., Josey, S. A., Mizielinski, M., and Shelly, A. (2016). Impact of ocean resolution on coupled air-sea fluxes and large-scale climate. *Geophysical Research Letters*, 43(19).

Robinson, A. R., Leslie, W. G., Theocharis, A., and Lascaratos, A. (2001). Mediterranean sea circulation. *Ocean currents: a derivative of the Encyclopedia of Ocean Sciences*, pages 1689–1705.

Robinson, C. J. (2016). Evolution of the 2014–2015 sea surface temperature warming in the central west coast of baja california, mexico, recorded by remote sensing. *Geophysical Research Letters*, 43(13):7066–7071.

Rodrigues, L. C., Bergh, J. C. V. D., Massa, F., Theodorou, J. A., Ziveri, P., and Gazeau, F. (2015). Sensitivity of mediterranean bivalve mollusc aquaculture to climate change, ocean acidification, and other environmental pressures: findings from a producer survey. *Journal of Shellfish Research*, 34(3):1161–1176.

Romanou, A., Tselioudis, G., Zerefos, C., Clayson, C., Curry, J., and Andersson, A. (2010). Evaporation–precipitation variability over the mediterranean and the black seas from satellite and reanalysis estimates. *Journal of Climate*, 23(19):5268–5287.

Rose, T., Smale, D., and Botting, G. (2012). The 2011 marine heat wave in cockburn sound, southwest australia. *Ocean Science*, 8(4):545–550.

Rouault, M., Illig, S., Bartholomae, C., Reason, C., and Bentamy, A. (2007). Propagation and origin of warm anomalies in the angola benguela upwelling system in 2001. *Journal of Marine Systems*, 68(3-4):473–488.

Ruiz, S., Gomis, D., Sotillo, M. G., and Josey, S. A. (2008). Characterization of surface heat fluxes in the mediterranean sea from a 44-year high-resolution atmospheric data set. *Global and Planetary Change*, 63(2-3):258–274.

Ruti, P., Somot, S., Giorgi, F., Dubois, C., Flaounas, E., Obermann, A., Dell'Aquila, A., Pisacane, G., Harzallah, A., Lombardi, E., et al. (2016). Med-cordex initiative for mediterranean climate studies, bams, doi: 10.1175. Technical report, BAMS-D-14-00176.1.

Salinger, J., Renwick, J., Behrens, E., Mullam, B., J Diamond, H., Sirguey, P., Smith, R., Trought, M., V Alexander, L., Cullen, N., Fitzharris, B., Hepburn, C., Parker, A., and J Sutton, P. (2019). The unprecedented coupled ocean-atmosphere summer heatwave in the new zealand region 2017/18: drivers, mechanisms and impacts. *Environmental Research Letters*.

Sánchez, E., Gallardo, C., Gaertner, M., Arribas, A., and Castro, M. (2004). Future climate extreme events in the mediterranean simulated by a regional climate model: a first approach. *Global and Planetary Change*, 44(1-4):163–180.

Sanchez-Gomez, E., Somot, S., Josey, S., Dubois, C., Elguindi, N., and Déqué, M. (2011). Evaluation of mediterranean sea water and heat budgets simulated by an ensemble of high resolution regional climate models. *Climate dynamics*, 37(9-10):2067–2086.

Sanchez-Gomez, E., Somot, S., and Mariotti, A. (2009). Future changes in the mediterranean water budget projected by an ensemble of regional climate models. *Geophysical Research Letters*, 36(21).

Scannell, H. A., Pershing, A. J., Alexander, M. A., Thomas, A. C., and Mills, K. E. (2016). Frequency of marine heatwaves in the north atlantic and north pacific since 1950. *Geophysical Research Letters*, 43(5):2069–2076.

Schaeffer, A. and Roughan, M. (2017). Sub-surface intensification of marine heatwaves off southeastern australia: the role of stratification and local winds. *Geophysical Research Letters*.

Schär, C., Vidale, P. L., Lüthi, D., Frei, C., Häberli, C., Liniger, M. A., and Appenzeller, C. (2004). The role of increasing temperature variability in european summer heatwaves. *Nature*, 427(6972):332.

Schiaparelli, S., Castellano, M., Povero, P., Sartoni, G., and Cattaneo-Vietti, R. (2007). A benthic mucilage event in north-western mediterranean sea and its possible relationships with the summer 2003 european heatwave: short term effects on littoral rocky assemblages. *Marine Ecology*, 28(3):341–353.

Schlegel, R. W., Oliver, E. C., Perkins-Kirkpatrick, S., Kruger, A., and Smit, A. J. (2017a). Predominant atmospheric and oceanic patterns during coastal marine heatwaves. *Frontiers in Marine Science*, 4:323.

Schlegel, R. W., Oliver, E. C., Wernberg, T., and Smit, A. J. (2017b). Nearshore and offshore co-occurrence of marine heatwaves and cold-spells. *Progress in Oceanography*, 151:189–205.

Schoetter, R., Cattiaux, J., and Douville, H. (2015). Changes of western european heat wave characteristics projected by the cmip5 ensemble. *Climate dynamics*, 45(5-6):1601–1616.

Schroeder, K., Garcìa-Lafuente, J., Josey, S. A., Artale, V., Nardelli, B. B., Carrillo, A., Gačić, M., Gasparini, G. P., Herrmann, M., Lionello, P., et al. (2012). Circulation of the mediterranean sea and its variability. In *The climate of the Mediterranean region*, pages 187–256. Elsevier.

Sein, D. V., Mikolajewicz, U., Gröger, M., Fast, I., Cabos, W., Pinto, J. G., Hagemann, S., Semmler, T., Izquierdo, A., and Jacob, D. (2015). Regionally coupled atmosphere-ocean-sea ice-marine biogeochemistry model rom: 1. description and validation. *Journal of Advances in Modeling Earth Systems*, 7(1):268–304.

Selig, E. R., Casey, K. S., and Bruno, J. F. (2010). New insights into global patterns of ocean temperature anomalies: implications for coral reef health and management. *Global Ecology and Biogeography*, 19(3):397–411.

Sevault, F., Somot, S., Alias, A., Dubois, C., Lebeaupin-Brossier, C., Nabat, P., Adloff, F., Déqué, M., and Decharme, B. (2014). A fully coupled mediterranean regional climate system model: design and evaluation of the ocean component for the 1980–2012 period. *Tellus A: Dynamic Meteorology and Oceanography*, 66(1):23967.

Sevault, F., Somot, S., and Beuvier, J. (2009). A regional version of the nemo ocean engine on the mediterranean sea: Nemomed8 user's guide. *Note de centre*, (107).

Shaltout, M. and Omstedt, A. (2014). Recent sea surface temperature trends and future scenarios for the mediterranean sea. *Oceanologia*, 56(3):411–443.

Smale, D. A., Wernberg, T., Oliver, E. C., Thomsen, M., Harvey, B. P., Straub, S. C., Burrows, M. T., Alexander, L. V., Benthuysen, J. A., Donat, M. G., et al. (2019). Marine heatwaves threaten global biodiversity and the provision of ecosystem services. *Nature Climate Change*, page 1.

Somot, S., Jorda, G., Harzallah, A., and , S. (2016). The mediterranean sea in the future climate projections (sub-chapter 1.2.3). in: The mediterranean region under climate change: A scientific update. *Editor:All-Envi in preparation of the COP22, Marrakech*.

Somot, S., Sevault, F., and Déqué, M. (2006). Transient climate change scenario simulation of the mediterranean sea for the twenty-first century using a high-resolution ocean circulation model. *Climate Dynamics*, 27(7-8):851–879.

Somot, S., Sevault, F., Déqué, M., and Crépon, M. (2008). 21st century climate change scenario for the mediterranean using a coupled atmosphere–ocean regional climate model. *Journal of Climate Dynamics*, 63:112–126.

Sotillo, M., Ratsimandresy, A., Carretero, J., Bentamy, A., Valero, F., and González-Rouco, F. (2005). A high-resolution 44-year atmospheric hindcast for the mediterranean basin: contribution to the regional improvement of global reanalysis. *Climate dynamics*, 25(2-3):219–236.

Sparnocchia, S., Schiano, M., Picco, P., Bozzano, R., and Cappelletti, A. (2006). The anomalous warming of summer 2003 in the surface layer of the central ligurian sea (western mediterranean). In *Annales Geophysicae*, volume 24, pages 443–452.

Tan, H. and Cai, R. (2018). What caused the record-breaking warming in east china seas during august 2016? *Atmospheric Science Letters*, 19(10):e853.

Thiébault, S. and Moatti, J.-P. (2016). *The Mediterranean region under climate change: a scientific update*.

Thorpe, R. B. and Bigg, G. R. (2000). Modelling the sensitivity of mediterranean outflow to anthropogenically forced climate change. *Journal of Climate Dynamics*, 16:355–368.

Tomassini, L. and Elizalde, A. (2012). Does the mediterranean sea influence the european summer climate? the anomalous summer 2003 as a test bed. *Journal of Climate*, 25(20):7028–7045.

Tseng, Y.-H., Ding, R., and Huang, X.-m. (2017). The warm blob in the northeast pacific—the bridge leading to the 2015/16 el niño. *Environmental Research Letters*, 12(5):054019.

Tsimplis, M. N., Marcos, M., and ab, S. (2008). 21st century mediterranean sea level rise: steric and atmospheric pressure contributions from a regional model. *Global and Planetary Change*, 63(2-3):105–111.

Tsimplis, M. N., Zervakis, V., Josey, S. A., Peneva, E. L., Struglia, M. V., Stanev, E. V., Theocharis, A., Lionello, P., Malanotte-Rizzoli, P., Artale, V., et al. (2006). Changes in the oceanography of the mediterranean sea and their link to climate variability. In *Developments in Earth and Environmental Sciences*, volume 4, pages 227–282. Elsevier.

Ulbrich, U., Xoplaki, E., Dobricic, S., García-Herrera, R., Lionello, P., Adani, M., Baldi, M., Barriopedro, D., Coccimiglio, P., Dalu, G., et al. (2013). Past and current climate changes in the mediterranean region. In *Regional assessment of climate change in the Mediterranean*, pages 9–51. Springer.

Vacelet, J. (1990). Report of a mission in tunisia, syria, cyprus,greece and turkey, 26 september-4 october and 25 october-12 november 1989 in the context of the programme 'fight against the epidemic decimating sponges in the mediterranean'. In *FAO Technical Cooperation. Programme,Rome*.

Van der Linden, P. and Mitchell, JFB, e. (2009). Ensembles: Climate change and its impacts-summary of research and results from the ensembles project.

Van Vuuren, D. P., Edmonds, J., Kainuma, M., Riahi, K., Thomson, A., Hibbard, K., Hurtt, G. C., Kram, T., Krey, V., Lamarque, J.-F., et al. (2011). The representative concentration pathways: an overview. *Climatic change*, 109(1-2):5.

Vaquer-Sunyer, R. and Duarte, C. M. (2013). Experimental evaluation of the response of coastal mediterranean planktonic and benthic metabolism to warming. *Estuaries and coasts*, 36(4):697–707.

Voldoire, A., Decharme, B., Pianezze, J., Lebeaupin Brossier, C., Sevault, F., Seyfried, L., Garnier, V., Bielli, S., Valcke, S., Alias, A., et al. (2017). Surfex v8. 0 interface with oasis3-mct to couple atmosphere with hydrology, ocean, waves and sea-ice models, from coastal to global scales. *Geoscientific Model Development*, 10(11):4207–4227.

Waldman, R., Somot, S., Herrmann, M., Bosse, A., Caniaux, G., Estournel, C., Houpert, L., Prieur, L., Sevault, F., and Testor, P. (2017). Modeling the intense 2012–2013 dense water formation event in the northwestern mediterranean sea: Evaluation with an ensemble simulation approach. *Journal of Geophysical Research: Oceans*, 122(2):1297–1324.

Walsh, J. E., Thoman, R. L., Bhatt, U. S., Bieniek, P. A., Brettschneider, B., Brubaker, M., Danielson, S., Lader, R., Fetterer, F., Holderied, K., et al. (2018). The high latitude marine heat wave of 2016 and its impacts on alaska. *Bulletin of the American Meteorological Society*, 99(1):S39–S43.

Weller, E., Min, S.-K., Lee, D., Kug, J.-S., Cai, W., and Yeh, S.-W. (2015). Human contribution to the 2014 record high sea surface temperatures over the western tropical and northeast pacific ocean. *Bulletin of the American Meteorological Society*, 96(12):S100–S104.

Wernberg, T., Bennett, S., Babcock, R. C., de Bettignies, T., Cure, K., Depczynski, M., Dufois, F., Fromont, J., Fulton, C. J., Hovey, R. K., et al. (2016). Climate-driven regime shift of a temperate marine ecosystem. *Science*, 353(6295):169–172.

Wernberg, T., Smale, D. A., Tuya, F., Thomsen, M. S., Langlois, T. J., De Bettignies, T., Bennett, S., and Rousseaux, C. S. (2013). An extreme climatic event alters marine ecosystem structure in a global biodiversity hotspot. *Nature Climate Change*, 3(1):78–82.

Wüst, G. (1961). On the vertical circulation of the mediterranean sea. *Journal of Geophysical Research*, 66(10):3261–3271.

Xoplaki, E. (2002). *Climate variability over the Mediterranean*. PhD thesis.

Xoplaki, E., González-Rouco, J., Luterbacher, J. u., and Wanner, H. (2004). Wet season mediterranean precipitation variability: influence of large-scale dynamics and trends. *Climate dynamics*, 23(1):63–78.

Xoplaki, E., González-Rouco, J. F., Luterbacher, J., and Wanner, H. (2003). Mediterranean summer air temperature variability and its connection to the large-scale atmospheric circulation and ssts. *Climate dynamics*, 20(7-8):723–739.

Xoplaki, E., Luterbacher, J., and Gonzales-Roucho, J. (2006). Mediterranean summer temperature and winter precipitation, large-scale dynamics, trends. *Nuovo Cimento della Societa Italiana di Fisica. C, Geophysics and Space Physics*, 29(1):45–54.

Xu, J., Lowe, R. J., Ivey, G. N., Jones, N. L., and Zhang, Z. (2018). Contrasting heat budget dynamics during two la nina marine heat wave events along northwestern australia. *Journal of Geophysical Research: Oceans*, 123(2):1563–1581.

Zaba, K. D. and Rudnick, D. L. (2016). The 2014–2015 warming anomaly in the southern california current system observed by underwater gliders. *Geophysical Research Letters*, 43(3):1241–1248.

Zhang, Z., Falter, J., Lowe, R., Ivey, G., and McCulloch, M. (2013). Atmospheric forcing intensifies the effects of regional ocean warming on reef-scale temperature anomalies during a coral bleaching event. *Journal of Geophysical Research: Oceans*, 118(9):4600–4616.

Zittis, G., Hadjinicolaou, P., Fnais, M., and Lelieveld, J. (2016). Projected changes in heat wave characteristics in the eastern mediterranean and the middle east. *Regional environmental change*, 16(7):1863–1876.

# Marine Heatwaves in the Mediterranean Sea : Detection, Past Variability and Future evolution

Sofia Darmaraki

Centre National de Recherches Météorologiques (UMR3589)
Météo-France, CNRS
42 avenue Gaspard Coriolis, Toulouse, France

**Abstract –** The Mediterranean Sea is considered a "Hot Spot" region for future climate change and depending on the greenhouse emission scenario, the annual mean basin sea surface temperature (SST) is expected to increase from +1.5 °°C to +3 °°C at the end of the 21st century relative to present-day. This significant SST rise is likely to intensify episodes of extreme warm ocean temperatures in the basin, named as Marine heatwaves (MHWs), that are known to exert substantial pressure on marine ecosystems and related fisheries around the world. In this context, the main aim of this PhD work is to study the past variability and future evolution of MHWs in the Mediterranean Sea. We propose a detection method for long lasting and large-scale summer MHWs, using a local, climatological 99th percentile threshold, based on present-climate daily SST. MHW probability of occurrence and characteristics in terms of spatial variability and temporal evolution are then investigated, using additional integrated indicators (e.g. duration, intensity, spatial extension, severity) to describe past and future events. Within the PhD and depending on the applications, the detection method is applied to various datasets : In-situ observation at buoys, high-resolution satellite product, various high- resolution and fully-coupled Regional Climate System Models including the recently developed CNRM-RCSM6 and the multi-model (5), multi-scenario (3) Med-CORDEX ensemble. The detection method is first tested on the 2003 MHW in order to assess its sensitivity to various tuning parameters. We conclude that its characterization is partly sensitive to the algorithm setting. Hindcast and historical mode simulations show that models are able to capture well observed MHW characteristics. We then assess past surface MHW variability (1982-2017) and their underlying driving mechanisms using the CNRM-RCSM6 model. We examine their characteristics from surface to 55m depth, where most thermal stress-related mass mortalities of Mediterranean ecosystems have been observed in the past. The analysis indicates an increase in duration and intensity of surface events with time, while MHWs of 2003, 2012 and 2015 are identified as the most severe events of the period. In particular, an anomalous increase in shortwave radiation and a lower-than-normal vertical diffusion and latent heat loss appeared to be responsible for the development of the MHW 2003, with wind playing a key role in the intensity of temperature anomalies at the sea surface. Differences on the dominant forcing, however, are sometimes evident in the different subbasin. We finally use the Med-CORDEX RCSM ensemble to assess the future MHW evolution in the basin over 1976-2100. Our results suggest longer and more severe events with higher global-warming rates. By 2100 and under RCP8.5, simulations project at least one long- lasting MHW every year, up to 3 months longer, about 4 times more intense and 42 times more severe than present-day events. Their occurrence is expected between June-October affecting at peak the entire basin. Their evolution is found to mainly occur due to an increase in the mean SST but an increase in daily SST variability plays also a noticeable role. Up to mid-21st century MHW characteristics rise independently of the choice of the emission scenario, whose influence becomes more evident by the end of the period. Further analysis finally reveals different climate change responses in certain configurations, more likely linked to their driving global climate model rather than to the individual regional model biases. This study provides a better understanding of Mediterranean Sea sensitivity to climate change considering for the first time the uncertainties related to global and regional climate models. We believe that this constitutes key information for the marine ecosystems and marine-related activities and societies in the basin that are under considerable risks due to the devastating effects of these events.

***Keywords*** *– Marine Heatwaves, Mediterranean Sea, climate change, extreme events, regional climate modeling*

**PhD supervisor –** Michel Deque, Samuel Somot

# Canicules océaniques en Méditerranée : Détection, Variabilité passée et Evolution future

Sofia Darmaraki

Centre National de Recherches Météorologiques (UMR3589)
Météo-France, CNRS
42 avenue Gaspard Coriolis, Toulouse, France

**Résumé –** L'objectif principal de ce travail de thèse est d'étudier la variabilité passée et l'évolution future des épisodes de températures océaniques anormalement chaudes en Méditerranée. Ces évènements, appelés canicules océaniques ou Marine Heatwaves en anglais (MHW), sont connues pour exercer une pression considérable sur les écosystèmes marins et les pêcheries associées un peu partout dans le monde. Nous proposons une nouvelle méthode de détection automatique des MHWs d'été basée sur le 99ème centile de la température quotidienne de la surface de la mer (TSM) en climat présent et tenant compte de la diversité géographique de la zone. La probabilité d'occurrence des MHWs et leurs caractéristiques spatio-temporelles sont ensuite étudiées. D'autres indicateurs intégrés tels que la durée, l'intensité, l'extension spatiale maximale ou la sévérité permettent de compléter la description des MHWs. Au cours de cette thèse et en fonction des applications, la méthode de détection est appliquée à différents types de données : observations in-situ aux bouées, produit satellitaire et différents modèles haute résolution et couplés haute fréquence du système climatique régional (RCSMs pour Regional Climate System Model en anglais) y compris le nouveau modèle CNRM-RCSM6 et l'ensemble Med-CORDEX multi-modèle (5) et multi-scénarios (3). L'algorithme de détection est d'abord testé sur la MHW de 2003 afin de montrer qu'il est peu sensible aux différents paramètres de réglage. L'évaluation des simulations rétrospectives et historiques montrent que les RCSMs sont capables dans l'ensemble de bien reproduire l'occurrence et les caractéristiques des MHWs observées par satellite. Nous étudions ensuite la variabilité passée des MHWs de surface (1982-2017) ainsi que leurs facteurs explicatifs en utilisant le modèle CNRM-RCSM6. Nous examinons, leurs caractéristiques entre 20-55 m de profondeur, là où la plupart des mortalités de masse liées au stress thermique des écosystèmes méditerranéens ont été observées dans le passé. L'analyse indique une augmentation de la durée et de l'intensité des évènements de surface au fil du temps, tandis que les MHWs de 2003, 2012 et 2015 sont détectées comme les évènements les plus sévères de la période. Par ailleurs, pour la canicule 2003 des différences importantes dans la contribution des échanges air-mer et de la diffusion vertical de chaleur sont mis en évidence pour les différents sous-bassins méditerranéens. Nous montrons également que la tension de vent joue un rôle clé sur l'intensité des anomalies de température en surface ainsi que leur propagation verticale. Enfin, nous utilisons l'ensemble Med-CORDEX de RCSMs pour évaluer l'évolution future des MHWs dans la région sur la période 1976-2100. Nos résultats suggèrent des évènements plus longs et plus sévères au fur et à mesure que le réchauffement climatique s'intensifie. D'ici à 2100 et dans le cadre du scénario le plus pessimiste (RCP8.5), les simulations projettent au moins une MHW de longue durée chaque année, jusqu'à 3 mois plus longue, environ 4 fois plus intense et 40 fois plus sévère que les évènements actuels. On s'attend à ce qu'elles se produisent entre juin et octobre, affectant au plus fort de leur extension l'ensemble du bassin. Cette évolution s'explique principalement par une augmentation de la TSM moyenne, mais l'augmentation de la variabilité quotidienne de la TSM joue également un rôle notable. Jusqu'au milieu du 21ème siècle, les caractéristiques des MHWs augmentent indépendamment du choix du scénario d'émission, dont l'influence devient plus évidente à la fin de la période. Enfin, l'analyse individuelle des modèles révèle différentes familles de réponses au changement climatique. Ces différences s'expliquent plus probablement par le choix du modèle global forçant, plutôt que par les biais individuels des modèles régionaux.

***Mots clés*** *– canicules oceaniques, Mediterranee, changement climatique, model climatic regional*

**Directeur de thèse –** Michel Deque, Samuel Somot
**Discipline –** Océan, Atmosphère, Climat